UC Berkeley
UC Berkeley Electronic Theses and Dissertations

Title
The Rate and Pattern of Deposition on Lowland River Floodplains

Permalink
https://escholarship.org/uc/item/5pz5n5tw

Author
Swanson, Kathleen

Publication Date
2013

Peer reviewed|Thesis/dissertation

eScholarship.org Powered by the California Digital Library
University of California

The Rate and Pattern of Deposition on Lowland River Floodplains

By

Kathleen Mary Swanson

A dissertation submitted in partial satisfaction of the

requirements for the degree of

Doctor of Philosophy

in

Engineering – Civil and Environmental Engineering

in the

Graduate Division

of the

University of California, Berkeley

Committee in charge:

Professor William E. Dietrich, Co-chair
Professor Mark Stacey, Co-chair
Professor John Dracup
Professor Mathias Kondolf

Fall 2013

The Rate and Pattern of Deposition on Lowland River Floodplains

Copyright © 2013

by

Kathleen Mary Swanson

Abstract

The Rate and Pattern of Deposition on Lowland River Floodplains

by

Kathleen Mary Swanson

Doctor of Philosophy in Engineering – Civil and Environmental Engineering

University of California, Berkeley

Professor William E. Dietrich, Co-Chair

Professor Mark Stacey, Co-Chair

On large lowland rivers, overbank flows can deposit as much as 40% of the river's sediment load across adjacent floodplain environments on an annual basis. The spatial pattern of this deposition and the corresponding grain size distributions are not well known, despite the importance of understanding floodplain evolution, the generation of alluvial architecture, and the spread of contaminants. The lack of field data of floodplain deposition also limits our ability to evaluate models of floodplain sedimentation. Here I report floodplain overbank depositional patterns and grain sizes on the Strickland River in Papua New Guinea, compare these data with similar data from the Fly River, to which the Strickland drains, and explore distinct differences between the two rivers using a simple 1-D diffusion-advection model to predict the field observations.

The Strickland and Fly Rivers join at just 6 m above sea level, and have experienced the same Holocene sea-level rise. Historically, the Strickland has carried about seven times as much sediment load and twice as much water discharge as the Fly. As a result of this higher sediment flux, the shorter lowland Strickland River floodplain should be more developed in response to Holocene sea-level rise and, consequently, should presently be storing proportionately less sediment than the floodplain of the middle Fly River. A field campaign to collect samples to document floodplain sedimentation rates was conducted in 2003. Mine-derived elevated Pb and Ag concentrations in 111 shallow (<1 m) floodplain cores collected in 2003 were used to determine sediment deposition rates across the lower Strickland floodplain. Observed sediment deposition rates decrease across the floodplain with distance from the channel bank, and the average rate of deposition was 1.4 cm/yr over the first 1 km.

The magnitude of overbank deposition along the lowland sand-bedded Strickland resulted in a ~13% loss of the total sediment load, corresponding to overbank deposition of about

~0.05% of the total load per km of channel length of the mainstem. Deposition rates over the first 1 km from the channel bank on the Strickland were about ten times higher than those estimated for natural sediment loads on the Fly. However, the proportion of the sediment load deposited per channel length on the Strickland was less than that of the Fly (0.09%/km of mainstem channel length) due to an extensive network of tributary and tie channels that convey sediment to the floodplain on the Fly. Furthermore, the lateral migration of the Strickland channel was ~5 times that on the Fly, such that most overbank deposits on the Strickland were returned to the channel, causing the net loss of sediment to the floodplain to be small.

In addition to the differences in the magnitude of deposition, the pattern of declining floodplain deposition with increasing distance from the channel differed between the two river systems: deposition decreased exponentially with distance from the channel on the Fly River floodplain and non-exponentially on the Strickland River floodplain. In order to assess the processes controlling this difference in the pattern of overbank deposition, sediment grain size distribution needed to be assessed. Particle size distributions for floodplain samples from the same cores used to determine deposition rates were measured using a Coulter LS laser particle sizer. Sediments from the Fly River floodplain did not vary much in size with distance from the channel and sand comprises about 5% of samples at all distances from the channel. This contrasted significantly with sediment size distributions across the Strickland floodplain, where sediments rapidly fined with distance from the channel. There was little sand or coarse silt present beyond 400 m from the channel and clay and fine silt comprised the majority of sediment beyond this distance.

Extensive studies of the Fly and Strickland River floodplain deposits motivated further study of the mechanisms of deposition. The differences in both the rate of deposition and the variation of grain size as a function of distance from the channel were hypothesized to be due to a difference in the relative importance of diffusive and advective transport of sediment from the channel to the floodplain. A 1-D numerical model was developed to investigate this hypothesis. The model indicated that lateral advection was the primary transport mechanism of sediment across both floodplains and that the key difference in depositional pattern may be explained by flocculation of all sediment particle sizes transported on to the swampy, highly-organic waters of Fly River floodplain and flocculation of primarily fine sediment transported across the less-swampy Strickland River floodplain. Lateral variability in accretion from overbank deposition can be explained by a mechanistically-derived exponential function that is solved by balancing a simple advection-deposition transport formula, but the parameters needed to evaluate the relationship are difficult to measure directly. Model parameters were estimated from the limited data available. A depositional length-scale was used to calculate the possible duration of active deposition, the effective settling velocity of flocculated particles, and floodplain flow velocity. The non-exponential deposition pattern observed on the Strickland River floodplain was likely the result of deposition of a distribution of particles sizes and a distribution of effective settling velocities. The observed non-

exponential accretion on the Strickland River floodplain arose from the sum of the exponential functions for each particle size. The flocculated particles on the Fly River floodplain likely had a single effective settling velocity resulting in the observed exponential deposition pattern and lack of fining in overbank deposits.

The Fly and Strickland Rivers serve as a unique natural laboratory where relatively undeveloped, large lowland river systems with similar climate, geology, ecology and history can be studied to examine the fundamental processes controlling the evolution of alluvial valleys. The extensive analysis of floodplain sediment cores demonstrated that the rate, pattern and proportional loss of sediment overbank was quite different on the two systems as a result of differing sediment loads, subsequent adjustment to Holocene sea level rise, and, probably, the relative importance of flocculation of sediments transported overbank. Despite these differences, the overbank deposition pattern on both river systems can be describe by a simple advection-settling model. The pattern of deposition can be used to evaluate the model parameters and quantify key variables such as particle and flow characteristics which are logistically difficult to obtain on large floodplains. This understanding enhances our ability to evaluate floodplain sediment transport dynamics based upon depositional records and identifies key measurements that should be incorporated into future studies.

Contents

Chapter 1
Floodplain Deposition and Previous Studies of the Middle Fly and Lower Strickland Rivers 1
1 Introduction 1
Figures 11

Chapter 2
Sediment load and floodplain deposition rates: comparison of the Fly and Strickland Rivers, Papua New Guinea 18
2.1. Introduction 20
2.2. Study site 20
2.3. Determination of floodplain sediment deposition rate using anthropogenic tracers 22
2.3.1 Sampling strategy and analysis 23
2.3.2 Sediment analysis 24
2.3.3 Determination of deposition rates 25
2.3.4 Derivation of background and mine-contaminated sediment concentrations 26
2.4. Deposition patterns on the Strickland River floodplain 27
2.4.1 Deposition of mine-derived sediment on the floodplain 27
2.4.2 Profile analysis 27
2.4.3 Calculated deposition rates 29
2.4.4 Floodplain sediment deposition rate 30
2.5. Discussion 33
2.6. Conclusions 37
Tables 39
Figures 45

Chapter 3
Sediment Particle Size Distribution of Overbank Deposits on Lowland River Floodplains 59
3.1 Introduction 60
3.1.1 Overbank Deposition 60
3.1.2 Observations of Floodplain Sediment Particle Size Distribution 61
3.2 Methods 62
3.3 Results 65
3.3.1 Strickland River Floodplain Sediment Particle Size Distribution 65
3.3.2 Fly River Floodplain Sediment Particle Size Distribution 68
3.4 Discussion 70
Tables 72
Figures 82

Chapter 4
A 1-D model to explore the lateral variation of floodplain deposition 107
4.1 Introduction 108
4.2 Theory 114
4.2.1 Floodplain deposition model 115
4.2.2 Turbulence model 117
4.2.3 Model scaling 119
4.3 Model parameterization 120
4.4 Results 122
4.5 Discussion 124
4.6 Conclusions 128
Tables 131
Figures 139
Appendix A 155
Appendix B 159
Tables 162
Figures 163

Acknowledgements

Throughout my time in graduate school I have had the opportunity to be surrounded lively, dedicated, and inspiring graduate students, researchers, postdoctoral researchers and professors in both Earth and Planetary Science and Environmental Engineering. It has been an amazing and enriching experience to be surrounded by so many wonderful people.

I owe my sincerest gratitude to my advisers, committee members, and professors, especially Bill Dietrich. He welcomed me to his group and taught me to view the landscape through the lens of mechanics and process. Bill always believed in me as a scientist and has been an inspiring mentor who never fails to as challenging questions. Mark Stacey has been an amazing teacher, an advocate for my work and his insights have been invaluable. Matt Kondolf and Jim Hunt provided thoughtful feedback and were generous with their time. John Dracup's kindness, encouragement and support has meant the world to me.

A special thank you to my lab mates and office mates. You all bring so many wonderful insights to our discussions and have been a wonderful source of support and friendship through the years. I don't know what I would have done without this amazing community. Thank you, Dino Bellugi, Christian Braudrick, Leslie Hsu, Ken Ferrier, Sarah Godsey, Vicky, Lee, Rebecca Leonardson, Toby Minear, Bill Mitchell, Marisa Palucis, Taylor Perron, Daniella Rempe, Johnny Sanders, Joel Rowland, Elowyn Yaeger, and so many others.

I have been fortunate to have been taught by some amazing instructors over the years. Dave Thomas introduced me to Environmental engineering and has been a lifelong mentor. Andy Schuler, Mike Gustafson and Gary Ybarra (among others) made my years at Duke intellectually rewarding, challenging and enjoyable. Bill Dietrich William Nazaroff, Jim Hunt, Vince Resh, John Dracup, Mark Stacey, David Schoellhamer, Zach Powell, and Kurt Cuffey have enriched my years at Berkeley.

I owe so much to the researchers who came before me and made so much of this work possible and to the intrepid crew who ventured to Papua New Guinea to sample the Strickland River floodplain by boat, helicopter, and on foot. Thank you, Rolf Aalto, Marie Bera, Geoff Day, Ian Hargreaves, Wes Lauer, Andrew Marshall, Cliff Reibe, Joel Rowland, and Johnny Sanders. Marie, you are missed. The trace metals analysis could not have been possible without the support of the scientists and staff at CSIRO Australia, Simon Apte, David Bishop, Stuart Simpson, and Elizabeth Watson. Special thanks got to Simon for all of his dedication to the research and his hospitality, delicious egg sandwiches, and fantastic book recommendations.

Financial support for this project primarily came from an NSF Margins (Source to Sink) grant with additional support for field work from Ok Tedi Mining Limited and Porgera Joint Venture. I was also supported by a Civil and Environmental Engineering graduate fellowship made possible through the generosity of UC Berkeley CEE alumni and friends.

Finally, it is my pleasure to thank my friends and especially my family for their unconditional support and love. My friends, especially Eric, Amy, Kristen, Christina and Shelley, have been my biggest cheerleaders. All of my family, especially my parents, has been unwavering in their encouragement and willingness to celebrate every milestone along the way. Michael, my partner, has been incredibly supportive and patient through this whole process. I am extraordinarily grateful and lucky to have him in my life.

Chapter 1

Floodplain Deposition and Previous Studies of the Middle Fly and Lower Strickland Rivers

1 Introduction

Floodplains are found on all river types and are an integral part of river systems. These landforms are often diverse and complex systems that respond to system changes heterogeneously and in space and time (Brige, 2003; Dunne and Aalto, 2013). Connectivity of rivers and floodplains is critical to riparian ecosystems providing off-channel aquatic habitat for sensitive species and exchanging water, sediment, nutrients and biota (e.g. Junk et al., 1989; Tockner et al., 1999; Kondolf et al., 2006; Tompkins, 2006). Floodplains are often impacted by upstream changes to sediment supply due to sediment capture by dams, increased sediment discharge from land use changes or mining, or are disconnected from rivers hydrologically by man-made levees and dykes to protect infrastructure from flooding and channel migration (e.g.Kondolf et al., 1997; Walling, 1999; Bridge, 2003; Rinklebe et al., 2007). The spatial and temporal complexity of these large, often anthropogenically altered features has proved a barrier to extensive research into the processes that control floodplain morphology and quantitative prediction of future changes in response to changing climate, sea level, land use or other forcings (Nanson and Croke, 1992; Dietrich et al., 1999; Blum and Törnqvist, 2000; Goodbred and Keuhl, 2000; Blum and Roberts, 2009; Dunne and Aalto, 2013).

Despite the fact that floodplains are of critical importance to human populations, ecosystems, and fluvial systems, a single mechanistic theory that can explain the lateral variability of floodplain sediment deposition and storage is lacking. Of specific interest are the following questions:

- Can we quantify river response to sea-level rise as a function of sediment load?
- Does the pattern of overbank deposition differ between floodplains as a result different states of response to sea-level rise or differing overbank transport processes?
- Can the observed depositional signals of floodplains inform our understanding of overbank deposition processes?

Perhaps the most robust dataset of modern floodplain deposition on a large lowland river floodplain is that on the middle Fly River in Papua New Guinea (eg. Dietrich et al 1999; Day et al., 2008; Lauer and Parker; 2008). The Fly River and its tributary, the Stirickland River, provide a natural laboratory where fluvial systems with differing sediment loads have responded to the same sea-level and climatic forcings. This dissertation explores the rate and pattern of deposition on the Strickland River floodplain then examines the depositional record of these two floodplains to evaluate the mechanisms that control floodplain deposition.

Nearly 40% of the River's sediment load is stored in the swampy floodplain (Day et al., 2008). Deposition decreases exponentially across the floodplain with increasing distance from any floodplain channel (Dietrich et al., 1999; Day et al. 2008). The Strickland River, carrying nearly twice as much water and seven times as much sediment as the Fly, is steeper and less swampy than the Fly River which it joins 150 km from the Gulf of Papua (Dietrich et al., 1999; Swanson et al., 2008)..

The Fly and Strickland Rivers drain from the Southern Fold Mountains (elev. ~4 km) of Papua New Guinea to the Gulf of Papua (Figure 1.1). The channels join ~150 km from the gulf with a bank elevation of ~6m (Dietrich et al. 1999). Upstream of their junction, the Fly catchment is 18,4000 km^2 with an average annual discharge of 2,244 m^3/s and an estimated natural sediment load of ~10 million tonnes/year (Dietrich et al., 1999). The Strickland River catchment is 36,000 km^2 with and average annual discharge of 3,110 m^3/s and a sediment load of 70-80 million tonnes per year (Dietrich et al., 1999; Day et al., 2008). Both channels occupy relatively wide (4-14km) alluvial valleys with moderately elevated scroll bar ridges (Figures 1.2 and 1.3) up to the gravel-sand transition several hundred km upstream of the junction (Dietrich et al., 1999). The middle Fly River has a slope of $1x10^{-5}$ at Everill Junction where it is joined by the Strickland and steepens upstream by a factor of 6 at the extent of the sand-bedded reach (Day et al., 2008). The Strickland River is an order of magnitude steeper throughout the 250-km extent of the sand bedded reach upstream of Everill junction with a slope of $1x10^{-4}$ (Figure 1.4; Swanson et al., 2008). The uplands of these rivers can receive up to 10-m of rainfall annually and 1-m of precipitation falls on the lowland floodplain (Day et al., 2008). La Niña events are associated with increased flooding and can lead to the middle Fly River floodplain being inundated continuously for months to more than a year. The less swampy Strickland River floodplain is not noted to be inundated for such prolonged periods.

Both the Fly and Strickland Rivers are largely undeveloped by modern standards without large cities or dams on the rivers, but both have mines in their headwaters. The Ok Tedi copper mine on a tributary of the Fly and Porgera Gold mine on a tributary of the Srtickland have contributed metal enriched sediments to the channels (Figure 1.1; Dietrich et al., 1999; Apte et al., 2001; Day et al., 2008; Swanson et al., 2008). The Ok Tedi Mine began operation in 1985 and increased the sediment load of the middle Fly

River ~4.5 times leading to bed aggradation, increased flooding and an increased rate of delivery of sediment to the floodplain (Day et al., 2008). Mine discharge to the Strickland River, which began in 1991, contributes ~10-15% of the sediment load in the lower reach of the river (Apte et al., 2001; Swanson et al., 2008; Markham, personal communication). This increase in load has not had an obvious impact on floodplain dynamics on the Strickland River. The presence of the mines in the headwaters of these river systems provides a readily available sediment tracer that can be used to identify sediment dispersal across the floodplains since the initiation of mining activities. Dietrich et al. (1999) and Day et al. (2008) estimate pre-mine floodplain deposition rates and patterns on the middle Fly River floodplain. Further analyses and discussions consider only with pre-mining estimates of deposition.

The Fly River floodplain was studied extensively from 1990 to 1994 to explore time impact of upstream mining on the channel and plain. A detailed description of the field and laboratory analysis can be found in Dietrich et al. (1999) and Day et al. (2008). Over 800 floodplain and off-river water body sediment cores were collected and analyzed during the five-year period (Figure 1.5). In each of the three longitudinal reaches of the middle Fly River floodplain, the forested, grassland and swamp reaches, deposition was clearly defined as decreasing exponentially with distance from the nearest channel up to 1 km from the channel and grainsize did not vary much beyond the channel levee (e.g. Figure 1.6; Dietrich et al., 1999; Day et al., 2008). Interestingly, a depositional web of tie channels, floodplain tributary channels and levee breaks transport ~20% of river discharge and associated sediment up to 40 km from the mainstem channel and the depositional pattern associated with floodplain channels is indistinguishable in magnitude and pattern from overbank deposition on the mainstem middle Fly River. An additional 20% of the sediment load from the channel was stored on the floodplain along the mainstem channel (Dietrich et al., 1999; Day et al., 2008). Figure 1.7 from Day et al. (2008) illustrates the expansive pattern of deposition from the main channel, tie channel-connected oxbow lakes and floodplain tributary channels.

The discharge of water and sediment from the Porgera mine in the headwaters of the Strickland River motivated an initial study of the surface sediments on the lowland floodplain to determine if metal concentrations in the deposited sediments exceeded environmental standards and to explore the areal extent of the impact to the floodplain (Apte, 2001). The study by Apte identified mine-derived metals in the sediment suitable for use as tracers in floodplains sediments and demonstrated that floodplain surface sediments had enriched metal concentrations relative to sediments at 29-30 cm depth.

The work presented in Chapter 2 built upon Apte (2001) to determine the rate and pattern of deposition of floodplain deposition on the lower Strickland River floodplain in 2003. As part of this study, duplicate cores were collected at most floodplain sampling locations. The geochronology of these duplicate cores was determined using ^{210}Pb providing both a verification of the rate and identified that deposition occurs periodically,

likely as the result of large floods (Aalto et al., 2008). The results of the work done by Aalto et al. (2008) are discussed in more detail in the Chapter 2.

Because the lower Strickland River has a shorter valley and a higher sediment load than the middle Fly, the channel should be more evolved in response to Holocene sea level rise and should be depositing less sediment on its floodplain (Lauer et al. 2008). Also, because the Strickland River floodplain is better drained and less swampy than they Fly, it is more likely to be dominated by advective transport of sediment across the plain than diffusive.

This dissertation explores the processes that control the rate, proportion and pattern of deposition on floodplains by addressing the following questions:

- Is the Strickland River floodplain more evolved than the Fly River floodplain in response to Holocene sea-level rise?
- Does the pattern of overbank deposition differ between the two floodplains as a result?
- Can these depositional signals inform our understanding of overbank deposition processes?

Changes in sediment and water supply or changes in base level can perturb the morphology or process of the river and that change can propagate up to several hundred km through the system (Schumm, 1993; Blum and Törnqvist, 2000). The sediment accommodation space created by sea-level rise tends to cause initially high net storage of sediment on the floodplain, but the sediment storage rate should decline as the river rebuilds its slope and infills the accommodation space (Muto and Swenson, 2005). Rivers with a large sediment supply should respond to relative SLR more quickly than their low supply counterparts (Paola, 2000) which would imply that the Strickland River should be more evolved in response to Holocene sea level rise and should be storing less sediment on the floodplain than the Fly (Lauer et al., 2008). The rate, proportion and spatial distribution of overbank floodplain deposition on the Strickland River floodplain determined using mine tracers is presented in Chapter 2 (previously published as Swanson et al., 2008). Though the magnitude of deposition on the Strickland River floodplain was higher than the calculated natural rate of deposition on the middle Fly River floodplain (Day et al., 2008), the proportion of the sediment load lost to the floodplain (~13%) and the proportion lost per channel length (0.05%/km) were both significantly lower than the corresponding measurements on the Fly indicating that the floodplain is in fact more "evolved" in response to sea-level rise. The deposition rate determined by Aalto et al. (2008) was slightly higher than but similar to the data presented here.

Overbank storage of sediment proportional to the total load on the Strickland River is relatively low when compared to other large river systems worldwide. The Rhine-Meuse stores ~19% of its annual load overbank (Middlekoop and Assleman, 1998) and while

just 10% of sediment load was deposited overbank on the Mississippi prior to human influence, an additional 30% was stored on levees and in crevasse splays (Kesel et al., 1992). As much as 30-70% of the sediment load in the Brahmaputra system may be stored overbank (Goodbred and Keuhl, 1998; Allison et al., 1998), and the magnitude of sediment storage on the Amazonian floodplain may be larger than the net flux of sediment out of the system (Dunne et al. 1998). Not only does the proportion of the load stored on the floodplain differ between the Fly and Strickland River floodplains, but the non-exponential deposition function observed on the Strickland River floodplain is far more typical (Swanson et al., 2008). Exponentially declining deposition rates have been observed on small UK rivers (Walling and He, 1998) and on the Fly River floodplain (Dietrich et al., 1999; Day et al., 2008), but deposition much more commonly decreases non-exponentially (e.g. Kesel et al., 1974; Allison et al., 1998; Aalto et al., 2003).

Quantifying the pattern of grain sizes across the floodplain can provide insight into the distribution and storage suspended sediment transported downstream, especially the washload carried by a channel (Higgins, 1990; Malmon et al., 2005), and the physical processes that were likely responsible for transporting and depositing sediment overbank (Allen 1978). When water overtops the levees there is an abrupt decrease in flow velocity and transport capacity resulting in the deposition of the coarsest material being carried in suspension by the river near the channel bank (Allen, 1965; Pizzuto, 1987; Asselman and Middelkoop, 1995; Walling et al., 1996; Asselman and Middelkoop, 1998; Dunne and Aalto, 2013). Sediment should fine with increasing transport distance from the channel (Asselman et al., 2003; Bridge, 2003; Dunne and Aalto, 2013). Chapter 3 establishes the particle size distribution of sediments deposited on the Strickland River floodplain and compares these data to the particle size distributions of deposited sediments on the Fly River floodplain. The Strickland River floodplain is dominated by fine silt, but fine sand is transported as much as 300 m from the channel bank. Strickland floodplain sediments fine rapidly with increasing distance from the channel and the distal floodplain is composed of only silt and clay. Fly River floodplain sediment particle sizes do not vary with distance from the channel and sand comprises ~5% of all floodplain sediments up to 1-km where active deposition ceases (Day et al., 2008). Day et al. (2008) argue that the often flooded and swampy floodplain may inhibit advective flows leading to a dominance of diffuse transport resulting in the exponential deposition pattern, but the lack of fining cannot be explained by either advective or diffusive transport alone.

The most important early models used to evaluate the lateral variability of overbank deposition were those by James (1985) and Pizzuto (1987). Both of these early models idealized a straight channel and confined floodplain with downstream velocities in the channel and plain which result in decreasing deposition rate and fining with increasing distance from the channel. Pizzuto (1987) concluded that lateral advection, which was not realistic in the idealized floodplain assumed to develop the model, would be required to transport sand and coarse sediment any significant distance from the channel. Many models of floodplain deposition (e.g Nicholas and Walling, 1997; Hardy et al., 2000; Moody and Troutman, 2000; Thonon, 2006) have been developed since James (1985) and

Pizzuto (1987), but none mechanistically address the mean lateral variability of floodplain deposition and particle size. Chapter 4 presents the development, scaling and application of a 1-D sediment transport and deposition model used to evaluate the relative importance of advective and diffusive transport on the Fly and Strickland River floodplains. A scaling of the model indicates that advective transport must be a dominant process on both floodplains and the balance of advection and settling across the plain yields an exponential deposition curve for each sediment size considered. The inclusion of multiple grainsizes results in a non-exponential deposition pattern and fining of deposited sediments with increasing distance from the channel. The lateral variability of particle size on the Fly River floodplain and clay on the Strickland River floodplain can only be explained by flocculation of the particles delivered overbank. Flocculation has been noted as an important process in deposition of sediments on floodplains (e.g. Nicholas and Walling, 1996 and Mertes, 1997), but a single effective floc size that incorporates all floodplain sediments, including sand, has not been observed *in situ*. The depositional length-scale developed for the model and characteristics of the floodplain deposits can be used to estimate key flood flow and particle characteristics that have not been measured directly.

References

Aalto, Rolf, et al. "Episodic sediment accumulation on Amazonian flood plains influenced by El Nino/Southern Oscillation." *Nature* 425.6957 (2003): 493-497.

Aalto, Rolf, J. Lauer, and William E. Dietrich. "Spatial and temporal dynamics of sediment accumulation and exchange along Strickland River floodplains (Papua New Guinea) over decadal-to-centennial timescales." *Journal of Geophysical Research: Earth Surface (2003–2012)* 113.F1 (2008).

Allen, John RL. "A review of the origin and characteristics of recent alluvial sediments." *Sedimentology* 5.2 (1965): 89-191.

Allen, J. R. L. "Studies in fluviatile sedimentation: an exploratory quantitative model for the architecture of avulsion-controlled alluvial suites." *Sedimentary Geology* 21.2 (1978): 129-147.

Allison, M. A., et al. "Importance of flood-plain sedimentation for river sediment budgets and terrigenous input to the oceans: Insights from the Brahmaputra-Jamuna River." *Geology* 26.2 (1998): 175-178.

Apte, Simon C., and Porgera Joint Venture. "Tracing mine-derived sediments and assessing their impact downstream of the Porgera gold mine." *Canberra: Commonwealth Scientific and Industrial Research Organization* (2001).

Asselman, Nathalie EM, and Hans Middelkoop. "Floodplain sedimentation: quantities, patterns and processes." *Earth Surface Processes and Landforms* 20.6 (1995): 481-499.

Asselman, Nathalie EM, and Hans Middelkoop. "Temporal variability of contemporary floodplain sedimentation in the Rhine–Meuse delta, The Netherlands." *Earth Surface Processes and Landforms* 23.7 (1998): 595-609.

Asselman, Nathalie EM, Hans Middelkoop, and Paul M. Van Dijk. "The impact of changes in climate and land use on soil erosion, transport and deposition of suspended sediment in the River Rhine." *Hydrological Processes* 17.16 (2003): 3225-3244.

Blum, Michael D., and Torbjörn E. Törnqvist. "Fluvial responses to climate and sea-level change: a review and look forward." *Sedimentology* 47.s1 (2000): 2-48

Blum, Michael D., and Harry H. Roberts. "Drowning of the Mississippi Delta due to insufficient sediment supply and global sea-level rise." *Nature Geoscience* 2.7 (2009): 488-491.

Bridge, J. S. "Rivers and Floodplains, 491 pp." (2003).

Day, Geoff, et al. "The depositional web on the floodplain of the Fly River, Papua New Guinea." *Journal of Geophysical Research: Earth Surface (2003–2012)* 113.F1 (2008).

Dietrich, William E., Geoff Day, and Gary Parker. "The Fly River, Papua New Guinea: Inferences about river dynamics, floodplain sedimentation and fate of sediment." *Varieties of Fluvial Form* (1999): 345-376.

Dunne, Thomas, et al. "Exchanges of sediment between the flood plain and channel of the Amazon River in Brazil." *Geological Society of America Bulletin*110.4 (1998): 450-467.

Dunne, T. and R. E. Aalto. “Large River Floodplains” in John F. Schroder (ed.) *Treatise on Geomorphology*, 9 (2013): 645-678.

Goodbred Jr, Steven L., and Steven A. Kuehl. "Floodplain processes in the Bengal Basin and the storage of Ganges–Brahmaputra river sediment: an accretion study u sing137Cs and 210Pb geochronology." *Sedimentary Geology* 121.3 (1998): 239-258.

Goodbred, S. L., and S. A. Kuehl. "The significance of large sediment supply, active tectonism, and eustasy on margin sequence development: Late Quaternary stratigraphy and evolution of the Ganges–Brahmaputra delta."*Sedimentary Geology* 133.3 (2000): 227-248.

Hardy, R. J., P. D. Bates, and M. G. Anderson. "Modelling suspended sediment deposition on a fluvial floodplain using a two-dimensional dynamic finite element model." *Journal of Hydrology* 229.3 (2000): 202-218.

Higgins, Roger J. "Off□river storages as sources and sinks for environmental contaminants." *Regulated Rivers: Research & Management* 5.5 (1990): 401-412.

James, C. S. "Sediment transfer to overbank sections." *Journal of Hydraulic Research* 23.5 (1985): 435-452.

Junk, Wolfgang J., Peter B. Bayley, and Richard E. Sparks. "The flood pulse concept in river-floodplain systems." *Canadian special publication of fisheries and aquatic sciences* 106.1 (1989): 110-127.

Kesel, Richard H., et al. "Lateral erosion and overbank deposition on the Mississippi River in Louisiana caused by 1973 flooding." *Geology* 2.9 (1974): 461-464.

Kesel, Richard H., Elaine G. Yodis, and David J. McCraw. "An approximation of the sediment budget of the lower Mississippi River prior to major human modification." *Earth Surface Processes and Landforms* 17.7 (1992): 711-722.

Kondolf, G. Mathias. "PROFILE: hungry water: effects of dams and gravel mining on river channels." *Environmental management* 21.4 (1997): 533-551.

Kondolf, G. Mathias, et al. "Process-based ecological river restoration: visualizing three-dimensional connectivity and dynamic vectors to recover lost linkages." *Ecology and Society* 11.2 (2006): 5.

Lauer, J., Gary Parker, and William E. Dietrich. "Response of the Strickland and Fly River confluence to postglacial sea level rise." *Journal of Geophysical Research: Earth Surface (2003–2012)* 113.F1 (2008).

Malmon, Daniel V., et al. "Influence of sediment storage on downstream delivery of contaminated sediment." *Water Resources Research* 41.5 (2005): W05008.

Mertes, Leal AK. "Documentation and significance of the perirheic zone on inundated floodplains." *Water Resources Research* 33.7 (1997): 1749-1762.

Middelkoop, Hans, and Nathalie EM Asselman. "Spatial variability of floodplain sedimentation at the event scale in the Rhine–Meuse delta, The Netherlands." *Earth Surface Processes and Landforms* 23.6 (1998): 561-573.

Moody, John A., and Brent M. Troutman. "Quantitative model of the growth of floodplains by vertical accretion." *Earth Surface Processes and Landforms* 25.2 (2000): 115-133.

Muto, Tetsuji, and John B. Swenson. "Large□scale fluvial grade as a nonequilibrium state in linked depositional systems: Theory and experiment." *Journal of Geophysical Research: Earth Surface (2003–2012)* 110.F3 (2005).

Nanson, G. C., and J. C. Croke. "A genetic classification of floodplains." *Geomorphology* 4.6 (1992): 459-486.

Nicholas, A. P., and D. E. Walling. "The significance of particle aggregation in the overbank deposition of suspended sediment on river floodplains." *Journal of Hydrology* 186.1 (1996): 275-293.

Nicholas, A. P., and D. E. Walling. "Modelling flood hydraulics and overbank deposition on river floodplains." *Earth Surface Processes and Landforms* 22.1 (1997): 59-77.

Paola, Chris. "Quantitative models of sedimentary basin filling." *Sedimentology* 47.s1 (2000): 121-178.

Pizzuto, James E. "Sediment diffusion during overbank flows." *Sedimentology*34.2 (1987): 301-317.

Rinklebe, Jörg, Christa Franke, and Heinz-Ulrich Neue. "Aggregation of floodplain soils based on classification principles to predict concentrations of nutrients and pollutants." *Geoderma* 141.3 (2007): 210-223.

Schumm, S. A. "River response to baselevel change: implications for sequence stratigraphy." *The Journal of Geology* (1993): 279-294.

Swanson, Kathleen M., et al. "Sediment load and floodplain deposition rates: Comparison of the Fly and Strickland rivers, Papua New Guinea." *Journal of Geophysical Research: Earth Surface (2003–2012)* 113.F1 (2008).

Thonon, Ivo. "Deposition of sediment and associated heavy metals on floodplains." *Nederlandse Geografische Studies/Netherlands Geographical Studies* 337 (2006).

Tockner, Klement, et al. "Hydrological connectivity, and the exchange of organic matter and nutrients in a dynamic river–floodplain system (Danube, Austria)." *Freshwater Biology* 41.3 (1999): 521-535.

Tompkins, Mark Robert. *Floodplain connectivity and river corridor complexity: implications for river restoration and planning for floodplain management*. University of California, Berkeley, 2006.

Walling, Des E. "Linking land use, erosion and sediment yields in river basins." *Man and River Systems*. Springer Netherlands, 1999. 223-240.

Walling, D. E., Q. He, and A. P. Nicholas. "Floodplains as suspended sediment sinks." *Floodplain processes* (1996): 399-440.

Walling, D. E., and Q. He. "The spatial variability of overbank sedimentation on river floodplains." *Geomorphology* 24.2 (1998): 209-223.

Figures

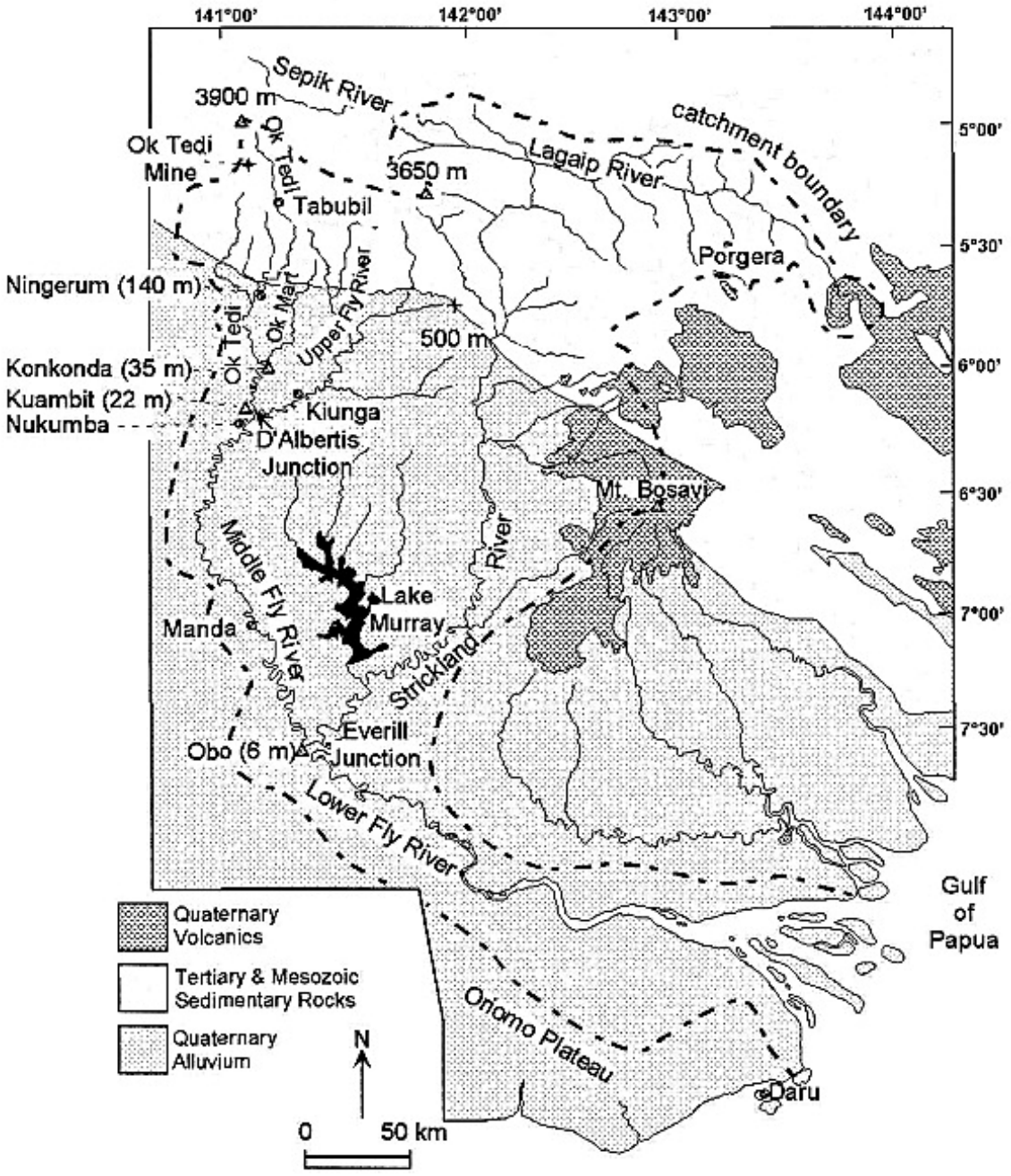


Figure 1.1 Map of the Fly River Inclusive of the Strickland River (from Day et al., 2008).

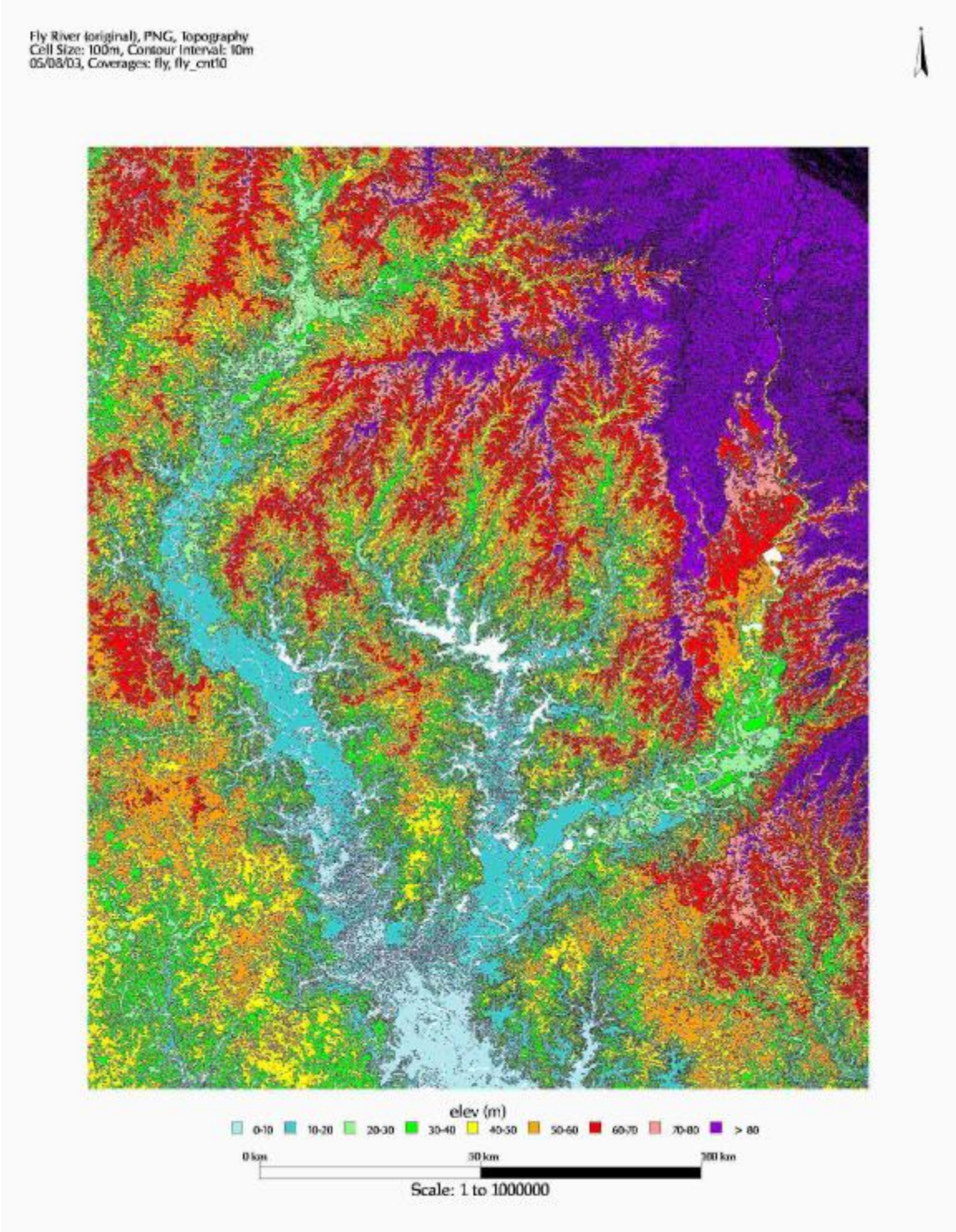


Figure 1.2 Digital elevation map (10-m contour) of the Fly and Strickland River basins from SRTM satellite data. Note the broad, low-slope channel belt of the Fly River and elevated channel-belt of the Strickland River floodplain.

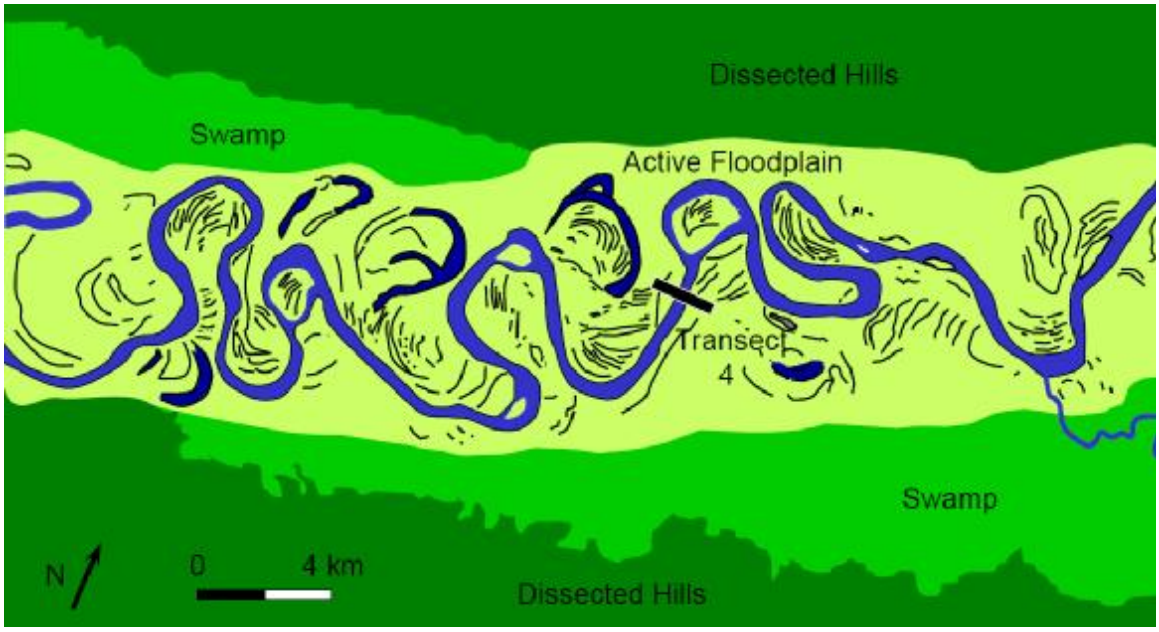


Figure 1.3. A detailed view of the Strickland River floodplain showing the elevated ridge, backswamp region, oxbows and scroll bars visible in satellite imagery. Also shown are transect 4 and the oxbow lake which has been breached and released floodwaters to the Mamboi drainage.

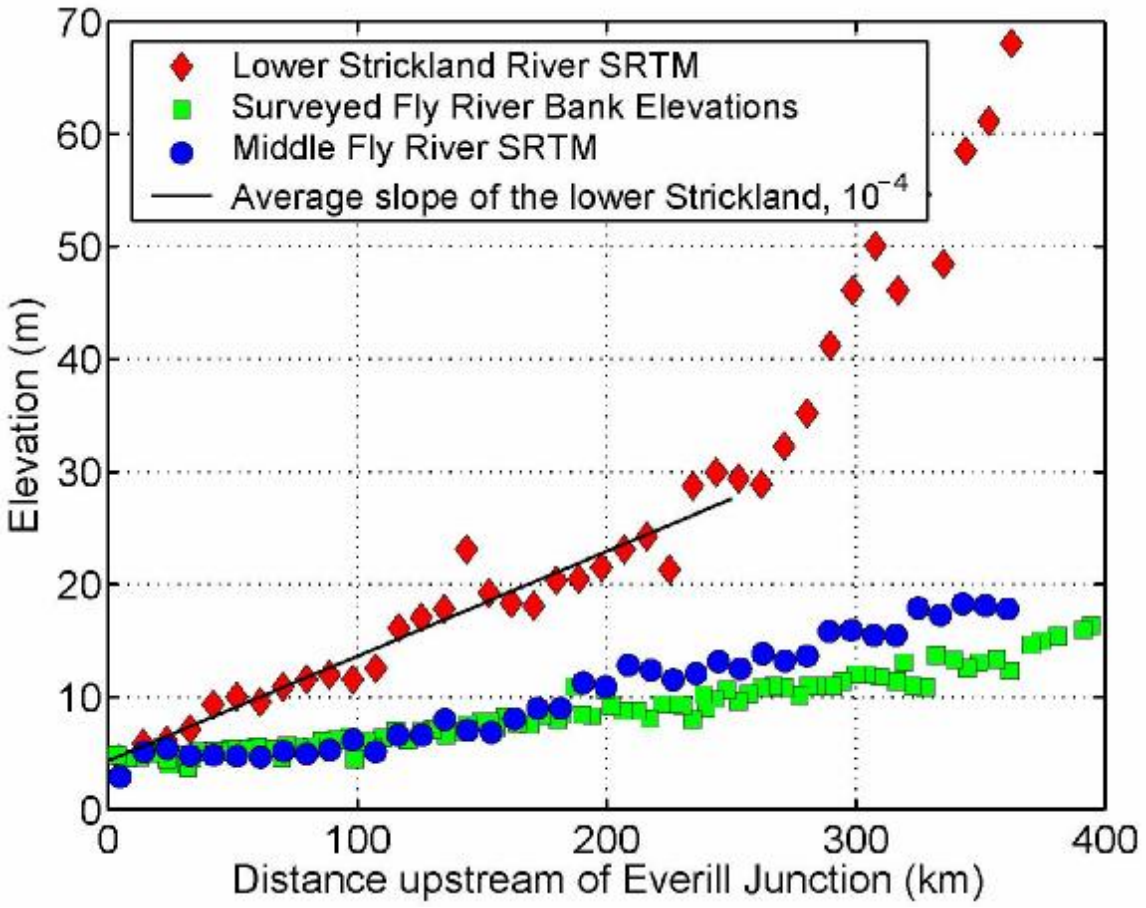


Figure 1.4 Longitudinal profiles of the Fly and Strickland Rivers derived from SRTM data. The Fly data are compared with a differential GPS survey on the Fly performed in 1995. This data agrees well with the 5-km averages of elevation along the Fly, derived from 90-m grid SRTM data. The Strickland data are also 5-km averages of elevation from 90-m grid SRTM data. The mean slope of the sand-bed reach of the Strickland, to 250-km upstream of Everill Junction, is 1 X 10^{-4}.

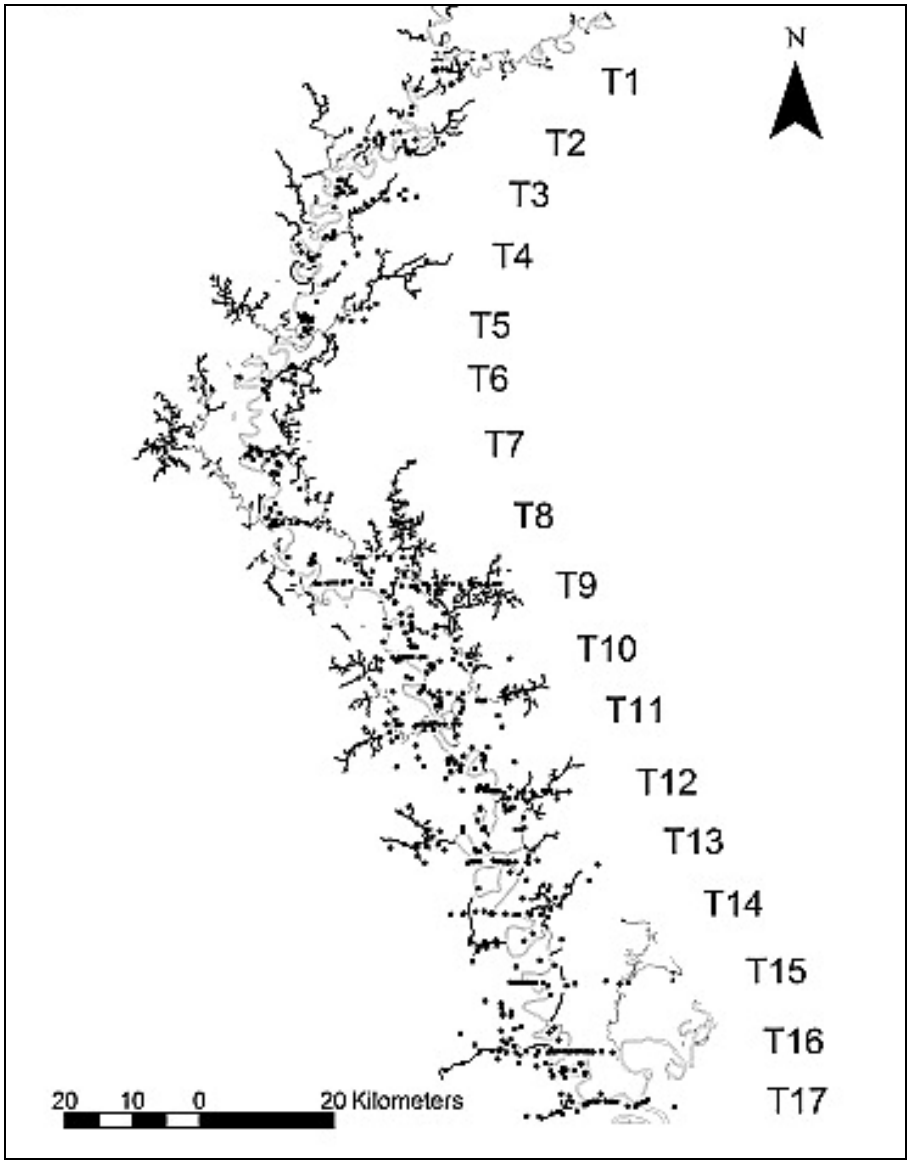


Figure 1.5 Extensive sediment core collection program established the pattern of floodplan deposition on the middle Fly River (from Day et al., 2008). Each dot represents a core location and the channel is shown in grey. Transect locations are numbered T1-T17 moving downstream.

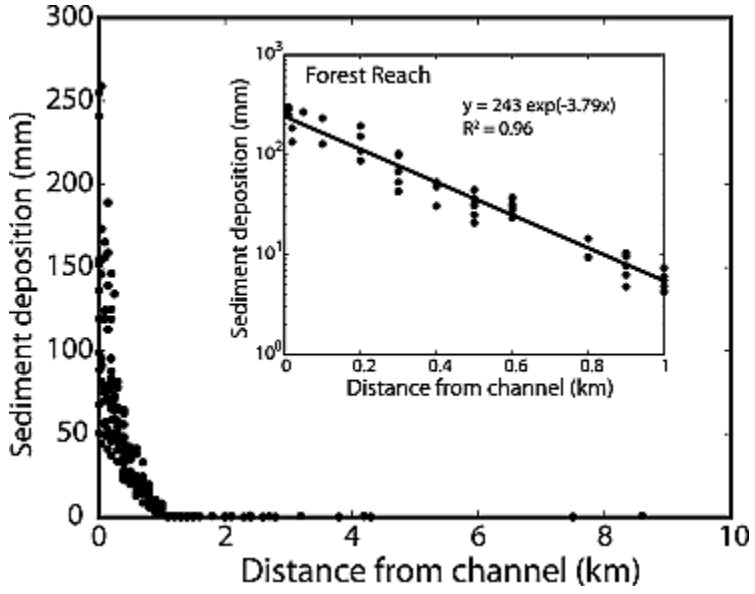


Figure 1.6 The calculated deposition rate for middle Fly River floodplain forested reach (from Day et al., 2008). The pattern varies exponentially as a function of distance from the nearest channel on all reaches but the magnitude varies between reaches.

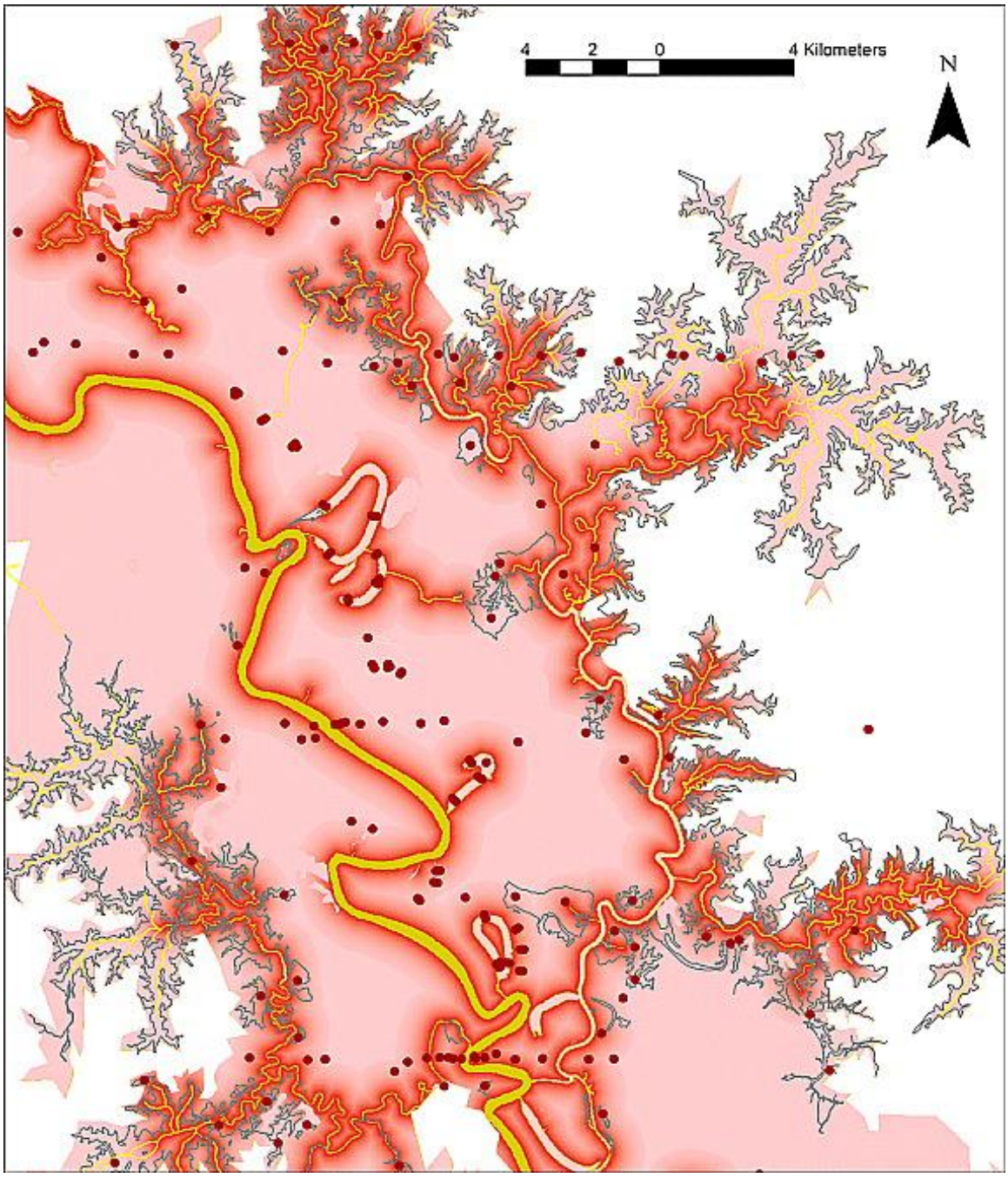


Figure 1.7 Depositional web on the Fly River floodplain (from Day et al., 2008). Dots indicate a core collection site. Red shading indicates the magnitude of deposition calculated from the distance to the nearest channel and the established deposition pattern.

Chapter 2

Sediment load and floodplain deposition rates: comparison of the Fly and Strickland Rivers, Papua New Guinea*

Abstract

Rates of aggradation and infilling of accommodation space along lowland channels in response to post-glacial sea-level rise should depend on sediment supply. The Strickland and Fly Rivers join at just 6 m above sea level, and have experienced the same Holocene sea-level rise. Historically, the Strickland has carried about seven times the sediment load and twice the water discharge as the Fly. Therefore, we hypothesize that the lowland Strickland floodplain should be more developed and, consequently, should presently be capturing proportionately less sediment than the floodplain of the lowland Fly River. We use mine-derived elevated Pb and Ag concentrations in 111 shallow (<1 m) floodplain cores collected in 2003 to determine deposition rates across the lower Strickland floodplain. Sediment deposition rates decrease across the floodplain with distance from the channel bank, and the average rate of deposition is 1.4 cm/yr over the first 1 km. Overbank deposition along the lowland sand-bedded Strickland results in ~13% loss of the total load, ~0.05%/km of channel length of the mainstem. Deposition rates over the first 1 km from the channel bank on the Strickland are about ten times those on the Fly (for estimated natural sediment loads), however, the proportional loss per channel length on the Strickland is less than that on the Fly (0.09%/km of mainstem channel length) due to an extensive network of tributary and tie channels that convey sediment to the floodplain on the Fly. Furthermore, the lateral migration of the Strickland channel is ~5 times that on the Fly, such that most overbank deposits on the Strickland are returned to the channel, causing the net loss of sediment to the floodplain to be small. We conclude that the Strickland River, which has a much higher overbank

* This work was first published as: Swanson, Kathleen M., et al. "Sediment load and floodplain deposition rates: Comparison of the Fly and Strickland rivers, Papua New Guinea." *Journal of Geophysical Research: Earth Surface (2003–2012)* 113.F1 (2008). It is reproduced here with the permission of the co-authors and the *American Geophysical Union*. Table 1 was improperly formatted in the original publication and has been corrected here. Color figures have been included where appropriate. Additionally, Appendix A, metal concentration data for each core, has been included.

deposition rate than the Fly River as a function of distance from channel bank, nonetheless has significantly less net accumulation than the Fly because: 1) a large proportion of the sediment load is conveyed up tributaries and tie channels on the Fly and, 2) lateral migration (which presumably results from the higher load) on the Strickland sweeps sediment back into the channel. Hence, our field observations support our initial hypothesis, though the primary reason for this is due to active lateral migration rather than low overbank deposition rates.

2.1. Introduction

All large lowland rivers entering the sea are in various states of response to post-glacial-maximum sea-level rise. The sediment accommodation space created by low sea-stand incision and then rapid sea-level rise tends to cause initially high net loss of sediment to the floodplain, but as the river rebuilds its slope and infills adjacent lowlands, the loss rate should decline (Muto and Swenson, 2005). The time scale over which a river shifts from significant net loss of sediment to primarily downstream sediment transfer should depend on the relative sediment supply and on rates of local subsidence and sea-level, or base-level, rise (Paola, 2000). This time scale is of fundamental significance to the offshore record because there is a time delay of sediment delivery to the marine environment. As the accommodation space infills, the depositional signal propagates through the fluvial system and could persist for more than 10,000 years (e.g., Pitman, 1978; Angevine, 1989). River morphology may also still be evolving in response to sea-level change (e.g., Aslan and Autin, 1999; Tornqvist, 1993; Latrubesse and Franzinelli, 2005).

The Fly River in Papua New Guinea provides an accessible fluvial system where the influence of sediment supply on river morphodynamics and net sediment storage response to rising base level may be studied. The middle Fly and lower Strickland Rivers join at Everill Junction, 400 km upstream of the delta front (all distances are streamwise unless otherwise noted, Figure 2.1). The Strickland drains twice the area and carries ~7 times the natural sediment load of the Fly River where they join. In this paper, we hypothesize that morphological differences between the rivers are the result of sediment-supply-driven differences in response to sea-level rise, and that the lower Strickland River, which is presumably more fully adjusted to modern sea level, should lose a much smaller proportion of its annual load to the floodplain than does the middle Fly.

Here, we briefly describe the morphologic differences between the Fly and Strickland channels and adjacent floodplains and then quantify a sediment deposition rate for ten years on the Strickland (1993-2003) using mine-derived tracers. These deposition rates are similar to those reported in a companion paper in which ^{210}Pb measurements provide timing of depositional events (Aalto et al., 2008). Our rates differ significantly from those reported by Day et al. (2008) for the middle Fly. Unexpectedly, we find that the average deposition rate for the first kilometer across the floodplain from the channel bank is much higher on the Strickland. High lateral migration rates (presumably due to the high sediment load) on the lower Strickland cause a relatively rapid return of this sediment to the channel, resulting in much lower net sediment deposition on the floodplain.

2.2. Study site

As shown in Figure 2.1, the Strickland and Fly Rivers drain the Southern Fold Mountains of Papua New Guinea, an area of rapid uplift (Pickup, 1984; Hill et al., 2002). They transport gravel down to broad lowlands, where the rivers transition to sand-dominated beds and a meandering channel planform across floodplains (<10 km wide) composed of elevated scroll-bar topography bordered by backswamps. Where the rivers join at Everill Junction (bankfull elevation ~6 m above sea-level), the median diameter of the Strickland River bed material is ~0.2 mm (Bera, 2005) and ~0.1 mm on the Fly (Dietrich et al., 1999). The lower Fly here is tidally influenced and flows to its delta, which terminates 400 km downstream. The Strickland drains 36,000 km^2, as compared to 18,400 km^2 for the Fly above Everill Junction. A greater proportion of the larger Strickland drainage is in the steep headwaters, and consequently, the sediment load is much greater than that delivered to the Fly. The natural load of the Fly is estimated to be just 10 million tonnes/year (Mt/yr), compared to 70-80 Mt/yr on the Strickland (Dietrich et al., 1999). Mean annual flow just above Everill Junction is 2244 m^3/s on the Fly and 3100 m^3/s on the Strickland (Dietrich et al., 1999). This difference is smaller than that of the drainage area because the headwaters of the Fly are exceptionally wet, often exceeding 10 m/yr of rainfall. The middle Fly channel length is ~420 km with another 70 km of river channel up the Ok Tedi to the gravel-sand transition. On the Strickland, the gravel-sand transition lies ~250 km upstream of Everill Junction. Hence, the potential sediment trap in the sand-bed reach is nearly twice as long on the Fly as on the Strickland. Surprisingly, despite the Fly system crossing a major region of tectonic activity, there is little evidence of significant uplift or subsidence in the reaches studied. On the Fly and Strickland, pre-Holocene terraces (with bright red sediment) occur at relatively low heights above the current floodplain. For more details about the geology, hydrology and geomorphology of the Fly system, see Dietrich et al. (1999).

The lower Strickland River is much steeper than the middle Fly River. Figure 2.2 shows estimates of channel longitudinal profiles for both systems from Shuttle Radar Topographic Mission (SRTM), provided by NASA. The middle Fly profile, which has also been surveyed using differential Global Positioning System (GPS), is concave up, dropping from 6.6×10^{-5} upstream to 1×10^{-5} at Everill Junction. The profile of the Strickland is much steeper, with the slope of the lower sand-bedded reach averaging 1×10^{-4}. Importantly, there are well-defined bars, commonly island bars, in the bends on the Strickland, whereas on the middle Fly there were no bars for the lower 170 km. On average, the Strickland shifts 5 m/yr laterally (Aalto et al., 2008), while the upper-middle Fly, prior to the introduction of mine waste, shifted ~1-2 m/yr. The lower-middle Fly showed no signs of lateral shift for over 50 years and lacked well-defined point bars (Dietrich et al., 1999). The common occurrence of oxbows and well-developed scroll bars along the lower-middle Fly led Dietrich et al. (1999) to propose that in relatively recent geologic time, this reach of river had become geomorphically inactive. Along the Fly, there are many tie channels (floodplain channels connecting the mainstem to off-river water-bodies (Blake and Ollier, 1971; Rowland et al., 2005), and tributary channels. In addition, a parallel channel system (the Agu River) cuts through uplifted sediment and drains the Fly for a considerable length before returning to it (see Day et al., 2008).

These channels are important dispersal pathways for sediment delivery to the floodplain. Day et al. (2008) report over 900 km of channels that convey sediment across the floodplain. Such channels are noticeably fewer on the Strickland.

One of the more striking features of the Strickland is the Holocene scroll-bar complex that forms an elevated ridge ~6 km wide surrounded by swamps across the floodplain. This feature is evident in elevation SRTM data shown in Figure 2.3, though it is possible that the ridge is accentuated in this data due to the tendency of trees to grow on the elevated, better-drained scroll-bar complex. A detailed view of the floodplain ridge and scroll-bar complex is shown in Figure 2.4. During 1998 and 2000 floods, flow spilled from the Strickland through an oxbow lake towards the north and traveled west along a tributary channel, the Mamboi River, into Lake Murray (Figures 2.1 and 2.4), and has remained an intermittent connection since that time (Porgera Joint Venture, 2003). The resulting extensive area of cutting and deposition associated with this process may foreshadow an eventual avulsion.

2.3. Determination of floodplain sediment deposition rate using anthropogenic tracers

In 1991, tailings and rock waste from the Porgera gold mine located in the headwaters of the Strickland began entering the system, introducing sediment with a variety of elevated metal concentrations (Apte, 2001). Silver and lead, the chosen tracers for this study, are ideal because of their post-depositional stability (Apte, 1995, 1996; Watson, 2006) and their presence at significantly elevated concentrations in mine-derived sediments discharged to the river system (Apte, 1995). Particulate Pb and Ag strongly covary both in suspended and floodplain sediments (Watson, 2006); hence measuring both elements serves as a data quality check. On the Strickland, Pb and Ag concentrations are only weakly influenced by the relative amount of organic matter in the sample, and grain size has a minor influence (Watson, 2006). The mine-derived tailings are mostly silt and clay (<63 μm), and the strongest Pb-Ag relationship was found in sizes <63μm. Only this size fraction was analyzed as a tracer in this study. There may be a tendency for samples rich in clay to be characterized by higher tracer concentrations, but our data cannot presently address this relationship of grain size and concentration. Suspended-sediment monitoring shows that near the mine, the suspended load is dominated by the mine waste (suspended load decreases with increasing discharge), but this effect ends with increasing discharge and drainage area downstream (Figure 2.5). A downstream decrease in trace-metal concentrations occurs due to dilution by uncontaminated sediments from tributaries and to sediment exchange with the bed and banks. Various estimates have been made of the mine-derived component of the sediment load down the Strickland. Using tracer techniques, Apte (2001) reports a value of 10-11% as of 2000 at SG 4 (Figure 2.1). Markham (personal communication, 2006) calculated a sediment budget for the river system and concluded that the mine-derived component at SG 4 progressively increased from 1991 to 1998, and since then has averaged ~15% of the suspended-sediment load. Further exchange and net deposition would make the mine-derived component even less

by the time the Strickland joins the Fly. This small contribution is in sharp contrast to the middle Fly, where sediment load has been elevated by ~4.6 times the natural load due to mining discharges (Day et al., 2008).

The period of significant mine operation is fairly short (ten years at the time of sample collection in 2003) and tailings discharge has varied with time. The mass of tailings discharged to the river increased progressively from 1992 to 1998 (Figure 2.6a). The concentration of Pb in the suspended sediment just 8 km downstream from the mine (SG1- Figure 2.1) increased during this time frame as well, but a very large spike occurred (due to lack of natural sediment dilution) during the 1997 – 1998 drought to flood cycle associated with a strong El Niño event (Figure 2.6b**)**. Figure 2.6c shows the mean daily flow at a gauging station (SG3) ~220 km above our upstream-most floodplain sampling location. Though located in the upper catchment, these data show the severe drought of 1997 and suggest the largest two flood events for the ten-year period ending in 2003 occurred in 1994 and 1998.

2.3.1 Sampling strategy and analysis

Two sampling campaigns were conducted on the Strickland floodplain to detect the spatial extent of mine-derived tracer accumulation across the Strickland floodplain. In 1997 (4 years after the commencement of significant discharge of mine tailings to the river, Figure 2.6a), five transects across the floodplain from near the gravel-sand transition (~410 km below the mine) to ~15 km upstream of Everill Junction (and 670 km below the mine) were sampled (Day et al., 1998). These transects, numbered 1-5, are shown in Figure 2.7. Pits were dug at distances of 0, 50, 100, 250, 500 and 1000 km from each bank, and a 1-cm slice was taken at the surface and at 29-30 cm below the surface. The floodplain was dry at the time and access was entirely via helicopter. For consistency in this survey, relatively straight sections were selected for each transect. Suspended load and bed-material samples were also collected, although river stage was particularly low when the samples were taken.

In 2003, the same transects were sampled in addition to 5 transects across actively shifting bends (Figure 2.7). Based on work investigating the Beni River in Bolivia (Aalto et al., 2003), it was anticipated that deposition rates would be higher if there was significant flow across the bends and out of the outer banks, particularly on the down-valley side of an actively migrating bend. In this report, data from three transects in bends, numbered transects 10, 13 and 15, are reported. Seven drop-cores were also collected from the deltaic front of a tie channel entering an oxbow and extending along a transect to its distal end, 3 km into the lake. Cores were collected along the shore of this oxbow as well, numbered transect 12 (Figure 2.7). Sampling was severely constrained by standing water remaining on the floodplain after a flood event that preceded our arrival and by a temporarily low river stage. Our access boat could only travel ~100 km upstream of Everill Junction. Sampling above this point was accomplished using small boats, canoe, or helicopter. On the floodplain it was difficult to travel farther than 500 m

from any bank without encountering deep standing water. Where possible, we sampled the transects at 5, 50, 100, 250, 350 and 500 m from each bank. Helicopter access was provided for a few days and distal cores (~1000 m) were collected on transects 1-5 for comparison to the 1997 study. To document whether Strickland sediment is currently spilling into Lake Murray via the Mamboi River (Figure 2.7), we used small boats to collect 27 cores along banks of the Mamboi and in Lake Murray.

At sample locations other than those sampled via helicopter, three separate cores were collected. A push core with a 2.5-cm-diameter, one-meter-long Polyethylene liner was used to collect most of our cores. Penetration was rarely the full 100-cm length, and the longer of the two cores was selected for ^{210}Pb analysis. Finally, a 5-cm-diameter hand PVC core liner was forced into the surface to ~10-cm depth and 1-cm slices were sub-sectioned from the cores and bagged in the field for shallow Pb and Ag analysis. At the helicopter sites, which were usually inundated, a single core was collected using a 5-cm gravity corer dropped from the hovering helicopter and retrieved with a rope. A total of 144 push cores for Pb and Ag analysis ~1-m in length, 197 push cores for ^{210}Pb analysis, and 97 hand cores were collected.

In order to characterize the bank and floodplain topography, each of the transects was surveyed (where access was not impeded by standing water) with a self-leveling transit. The coordinates for each core location were also recorded. Channel-depth measurements were made with a sonar scanner.

2.3.2 Sediment analysis

Chemical analyses were conducted at the Center for Environmental Contaminants Research of CSIRO Land and Water, Sydney, Australia, where well-developed analytical procedures were already in place. Cores were initially sectioned into 1-cm samples at 0-1, 1-2 and 29-30 cm depths. Then additional subsamples were analyzed to increase the resolution of data, so as to document vertical variation in deposition rate. In total, over 800 core sections were analyzed.

As noted above, only the fraction of the sediment that is <63 μm was analyzed for this study in order to better isolate the mine-derived signal. The <63-μm sediment fractions were isolated by wet sieving, dried and subjected to microwave-assisted digestion in a mixture of concentrated HCl and HNO_3. Metal concentrations in the resulting digest solutions were then determined using a combination of inductively coupled argon plasma emission spectrometry (ICP-AES), inductively coupled plasma mass spectrometry (ICP-MS) and graphite furnace atomic absorption spectrometry (GF-AAS). Further details can be found in the work by Day (1998) and Watson (2006). For quality-assurance purposes, one standard reference sample (PACS-2, National Research Council, Canada) and one blank were included in each analytical batch.

The organic carbon (OC) content was estimated for each sample through loss on ignition. Though OC% in each sample was generally small (~9%). The concentration of metals measured by the ICP-AES and GF-ASS was corrected to discount the average mass of organic material in the sample so as not to under-estimate trace-metal concentrations.

2.3.3 Determination of deposition rates

We used two different approaches to calculate sediment deposition rates from the Pb and Ag core profiles. In both approaches we assumed that by the time the mine-derived sediment reaches the Strickland floodplain system, it is well mixed with the natural load and has the same physical characteristics and behavior as natural sediment when it disperses across the floodplain.

The first method (inventory approach) assumes that the concentration of the tracers transported to the spot of deposition is a temporal and spatial constant. An integrated concentration (i.e., inventory) of the tracer is then measured through the core, and a deposition rate is calculated from the total amount of mine-derived sediment (for details see Day et al. (2008)). Deviations at depth from the incoming tracer concentration are assumed to be due to mixing of mine-derived sediment with background floodplain sediment (i.e., through bioturbation and physical mixing processes), which may cause dilution of the signal and deeper penetration of mine-derived tracers than would occur by burial alone. The effective depth of sedimentation, L_c, is calculated by determining the proportion of each core interval that is composed of sediment with a set incoming trace-metal concentration, $e_{ci,}$ and a typical bulk density of contaminated surface sediment, r_c. This calculation is done for each interval depth (i) between successive subsamples and summed to get the equivalent depth of sedimentation with elevated mine-derived particles as shown in equation 2.1:

$$L_c = \sum_{i=1}^{n} \frac{z_i \cdot r_b(\overline{e_{s_i}} - e_b)}{r_c(e_{c_i} - \overline{e_{s_i}}) - r_b(e_b - \overline{e_{s_i}})}. \qquad (2.1)$$

Here r_b is the bulk density of uncontaminated sediments, $\overline{e_{s_i}}$, is the average, or measured, metal concentration for the interval length z_i, and e_b is the background metal concentration. To apply (1), estimates must be made of incoming metal concentrations, e_{ci}, which as indicated by subscript, i, could vary with time and therefore depth. We also need to estimate the background concentration, e_b, and directly measure the other properties. Measured trace-metal concentrations above the calculated incoming concentrations are assumed to be unmixed and the entire interval length is included in the equivalent depth of sedimentation.

The other method used here (the depth-of-occurrence approach) assumes that the deposition rate is high enough and the depositional period short enough that bioturbation

is ineffective, and that vertical variation in mine-derived Pb and Ag is due to variations in the concentration of tracer being delivered. In this second case we assume that the first occurrence of any elevated concentration of Pb or Ag relative to background defines the arrival of mine-derived sediment. This depth-of-occurrence directly translates to a rate for the time since the commencement of mining. Because the metal concentration of each core is defined by a series of discrete subsamples that may not capture the exact depth at which this occurs, the depth of first occurrence is linearly interpolated based on the respective depths and concentrations of adjacent subsamples. As in the inventory case, a background concentration has to be assigned.

Both methods also include a density correction. Reported sediment deposition rates are for sediments with a bulk density of 1.5 g/cm^3 (Aalto et al., 2008). Once the sediment deposition rate was calculated for each core, we then explored the spatial pattern of deposition to determine how to obtain the total flux of overbank sediment.

2.3.4 Derivation of background and mine-contaminated sediment concentrations

Data from suspended material and floodplain sediment analyses were used to determine both background and incoming concentrations. First, the upper limit of trace-metal concentrations was determined for suspended-sediment samples from Strickland River tributaries not influenced by mining (32 μg/g Pb, 0.32 μg/g Ag, as reported in Apte (2001). To quantify the background metal concentrations, we reviewed 111 cores to determine the depth of first occurrence for concentrations greater than any measured in the tributaries. A histogram of Pb and Ag concentrations in the samples taken below this first occurrence was then plotted (198 samples in total, Figure 2.8). The Pb values were approximately normally distributed with a median value of 16 μg/g, and 95% of the subsamples contained 25 μg/g Pb or less. The 80th percentile value for Pb was 22 μg/g. The Ag values were skewed towards the smaller concentrations with a median value of 0.07 μg/g, a 95th percentile value of 0.16 μg/g, and a distinct break at the 80th percentile of 0.1 μg/g. Based on this analysis, we used 25 μg/g Pb and 0.16 μg/g Ag with the understanding that 22 μg/g Pb and 0.1 μg/g Ag represent more conservative alternatives. The deposition rate was determined for both methods described below using both the 95th percentile and 80th percentile background values. Lead and silver concentrations were closely correlated in floodplain sediments (r=0.85, n=706). For the sake of brevity, we will primarily discuss the results for the analysis of Pb with a background value of 25 μg/g.

The concentrations of the first two subsamples from each core, 0-1 and 1-2 cm respectively, where there was a distinct variation above the background values for both Pb and Ag were plotted to determine the incoming trace-metal concentrations (n=109). These data were normally distributed and had mean values of 49 μg/g Pb and 0.5 μg/g Ag, respectively (Figure 2.9). These values are in agreement with the measured concentrations of what appeared to be very young deposits in the field and with

concentrations measured in suspension during the falling limb of the 2003 flood (60 μg/g during a discharge of about 3100 m^3/s).

2.4. Deposition patterns on the Strickland River floodplain

2.4.1 Deposition of mine-derived sediment on the floodplain

Figure 2.10 shows examples of cross-stream variation in surface and 30 cm depth Pb concentrations at transect 5 for the 1997 and 2003 survey, 4 and 10 years, respectively, after significant volumes of mine-derived sediment entered the Strickland (Figure 2.6a). These data clearly reveal the overbank deposition of mine-derived sediment, with initial deposition closer to the channel, followed by a widening of the active depositional area and significant elevation of Pb concentrations in the surface sediments in 2003. As shown in Figure 2.6a, tailings loading reached full-mine operation level in 1998. So, the large change is in keeping with this increased loading, and with the spike in Pb concentrations that occurred during 1997 and for a period thereafter. Note that all measured concentrations at 29-30 cm were below background in 1997, but were elevated above background near the channel on both banks by 2003.

2.4.2 Profile analysis

Core profiles generally showed a consistent trend of Pb and Ag accumulation in surficial sediments. A complete record of the deposition rate calculated for each sediment core using mine tracers is provided in appendix A. In this section, Transect 5 is discussed in detail in order to illustrate some key observations. Figure 2.11 shows the cross-sectional topography and corresponding Pb concentration profiles for 11 cores taken across the floodplain. As seen in Figure 2.12 (a satellite image of the location), Transect 5 is at the downstream portion of the bend, which is cutting into a floodplain composed of oxbows, channel traces and scroll bars. Analysis of satellite photographs indicates that the channel here shifted ~225 m toward the right bank (looking downstream) between 1972 and 2000, hence the left bank is composed of recently deposited sediments whereas the higher right bank is composed of older deposits capped with recent overbank sediments. This transect is in the gravel-sand transition area, with gravel present on the bed and bars, but not on the floodplain.

Transect 5 has several features common to others collected throughout the floodplain. The deeper, clearly uncontaminated sediments indicate that background values of Pb (and Ag) vary greatly, and in this transect, Pb concentrations as low as 9 and as high as mid-20's (μg/g) are measured in what are viewed as pre-mine or background sediments. The Pb concentrations generally increase towards the surface, but only in one case (150 m right side) is the increase abrupt relative to background values. Although this might be evidence of bioturbation generally smoothing abrupt changes, it is also the case that the suspended load of Pb-rich mine-derived sediment increased gradually for the first several years (see Figure 2.6b). Hence, the gradual shift may simply reflect this change. The

profiles, when sampled intensively, unexpectedly reveal considerable vertical variation, and there are distinct subsurface concentration maxima. The right bank 150-m core has a spike (153 μg/g Pb, the highest recorded in any floodplain core) at 35-36 cm below the surface. On the left bank, the spike is at 3-4 cm below the surface (at 5, 150, and 250 m from the bank), and the measured concentrations are smaller. We suggest the vertical variation in Pb and the spike record the temporally variable and stage-dependent metal concentration in the suspended load (see Watson (2006), for more discussion). Although on an annual basis the mine load is ~15% of the total load at SG 4 (360 km from the mine), during periods of low flow and periods of drought, the proportion of the sediment that is derived from the mine can increase considerably. Conversely, during floods, the large introduction of natural sediments dilutes the concentrations of mine-derived tracers to low values. The spike in concentration may record the first flush of sediment after the 1997 drought (Watson, 2006), with the higher proportion of mine-derived sediment in this material causing a significant increase in metal concentrations in the floodplain sediment. Continued overbank flow, and subsequent flood events with increased natural sediment loads would then reduce the Pb and Ag concentrations. This may be the case in three cores where the concentrations in the first 1 cm approach background levels (5 m left, 50 m and 150 m right).

The cores reveal deposition patterns across the floodplain that are consistent with the position of the transect in a bend and with local topographic effects. In Figure 2.11, we have labeled each profile with the depth where we infer mine-related sedimentation began, given a background concentration of 25 μg/g. The deposition rate is then calculated by correcting for density variation and dividing by ten years. On the right cut-bank side of the bend, overbank deposition rates were 3.5-6 cm/yr out to 150 m. Further coring across the floodplain was not possible because of deep standing water and time constraints (access to distal cores was entirely by helicopter). We calculated a deposition rate of ~1.0 cm/yr for a core collected by helicopter >1 km from the right bank, where it is crossed by the transect. This site, however, was ~800 m from the nearest bank upstream. On the left bank side 5 and 50 m from the bank, the cores are contaminated through their entire depth (60 and 73 cm, respectively). These deposits probably record rapid vertical accretion on the advancing point bar. Hence, the strong vertical variation probably records stage-dependent Pb concentration in the suspended load. Farther across the floodplain, the deposition rate drops to 1.2-1.3 cm/yr until the 1000-m core is reached, where the net deposition rate increases to 1.8 cm/yr. We note that this site is closer to the outer bank of an upstream bend (~500 m from the bank) and suggest that the increase in sediment accumulation rate records the influence of this upstream bend. This finding caused us to correct all distances relative to the nearest bank rather than along a particular transect.

To estimate the sediment deposition rate from the inventory method at transect 5 and subsequent transects, we apply equation (2.1) assuming the background values for Pb of 25 μg/g and Ag of 0.16 μg/g in the higher case, and 22 and 0.1 μg/g in the lower case. Incoming concentrations at flood stages have not been monitored, and as suggested by

the analysis of transect 5, the concentrations will be highly variable. We did not attempt to estimate the temporal record of c_{ci}, given the likelihood that incoming concentrations are highly variable with both seasonal and stage effects, which would be extremely difficult to measure and predict. This method provides a lower estimate for the average deposition rate, about half that indicated by the depth-of-occurrence method, but mirrors the spatial patterns. For transect 5, the calculated deposition rates for 25 μg/g Pb background concentration on the right cut bank has a range of 1.4-3.1cm/yr in the near-channel cores with the distal core recording 0.4 cm/yr. The corresponding rates on the left bank are >3.5 and 5 cm/yr at 5 and 50 m from the channel, respectively, dropping below 0.7 cm/yr at 250 m from the channel and increasing to 1.0 cm/yr in the distal core.

2.4.3 Calculated deposition rates

Table 2.1 summarizes the sediment deposition rate for each core site across all transects sampled, and Figure 2.13a shows the deposition rate for each core as a function of distance from the nearest channel bank. It should be noted that vertically adjacent core subsamples from which the linear interpolation of the depth-of-occurrence is calculated are more than a 10 cm apart for 21 of the cores sampled. Of the 111 cores analyzed in this study, 28 were contaminated throughout their depth (hence we have only a minimum deposition rate) and 9 showed no evidence for deposition of mine-derived sediment. For the remaining 74 cores, the depth of first mine sediment occurrence was linearly interpolated between two values separated by an average core length of 10.4 cm with a standard deviation of 10.4 cm. Through this 10-cm depth interval, Pb concentration gradients averaged 5.5 μg/g-cm with a standard deviation of 7.1 μg/g-cm. With the linear interpolation procedure, the estimated depth of first mine-derived sediment would decrease with increasing metal concentration in the upper layers. Thus, our deposition rates depend to some degree on the incoming metal concentrations, which vary spatially and temporally across the floodplain.

As shown in Table 2.1, the average deposition rate for each side of the channel, calculated as the numeric integral of sediment deposition rate as a function of distance from the channel divided by transect width, varies from 0.04 cm/yr (on the right bank of transect 4) to 4.85 cm/yr (right bank of transect 10). The average deposition rate per channel distance decreases from nearly 5 cm/yr near the bank to 0.35 cm/yr 1450-2000 m from the channel. Figure 2.13a separates cores from straight sections, with relatively slowly shifting banks (transects 1-4) from cores in bends (transects 5, 10, 13, and 15), and from a core collected on the banks of an oxbow (transect 12).

Several patterns emerge. Deposition rate generally decreases with distance from the bank, but local values are highly variable. An exponential function is commonly applied to floodplain sedimentation data (e.g., Tornqvist and Bridge, 2002; Walling and He, 1998; Day et al., 2008). Figure 2.13b shows that the data generally follow an exponential decline, but near the bank the rate of decline is systematically higher than predicted by the function. Several of the near-bank cores may record the effects of lateral shifting and

rapid vertical accretion on newly emergent bars. Farther out, overbank deposition was the dominant process. This change in process may explain the shift in deposition rate with distance, which is apparent in the data.

On a given transect, deposition generally differed between the left and right banks. Although picked for their generally straight reaches, none of the five transects established in 1997 were in perfectly straight channels. Transects 1, 2, 4 and 5 show curvature and in each case the bank and the adjacent floodplain for a few 100 m was higher on the outer bank. Transect 3 is centered in a relatively straight reach between two bends in which the channel width progressively increases downstream. In all cases, the sediment deposition rate was higher on the bank with the higher floodplain elevation, suggesting that the higher rate was associated with stronger overbank flows due to bank curvature.

As expected, the more strongly curved transects (5, 10, 13 and 15) had higher overbank deposition rates (over the comparatively short distances from the channel that were measured). The reach with the least floodplain sediment deposition was transect 4. Comparison of 2000 and 1972 satellite imagery reveals this section to be the most stable of all the transects, showing no visible shifting. Transect 12 samples were collected on the banks of an oxbow rather than normal to the bank of the active channel. To compute deposition as a function of distance we measured the distance to the nearest bank of the Strickland mainstem. Sediment deposition was low along the entire transect, ranging from 0.1-0.4 cm/yr.

2.4.4 Floodplain sediment deposition rate

There are several approaches that could be used to estimate total floodplain deposition of sediment (M, tonnes/ year). One would be take the average rate (in cm/yr), D_a of all cores, multiply that times the active area (A) of deposition on both sides of the channel, and apply an appropriate average bulk density (ρ_s), i.e.:

$$M = \rho_s D_a A. \qquad (2.2)$$

Our samples, however, are strongly biased towards areas near the bank (due to access difficulties). Instead, we estimated a distance-dependent deposition function for the entire data set and integrated that function across the floodplain. Sparsely sampled regions as defined by distance from channel were grouped with adjacent samples to reduce the bias toward individual samples, as demonstrated in Table 2.1. Figure 2.13a shows that deposition rates are similar for straight and curved reaches very close to the channel, because of high deposition rates associated with relatively minor channel shifting. Sediment deposition rates remain high farther from the channel banks on reaches with sharp channel curvature than on straight reaches. Inspection of the maps of the Strickland (Figure 2.7**)** suggests that the proportion of bank length in bends and straight sections is roughly equal, so we will treat the deposition data as a single data set. An exponential fit to data binned by distance from the channel (Table 2.2) systematically

under estimates the high rates of deposition near the channel bank (Figure 2.13b). Rather than impose a function on these data, we numerically integrated the data and divided by the active deposition width to get a mean deposition rate (cm/yr). We then assigned this average rate to D_a in (2.2), with the associated channel area.

The distances over which equation (2.2) can be applied were limited to the region where the pattern of deposition was well defined. There are only 4 data points beyond 1 km from the channel bank, and two of these points show very low values (0 and 0.1 cm/yr). Hence, the deposition rate is not well constrained farther out, though the rate there is distinctly lower than near bank values. Furthermore, because of channel sinuosity, projection of deposition rate beyond 1 to 1.5 km for the width, w, is problematic because there is significant overlap of bank-normal projections. On the Strickland, the actual area of the floodplain bordering 1 km either side of the 267-km study reach is 455 km^2, and for 1.5 km out it is 597 km^2 (compared to the estimated total floodplain area of 1165 km^2, with channel surface area deleted from the total). If we estimate the average deposition beyond 1-km and apply it to the total floodplain area, we will ultimately underestimate the total loss to deposition, because the area increases by only 30% when the active depositional width increases by 50%. For these reasons, we estimate the deposition based on a 1 km width. The use of 1 km is more conservative and makes the width identical to that used on the Fly River, to which we wish to make comparisons (Day et al., 2008). We also use the GIS determined area of 455 km^2 for the Strickland floodplain.

Our upstream-most sample location (267 km from Everill Junction), transect 5, is in a gravel-bedded reach that progressively steepens upslope. Based on satellite imagery, floodplain borders the channel for another 49 km upstream, but in this reach the channel shifts more slowly (Aalto et al., 2008), and the discharge is flashier than in the lower Strickland. It seems possible that rates and patterns of overbank deposition may change significantly up the canyon. In order to compare with the sand-bedded Fly rates, it is perhaps most appropriate to use the 267 km length of sand-bedded channel below transect 5 when calculating A in equation (2.2). However, for consistency with the deposition rates presented by Aalto et al. (2008) who perform their analysis for the ~318 km of sinuous single thread lowland Strickland, we also report results for a 318-km lowland channel length. Aalto et al. (2008) calculate channel area, A, as channel length times the 1-km active width of deposition on either side of the channel ($A = 636$ km^2), and acknowledge that this leads to an ~10% overestimate of the total area because of overlapping bank-normal projections. For consistency with their results, we use $A = 636$ km^2 when calculating the floodplain losses for the longer channel length.

Table 2.2 summarizes the 1-km average sediment deposition rate (corrected to a bulk density of 1.5 g/cm^3), D_a in equation (2.2), for both the inventory and depth-of-occurrence methods employing different assumptions about background and incoming Pb and Ag levels. We also report the total annual mass deposited overbank (M in equation 2.2) and its proportion of the total sediment load (estimated to be 70 Mt/yr). The

inventory method yields smaller values because this method assumes that values between background and estimated incoming concentration represent dilution by bioturbation with uncontaminated sediments. These rates define the lowest probable deposition rate. The highest rate was associated with the lowest estimated background Pb and Ag concentrations using the depth-of-occurrence method. This sediment deposition rate is probably too high, as deep cores, clearly not contaminated, at transect 12 were counted as contaminated throughout their entire length because the uniformly low Pb concentrations were slightly above the assigned background concentration.

Our best estimate, based on the depth-of-occurrence method is that the mean sediment deposition rate across the floodplain to 1 km from the channel bank is 1.4 cm/yr or 9.2 Mt/y for the sand-bedded river length of 267 km or 13 Mt/y for 318 km of active lowland channel. These deposition rates equal 13 and 19% of the estimated mean annual load of 70 Mt/yr. These rates normalized by channel length are 0.05 %/km and 0.06 %/km, respectively.

Two other depositional processes are not accounted for in this analysis. One oxbow connected via a tie channel was sampled and high rates of sediment accumulation were measured there. All core samples to a depth of 40 cm (bottom of core) were contaminated out to a distance of 0.5 km. Elevated metal concentrations were found to depths of 7 cm over 3 km from the tie channel inlet. There are many partially filled oxbows on the Strickland (Figure 2.4) but not many tie channels (that we have been able to detect). There are as many as 7 oxbow lakes that have maintained a connection to the main stem of the river, but not all of these are connected via a developed tie channel. The sediment deposition into the oxbows is estimated to be a small part of the total budget because of the lack of well-developed tie channel connections. The other depositional process occurs where the Strickland spills out of its banks and flows into the Mamboi River (Figure 24). This breakout occurs via a breached oxbow, which is partially infilled. In 1998, several square kilometers of floodplain received large quantities of sediment, but the overflowing currents also scoured the floodplain surface. A large amount of sediment partially filled the breached oxbow. Core samples along the length of the Mamboi and into Lake Murray (Figure 2.7) and suspended-load measurements along the Mamboi revealed that mine-derived sediment was present through the entire system, with suspended-sediment Pb concentrations of 36-97 μg/g. Because the outflow is only intermittent, however, we estimate that the loss of sediment to the floodplain had been relatively minor compared to the total load at the time of our fieldwork in 2003.

2.5. Discussion

Morphologic and deposition rate differences between the Fly and Strickland Rivers support the hypothesis that the higher sediment load on the Strickland has resulted in a greater infilling of accommodation space and a smaller proportion of its sediment load currently being deposited on the floodplain. The morphologic differences are profound. The Strickland is much steeper, has a coarser bed and large sandy point bars (often

broken into island bars), and erodes its banks at a much greater pace. There are fewer tie channels connecting to oxbows and blocked valley lakes. We suggest all these features are signatures of chronic high sediment load. Although we have not quantified the Holocene sediment discharge to the lower Strickland, there is no evidence of major stream capture at this time, or of large climatic shifts. Hence, the elevated load on the Strickland, derived from headwater channels cutting deep canyons into rapidly uplifting lands, has most likely occurred throughout this period. Radiocarbon dates in cores up to 15 m deep obtained along the middle Fly and lower Strickland demonstrate that aggradation kept pace with sea-level rise, even during early post-glacial rapid rise (Chappell and Dietrich, 2003). Lauer et al. (2008) infer through modeling that the sediment load on the Strickland was much higher than the Fly over this period. The Fly, on the other hand, did experience an early Holocene pulse of sediment due to a 7 km^3 landslide in its headwaters 8800 years before present (Blong, 1991). Much of that sediment remains in the headwaters, but initial erosion of the deposit may have contributed to the Fly River keeping pace with the rapid sea-level rise then and not becoming an inland estuary.

Differences in morphology associated with sustained differences in sediment load on rivers responding to sea-level rise are seen on other rivers, notably the Rio Negro and the Solimoes-Amazon River. Dunne et al. (1998) describe the morphologic diversity and dynamics of the Amazon, emphasizing that sediment exchanges between the floodplain and the channel exceed the 1200 Mt/yr annual load. There are extended reaches with large bars, rapid lateral channel shifting, and extensive floodplain deposition. In contrast, the Rio Negro, which drains 27% of the Amazon basin where they join, discharges only 8 Mt/yr to the Amazon (Latrubesse and Franzinelli, 2005). The lower 300 km of the Rio Negro consists of a system of islands, lakes and channels dominated by backwater effects of the Amazon. Latrubesse and Franzinelli (2005) argue that the Rio Negro progressively responded to Quaternary climate change and sea-level rise, but that the lower reach of the river did not have sufficient sediment load to keep pace with post glacial sea-level rise on the Amazon. Consequently, the mainstem Amazon response to sea-level is driving the morphodynamics of the lower Negro.

Although modest in extent compared to the Fly survey (Day et al., 2008), the cores on the Strickland define a clear pattern of sediment deposition. Importantly, the two entirely independent means of documenting rates of sedimentation, ^{210}Pb dating and mine-tracer occurrence, give remarkably comparable results, 1.6 cm/yr and 1.4 cm/yr respectively. Consistent with our slightly lower average deposition rate, the percentage of sediment load deposited overbank is 19% compared to 17-27% reported by Aalto et al. (2008) for the 318-km lowland reach length. Figure 2.14 shows the data reported in this paper with that given by Aalto et al. (2008). It is encouraging that both the magnitude and pattern of deposition compare well. Our measurements are somewhat lower at distances closer than 150 m and higher at distances beyond about 500 m. If metal concentration does vary with clay content, then this difference could be associated with a systematic increase in clay content with distance from the channel as noted by Aalto et al. (2008).

Comparable rates of floodplain deposition have been documented on other large lowland rivers. On the Brahmputra-Jamuna River, Allison et al. (1998) report deposition rates as a function of distance from channel banks (like our Figures 2.13 and 2.14) and fit a power law to their data. The function defined by Allison et al. (1998) matches with our observations and those of Aalto et al. (Figure 2.14). Allison et al. (1998) also note, as we have found, that an exponential function represents the data poorly. For their study reach, they report 8% of the sediment load was being deposited on the floodplain over 110 km, or a value of 0.07%/ km of channel reach, a rate similar to our measurements. On the tidal reach of the Amazon below Obidos, Dunne et al. (1998) conclude that there is a loss of 350 Mt/yr relative to a total load of 1200 Mt/yr as the river travels 450 km towards the sea. This gives a deposition rate of 0.065%/km of channel length. On the 833 km reach between Sao Paulo de Olivenca and Obidos, which is not tidally influenced, floodplain deposition rate is ~0.1% of total load/km of channel length. On the Mississippi, Kesel et al. (1992) report a 39% loss of sediment to the floodplain over 1674 km, or 0.02%/km of channel length. Much higher rates of loss per channel length (well above 0.1%/km of channel length) are found on the relatively small rivers studied by Nicholas et al. (2006) in the United Kingdom. Overall, the values we find for the Strickland are similar to those reported elsewhere for most large rivers, although they are lower than those reported for the Beni River, Bolivia (Aalto et al., 2003).

Comparison of depositional rates on the Strickland and Fly reveal some surprising results. The deposition rate for the first 1 km of floodplain from the bank is nearly 10 times greater on the Strickland (1.4 cm/yr) than that documented for the natural load on the Fly (0.1 to 0.2 cm/yr, Day et al. 2008). Figure 2.14 shows the measured rates on the Fly compared to those of the Strickland, but these rates are elevated due to mine waste loading on the Fly. Day et al. (2008) propose that these rates are elevated in proportion to the increased load by the mine, hence the natural load rates are estimated to be ~4.6 times lower. Given that the Strickland carries ~7 times the natural load of the Fly annually, it makes sense that annual accumulation rates would be greater. This may seem to contradict our stated hypothesis, but other differences become important. We note that the Strickland deposits 13-19% of its total sediment load overbank through its lower reaches, whereas, on the middle Fly, 40% of the annual load is sequestered. This difference is partially a result of the longer reach on the Fly, but correcting for length, the sediment deposition rate as a proportion of the load is 0.05-0.06%/km per channel length on the Strickland, and 0.09%/km channel length on the Fly. On the Fly, however, half of the sediment deposition occurs when sediment-laden flows are pushed up tributary and tie channels and spill onto to the floodplain at a considerable distance from the mainstem. Including these additional channels, the effective channel length on the middle Fly is 1325 km (as compared to just the mainstem of 420 km). Normalizing by this greater length gives a sediment loss rate of 0.03%/km of channel length on the Fly. Thus, per mainstem channel length, the lower load on the Fly leads to lower floodplain deposition rates, but the extensive network of tributaries and tie channels into which the Fly pumps

sediment causes it to deposit a much greater proportion of its sediment load on the floodplain than does the Strickland.

Although the percentage sediment load deposition per unit mainstem channel length is less on the Strickland, the absolute deposition rate in Mt/y is much higher than the natural rate on the Fly. However, this does not mean that the Strickland is still rapidly infilling the accommodation space (*sensu*, Blum and Tornqvist, 2000) associated with post-glacial sea-level rise. The average migration rate of 5 m/yr on the Strickland (Aalto et al., 2008) implies that the channel can easily migrate across the 1-km wide depositional width in just 200 years, sweeping most of the deposited sediment back into the channel. Furthermore, the exchange rate (in Mt/yr) with the floodplain due to lateral migration is much higher than the overbank deposition rate. A lateral migration rate of 5 m per year, times a channel distance of 318 km and an estimated average bank height of 13 m yields ~30 Mt/yr (for a density of 1.5 gm/cm^3). In contrast, on the Fly, the migration rate is 1-2 m/yr in the upper two-thirds of the middle Fly and zero in the lower third of the middle Fly. Dietrich et al. (1999) estimate that bank migration causes only ~4 Mt/yr of erosion. Also, at least half the sediment deposited onto the Fly floodplain occurs via tributary and tie channels, which do not migrate. Hence, while most of the sediment deposited along the Strickland will be rapidly swept back into the channel, on the Fly, much of the sediment is going into long-term storage. Hence, although the annual overbank deposition rate (in Mt/yr) is greater on the Strickland, the long-term accumulation rate may now be approaching zero (perhaps just keeping pace with aggradation due to the gradual extension of the delta into the ocean, Aalto et al. (2008)).

This analysis points to two important issues: 1) topographic controls on a river's response to sea-level rise, and 2) the long-term stratigraphic record versus the short-term deposition rates. Figures 2.3 and 2.4 show that the Strickland has built a scroll-bar ridge (or meander belt) across a wider valley trough. Potential accommodation space on the Strickland River is still plentiful in backswamp areas bordering this belt and in Lake Murray. Former meander belts, similar to those that populate the Holocene alluvial surfaces of other large systems such as the Mississippi River (e.g., Aslan and Autin, 1999) and Colorado River (e.g., Blum and Tornqvist, 2000), however, are absent. The recent flood outbreak down the Mamboi River (Figure 2.7) into Lake Murray defines a potential avulsion path, which, should the Strickland shift there, would cause a significant channel displacement and lead to large areas of sediment accumulation. We note that the current outflow channel of Lake Murray, the Herbert River, seems much too wide for its drainage area, and is bordered by oxbows despite the current absence of bars or lateral migration of the channel. One possibility is that the Herbert River was an earlier path of the Strickland, and the path down the Mamboi was exploited much earlier in the Holocene.

Blum and Tornqvist (2000) suggest that on the Colorado system complete filling of the accommodation space would favor avulsion. Slingerland and Smith (2004) emphasize the tendency for aggrading floodplain systems to avulse. On the Strickland, even with

more infilling of backswamps, the valley width is still relatively narrow and may inhibit avulsion but for the path down the Mamboi. Our measurements of floodplain deposition and lateral migration also indicate that despite the extensive backswamp areas bordering the channel, little net sediment accumulation appears to be occurring in these distal locations. Hence, well before complete "filling" of accommodation space, the rate of floodplain sediment accumulation appears to have dropped to low values. Three factors appear to contribute to this state. First, as just reviewed, there is limited space for avulsion and potential accommodation areas are not reached. Second, the rapid drop off in sediment deposition on the floodplain with distance from the channel means limited sediment delivery to more distal portions of the floodplain. Third, vertical accumulation rate may be relatively low. This rate will tend to keep pace with the combined effects of subsidence, sea-level rise and delta extension (Aalto et al., 2008). There may also be some effect of hydrostatic warping due to sea-level rise (Chappell and Dietrich, 2003). We see little evidence for either subsidence or uplift on the lower Strickland. The late Holocene slow sea-level rise and delta growth, then, requires little accumulation along the Strickland to keep pace.

Another important issue is the disparity on the Strickland between the relatively rapid short-term floodplain deposition rates and the apparent slow accumulation rates over the long-term. An inverse relationship between deposition rate and period of observation was noted by Sadler (1981) and often referred to as the "Sadler effect". Bridge (2003) notes specifically that average floodplain deposition rates tend to decrease with increasing time interval of record. Mechanisms for this disparity, found throughout sedimentary systems, have been debated (e.g., Sommerfield, 2006). Here it appears that a net balance between short term (event and decadal) overbank deposition and progressive lateral migration could lead to a small net accumulation over the long time scales. In this case, the inverse relationship between deposition rate and observation time emerges from the changing balance of processes over time.

2.6. Conclusions

The Fly River system provides us with a natural experiment in which two large rivers with greatly different sediment loads respond to the same post-glacial sea-level rise. Our field investigations and modeling reported here and in companion papers (Aalto et al., (2008; Day et al., 2008; and Lauer et al, 2008) document modern floodplain deposition rates and place constraints on longer term accumulation rates. Together these data demonstrate strong differences between the Strickland and Fly Rivers that arise due to sediment load.

The Strickland discharges ~7 times the natural load of the Fly. Close to where the two rivers join, the Strickland is nearly 10 times steeper, carries bed material whose median size is twice that of the Fly, and has a lateral migration rate of 5 m/yr as compared to nearly zero (in the past 50 years) on the Fly. Furthermore, the Strickland has wide shallow point bars that commonly are divided into partially vegetated islands, whereas

the lower 170 km of the Fly upstream from the junction with the Strickland is essentially bar-free. The Fly discharges sediment into tributaries and tie channels leading to net accumulation in the floodplain. Slow lateral channel shifting also means that overbank deposition is contributing to net accumulation, although natural rates of deposition are slow (0.1-0.2 cm/y to 1 km from the bank) on the Fly. In contrast, the Strickland deposits sediment overbank at 1.4 cm/yr averaged over 1 km from the channel bank, but high lateral migration rates sweep sediment back into the river, leading to relatively low net sediment accumulation rates. Hence, the river with the higher load has a higher floodplain deposition rate, but a faster lateral migration rate, leading to much less of its floodplain overbank deposits contributing to the total net storage and infilling of accommodation space. This dynamic balance supports our initial hypothesis that the Strickland has infilled more of its accommodation space and is correspondingly losing less of its sediment load to floodplain deposition. The current low rates of accumulation within the scroll-bar complex are set by the combined effects of sea-level rise and delta advance (both of which have been slow in the late Holocene). The relatively narrow valley in which the Strickland flows may have prevented multiple Holocene meander belts from forming as has been found elsewhere.

Deposition rate decreases rapidly with distance from channel bank, but the pattern differs between the Strickland and the Fly. Both the mine-tracer occurrence measurements reported here and the ^{210}Pb data reported by Aalto et al. (2008) show an abrupt decrease in floodplain deposition rate with distance from the channel bank that is not well represented by an exponential function (often used to characterize near bank deposition, (e.g., Tornqvist and Bridge, 2002). Deposition extends beyond 1 km, and can occur out to 2 km from the channel. Rates of overbank deposition were greater farther from the channel on bends than on straight sections. Interestingly, the average deposition rate as a function of distance from bank on the Strickland is very similar to that reported on the Brahmaputra-Jamuna River (Allison et al., 1998) and Beni River (Aalto et al., 2003). In contrast, the Fly River overbank deposition rates are well defined by an exponential, and deposition essentially ceases 1 km from the bank. These documented rates, and their similarities and differences between river systems, are not yet explained quantitatively.

We have argued from inference and modeling that the long-term (Holocene) sediment load on the Strickland has probably been persistently higher than the Fly because of the greater drainage area in the rapidly uplifting and eroding headwater mountains. It is difficult, however, to reconstruct this history. Knowledge of the depth and rate of sediment accumulation over the Holocene along the Strickland would help provide some important constraints. Seismic surveys and dating of sediments obtained from deep cores across the floodplain would be invaluable.

Taken together, these observations argue that the time evolution (and resulting morphodynamics and stratigraphic record) of a large lowland river in response to sea-level rise will depend strongly on upstream sediment load to the river. That load, however, is not necessarily uniformly dispersed into available floodplain accommodation

space. Low sediment load leads to slow development, and even after 20,000 years since the onset of sea-level rise and more than 6000 years of nearly constant sea level, the Fly River continues to lose a large proportion of its sediment load to its floodplain. In contrast, the Strickland has more fully responded, and transfers the majority of its sediment load through its lowland valley, even though substantial areas of accommodation space remain unfilled.

Acknowledgements

Primary support for this project came from an NSF Margins (Source to Sink) grant (NSF EAR-0203577). Development and refinement of the ^{210}Pb dating technique was supported in part by NSF EAR-0310339 and EAR-0403722. Some support also came from the National Center for Earth-surface Dynamics. The Western Venturer, which was essential to the program, was provided by Ok Tedi Mining Limited (with a special thanks to Jim Veness). Helicopter and food support in the field, and support for laboratory analysis was provided by Porgera Joint Venture (Tim Omundsen, Charlie Ross and Jim McNamara). Valuable hydrologic monitoring data were also provided by Porgera Joint Venture (through the help of Andrew Markham (Hydrobiology, Australia)). Lihir Mining (Geoff Day) gave valuable logistical assistance in Port Moresby and provided some equipment. Cliff Reibe, John Sanders and Ian Hargreaves were invaluable to the field campaign. Stuart Simpson and David Bishop (CSIRO) are thanked for their contributions to the chemical analyses undertaken as part of this project. The authors are grateful for the reviews and comments provided by Michael Blum, Gary Parker and Charles Nittrouer.

Transect		Distance From Channel (m)																Transect Average
		5	20-25	50	75	100	135	150	200	250	275-325	350	400-425	475-625	800-850	1000-1025	1450	1875-2000	
1	Left	3.1		3.1						2.5				1.9		1.2		0.9	1.53
	Right	2.4	1.3	1.4										0.4		1.5			0.96
2	Left		7.8	1.9		2.6		1.6	0.8	1.9	2.3			0.7		1.4			1.61
	Right	2.3	3.2	1.5	0.2	0.7		0.7	0.6	1.5		0.2	0.3			0.9			0.71
3	Left	6.8		0.6		0.5		0.0		0.0		0.0		0.0					0.37
	Right	1.2		0.6		0.7		0.5		0.7		2.0		2.2					3.25
4	Left	0.4		0.2		0.0		1.0										0.0	1.09
	Right	0.9		0.0		0.1		0.0		0.1		0.0		0.1					0.04
5	Left	5.0		7.2		1.3		1.3		1.2				1.8					3.07
	Right	4.9		5.0		5.7		3.5							1.0				3.92
10	D. Left	0.4	5.5	1.5		5.1	0.8	1.8			0.7								2.08
	U. Left	3.3		5.5		5.9		7.0	3.5		2.1		2.9	0.4					3.25
	D. Right	3.0		5.9	5.6	4.8													4.85
13	Left	2.7		2.3		4.8				2.2									3.29
	Right	2.1	4.4	4.8				3.3											3.94
15	Left	2.3		6.8		1.0													4.11
	Right	5.1		4.0		7.0		6.4		1.6	2.3								4.65
12													0.2		0.1	0.2	0.1	0.4	
Average		2.87	4.46	3.07	2.87		2.14		1.65	1.29	1.88	0.56	1.15	0.95	0.91		0.35		

Table 2.1 Summary of sediment accumulation rate calculated for each core using the depth-of-occurrence method for a background concentration of 25 mg/g Pb. Numerically integrated average deposition for each transect is shown; units are cm/a. Data were combined with adjacent samples where two or fewer cores recorded the deposition rate for a single distance from the channel.

Method	Distance From River Bank (m) 5	24	50	97	149	200	250	300	350	400	500	954	1830	1-km Average	2-km Average	Mass Lost (mt)	Mass Lost (%)
Depth-of-Occurrence																	
25 µg/g Pb	2.9	4.5	3.1	2.9	2.1	1.6	1.3	1.9	0.6	1.2	0.9	0.9	0.4	1.4	1.0	9.2	**13.2**
22 µg/g Pb	2.9	4.5	3.4	3.0	2.3	1.7	1.5	3.9	0.6	2.4	1.1	1.9	1.6	1.8	1.7	12.2	**17.4**
0.16 µg/g Ag	2.7	2.5	3.2	3.0	2.3	1.5	1.3	1.4	0.6	1.4	1.2	1.1	0.2	1.4	1.0	9.2	**13.2**
0.1 µg/g Ag	3.3	3.8	3.3	3.4	2.7	1.8	1.8	2.0	0.8	2.2	1.6	1.6	0.4	1.8	1.3	12.2	**17.4**
Inventory																	
25, 49 µg/g Pb	1.4	2.8	1.6	1.4	0.8	0.6	0.9	1.4	0.3	0.4	0.6	0.5	0.1	0.7	0.5	4.7	**6.7**
22, 49 µg/g Pb	2.0	3.4	2.3	2.0	1.3	1.0	1.1	1.7	0.3	0.6	0.6	0.5	0.1	0.9	0.6	5.9	**8.4**
0.16, 0.5 µg/g Ag	1.3	2.8	1.5	1.4	0.9	0.5	0.8	1.1	0.3	0.3	0.5	0.4	0.1	0.6	0.4	4.2	**5.9**
0.1, 0.5 µg/g Ag	1.9	3.5	2.4	2.2	1.6	1.1	1.0	1.7	0.3	0.5	0.7	0.4	0.1	0.9	0.6	6.0	**8.6**

Table 2.2. A summary of results for each method using both the 80% and 95% values for background concentration. Rates are recorded in cm/yr. The average rate is determined by numeric integration to 1 km divided by width. The proportion of the load lost is calculated for 1 km on either side of the channel for the entire 455-km^2 floodplain (for the 267-km sand-bedded channel reach) relative to the discharge of 70Mt/yr load.

References

Aalto, Rolf, et al. "Episodic sediment accumulation on Amazonian flood plains influenced by El Nino/Southern Oscillation." *Nature* 425.6957 (2003): 493-497.

Aalto, Rolf, J. Lauer, and William E. Dietrich. "Spatial and temporal dynamics of sediment accumulation and exchange along Strickland River floodplains (Papua New Guinea) over decadal-to-centennial timescales." *Journal of Geophysical Research: Earth Surface (2003–2012)* 113.F1 (2008).

Allison, M. A., et al. "Importance of flood-plain sedimentation for river sediment budgets and terrigenous input to the oceans: Insights from the Brahmaputra-Jamuna River." *Geology* 26.2 (1998): 175-178.

Angevine, Charles L. "Relationship of eustatic oscillations to regressions and transgressions on passive continental margins." *Geophysical Monograph Series*48 (1989): 29-35.

Apte, S.C. "Factors affecting the release of metals from discharged mine tailings in the Porgera/Strickland River system." CSIRO Investigation Report CET/LH/IR394 prepared for Porgera Joint Venture. CSIRO Australia (1995): 73 pp.

Apte, S.C. "Porgera mine tailings leaching study." CSIRO Investigation Report CET/LH/IR 483R prepared for Porgera Joint Venture. CSIRO, Australia (1996): 18 pp.

Apte, S.C. "Tracing mine derived sediments and assessing their impact downstream of the Porgera Gold Mine." Report No. ET/IR385 prepared for Porgera Joint Venture CSIRO, Australia (2001): 55 pp.

Aslan, Andres, and Whitney J. Autin. "Evolution of the Holocene Mississippi River floodplain, Ferriday, Louisiana; insights on the origin of fine-grained floodplains." *Journal of Sedimentary Research* 69.4 (1999): 800-815.

Bera, M., W.E. Dietrich, and H. Davies "Sediment Transport of the Lower Strickland River." Proceedings of the Seventh PNG Geology, Exploration and Mining Conference. Lae, PNG. (2005).

Blake, D. H., and C. D. Ollier. "Alluvial plains of the Fly River, Papua." *Z. Geomorphol* 12 (1971): 1-17.

Blong, R. J. "The magnitude and frequency of large landslides in the Ok Tedi catchment." *Report to Ok Tedi Mining Ltd, Tabubil, Papua New Guinea* (1991).

Blum, Michael D., and Torbjörn E. Törnqvist. "Fluvial responses to climate and sea-level change: a review and look forward." *Sedimentology* 47.s1 (2000): 2-48.

Bridge, John S. *Rivers and floodplains: forms, processes, and sedimentary record*. Wiley. com, 2009.

Chappell, J., and W. E. Dietrich. "Holocene evolution of the middle Fly River, Papua New Guinea." *AGU Fall Meeting Abstracts*. Vol. 1. 2003.

Day, G.M., S.C. Apte, G.E. Batley, and J. Skinner "Strickland River Floodplain Coring Project. Project Report." Ecowise Environmental Ltd., Limnos Environmental Consultants Pty Ltd., and CSIRO, Australia. (1998): 55 pp.

Day, Geoff, et al. "The depositional web on the floodplain of the Fly River, Papua New Guinea." *Journal of Geophysical Research: Earth Surface (2003–2012)*113.F1 (2008).

Dietrich, William E., Geoff Day, and Gary Parker. "The Fly River, Papua New Guinea: Inferences about river dynamics, floodplain sedimentation and fate of sediment." *Varieties of Fluvial Form* (1999): 345-376.

Dunne, Thomas, et al. "Exchanges of sediment between the flood plain and channel of the Amazon River in Brazil." *Geological Society of America Bulletin*110.4 (1998): 450-467.

Hill, K. C., et al. "Copper–gold mineralisation in New Guinea: tectonics, lineaments, thermochronology and structure." *Australian Journal of Earth Sciences* 49.4 (2002): 737-752.

Kesel, Richard H., Elaine G. Yodis, and David J. McCraw. "An approximation of the sediment budget of the lower Mississippi River prior to major human modification." *Earth Surface Processes and Landforms* 17.7 (1992): 711-722.

Lauer, J., Gary Parker, and William E. Dietrich. "Response of the Strickland and Fly River confluence to postglacial sea level rise." *Journal of Geophysical Research: Earth Surface (2003–2012)* 113.F1 (2008).

Latrubesse, Edgardo M., and Elena Franzinelli. "The late Quaternary evolution of the Negro River, Amazon, Brazil: implications for island and floodplain formation in large anabranching tropical systems." *Geomorphology* 70.3 (2005): 372-397.

Muto, Tetsuji, and John B. Swenson. "Large-scale fluvial grade as a nonequilibrium state in linked depositional systems: Theory and experiment." *Journal of Geophysical Research: Earth Surface (2003–2012)* 110.F3 (2005).

Nicholas, A. P., et al. "Development and evaluation of a new catchment-scale model of floodplain sedimentation." *Water resources research* 42.10 (2006).

Paola, Chris. "Quantitative models of sedimentary basin filling." *Sedimentology*47.s1 (2000): 121-178.

Pickup, G. "Geomorphology of tropical rivers: I. Landforms, hydrology and sedimentation in the Fly and lower Purari, Papua New Guinea." *Catena Suppl* 5 (1984): 1-17.

Pitman, Walter C. "Relationship between eustacy and stratigraphic sequences of passive margins." *Geological Society of America Bulletin* 89.9 (1978): 1389-1403.

Porgera Joint Venture "Porgera's impact on rivers." Enga, PNG (2003): 6 pp.

Rowland, Joel C., et al. "Tie channel sedimentation rates, oxbow formation age and channel migration rate from optically stimulated luminescence (OSL) analysis of floodplain deposits." *Earth Surface Processes and Landforms* 30.9 (2005): 1161-1179.

Sadler, Peter M. "Sediment accumulation rates and the completeness of stratigraphic sections." *The Journal of Geology* (1981): 569-584.

Slingerland, Rudy, and Norman D. Smith. "River avulsions and their deposits."*Annu. Rev. Earth Planet. Sci.* 32 (2004): 257-285.

Sommerfield, Christopher K. "On sediment accumulation rates and stratigraphic completeness: Lessons from Holocene ocean margins." *Continental Shelf Research* 26.17 (2006): 2225-2240.

Tornqvist, Torbjorn E. "Holocene alternation of meandering and anastomosing fluvial systems in the Rhine-Meuse Delta (central Netherlands) controlled by sea-level rise and subsoil erodibility." *Journal of Sedimentary Research* 63.4 (1993): 683-693.

Törnqvist, Torbjörn E., and John S. Bridge. "Spatial variation of overbank aggradation rate and its influence on avulsion frequency." *Sedimentology* 49.5 (2002): 891-905.

Walling, D. E., and Q. He. "The spatial variability of overbank sedimentation on river floodplains." *Geomorphology* 24.2 (1998): 209-223.

Watson, E. “The use of lead and silver to study recent sedimentation on a tropical floodplain: assessment of post-depositional stability and of temporal and spatial trends in mine-derived sedimentation.” Unpublished Honors thesis, Macquarie University, Sydney, Australia. (2006).

Figures

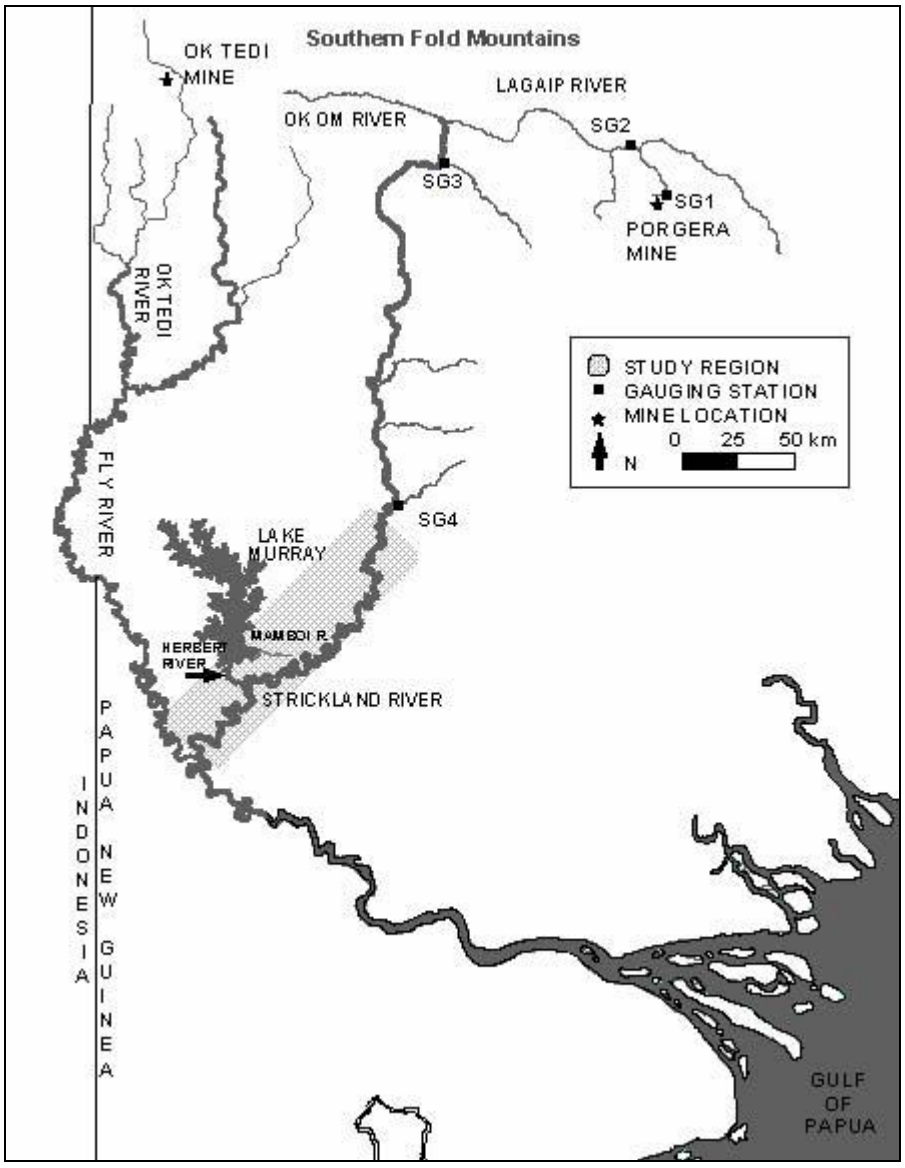


Figure 2.1. Watershed map showing the Strickland and Fly Rivers. Stream gauging stations, labeled "SG", are intermittently monitored by Porgera mine.

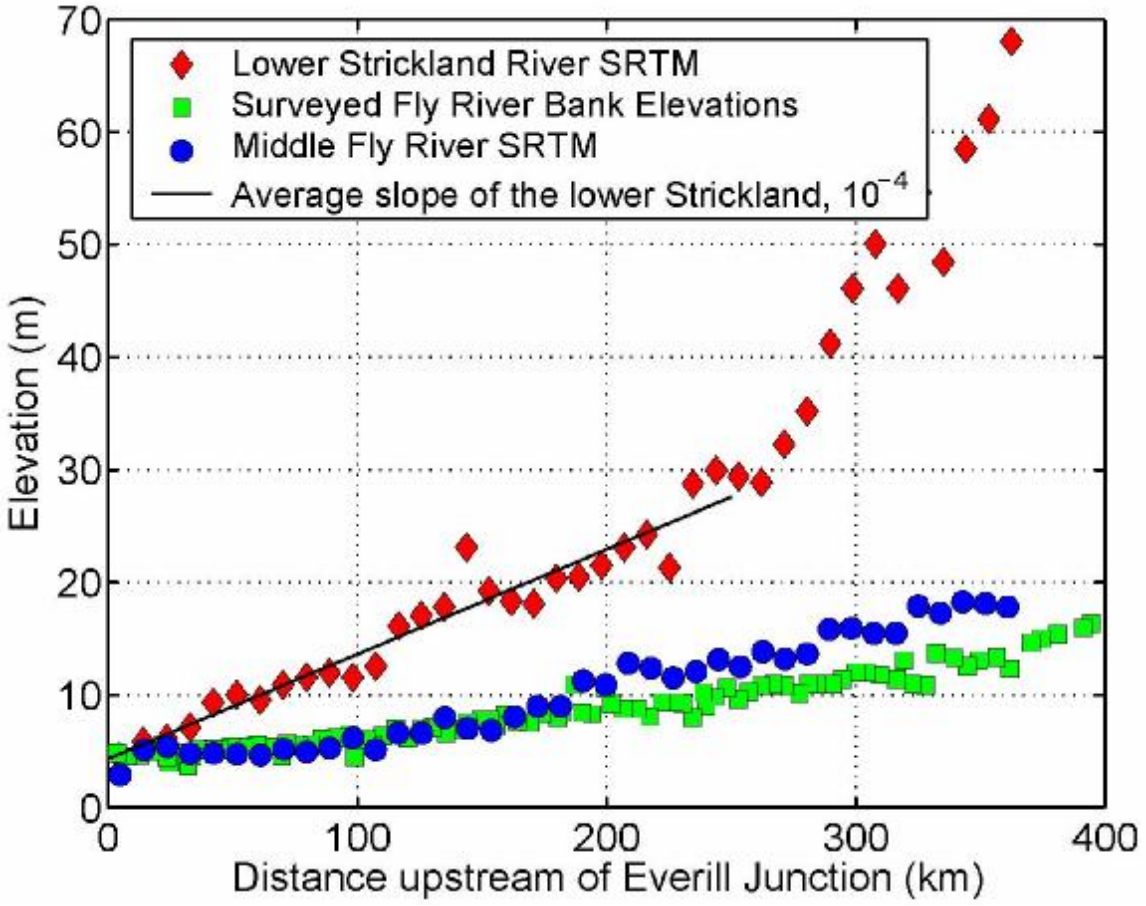


Figure 2.2. Longitudinal profiles of the Fly and Strickland Rivers derived from SRTM data. The Fly data are compared with a differential GPS survey on the Fly performed in 1995. This data agrees well with the 5-km averages of elevation along the Fly, derived from 90-m grid SRTM data. The Strickland data are also 5-km averages of elevation from 90-m grid SRTM data. The mean slope of the sand-bed reach of the Strickland, to 250-km upstream of Everill Junction, is 1 X 10^{-4}.

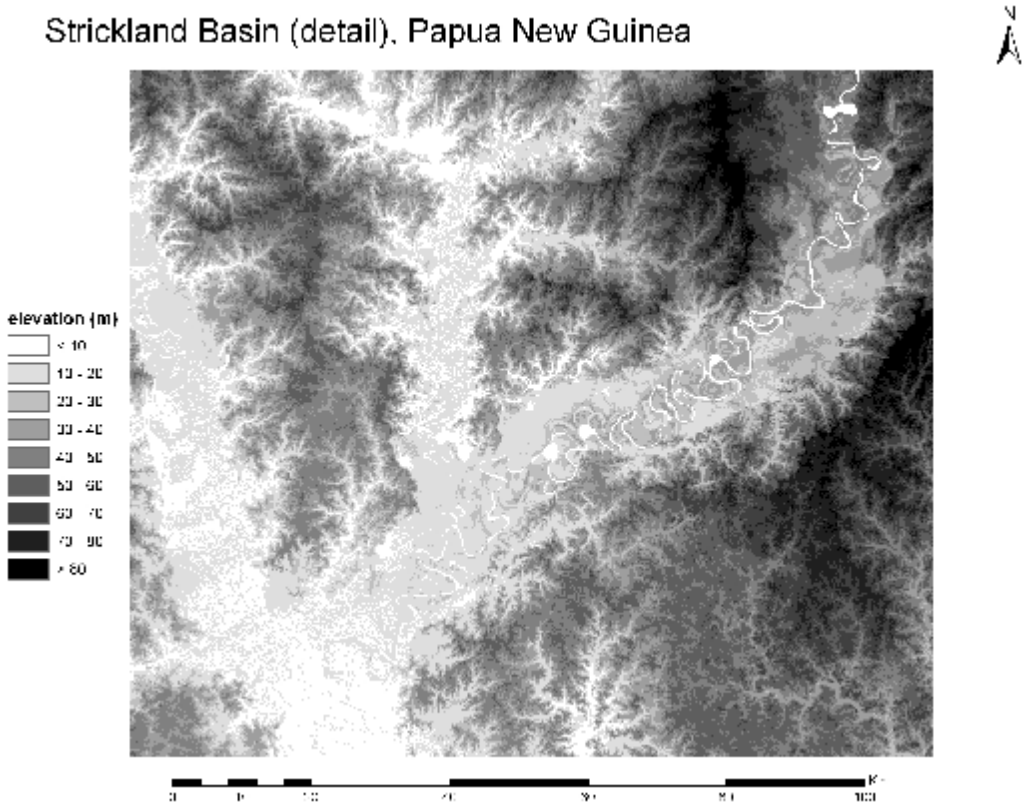


Figure 2.3. Topography of the lower Strickland area. Note the narrow floodplain valley is confined by dissected hills and bordered by low-lying swamp reaches. The meander belt has built an elevated ridge and scroll-bar complex proximal to the channel.

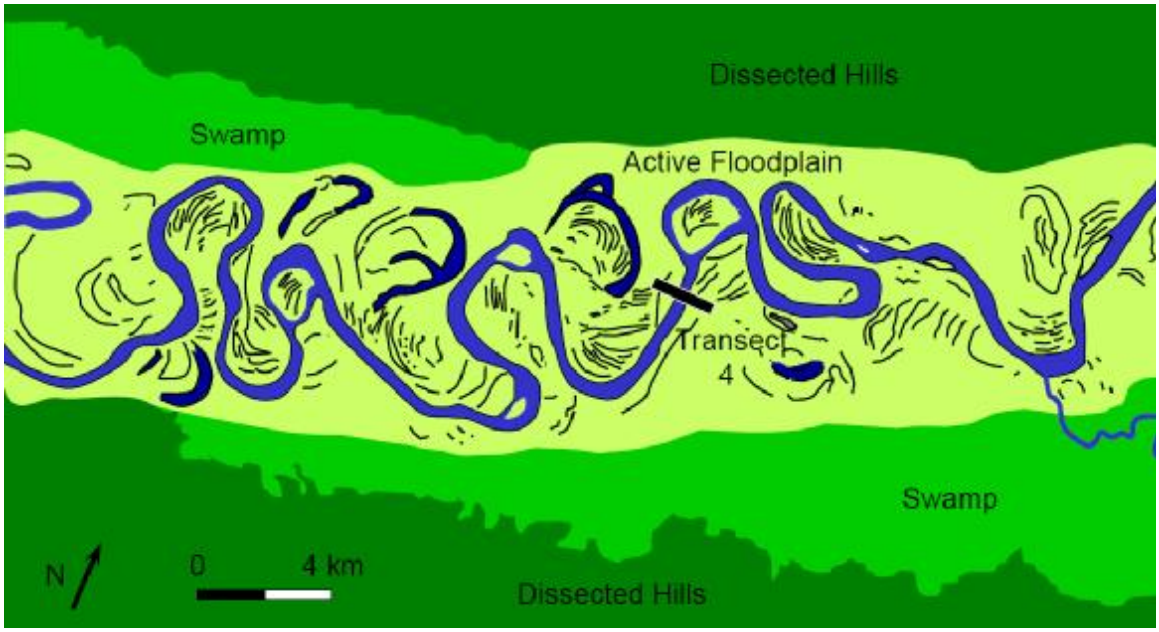


Figure 2.4. A detailed view of the Strickland River floodplain showing the elevated ridge, backswamp region, oxbows and scroll bars visible in satellite imagery. Also shown are transect 4 and the oxbow lake which has been breached and released floodwaters to the Mamboi drainage.

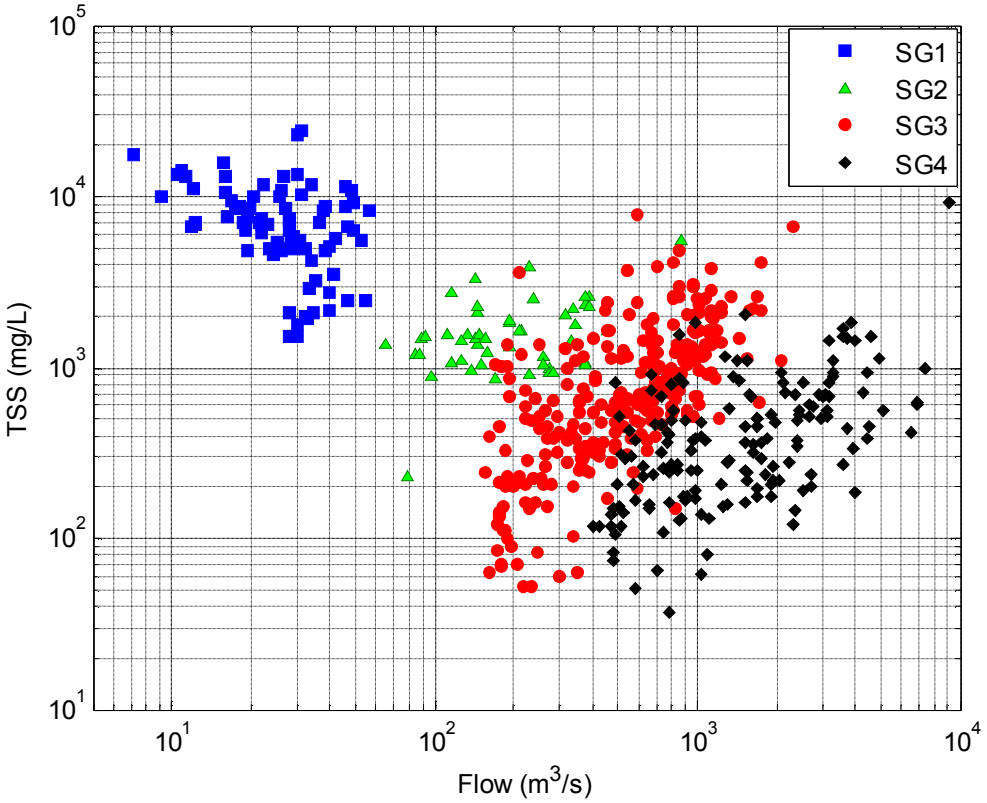


Figure 2.5. Suspended-sediment concentrations measured at increasing distances downstream from Porgera Mine. Note that suspended-sediment concentration decreases with increasing discharge near the mine, SG1, indicating dilution, but increases with increasing flow farther downstream, SG4. This indicates that the mine loading does not have a large effect on the total load transported by the river, especially during large flows.

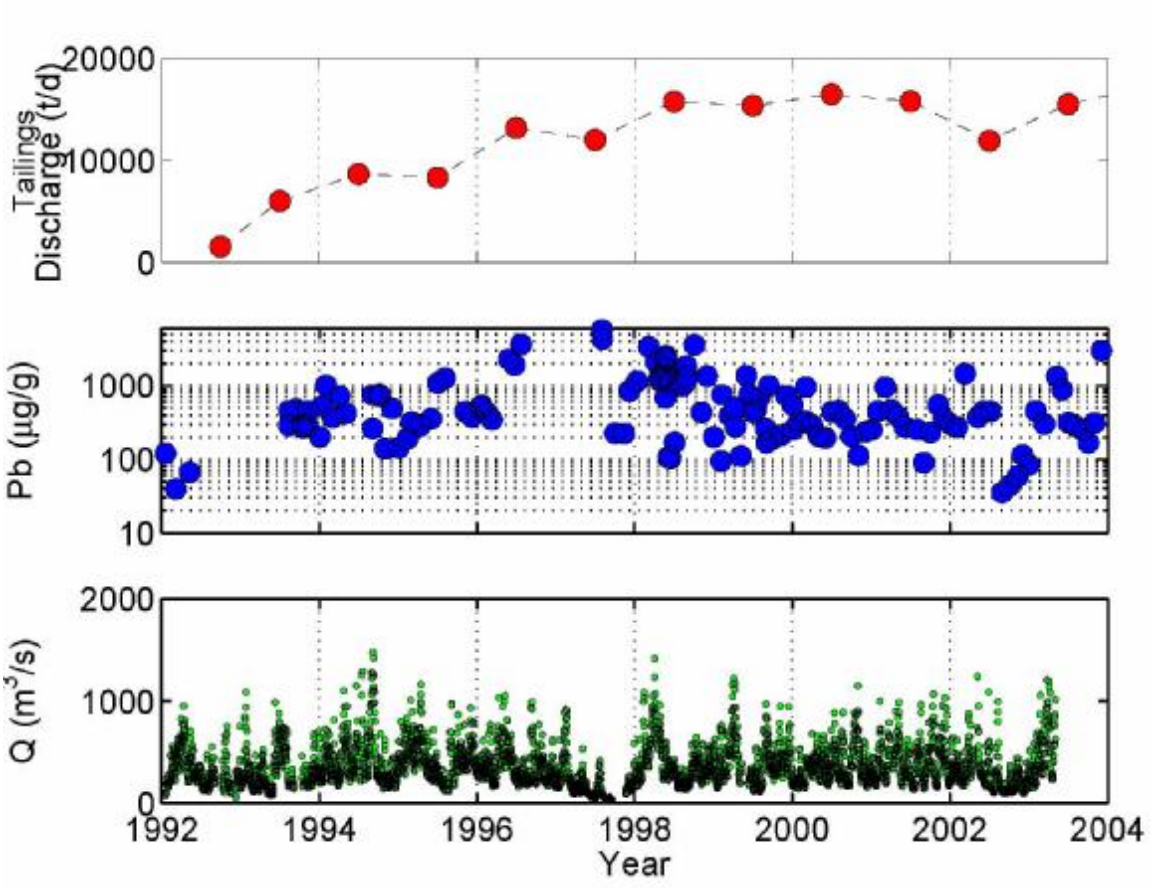


Figure 2.6. Tailings discharge, Pb concentrations, and mean daily flow in the Strickland River a) Daily tailings discharge into the Strickland by Porgera mining (annual load in 1991 was similar to 1993, but daily discharge values were not available). b) Particulate lead concentration at SG1, just downstream of the mine. c) Daily flow records for SG3, 165 km from the mine, and 470 km upstream from Everill Junction shown in Figure 2.1 (Data provided by Porgera Joint Venture).

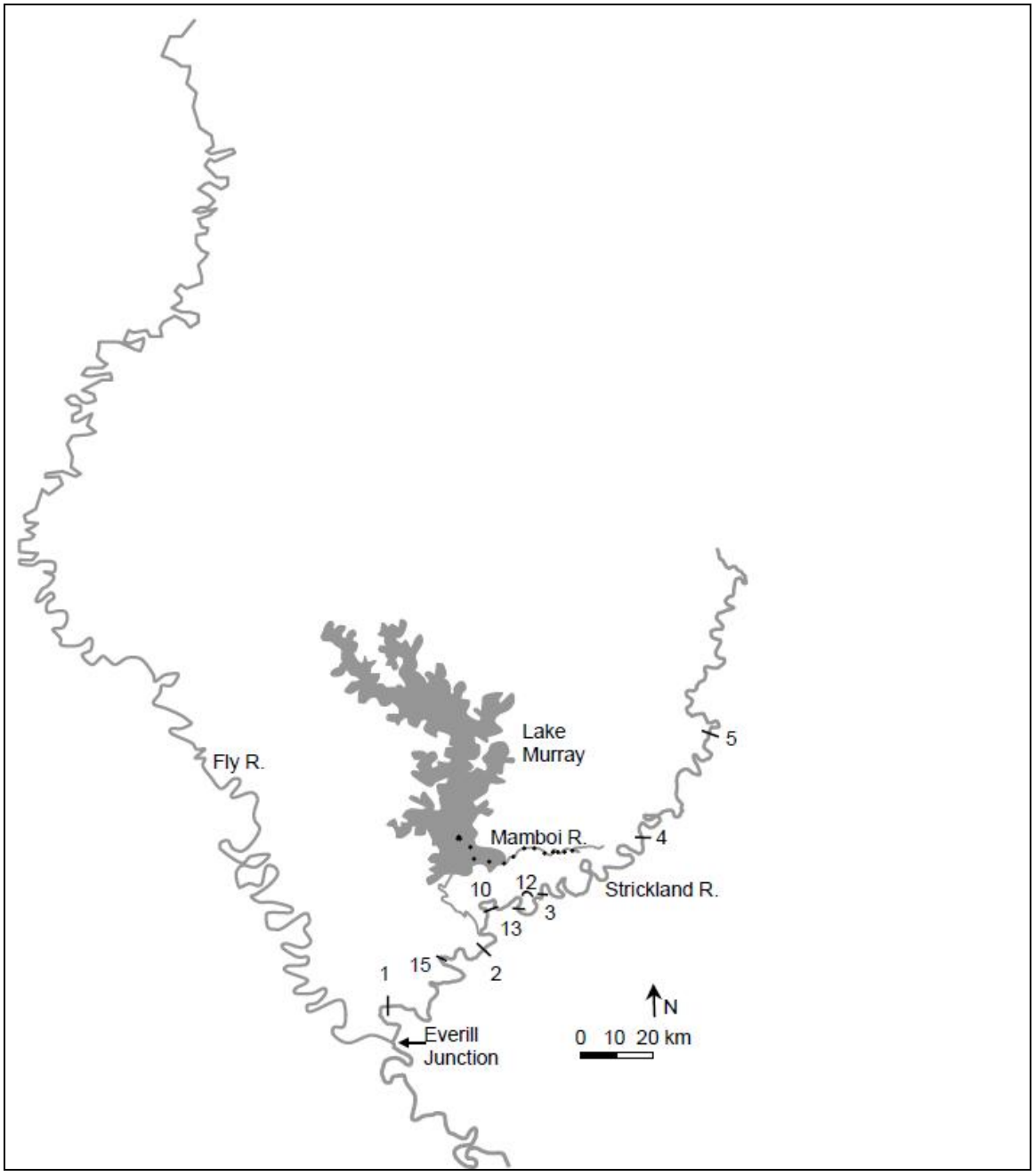


Figure 2.7. Transect location map. Locations include straight transects 1-4, moderately curved transect 5, oxbow transect 12 and curved transects 10, 13 and 15.

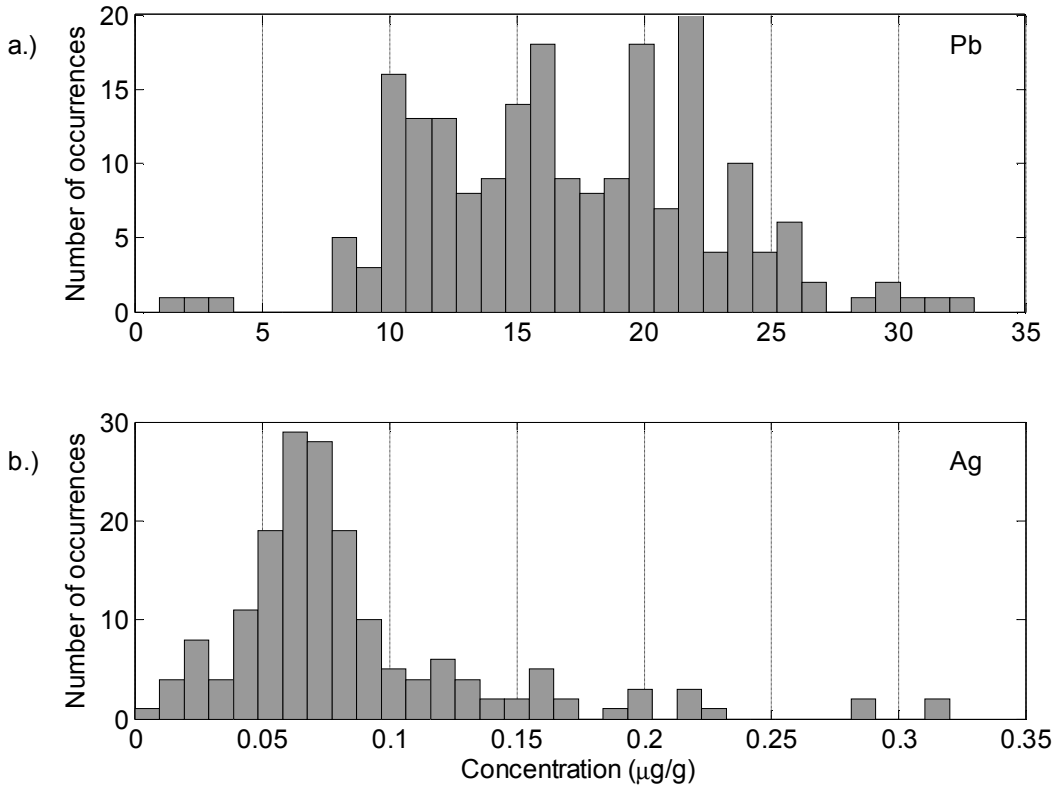


Figure 2.8. Histogram of background trace-metal concentrations measured on the floodplain; a.) shows Pb occurrences, b.) shows Ag occurrences.

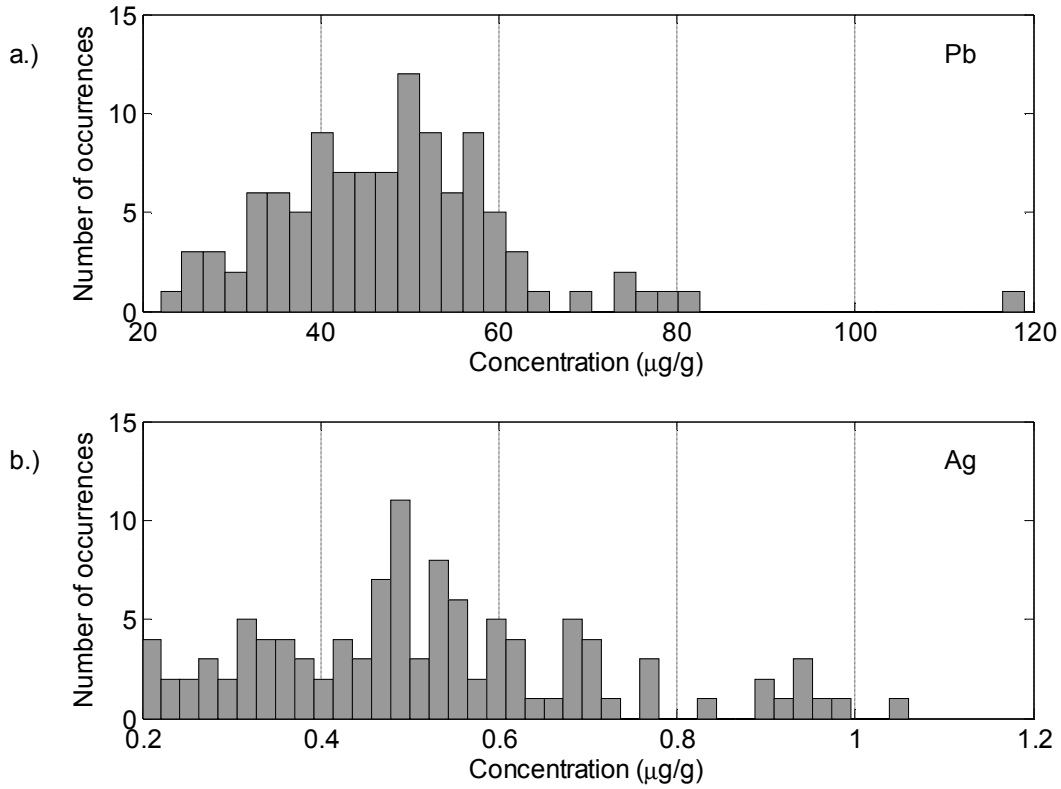


Figure 2.9. Histogram of incoming, or surface, trace-metal concentrations measured on the Strickland River floodplain; a.) shows Pb occurrences, b.) shows Ag occurrences.

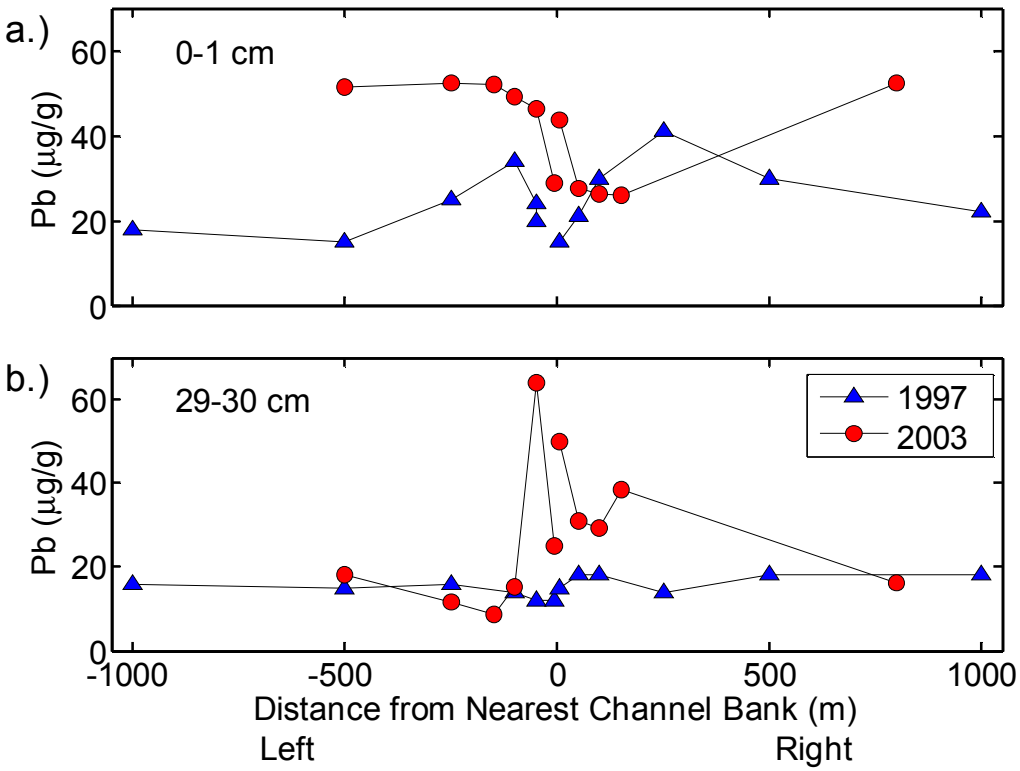


Figure 2.10. Comparison of Pb concentration in surface and 29-30 cm samples taken in 1997 and 2003 at transect 5. Note the overall increase in concentrations at the surface and at depth as well as the spread of contamination across the floodplain over time. The distances plotted are to the nearest location on the main channel.

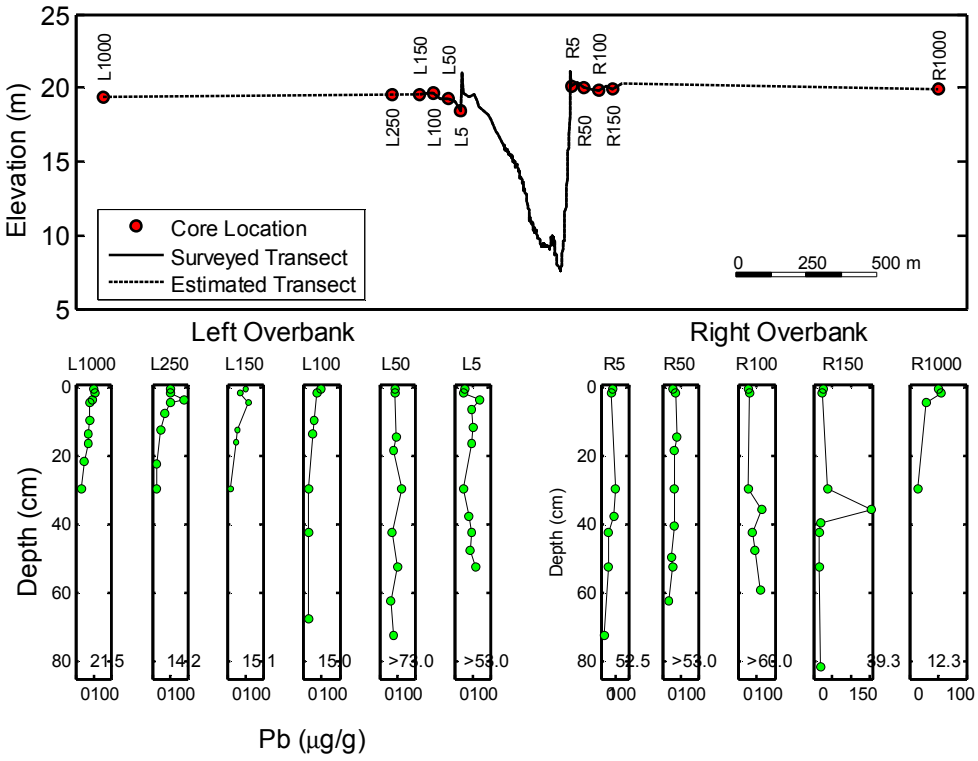


Figure 2.11. Transect 5 topography and individual core concentration profiles.

a) Field-surveyed topography (distal elevations are estimated) with core locations shown. The distances shown are along the transect, but the distal cores are actually closer to upstream reaches of the channel. b) Pb concentration profiles for each of the 11 cores along transect 5. The distal cores, L1000 and R1000, are approximately 500 and 800 m from the upstream left and right banks, respectively. The number at the bottom of each subplot is the interpolated depth at which the Pb concentration would equal the background value of 25 μg/g.

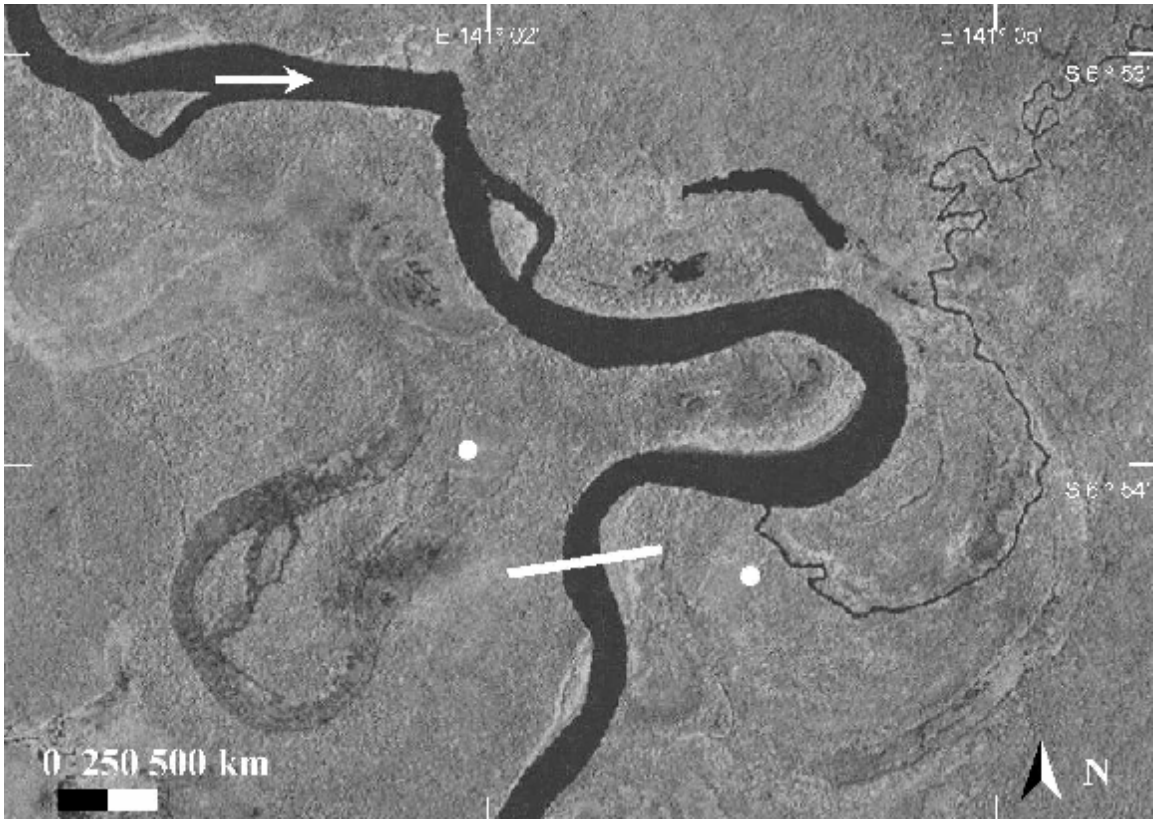


Figure 2.12. Transect 5 Satellite Image (obtained from Landsat.org, 2006). The surveyed transect is indicated by the white line. The two distal core locations, sampled by helicopter, are shown as points. The channel is 250 m wide at the transect location. North is upward and the arrow shown indicates flow direction.

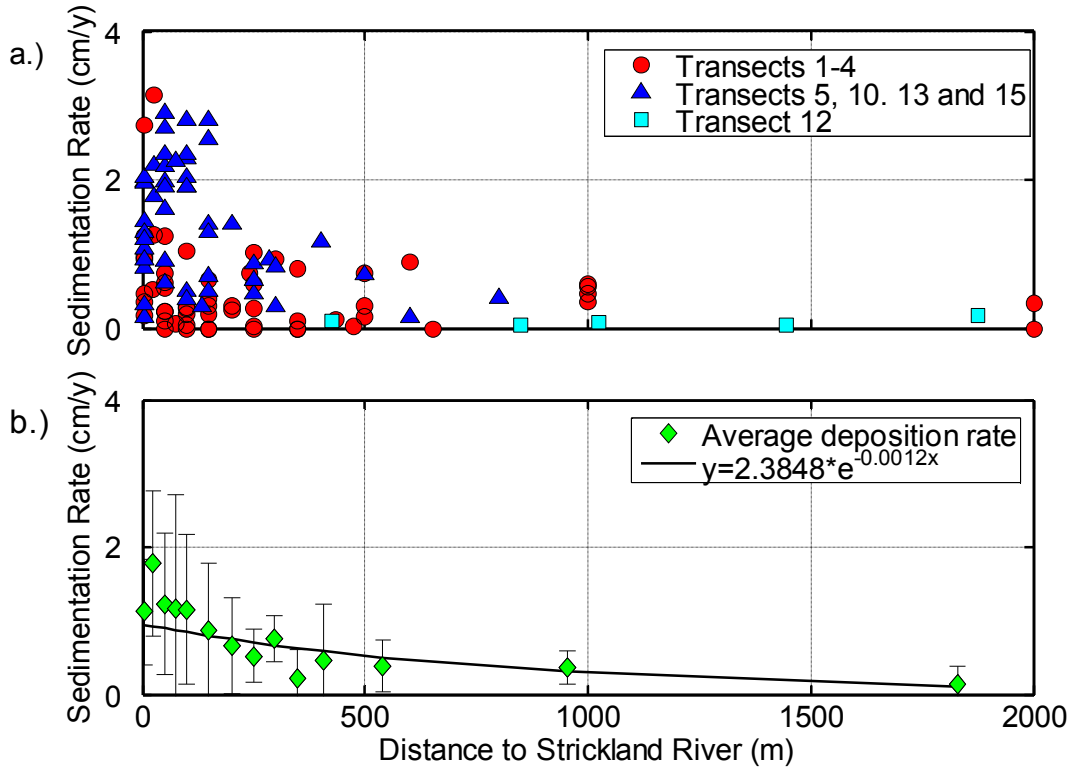


Figure 2.13. Sediment deposition rate as a function of distance from bank. a) All core samples (rates based on depth-of-occurrence for 25 µg/g Pb background). Transect 12 is along the shore of an oxbow, and is therefore plotted separately. All distances are to the nearest portion of the Strickland. b) Sediment deposition rate averaged by sampling distance. If one or two cores were sampled at a given distance, they were binned with adjacent samples and plotted versus the weighted average of the distances. The exponential fit has an R^2=0.67

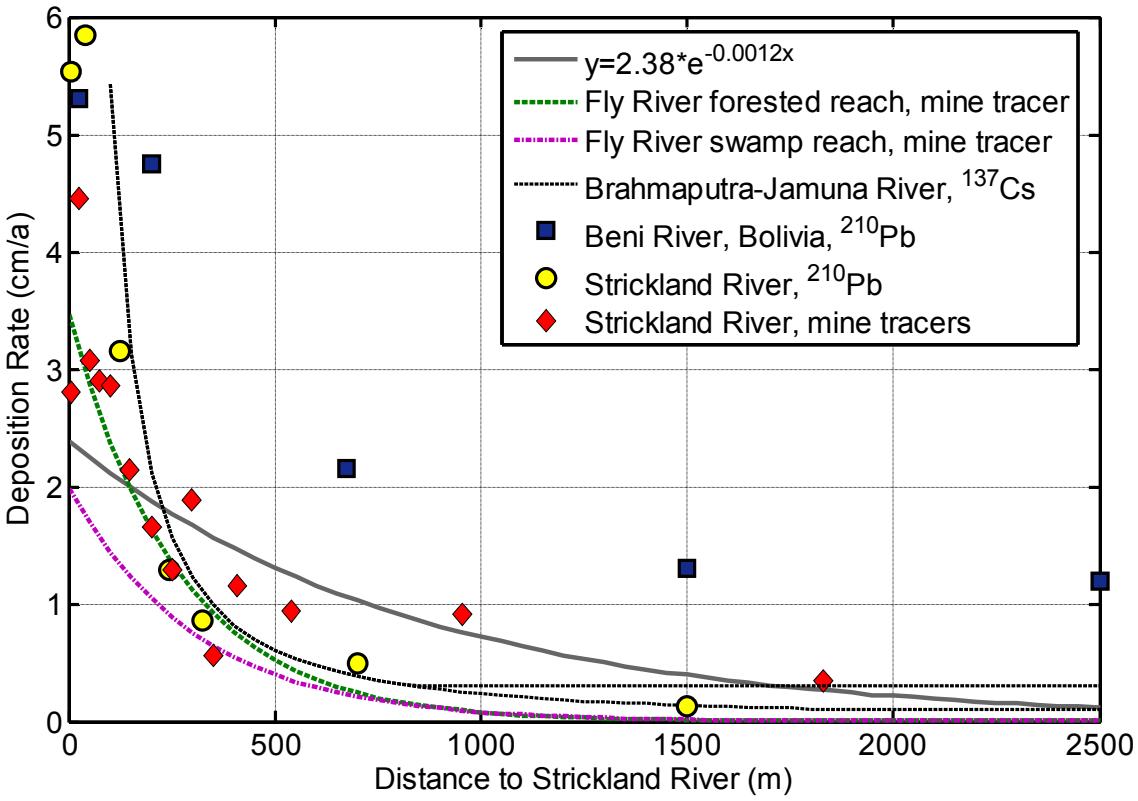


Figure 2.14. Average Strickland River deposition rate and exponential trend from Figure 2.13 plotted with the accumulation rate functions measured on other large river floodplains**.** The deposition function measured using ^{210}Pb dating (*Aalto et al*., 2008) is plotted in yellow. Post-mine deposition rates on the Fly River were described in *Day et al*. (2008). The power law describing deposition rate as a function of distance from the Brahmaputra-Jamuna River is also shown (*Allison et al*., 1998). The relationship developed by *Allison et al*. (1998) required that a minimum deposition rate of 0.1 or 0.3 cm/yr be assigned based on channel reach. Deposition on the Beni River, Bolivia, was measured by *Aalto et al.* using ^{210}Pb (2003).

Chapter 3

Sediment Particle Size Distribution of Overbank Deposits on Lowland River Floodplains

Abstract

The Strickland and Fly Rivers join at just 6 m above sea level, and have experienced the same Holocene sea-level rise. Historically, the Strickland has carried about seven times the sediment load and twice the water discharge as the Fly. Deposition rates over the first 1 km from the channel bank on the Strickland were about ten times those on the Fly (for estimated natural sediment loads), however, the proportional loss per channel length on the Strickland was less than that on the Fly (0.09%/km of mainstem channel length) due to an extensive network of tributary and tie channels that convey sediment to the floodplain on the Fly. Additionally, deposition decreased with a clear exponential pattern with increasing distance from the nearest channel on the Fly River floodplain, while the decrease in deposition rate with distance from the channel was non-exponential on the Strickland River Floodplain, indicating a further difference in sediment transport and deposition processes. Particle size distribution for floodplain subsamples from the same cores used to determine deposition rates was measured using a Coulter LS laser particle sizer. Sediments from the Fly River did not vary much in size with distance from the channel though there was a slight decrease in the percent composition of fine sediments (clay and fine silt) and an increase in relative contribution of coarser sediment (medium and coarse silt) with distance from the channel. Sand composed about 5% of samples at all distances from the channel. This contrasted significantly with sediment size distributions across the Strickland floodplain, where sediments rapidly fined with distance from the channel. There was little sand or coarse silt present beyond 400 m from the channel and clay and fine silt comprised the majority of sediment beyond this distance. These strikingly different patterns of sediment particle size distribution across the floodplains were likely due to strong flocculation of all sediment sizes across the Fly River floodplain and relatively weaker flocculation on the Strickland River floodplain.

3.1 Introduction

Overbank deposition, lateral migration, and channel avulsion are the primary processes responsible for floodplain building. Lowland river floodplain sediments have not been widely studied, but the fine sediments are often contaminated by metals and other natural and anthropogenic pollutants (Rinklebe et al., 2007). Quantifying the pattern of grain sizes across the floodplain can provide insight into the distribution and storage of potentially hazardous waste associated with suspended sediment transported downstream, especially the washload carried by a channel (Higgins, 1990; Malmon et al., 2005) and provide insights into the physical processes that were likely responsible for transporting and depositing sediment overbank (Allen 1978). In order to assess the transport processes responsible for forming floodplains one must quantifying the pattern of both the amount of sediment deposited and the grain size distribution of that sediment. This enhanced understanding also allows for the interpretation of the sedimentary record of floodplains and better prediction of floodplain response to changing forcings such as climate, base level or sediment load.

This chapter presents a detailed study of the sediment size distribution across the middle Fly River floodplain (Day et al., 2008) and the lowland Strickland River floodplain. This data set is among the most extensive and detailed datasets of lowland floodplain sediment particle size distribution. These data, combined with the magnitude of overbank deposition (Swanson et al., 2008; Day et al., 2008), are used in Chapter 4 to motivate a mechanistic overbank floodplain transport and deposition model to identify the processes that control the rate and pattern of deposition on lowland river floodplains.

In this chapter, the particle size distribution (used here to mean the full grain size distribution of a depositional layer or transported sediment) of the sediment delivered to the floodplain of the lower Strickland River floodplain was measured and compared to that found along the middle Fly River floodplain by Day et al. (2008). The number and detail of these data are unique for large river system floodplains. The fate of mine contaminants being stored in the fine grained sediments on floodplain, the role of mechanisms like advection, diffusion and flocculation in floodplain sediment transport, and the geologic record of floodplain sediments can better understood by characterizing the particle size distribution of sediments on the floodplain.

3.1.1 Overbank Deposition

Early observations of floodplain alluvium were often qualitative, but these qualitative observations led to a rich study of the linkages between alluvial stratigraphy, channel morphology and process. Allen (1965) presented an early qualitative model of how floodbasin fill particle size distribution and pattern related to channel type and process as shown in Figure 3.1. Subsequent quantitative models predicted how alluvial architecture was dependent on aggradation rate and floodplain accommodation space during relative

sea-level change (Marriott 1999) and simulated cross-valley stratigraphy under various forcings (Mackey and Bridge, 1995). These models generally considered overbank deposits as a single "fine sediment" unit on lowland floodplains with coarser sand and larger sediments as channel fill, bed, and bar material. Sandy clay deposits were often interpreted as being channel levee deposits while clay would indicate sediment deposited on the distal floodplain (e.g. Figure 3.2 from Stouthamer 2001). Clearly identifying the processes that control floodplain deposition rate and sediment particle size distribution would lead to an enhanced understanding of floodplain stratigraphy and interpretation of the stratigraphic record.

Overbank transport can occur when the stage of the channel tops the levees or channel bank and there is a head gradient from the channel to the floodplain or when both the channel and floodplain are above bankfull stage and sediment laden water from the channel exchanges with water from the floodplain in vortices at the channel margin (Bridge, 2003). Overbank deposits can be described as successive layers of sediment draped across the floodplain (Moody et al., 1999). When water overtops the levees there is an abrupt decrease in flow velocity and transport capacity resulting in the deposition of the coarsest material being carried in suspension by the river near the channel bank (Allen, 1965; Pizzuto, 1987; Asselman and Middelkoop, 1995; Walling et al., 1996; Asselman and Middelkoop, 1998). As the water spreads across the floodplain, frictional losses and increasing flow depth can often result in additional decreases in flow velocity and transport capacity leading to a fining of deposited sediment with increasing distance from the channel (Walling et al. 1992; Asselman et al. 2003). In areas where advective transport dominates, theory suggests that the grain sizes will decrease gradually across a broad floodplain while narrow floodplains adjacent to a channel that are dominated by diffusive transport will fine more rapidly (Pizzuto, 1987; Adams et al. 2004).

The grain size distribution on the floodplain is a function of both the supply and the transport of sediment onto and across the floodplain from the channel and can vary spatially and temporally (Knox, 1987; Bridge, 2003). Additionally, the transport of fine sediment can be affected by flocculation which may alter the pattern of sediment deposited on the floodplain by changing the effective settling velocity of the aggregated particles relative to their individual or ultimate settling velocities (Nicholas and Walling, 1996; Nicholas and Walling, 1998).

3.1.2 Observations of Floodplain Sediment Particle Size Distribution

Fining of overbank sediment deposits with increasing distance from the channel has been observed on the Mississippi River, Powder River and elsewhere (e.g. Autin and Aslan, 2001; Moody et al., 1999). Moody et al. (1999) found that the narrow floodplain bench of the gravel and sand bedded Powder River fined with increasing distance from the channel. Though sand comprised about 18% of the suspended load of the Powder River and clay 47%, 55% of the sediment nearest the channel bank on the floodplain was sand and only about 10% in the floodplain trough. Conversely, the floodplain crest was

composed of 10% clay and the trough 40% (Moody et al., 1999). Adams et al. found that D50 of the surface sediment decreased exponentially across the width of the levees on the Saskatchewan River (2004). Walling and He (1998) observed a decrease in particle size with distance from the channel in surface sediments on small rivers in the UK, but differentiated two unique deposition processes, an exponential decrease in coarse sediment deposition with distance from the channel and a layer of fine sediment deposited in proportion to the depth of the overlying flood water in the distal floodplain or flood basin, likely the result of clay settling from impounded waters trapped on the plain following the initial flooding. Walling et al. (1997) found that most sand deposited within 20-40m from the channel following a large flood event on the River Ouse with a D50<100 μm near the channel and that D50 decreases to <20 μm beyond 100m from the relatively small channel. Marriot (1992) found a similar trend in the fining of floodplain sediment of the River Severn, UK, which was consistent with the diffusion model proposed by James (1985).

Because of the difficulty in sampling large floodplains with the resolution to resolve complex spatial patterns or adequately defining spatial patterns based on limited point sampling, relatively few studies have been done on large floodplains. Though studied extensively, there is little information about the lateral variation in particle size on many of the world's larger rivers such as the Amazon River (e.g. Dunne et al., 1998; Mertes, 1994; Dunne and Aalto, 2103). Thonon et al. (2007) found that sediment deposition pattern and particle size distribution were a function of distance from the channel on a relatively unconstrained reach of the Rhine system, but varied little on a diked reach. On the wider reach, less sand was deposited relative to the total amount of sediment delivered and clay and organic matter content increased with increasing distance from the channel. The Brahmaputra River system deposited sediment at a rate that decreases as a power law function with increasing distance from the channel, but there was very little channel bed material, in this case sand (2-6%) in the measured cores and deposits fined rapidly with increasing distance from the channel because of the near constant deposition rate of sand on the distal floodplain (Allison et al., 1998).

Perhaps the most detailed study of large lowland river floodplain deposition was conducted by Day et al. (2008) on the Fly River. The middle Fly River floodplain, unlike most other large lowland river floodplains, did not fine with increasing distance from the channel. Sand comprised about 5% of all floodplain sediment up to 1 km from the channel. The results of the particle size analysis on the Fly River are discussed more extensively throughout this chapter.

3.2 Methods

Core sample locations were reported in Chapter 2 and Day et al. (2008) Sediment subsamples were prepared then analyzed optically with a Coulter LS laser particle sizer based on the methods of Rowland et al. (2005). The Coulter LS was chosen for the analysis because of the ease of analysis and resolution over the desired range of particle

sizes that laser diffraction provides over other techniques such as sieve-hydrometer analysis (Wen et al. 2002). The Coulter LS measured light strength and scatter for 60 seconds while the sample was continuously stirred. The optical measurements were then converted to particle diameters with a range of 0.4-900 μm using the Fraunhofer model (Loizeau et al., 1994). Laser size diffraction provides precise results, but can produce errors when particles are non-spherical and does not measure or incorporate variable particle density into the calculations (Beuselinck et al., 1998). Typically, the presence of non-spherical particles results in the measurement of a broader distribution than is actually present, but the mean particle diameter is usually measured with reasonable accuracy despite the error in the distribution.

Surplus sediment samples from metals analysis (when available) or from slices adjacent to those analyzed for mineral content were subsampled for particle size distribution analysis. See Chapter 2 for description of the collection process. Approximately 0.5 mg of wet sediment was subsampled with a clean spatula and placed in pre-labeled glass beakers. The subsample was then suspended in 20 mL of ultrapure filtered water and stirred mechanically with the spatula. Approximately 5 mL of 30% H_2O_2 was added and each sample which was stored at room temperature for 24 to 48 hours to oxidize organic matter. If oxidation was still incomplete after 48 hours, as evidenced by continued effervescence, the sample was stored for an additional 24 hours. Samples were then stirred mechanically and sonicated in a hydrosonic water bath at 25 C for 5 minutes to break up any aggregated materials. A magnetic stirring rod was not used because magnetic sediments in the samples proved difficult to remove from the stirring rod. Subsamples of the material where then analyzed using a Coulter LS100 Laser Particle Sizer, hereafter referred to as the Coulter LS.

Output from the Coulter LS can be viewed as percent of subsample composition by number, area or volume as calculated from the particle diameter conversion. Since variable particle density is not considered the conversion to percent composition by mass was computed by multiplying the percent by volume by a constant particle density. The particle density of quartz, 2.65 g/cm^3, was assumed for all calculations below. Three consecutive measurements were averaged and the process was repeated with the same conserved sample until the result no longer changed from continued disaggregation of particles due to stirring in the Coulter LS analysis chamber and 2 standard deviations of the 3 consecutive measurements was small upon visual inspection of the plotted mean and deviation for each bin size. An example particle size distribution is plotted in Figure 3.3. The result of this analysis represents the ultimate or dispersed particle size distribution, but may not represent the effective or flocculated particle size that was transported *in situ* on the floodplain.

A total of 280 samples from 77 cores from the 8 transects on the Strickland River floodplain were analyzed. The spacing and distribution of subsamples is summarized in Figure 3.4 and Table 3.1. X-Ray images and ^{210}Pb geochronology of Strickland River floodplain cores showed banding several mm to dm thick indicative of distinct sediment

packages of similar grainsize (Aalto, 2008) which, when combined with the preserved spike in metal concentration assosciated with a large flood (Watson, 2006; Swanson et al., 2008), indicate a lack of mixing in the deposited sediments. In order to reduce the bias that may be introduced by under-sampling a core or only sampling individual sediment layers, several depths from cores were analyzed when subsamples were available. Generally, there were not enough samples from any single core to reliably evaluate upward fining or coarsening of sediment that may be caused by channel migration away from or towards a sediment core. About 65% of the analyzed samples were sectioned from the top 15cm of the cores. Only 7 cores and 10 subsamples were measured at 1-2 km from the channel, which may introduce a bias in the data towards the values nearer the channel. Cores were binned by distance, as was done in Chapter 2, and presented in Table 3.1. Particle size distributions (PSDs) from each distance bin were averaged to assess the lateral trends in grainsize.

The results of particle size and deposition rate as a function of distance from the channel were compared to the corresponding results from Day et al. (2008). Because combustion was used to eliminate organic matter from the Fly River floodplain samples, some of the clay and fine silt may not have been fully disaggregated during analysis. Thirty-five of the 281 samples analyzed by Day et al. for PSD had unusually coarse tails with measured diameters often exceeding 800 μm (>1% by volume >400 μm). Since sediment of this diameter was not evident in the suspended material in the channel and was not present in thin sections of the cores examined visually (Dietrich, personal communication), these 35 samples and an additional 14 cores with insufficient identifying data were excluded from the data set leaving 280 samples from 212 cores for comparison to the Strickland River floodplain sediments (Figure 3.5 and Table 3.2). The Fly River floodplain sediment subsamples adjacent to the surface sediment used for metals analysis (0.6-1.2 cm depth) were analyzed for particle size distribution. Some duplicate analyses were included. Duplicate analyses from the same depth of the same core (all samples are from 0.6-1.2 cm for Fly River PSD analysis) were averaged, leaving 212 samples for comparison with the Strickland River floodplain sediments. Sampling of the floodplain was more evenly spaced with distance from the channel when compared to the Strickland River sample spacing.

The magnitudes and trends in particle size distribution with increasing distance from the channel and possible differences in overbank transport between straight and curved reaches of the channel were explored. PSD is reported as the % by mass in particle size classes for clay, silt and sand sizes as well as the geometric mean grain size and 10^{th}, 50^{th} and 90^{th} percentile particle sizes by mass. These measures of grain size and distribution were chosen to display the absolute composition of the sediment samples as well as to adequately characterize trends in the spatial distribution of grainsizes on the floodplain. Though assessing the particle size distribution of the surface sediment is an important characterization of the 2-D floodplain surface (from the binned-average PSD) and can provide insight into the transport dynamics across the floodplain, characterizing the sediment delivered to the floodplain from the channel and the overall composition of

accumulated sediment stored in the floodplain can only be accomplished when the lateral variability in deposition rate and particle size distribution of deposited sediments are combined. The particle size distribution of the sediments that were delivered overbank were also calculated by combining the distance-dependent measured deposition rate for each floodplain with the binned average PSD. The PSD for this integrated sediment package is presented to both 1-km and 2-km since only one subsample was measured 2 km from the Strickland River floodplain channel and metals analysis from Day at al. (2008) and Swanson et al. (2008) defined the active zone of deposition as the first 1 km from the channel.

The overall percent contribution of each size class in the wedge of deposited sediment can be calculated from this depth-integrated approach. The total volume per unit width, $\forall$, of sediment deposited across the transect was calculated and the relative contribution of each size class, i, is evaluated,

$$\forall_i = \sum_{i,j} h_j * P_{ij} \cdot L_j \tag{3.1}$$

where $h(j)$ is the amount of sediment deposited annually at position j, P_{ij} is the percent composition of particle size class i at position j, and L_j is the length of the transect represented by the measurements taken at the given distance from the channel. The annual deposition rate is defined as the binned average deposition rate on the Strickalnd River floodplain (Swanson et al., 2008) or is calculated from the exponential deposition function for the Fly River floodplain (Day et al., 2008).

3.3 Results

3.3.1 Strickland River Floodplain Sediment Particle Size Distribution

Strickland River floodplain sediments decreased in size with distance from the channel. The median grain diameter by volume, D50, up to 100 m from the channel ranged from about 2-80 μm with a mean of 13.2 μm (Figure 3.6). The coarsest D50 occured 100 m from the right bank on the downstream section of transect 10 in a meander. The smallest D50 was observed at the most distal core sampled, 2000 m from the left bank at the downstream most transect, transect 1. The binned average data for D50 are presented in Figure 3.7 and Table 3.3. The binned-average D50 decreased from 15.7 to 2.0 μm with increasing distance from the channel.

The smallest 10% of the sediment by volume, D10, was dominated by clay size material. The D10 data ranges from 0.6 to 9.0 μm with a bulk mean of 1.3 μm (Figure 3.6). The lower bound of the range was probably influenced by the smallest discernible diameter measured by the Coulter LS, 0.4 μm. The maximum D10 occurred just 5 m from the right

bank of transect 15 in what was most likely a bar. The distance averaged D10 decreased from 1.5 μm near the channel to 0.7 μm 2 km from the channel (Figure 3.7).

The coarsest 10% of the sediment measured across the entire floodplain was dominated by coarse silt (Figure 3.6). The coarsest D90, 165.8 μm, was sampled 100 m from the right bank on the downstream section of transect 10, where the coarsest median grain size was also observed. The D90 decreased sharply away from the channel, but the minimum D90, 5.1 μm, occurred 150 m from the right bank of transect 2, a relatively swampy region of the lower floodplain. The binned averaged D90 decreased from 68.9 to 7.2 μm with increasing distance from the channel (Figure 3.7).

The geometric mean grain size calculated from the binned average data, presented in Figure 3.8, was 12.6 μm near the channel bank and decreased non-linearly with increasing distance from the channel to 2.2 μm 2 km from the bank. A logarithmic function fit to the data explains nearly 70% of the variation in mean particle diameter with distance from the channel.

The cumulative percent of sediment finer than a given grain size is plotted in Figure 3.9 for all Strickland River floodplain samples analyzed. Though some samples were relatively coarse, it is evident from this plot that the majority of the samples were dominated by clay and silt sizes.

The binned-average cumulative percent composition is plotted in Figure 3.10. The binned-average 5 m from the channel was the coarsest and the binned-averages 1000-m and 2000 m from the channel were the finest. Though the trend was not absolute, the concave downward curves generally represent cores >500m from the channel and the concave upward curves represent cores much closer to the channel. This indicates a fining of sediment with distance from the channel.

The Strickland River floodplain sediments were dominated by clay and silt. This was further demonstrated by the plots of the D10, D50 and D90 as a percent by number of the same samples (Figure 3.11). The calculated D10 by number was less than the lower bound of the Coulter LS for all samples and was interpolated from the slope of the cumulative % finer than PSD at the lower bound. The D50 and D90 were also clay dominated when calculated as a percent by number. This is especially important for tracking heavy metal-contaminated sediments because the metals adhere to surfaces and the highest concentrations are associated with the smallest particles (Ackroyd et al., 1986; Stewart and Thomson, 1997).

There was a noticeable decrease in sand composition and increase in clay composition with increasing distance from the channel on the Strickland River floodplain (Figure 3.12 Binned-average clay silt and sand size fractions are plotted in Figure 3.13. and Table 3.3 lists the binned-average for 0-2 μm, 2-8 μm, 8-16 μm, 16-32μm, 32-64μm, 64-128 μm

and >128 μm diameter particles. The percent by volume of clay (<2 μm), very fine silt (2-8 μm), fine silt (2-16 μm), medium silt (16-32 μm), coarse silt (32-62 μm) and sand (>62 μm) and the relative magnitude and contribution of each size class to the annual deposition function are shown in Figure 3.14 and Table 3.4.

Clay content increased from 13% to 50% of the measured sediments from 5 to 2000 m respectively (Figures 3.13 and 3.14). From equation 3.1, 22.5% of the sediment deposited on the floodplain, by volume, was clay to 1-km and 28.1% to 2 km (Figure 3.14 and Table 3.4). Though the percent clay increased with increasing distance from the channel, the relative increase in clay content was offset by the decrease in deposition rate on the distal floodplain (Figure 3.14).

Silt content initially increased with increasing distance across the floodplain from the Strickland River, but decreased at 1-km and 2 km from the channel (Figure 3.13 and Table 3.3). This may have been due to the preferential deposition of sand near the channel leading to a reatively larger proportion of silt in the water column. Silt content increased from 72.9% 5 m from the channel to 79.1% 450 m from the channel and decreased to 62.3% 1 km from the channel (Table 3.3). Distal samples, 1–km and 2 km from the channel, contained mostly very fine silt 2-8 μm in diameter. Coarser silts were more abundant <450m from the channel. Very fine silt also dominated the composition of the floodplain deposits (as calculated from equation 3.1) comprising 36.9% and 40.2% of the deposited sediments to 1 and 2 km respectively (Table 3.4). All silt (2-64 μm) comprised 78.0% and 70.3% of the deposited volume to 1 and 2 km respectively.

Sand content decreased from 13.3% 5 m from the channel to 0.1% 1 km from the channel and 0% 2 km from the channel (Figures 3.13 and 3.14). Coarse sand, ≥128μm, comprised only 0.5% of the sediment deposited 5 m from the channel and was not found in any samples beyond 300 m from the channel (Table 3.3). Only a fraction of a percent of any samples beyond 300 m was composed of fine sand, 64-128 μm (Table 3.3). Volume integration of the deposited floodplain sediments yielded a sand content of only 2.2% by volume to 1-km and 1.5% to 2-km (Table 3.4).

As demonstrated in Chapter 2, the rate of deposition in curved reaches was higher than in straight reaches. More samples were collected from curved reaches (n=208) than straight reaches (n=72), but all samples analyzed for PSD beyond 400m from the channel were collected at straight reaches. There was not a significant difference in mean particle diameter between these two populations (Figure 3.15 t-test P=0.19). This held true for D50 and D90, indicating that the average and larger particle sizes were transported equally on the floodplain adjacent to both straight and curved reaches.

The D10 appeared to be larger for curved reaches than straight reaches, plotted in Figure 3.16. A t-test indicates that there was a statistically significant difference between the two groups ($P=10^{-8}$). This may indicate that overbank flow adjacent to curved reaches was

more energetic than flow adjacent to straight reaches and fine sediment was kept in suspension rather than depositing near the channel. Increased turbulence may also break apart flocculated particles that would otherwise settle. This difference was only observed in the smallest size fraction and not in the other size classes.

3.3.2 Fly River Floodplain Sediment Particle Size Distribution

Middle Fly River floodplain sediments were coarsest directly adjacent to the channel, but did not appear to fine with increasing distance beyond the channel bank (Day et al., 2008). Measurements of D10, D50and D90 from all of the sampled cores are presented in Figure 3.17. There was more variability in the measurements near the channel where sampling density was higher, but this could also be a result of heterogeneous deposition patterns near the channel bank.

The D50 by volume ranged from 3.2 to 100.2 μm (Figure 3.17). The coarsest D50 occurred 10m from the bank on transect 1; the finest D50 occurred 50 m from the bank on transect 3. The binned-average data for Fly River floodplain sediments are presented in Figure 3.18 and Table 3.5. Binned-average D50 was greatest 10 m from the channel, 18.2 μm, and least 50 m from the channel, 9.2 μm. The mean and the standard deviation of the binned-average D50 data were 12.3 μm and 2.3 μm respectively.

The D10 ranged from 0.98-7.3 μm with the coarsest D10 10 m from the bank on transect 1 and the finest 50 m from the bank on transect 3. Binned-average D10 was also greatest 10 m from the channel, 3.1 μm, and least 1000-1200 m from the channel, 1.8 μm. It should be noted that the binned-average D10 was also 1.8 μm 50-m and 250 m from the channel. The mean and the standard deviation of the binned-average D10 data were 2.2 μm and 0.36 μm respectively.

The D90 by volume ranged from 10.2-163.1 μm (Figure 3.17). The coarsest D90 occurred 10 m from the bank on transect 1; the finest D90 occurred 400 m from the bank on transect 7. The binned-average D90 was greatest 10 m from the channel, 110.5 μm, and least 1000-1200 m from the channel, 34.8 μm. The D90 >2400 m from the channel was also 34.8 μm. The mean and the standard deviation of the binned-average D90 data were 46.5 μm and 17.5 μm respectively.

Mean diameter ranged from 3.9-69.9 μm. The minimum value occurred 400 m from the nearest channel on transect 7 and the largest 10 m from the channel on transect 1. Binned-average mean particle diameters are reported in Table 3.5 and ranged from 8.8 μm 50 m from the channel to 17.7 μm 10 m from the channel with a mean and standard deviation of 11.1 and 2.1 μm respectively. Geometric mean diameter of floodplain sediments was also coarsest nearest the channel but did not decrease with distance from the nearest channel systematically as mean diameter did for Strickland River floodplain sediments (Figure 3.19). Unlike the trend for the Strickalnd River floodplain sediments,

a best fit function, an exponential function, explained just 10.78% of the trend in this data. With the exception of the 10 m average, the data were between 8 and 14 μm and more closely resemble a horizontal line than an exponential or decreasing function.

The cumulative percent of sediment finer than a given grain size is plotted in Figure 3.20 for all Fly River floodplain samples analyzed. Very few (4) of the particle size distributions plotted were more than a few percent by volume greater than 100 mm. The binned-average cumulative PSDs are plotted in Figure 3.21. The distributions were very similar to one another with the exception of the 10-m average that was coarser than the other distributions.

Much like the observations on the Strickland River, the percent by number PSDs for the Fly River floodplain sediments indicated a very fine floodplain (Figure 3.22). Most D10 values were <0.5 μm (all but 7 values) and only 1 measurement had a D10 by number greater than 2 μm. The D10 by number was 3.53 μm 1600 m from the nearest channel on transect 10. That same sample also had the coarsest D50 and D90 measured. The D50 measurements ranged from 0.58 to 4.74 μm. All D50 measurements except for the maximum were below 1 μm. The D90 measurements ranged from 1.26-8.35 μm with all measurements other than the max not exceeding 2.6 μm.

Percent clay did not vary strongly with distance from the middle Fly River channel (Figure 3.23). Binned-average floodplain sediments were 6.6-13.6% clay with no clear trend in clay content with distance from the channel (Table 3.5 and Figure 3.24). The volume integration calculation yielded 9.3% clay by volume to both 1-km and 2 km from the channel bank (Table 3.6).

Silt was the greatest contributor to middle Fly River floodplain sediments; 75.8-91.6% of binned-average sediment composition (Figure 3.24, Table 3.5). Silt content increased slightly with increasing distance from the channel as sand content and clay content droped (Figures 3.24 and 3.25). Very fine, fine and medium slit each contributed ~17-35% to the sediment composition while coarse and very coarse silt contributed ~1-14% (Table 3.6). The volume integrated silt content was 85.4% to 1-km and 85.6% to 2-km.

Though the highest sand content values were near the channel, there was not a trend in sand content with distance from the channel (Figure 3.23, 3.24). Fromthe binned-averages, sand comprised 17.6% of the sediment 10 m from the channel but ranged from 1.2-6.4% from 20 to >2400 m from the channel with no clear dependence on distance (Table 3.5). The volume integrated sand content was 5.3% to 1-km and 5.2% to 2-km.

Instead of sediment fining as coarser particles settle out, the sediment deposited on the middle Fly River floodplain appeared to coarsen slightly with the relative contribution of medium silt increased slightly and the relative contributions of very fine silt and clay decreased slightly with increasing distance from the channel (Figure 3.25).

3.4 Discussion

The Strickland River floodplain deposits were dominated by silt and clay and only a small fraction of the floodplain was composed of sand-the dominant bed material. Floodplains and flood basins are typically composed of washload when overbank deposition is a primary mechanism for building and storing sediment in the floodplain (Bridge, 2003). The floodplain sediment deposits also fined with increasing distance from the channel, as one would expect based on differential settling velocities of particles of differing diameters being transported away from the channel (Allen, 1965; Pizzuto, 1987; Asselman and Middelkoop, 1995, Adams et al., 2004; Dunne and Aalto, 2013). Most sand was deposited in the first 400 m from the channel. Though most previous studies of floodplain particle size distribution (e.g. Pizzuto, 1997; Asselman and Middelkoop, 1995; Walling et al, 1996) noted little to no sand at this distance, the Strickland River and floodplain sediments were much larger than most of those studied. The distance sand traveled was likely limited by the strength of lateral advection and turbulence in the shear layer between the floodplain and channel. The D50 and mean particle diameter decreased exponentially with increasing distance from the channel as was observed on floodplains by Walling and He (1998) and in levee deposits by Adams et al. (2004).

Fine sediments were inhibited from depositing on meander reaches of the floodplain as indicated by a larger D10. This effect was not observable in the distal floodplain, possibly because of the spatial distribution of sampling sites. The D50, D90 and mean particle sizes of meandering and straight floodplain reaches were not distinguishable. This may indicate that a stronger advective flow, either lateral or longitudinal, generated a shear stress that reduces clay and silt deposition. It is likely that the flow was much stronger across the floodplain between meanders and fine sediments, clay and fine silt, which would normally be flocculated, are broken apart resulting in slower effective settling velocities. The slower settling velocities result in a lower deposition rate in these floodplain sections.

The pattern and particle size distribution of deposition on the lower Strickland River floodplain differed distinctly from the pattern of floodplain sediment deposition on the middle Fly River. Deposition rate on the Strickland River floodplain decreased with increasing distance from the channel, but not exponentially, and grain size decreased exponentially with increasing distance from the channel. Deposition rate decreased exponentially away from the channel on the Fly River floodplain, but the grain size of floodplain sediments was markedly constant as a function of distance from the channel. The differing patterns of both the rate and particle size distribution of deposited sediments on the Fly and Strickland River floodplains indicate that there is a difference in the overbank process that builds these floodplains despite their shared geology and sea-level rise history.

The dispersal of coarse sediment across the floodplain can be observed in crevasse splays on other rivers (Aalto et al. 2003), but energetic flows across the floodplain, crevasse splays, and levee failures were not observed on the Fly during the study period where sand content in deposited sediment was nearly uniform spatially. A more reasonable explanation for the pattern of deposition on the Fly River floodplain may be the relative strength or influence of flocculation on particle settling velocities. By increasing the effective settling velocity of fine sediment and decreasing the effective settling velocity of coarse grained particles (Mertes, 1997; Manning, 2001; Winterwerp and van Kesteren, 2004; Manning and Schoellhamer, in review), flocculation may be able to produce the observed pattern of deposition on the swampy Fly River floodplain. Flocculation may also occur on the Strickland River floodplain, but with better drainage and less organic-rich standing water on the floodplain, it is likely that flocculation would be weaker or less prominent on the Strickland River floodplain. This hypothesis is explored further in the next chapter.

Tables

	Distance From Channel (m)																
	5	20-25	50	75	100	135	150	200	240-250	275-325	350	400-425	475-625	900	1000-1025	1450	1875-2000
Number of transects	6	4	7	2	6	1	5	2	4	3	2	1	1	0	4	0	1
Number of Cores	11	4	14	3	8	1	5	3	5	4	2	1	1	0	5	0	1
Number of Subsamples	49	14	64	8	51	7	31	5	13	16	3	7	1	0	9	0	1

Table 3.1 The number of transects, cores and subsamples analyzed at each distance from the Strickland River.

	Distance From Channel (m)																
	10	20	50	100	130-150	200	250	300	400	500	600	700-750	800	900	1000-1200	1300-2000	≥2400
Number of transects	7	3	7	11	6	10	5	12	10	11	9	6	7	6	7	11	2
Number of Cores	12	4	10	27	11	25	6	22	18	14	13	7	8	8	10	13	4
Number of Subsamples	22	5	15	37	15	39	7	30	18	14	13	11	8	14	13	13	6

Table 3.2 The number of transects, cores and subsamples analyzed at each distance from the Fly River.

	Distance From Channel (m)																
	5	25	50	75	100	135	150	200	248	296	350	400	450	900	1000	1450	2000
Mean D µm	12.6	5.8	9.6	7.2	8.4	4.1	8.5	9.2	6.2	6.8	4.4	5.1	5.2	-	2.8	-	2.2
D10	1.5	1.1	1.3	1.2	1.2	0.9	1.2	1.1	1.1	1.1	1.0	1.0	1.1	-	0.8	-	0.7
D50	15.7	5.9	10.5	7.8	9.0	4.2	9.2	11.2	6.7	7.3	4.7	5.4	5.8	-	2.8	-	2.0
D90	68.9	29.4	57.2	37.8	47.3	17.8	49.2	53.7	29.1	33.3	17.4	21.7	19.6	-	9.3	-	7.2
<2 µm %	13.8	21.2	16.5	18.9	17.7	27.3	18.3	19.5	20.1	19.3	25.1	22.8	20.9	-	37.5	-	50.3
2-8 µm	23.1	37.7	27.6	32.0	29.5	44.5	28.7	24.7	35.0	33.7	42.8	39.6	40.2	-	49.6	-	41.2
8-16 µm	8.5	11.6	9.4	11.0	10.4	11.5	9.2	7.5	12.9	12.2	13.5	13.4	15.2	-	6.8	-	3.1
16-32 µm	21.1	21.3	21.9	24.4	23.3	14.1	22.7	23.4	23.9	24.4	18.0	20.8	22.8	-	5.2	-	5.5
32-64 µm	20.2	7.7	16.3	12.4	14.4	2.5	15.8	18.2	6.6	7.5	0.6	3.3	0.9	-	0.6	-	0.1
64-128 µm	12.8	0.5	8.0	1.3	4.3	0.2	5.2	6.7	1.5	2.6	0	0.1	0	-	0.1386	-	0.0
>128 µm	0.5	0	0.3	0	0.5	0	0.02	0.01	0.00	0.4	0	0	0	-	0	-	0

Table 3.3 Binned averages of sediment size measurements on the Strickland River. Percent composition calculations are subject to rounding errors.

Total distance	Grain size class µm						
	0-2	2-8	8-16	16-32	32-62	62-128	>128
1000	22.5%	36.9%	17.3%	13.5%	7.6%	2.1%	0.1%
2000	28.1%	40.2%	14.4%	10.3%	5.4%	1.4%	0.1%

Table 3.4 Relative contribution to the total volume of each size class of sediment deposited on the Strickland River floodplain when computed to 1 and 2 km.

	Distance From Channel (m)																
	10	20	50	100	130-150	200	250	300	400	500	600	700-750	800	900	1000-1200	1300-2000	≥2400
Mean D μm	17.7	10.7	8.8	9.8	12.4	9.7	9.2	11.0	11.4	11.5	11.4	9.9	10.0	12.3	8.8	12.5	11.1
D10	3.1	2.1	1.8	2.0	2.3	1.9	1.8	2.0	2.3	2.0	2.2	2.1	2.0	2.1	1.8	2.9	2.6
D50	18.2	11.3	9.2	10.7	14.0	10.1	9.9	11.9	13.0	13.6	12.9	10.9	11.3	14.3	9.7	14.8	13.0
D90	110.5	43.9	38.3	39.8	53.2	43.9	39.3	48.7	42.6	46.0	43.8	37.3	39.8	55.1	34.8	38.7	34.8
<2 μm %	6.6	10.7	13.3	11.5	9.8	12.6	13.5	11.5	9.3	11.2	10.0	11.0	11.4	11.0	13.6	7.0	8.1
2-8 μm	22.9	31.8	35.7	32.7	26.9	33.6	33.5	30.2	28.9	27.5	28.7	32.3	31.1	27.0	33.8	25.6	26.2
8-16 μm	19.9	22.2	22.6	22.6	20.9	20.8	19.6	20.7	22.3	19.5	21.9	23.9	23.0	18.0	22.2	24.9	27.4
16-32 μm	20.7	20.7	17.0	20.7	22.1	18.7	20.9	21.7	24.3	24.0	24.2	21.7	21.7	22.8	21.0	29.8	26.9
32-64 μm	12.4	10.3	8.8	10.2	15.0	9.8	10.1	10.0	12.9	14.3	11.4	7.9	11.1	14.7	8.3	11.4	7.8
64-128 μm	12.3	2.3	1.8	1.8	4.3	3.4	1.8	4.1	1.6	2.4	2.6	2.3	1.4	5.0	0.8	1.1	1.2
>128 μm	5.3	2.0	0.8	0.5	1.0	1.1	0.5	1.8	0.7	1.1	1.2	0.8	0.4	1.4	0.4	0.2	0.5

Table 3.5 Binned averages of sediment size measurements on the Fly River floodplain. Percent composition calculations are subject to rounding errors.

Total distance	Grain size class μm						
	0-2	2-8	8-16	16-32	32-62	62-128	>128
1000	9.3%	29.0%	20.9%	21.7%	13.9%	3.7%	1.5%
2000	9.3%	28.9%	21.0%	21.8%	13.8%	3.7%	1.5%

Table 3.6 Relative contribution to the total volume of each size class of sediment deposited on the Fly River floodplain when computed to 1 and 2 km.

References

Aalto, Rolf, et al. "Episodic sediment accumulation on Amazonian flood plains influenced by El Nino/Southern Oscillation." *Nature* 425.6957 (2003): 493-497.

Ackroyd, DR el, et al. "Distributions and behaviour of dissolved Cu, Zn and Mn in the Tamar Estuary." *Estuarine, Coastal and Shelf Science* 23.5 (1986): 621-640.

Adams, Peter N., Rudy L. Slingerland, and Norman D. Smith. "Variations in natural levee morphology in anastomosed channel flood plain complexes."*Geomorphology* 61.1 (2004): 127-142.

Allen, John RL. "A review of the origin and characteristics of recent alluvial sediments." *Sedimentology* 5.2 (1965): 89-191.

Allen, J. R. L. "Studies in fluviatile sedimentation: an exploratory quantitative model for the architecture of avulsion-controlled alluvial suites." *Sedimentary Geology* 21.2 (1978): 129-147.

Allison, M. A., et al. "Importance of flood-plain sedimentation for river sediment budgets and terrigenous input to the oceans: Insights from the Brahmaputra-Jamuna River." *Geology* 26.2 (1998): 175-178.

Asselman, Nathalie EM, and Hans Middelkoop. "Floodplain sedimentation: quantities, patterns and processes." *Earth Surface Processes and Landforms*20.6 (1995): 481-499.

Asselman, Nathalie EM, Hans Middelkoop, and Paul M. Van Dijk. "The impact of changes in climate and land use on soil erosion, transport and deposition of suspended sediment in the River Rhine." *Hydrological Processes* 17.16 (2003): 3225-3244.

Beuselinck, Laurent, et al. "Grain-size analysis by laser diffractometry: comparison with the sieve-pipette method." *Catena* 32.3 (1998): 193-208.

Bridge, John S. *Rivers and floodplains: forms, processes, and sedimentary record*. Wiley. 2009.

Day, Geoff, et al. "The depositional web on the floodplain of the Fly River, Papua New Guinea." *Journal of Geophysical Research: Earth Surface (2003–2012)*113.F1 (2008).

Dunne, Thomas, et al. "Exchanges of sediment between the flood plain and channel of the Amazon River in Brazil." *Geological Society of America Bulletin*110.4 (1998): 450-467.

Dunne, T. and R. E. Aalto. “Large River Floodplains” in John F. Schroder (ed.) *Treatise on Geomorphology*, 9 (2013): 645-678.

Higgins, Roger J. "Off.river storages as sources and sinks for environmental contaminants." *Regulated Rivers: Research & Management* 5.5 (1990): 401-412.

James, C. S. "Sediment transfer to overbank sections." *Journal of Hydraulic Research* 23.5 (1985): 435-452.

Knox, James C. "Historical valley floor sedimentation in the Upper Mississippi Valley." *Annals of the Association of American Geographers* 77.2 (1987): 224-244.

Loizeau, J-L., et al. "Evaluation of a wide range laser diffraction grain size analyser for use with sediments." *Sedimentology* 41.2 (1994): 353-361.

Mackey, Scudder D., and John S. Bridge. "Three-dimensional model of alluvial stratigraphy: theory and application." *Journal of Sedimentary Research* 65.1 (1995).

Malmon, Daniel V., et al. "Influence of sediment storage on downstream delivery of contaminated sediment." *Water Resources Research* 41.5 (2005): W05008.

Manning, A.J. A study of the effects of turbulence on the properties of flocculated mud. Ph.D. Thesis. Institute of Marine Studies, University of Plymouth, Plymouth, UK, (2001): 282p.

Manning, A.J., and D.H. Schoellhamer, “Sediment floc characteristics in San Francisco Bay, USA” *Marine Geology* (*In review)*.

Marriott, Susan. "Textural analysis and modelling of a flood deposit: River Severn, UK." *Earth Surface Processes and Landforms* 17.7 (1992): 687-697.

Marriott, S. B. "The use of models in the interpretation of the effects of base-level change on alluvial architecture." *Fluvial Sedimentology VI:(Special Publication 28 of the IAS)* 28 (1999): 271.

Mertes, Leal AK. "Rates of flood-plain sedimentation on the central Amazon River." *Geology* 22.2 (1994): 171-174.

Mertes, Leal AK. "Documentation and significance of the perirheic zone on inundated floodplains." *Water Resources Research* 33.7 (1997): 1749-1762.

Middelkoop, Hans, and Nathalie EM Asselman. "Spatial variability of floodplain sedimentation at the event scale in the Rhine–Meuse delta, The Netherlands."*Earth Surface Processes and Landforms* 23.6 (1998): 561-573.

Moody, John A., James E. Pizzuto, and Robert H. Meade. "Ontogeny of a flood plain." *Geological Society of America Bulletin* 111.2 (1999): 291-303.

Nicholas, A. P., and D. E. Walling. "The significance of particle aggregation in the overbank deposition of suspended sediment on river floodplains." *Journal of Hydrology* 186.1 (1996): 275-293.

Nicholas, A. P., and D. E. Walling. "Modelling flood hydraulics and overbank deposition on river floodplains." *Earth Surface Processes and Landforms* 22.1 (1997): 59-77.

Pizzuto, James E. "Sediment diffusion during overbank flows." *Sedimentology*34.2 (1987): 301-317.

Rinklebe, Jörg, Christa Franke, and Heinz-Ulrich Neue. "Aggregation of floodplain soils based on classification principles to predict concentrations of nutrients and pollutants." *Geoderma* 141.3 (2007): 210-223.

Rowland, Joel C., et al. "Tie channel sedimentation rates, oxbow formation age and channel migration rate from optically stimulated luminescence (OSL) analysis of floodplain deposits." *Earth Surface Processes and Landforms* 30.9 (2005): 1161-1179.

Stewart, C., and J. A. J. Thompson. "Vertical distribution of butyltin residues in sediments of British Columbia harbours." *Environmental Technology* 18.12 (1997): 1195-1202.

Stouthamer, Esther. "Sedimentary products of avulsions in the Holocene Rhine–Meuse delta, The Netherlands." *Sedimentary Geology* 145.1 (2001): 73-92.

Swanson, Kathleen M., et al. "Sediment load and floodplain deposition rates: Comparison of the Fly and Strickland rivers, Papua New Guinea." *Journal of Geophysical Research: Earth Surface (2003–2012)* 113.F1 (2008).

Thonon, Ivo, et al. "Modelling floodplain sedimentation using particle tracking." *Hydrological processes* 21.11 (2007): 1402-1412.

Walling, D. E., T. A. Quine, and Q. He. "Investigating contemporary rates of floodplain sedimentation." *Lowland floodplain rivers: Geomorphological perspectives* (1992): 165-184.

Walling, D. E., Qand He, and A. P. Nicholas. "Floodplains as suspended sediment sinks." *Floodplain processes* (1996): 399-440.

Walling, D. E., P. N. Owens, and G. J. L. Leeks. "The characteristics of overbank deposits associated with a major flood event in the catchment of the River Ouse, Yorkshire, UK." *Catena* 31.1 (1997): 53-75.

Walling, D. E., and Q. He. "The spatial variability of overbank sedimentation on river floodplains." *Geomorphology* 24.2 (1998): 209-223.

Wen, Baoping, Adnan Aydin, and Nurdan S. Duzgoren-Aydin. "A comparative study of particle size analyses by sieve-hydrometer and laser diffraction methods." *ASTM geotechnical testing journal* 25.4 (2002): 434-442.

Winterwerp, Johan C., and Walther GM Van Kesteren. *Introduction to the physics of cohesive sediment dynamics in the marine environment*. Access Online via Elsevier, 2004.

Figures

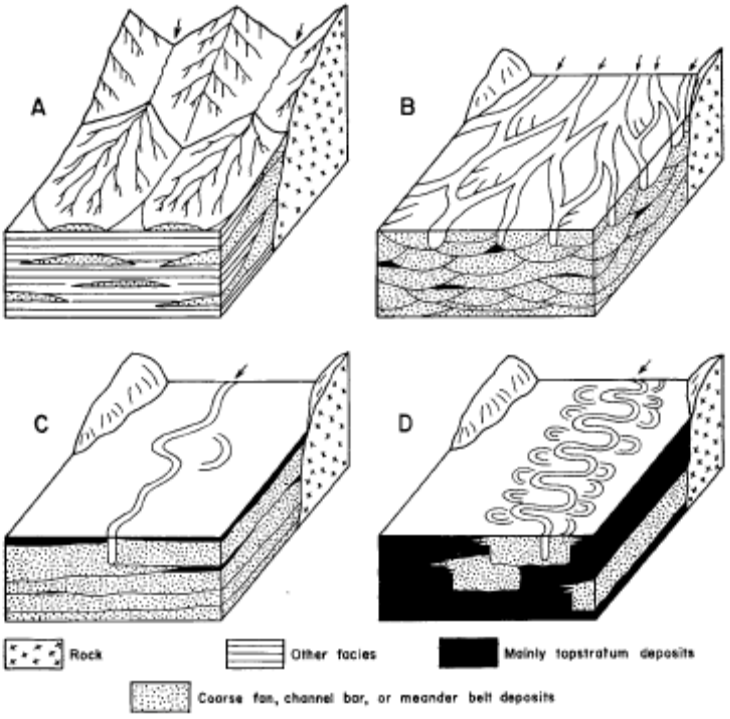


Figure 3.1 From Allen (1965), these hypothetical models of particle size distribution and geometry of common alluvial facies. A. Alluvial fan. B. Braided stream. C. Low sinuosity stream. D. Meandering stream.

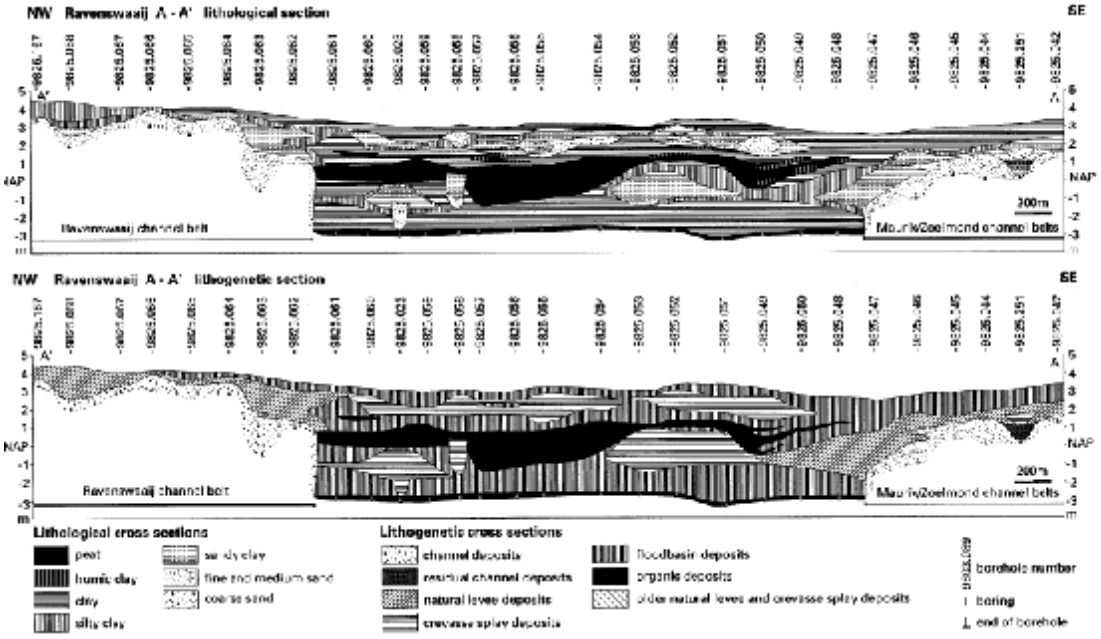


Figure 3.2. The particle size distribution (top) and stratigraphic interpretation (bottom of a cross section of a floodplain transect from Stouthamer (2001). Sandy clay are crevasse-splay and levee deposits while clay is generally a floodbasin deposit.

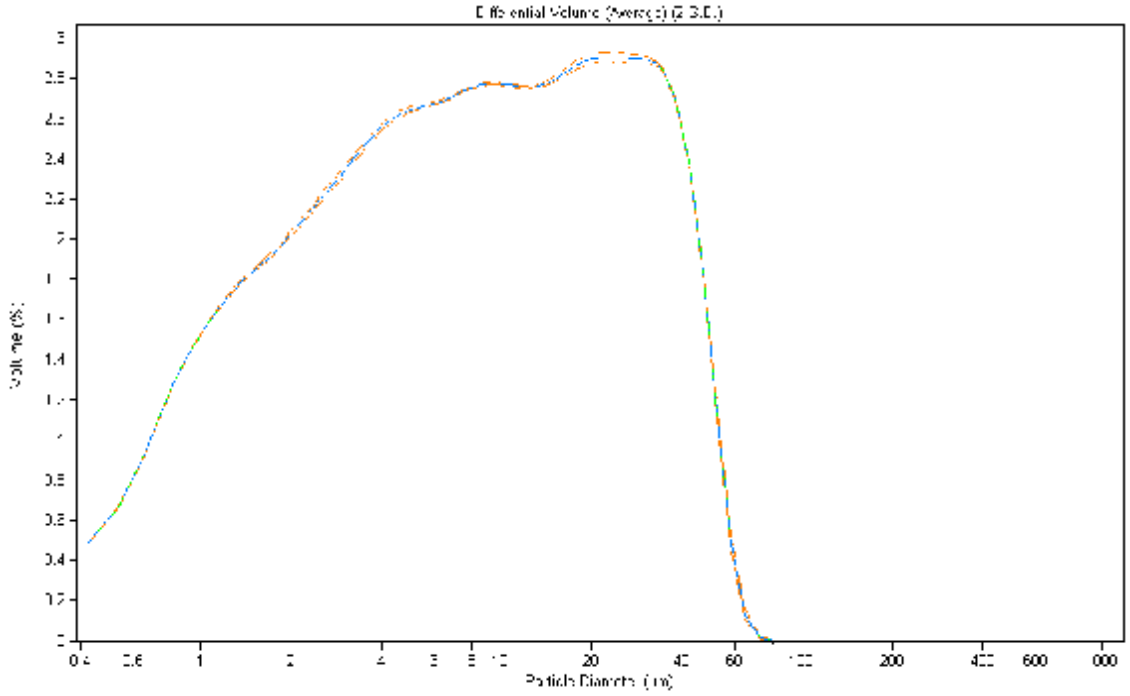


Figure 3.3 Sample Coulter LS result from transect 2 left bank 100 m from channel 10-11 cm depth. The blue line represents the average percent by volume as a function of particle diameter of 3 1-min sample analyses and the dashed orange lines indicate 2 standard deviations from the mean.

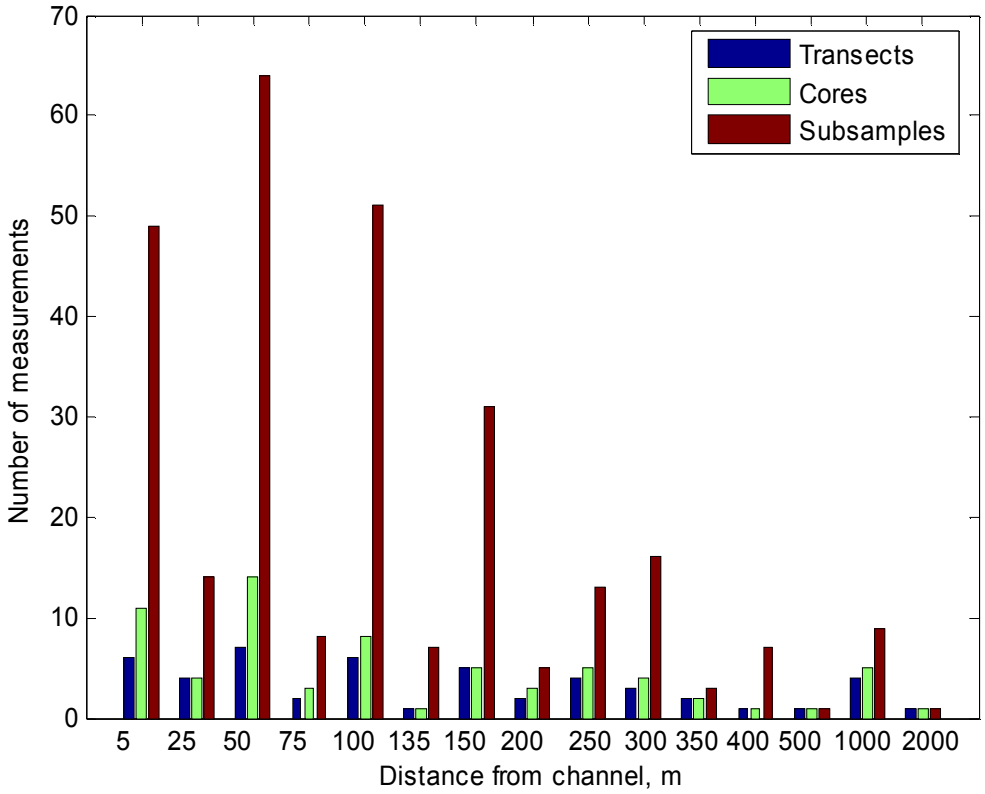


Figure 3.4 The number of transects, cores and subsamples analyzed at each distance from the Strickland River channel.

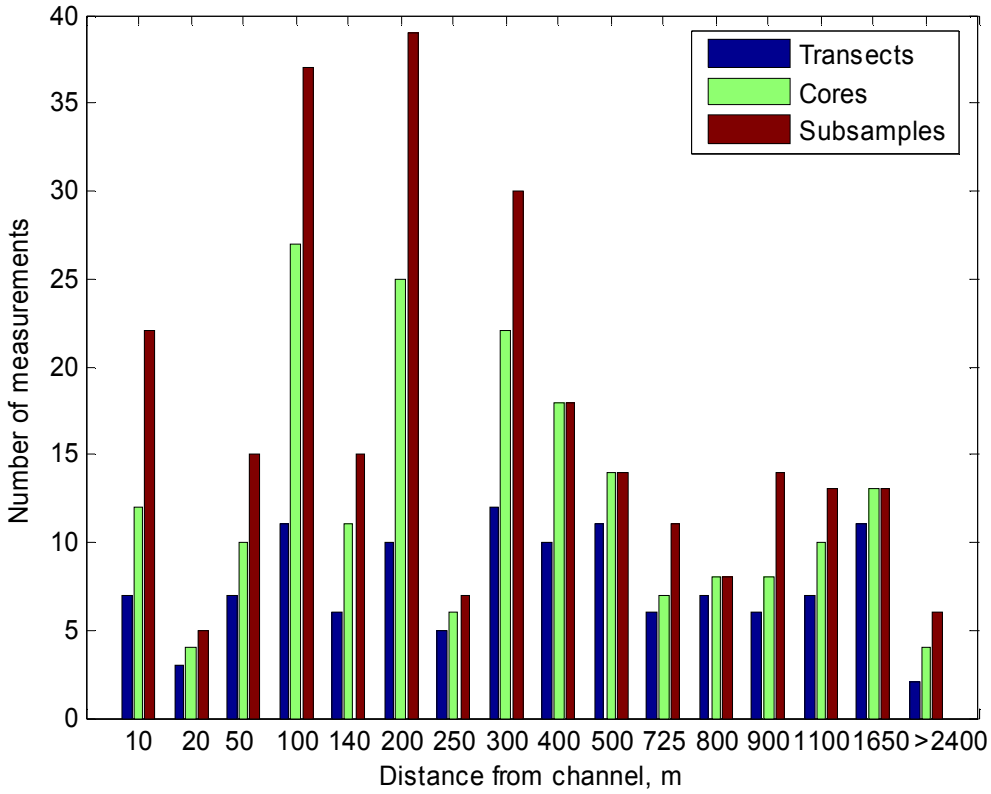


Figure 3.5 The number of transects, cores and subsamples analyzed at each distance from the Fly River channel. Median values are used when data is binned for more than a single distance from the channel.

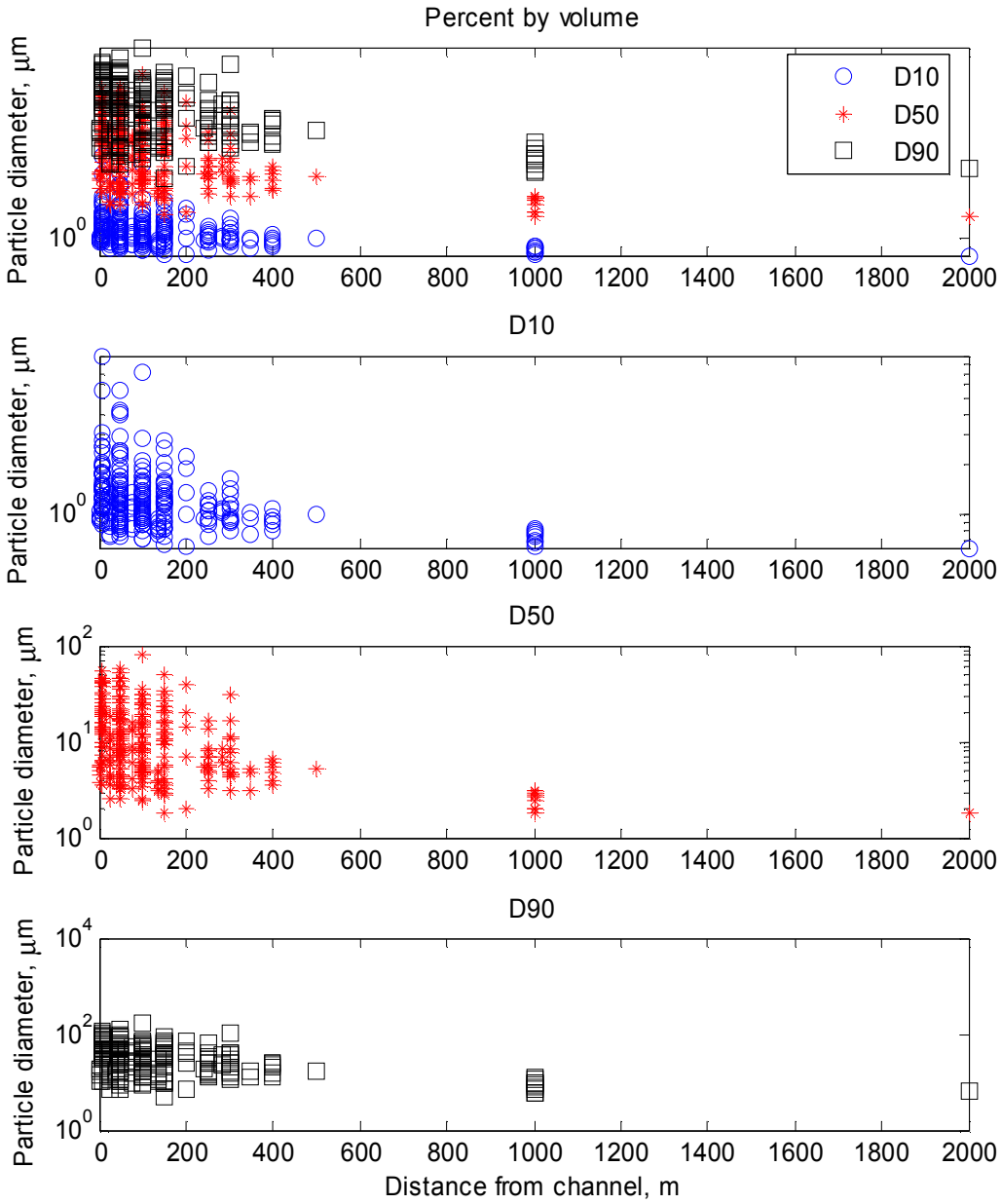


Figure 3.6 Strickland River floodplain sediments D10, D50 and D90 as a function of distance from channel.

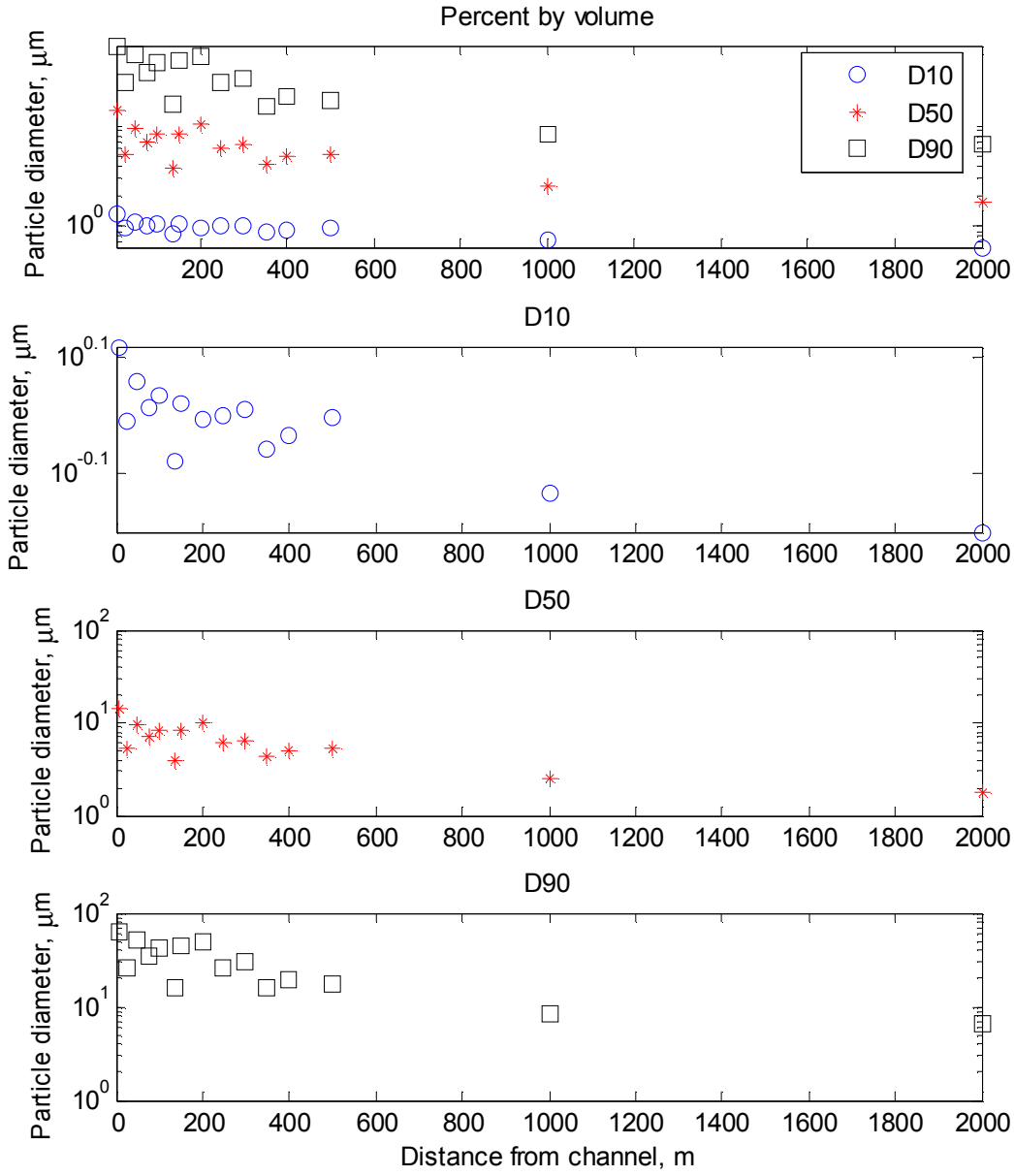


Figure 3.7 Binned-average Strickland River floodplain sediments D10, D50 and D90 as a function of distance from channel.

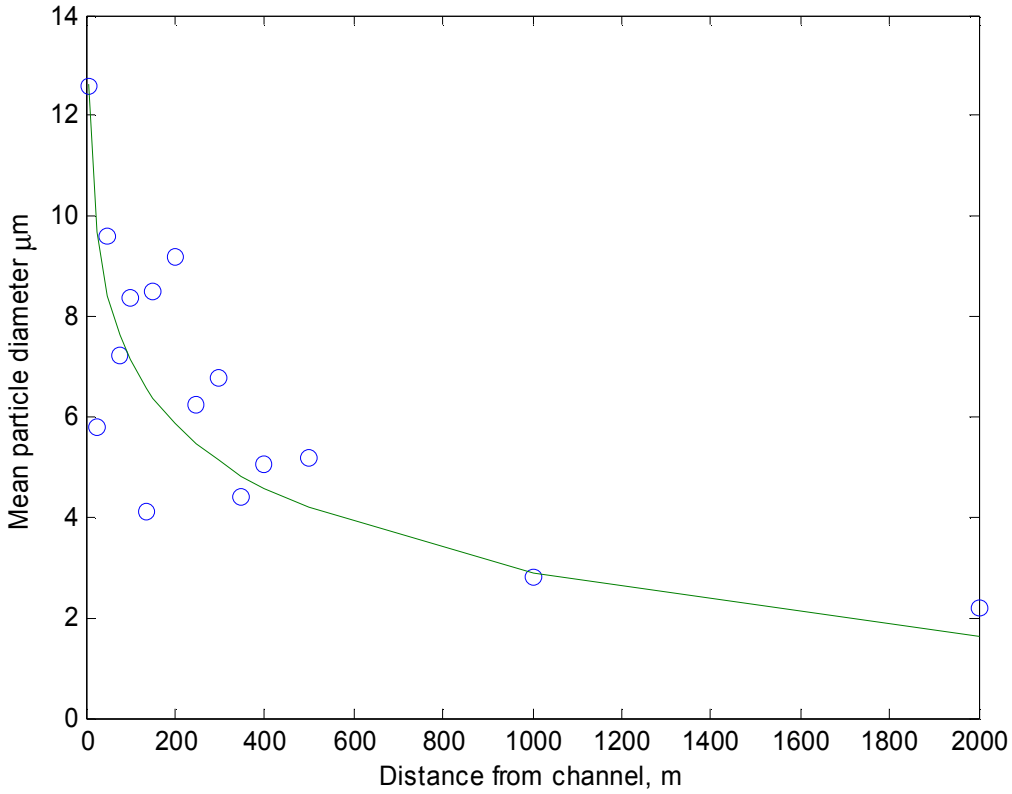


Figure 3.8 Binned-averaged mean particle diameter for lower Strickland River floodplain sediments. The green line represents the best fit function $y = -1.832\ln(x) + 15.561$ and $R^2 = 0.6967$.

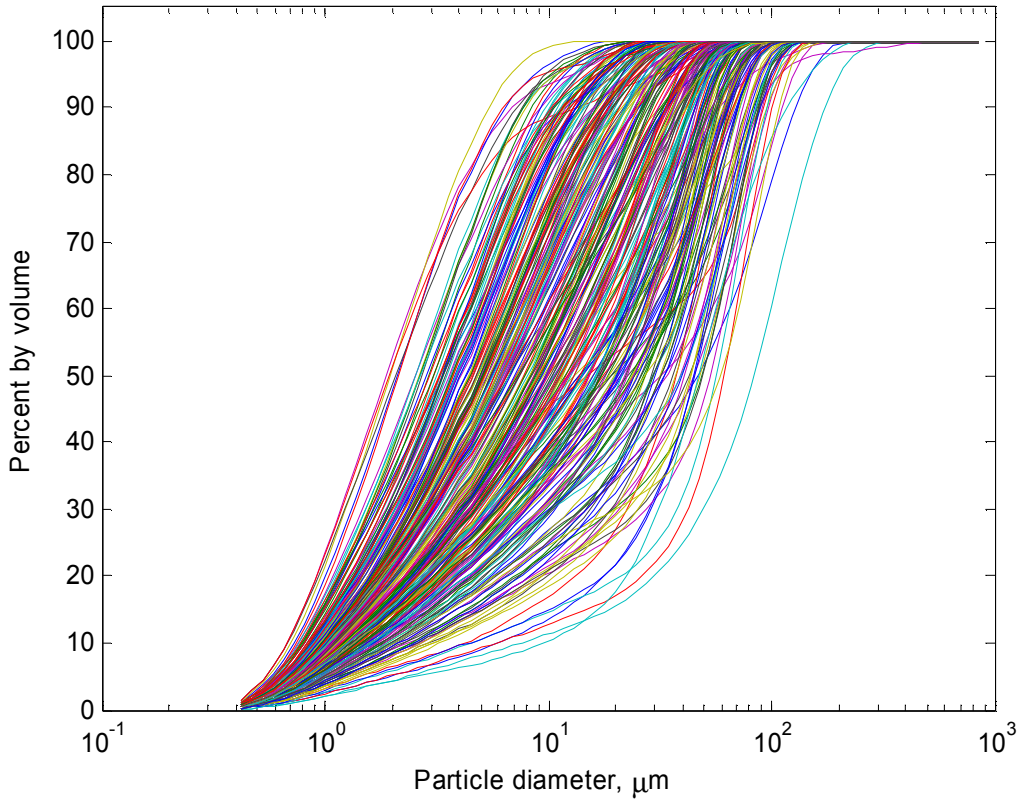


Figure 3.9 Cumulative percent finer than by volume for all Strickland River floodplain samples.

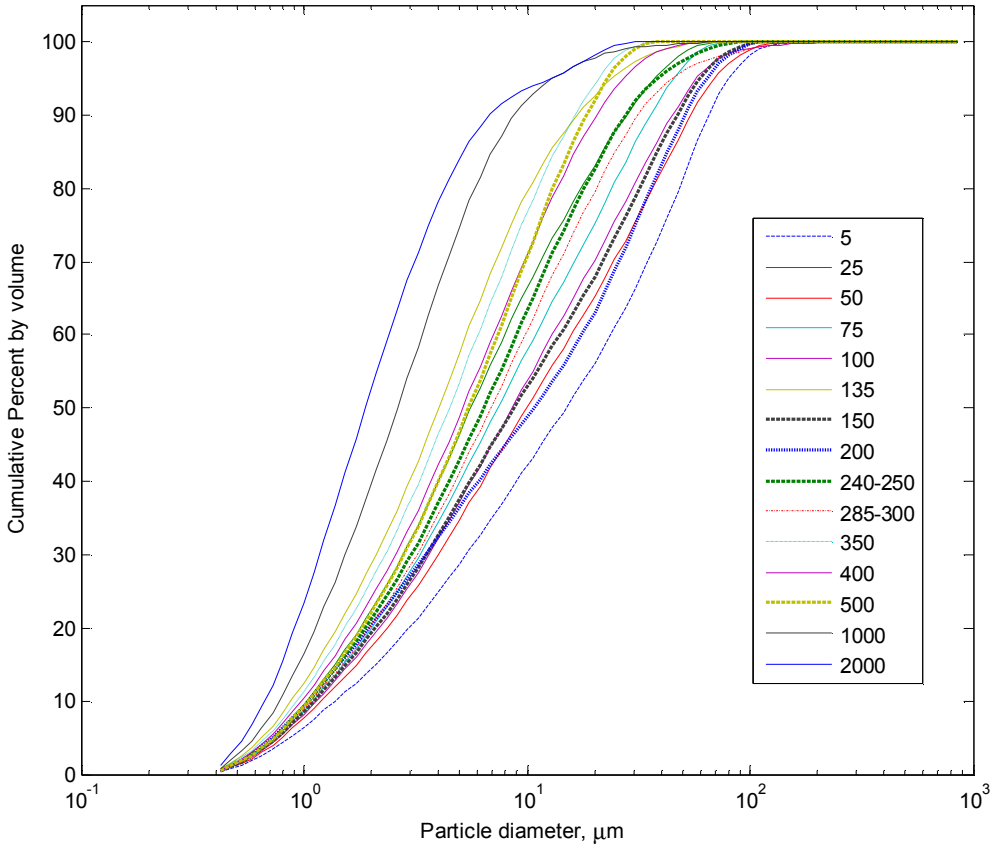


Figure 3.10. Binned-average cumulative percent composition for lower Strickland River floodplain sediments for each distance bin (m). Samples farther from the channel are generally finer than those taken from near the bank.

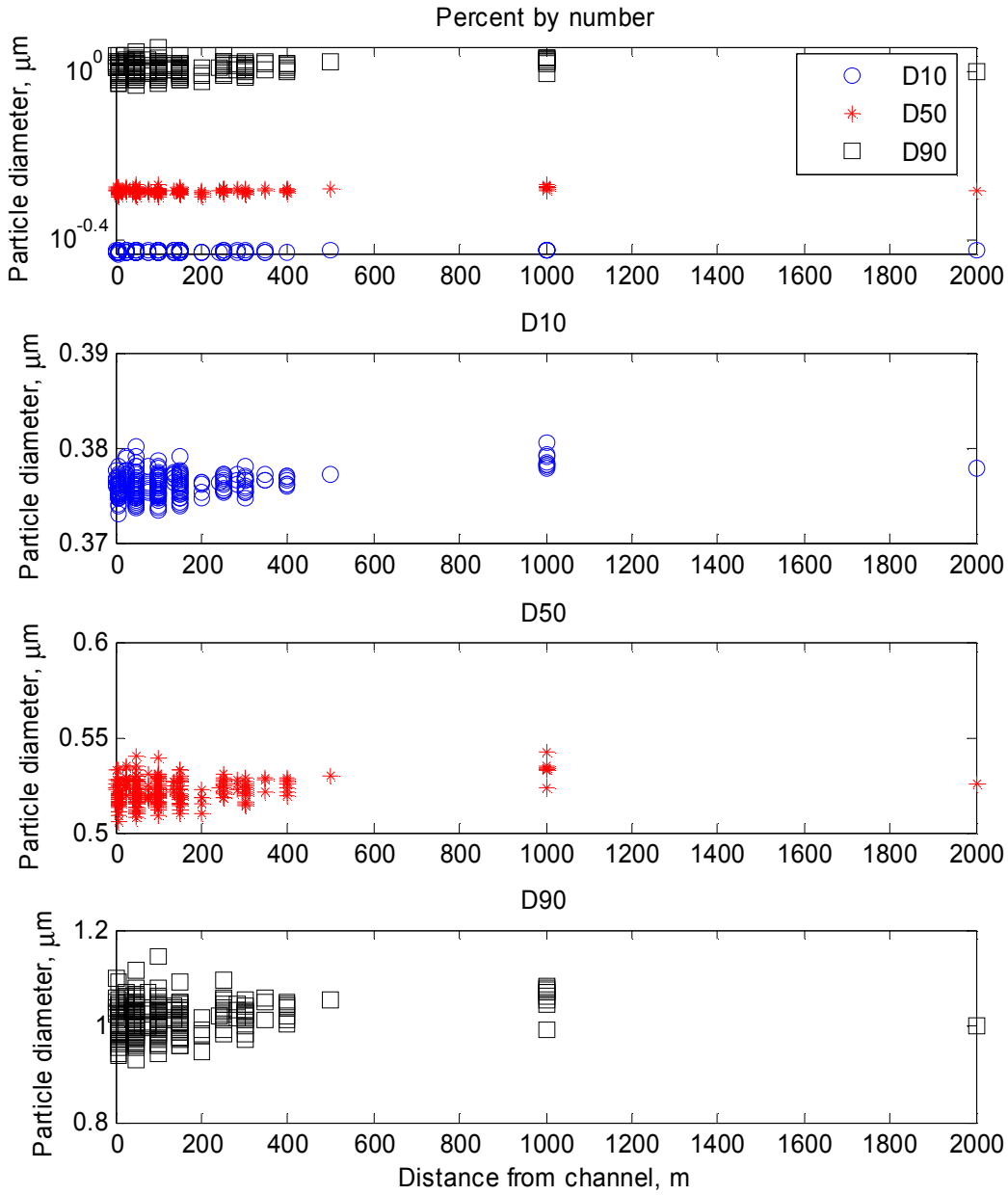


Figure 3.11 Particle diameters for D10, D50 and D90 calculated as a percent by number for Strickland River floodplain sediments.

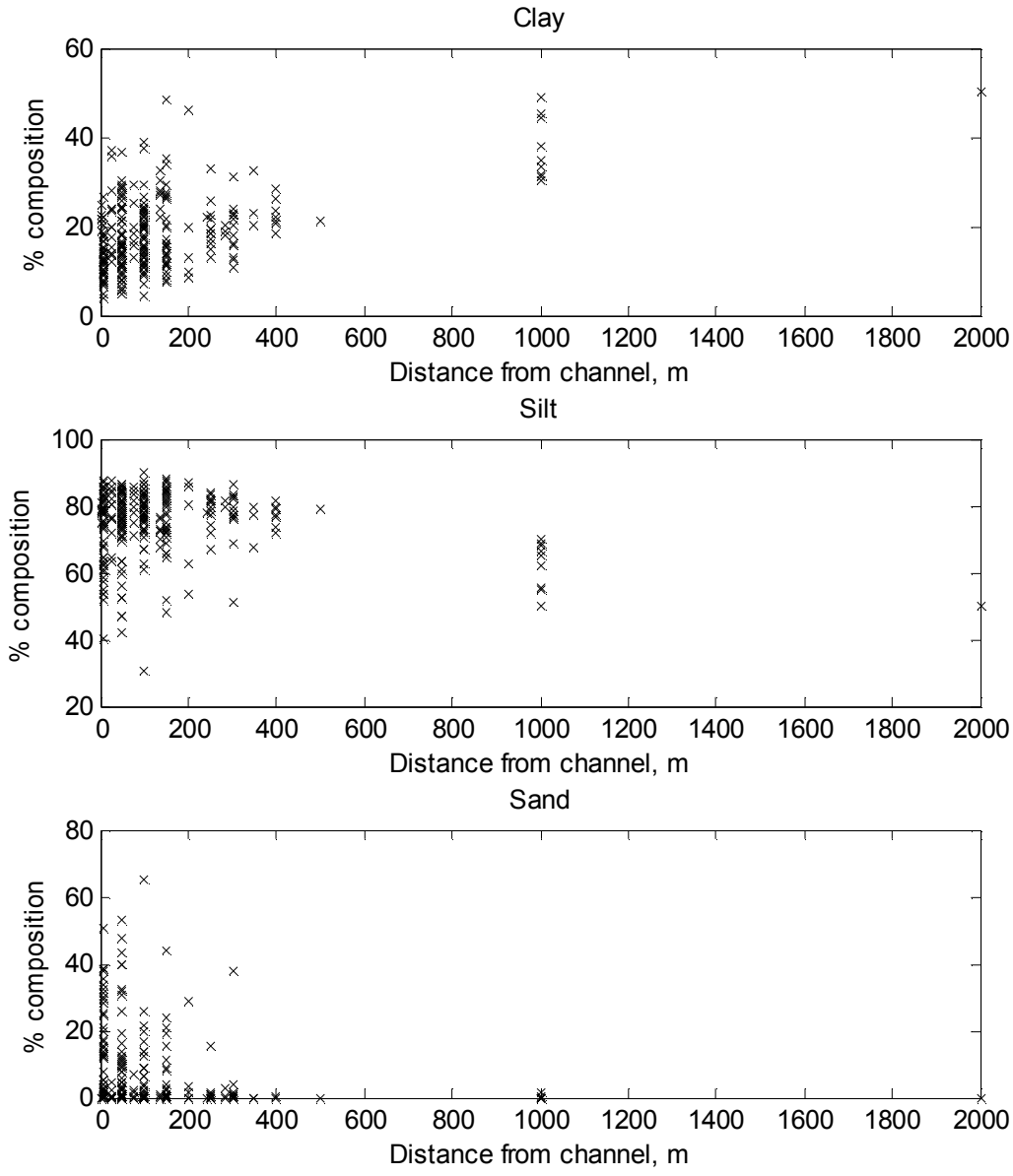


Figure 3.12 Fraction of clay silt and sand in Strickland River floodplain sediment as a function of distance from the channel.

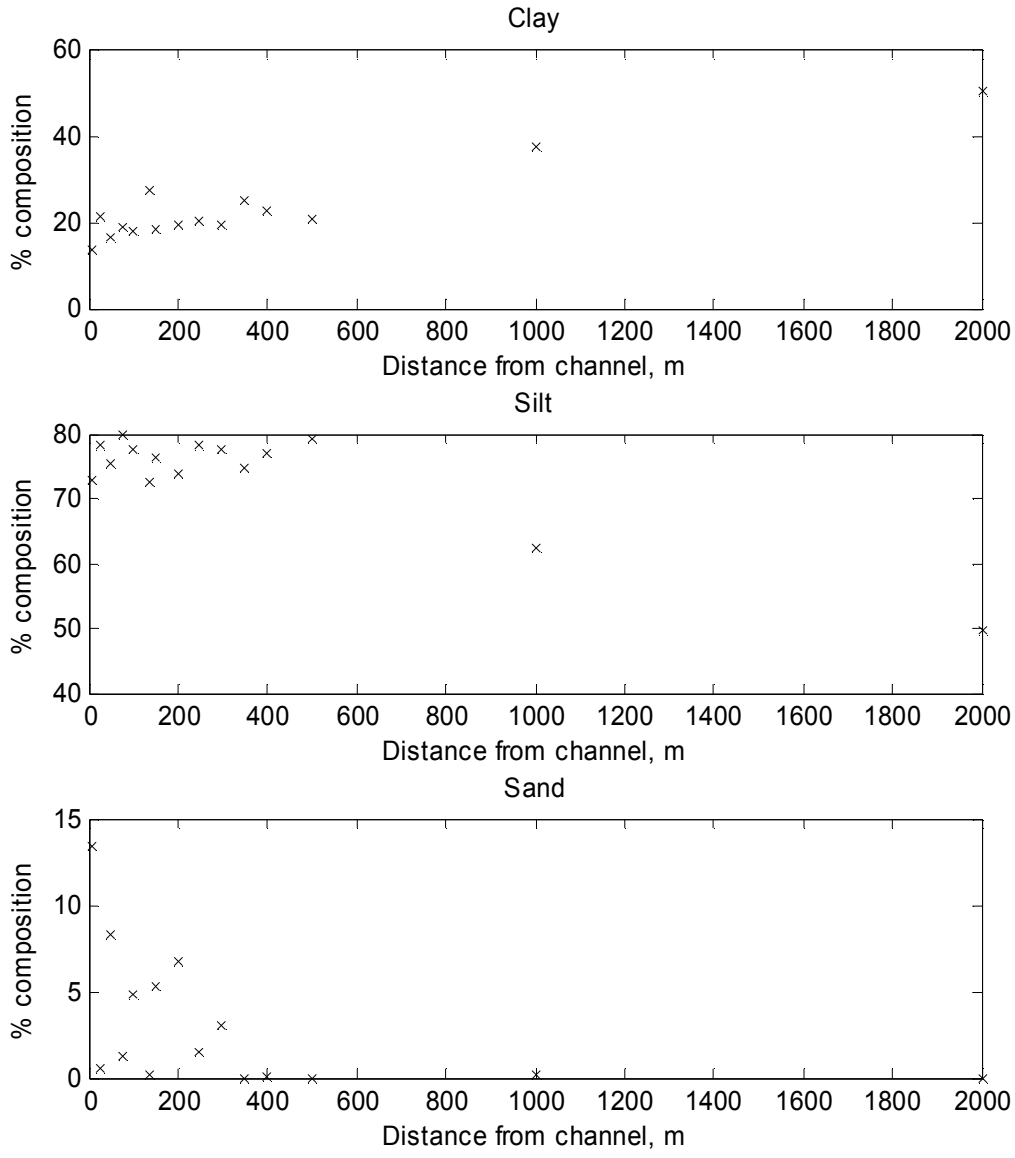


Figure 3.13 Binned-averages of percent clay silt and sand as a function of distance from the Strickland River.

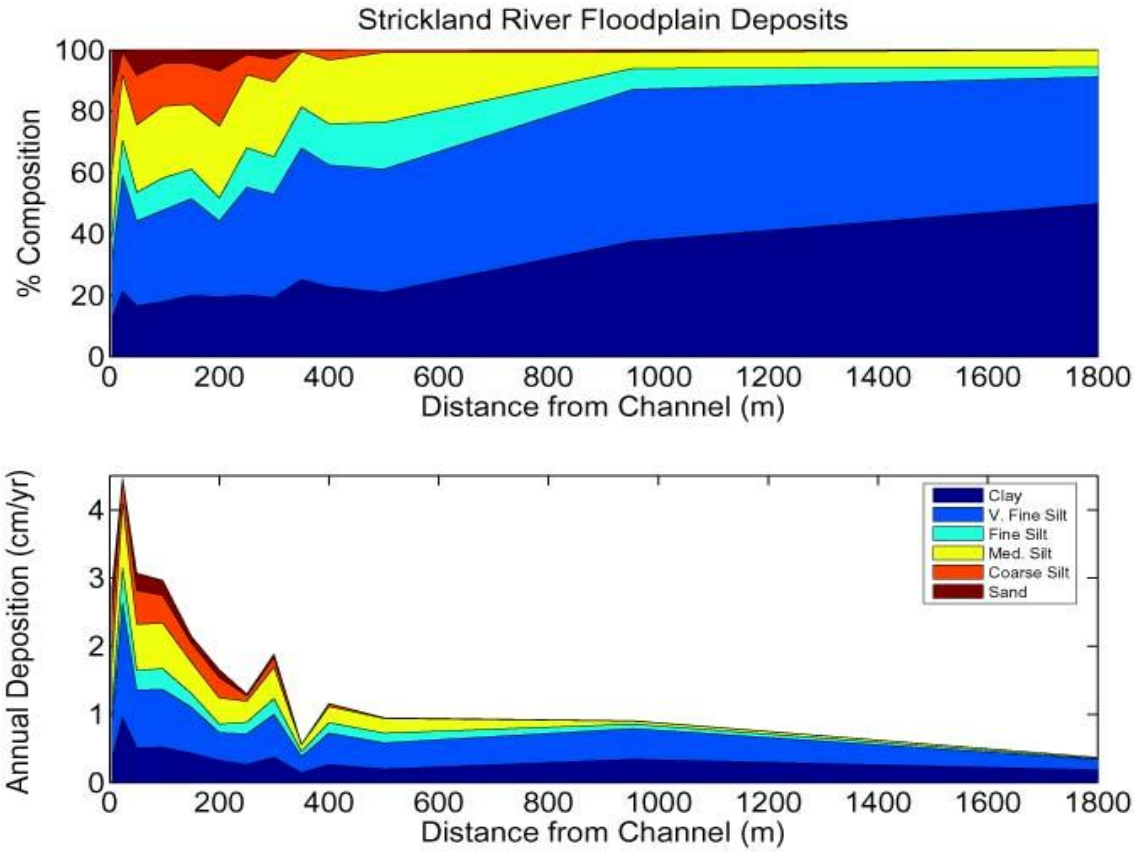


Figure 3.14 Average percent composition by volume of Strickland River floodplain deposits for each size class of clay (<2 μm), very fine silt (2-8 μm), fine silt (2-16 μm), medium silt (16-32 μm), coarse silt (32-62 μm) and sand (>62 μm). The lower panel shows both the relative contribution and magnitude of deposition of each size class.

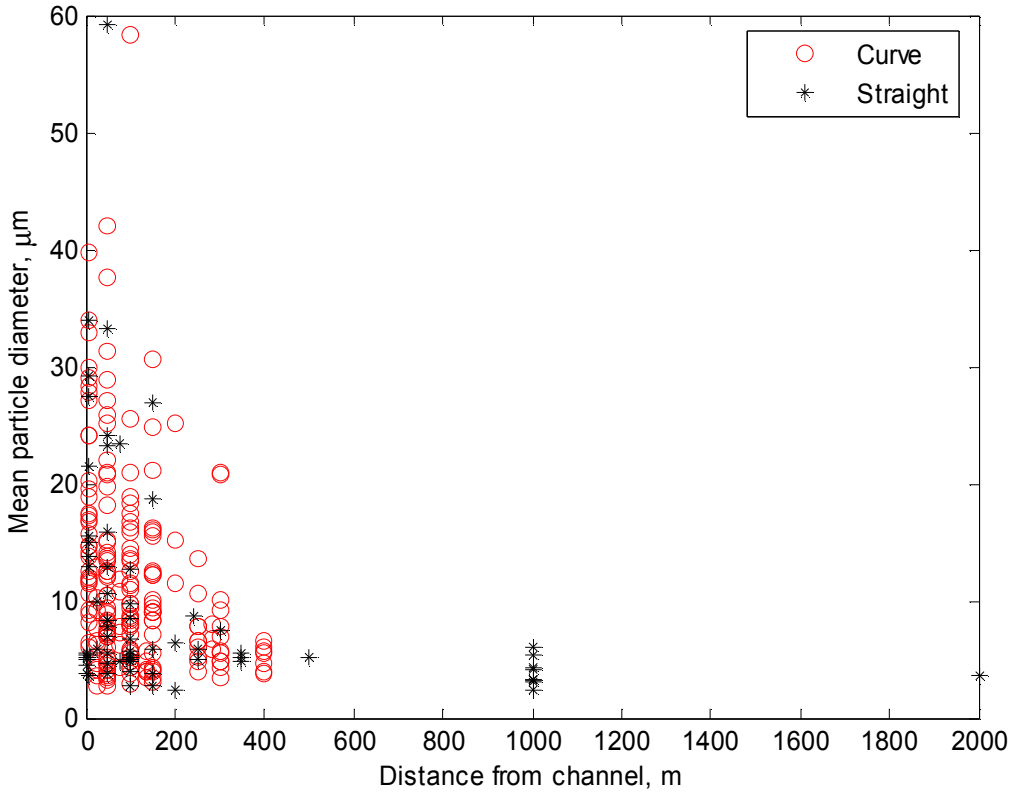


Figure 3.15 Mean particle diameter of Strickland River floodplain sediments measured on curved and straight reaches as a function of distance from the channel.

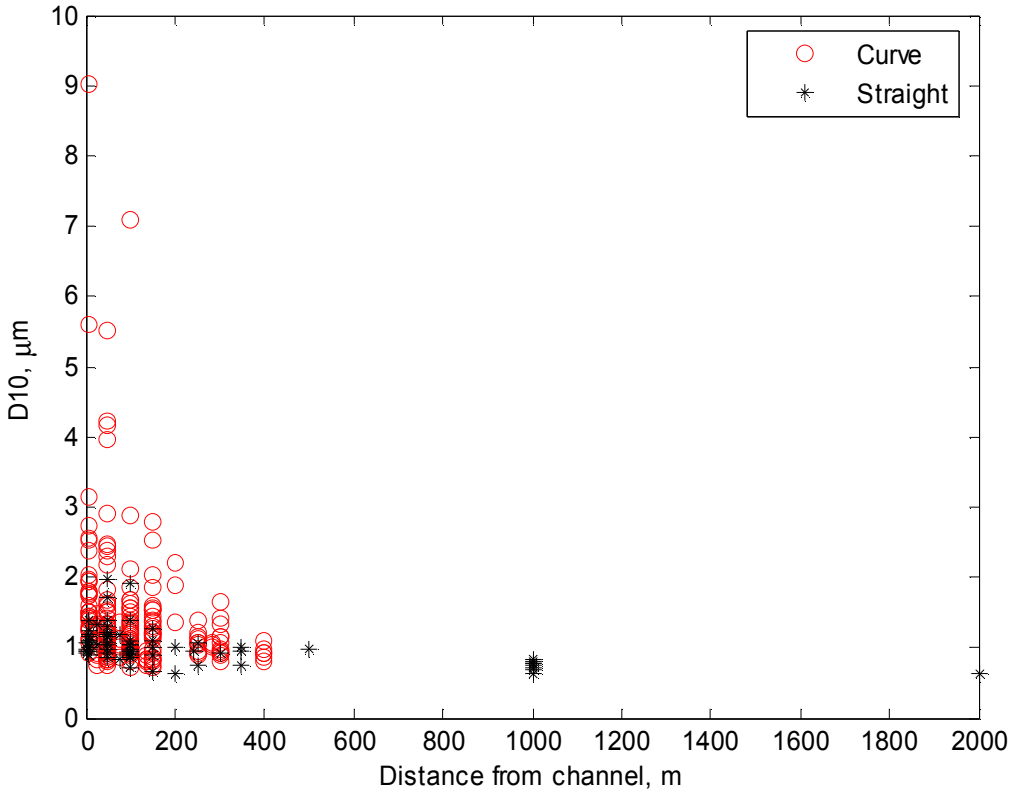


Figure 3.16 D10 of Strickland River floodplain sediments for curved and straight reaches as a function of distance from the channel.

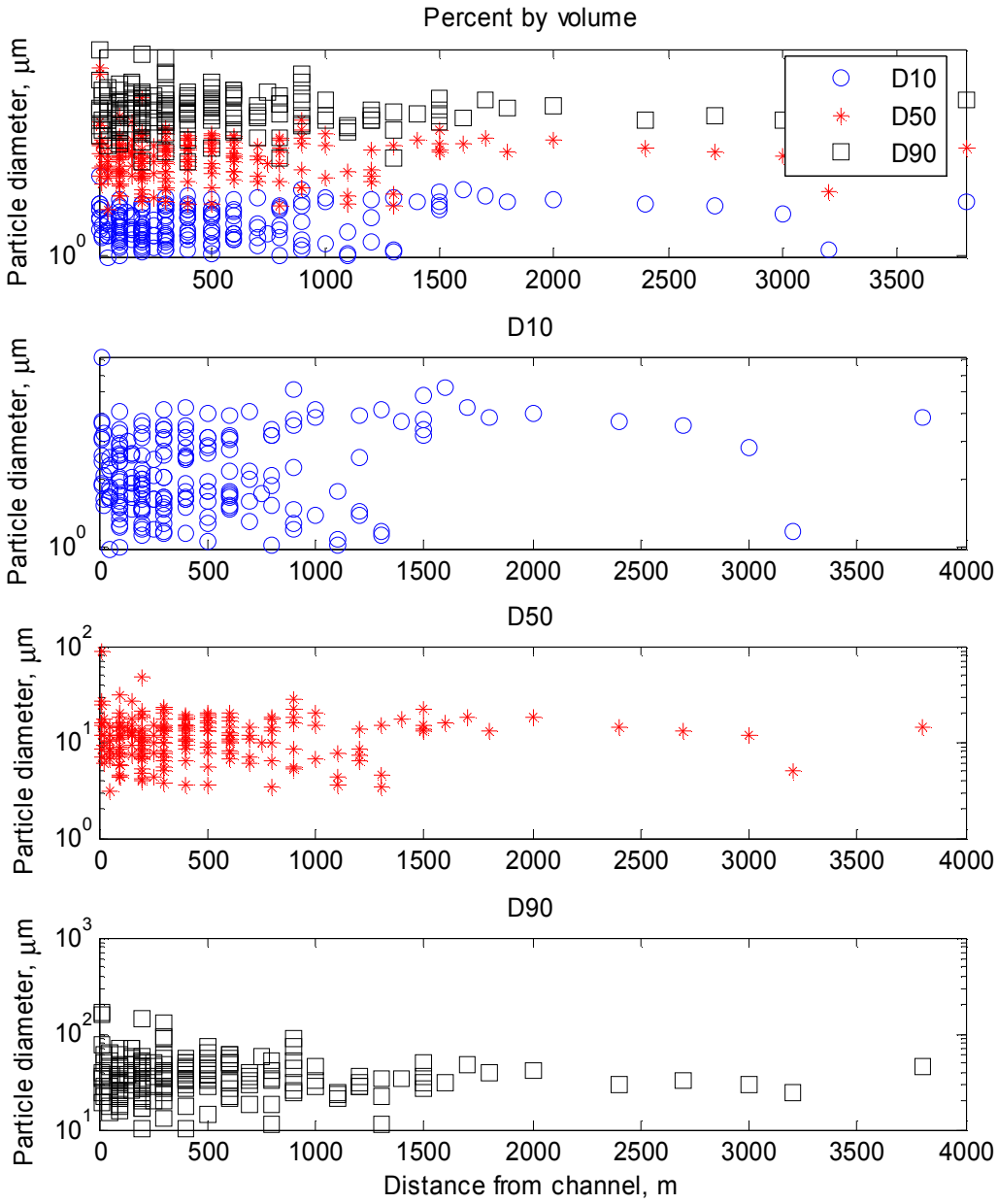


Figure 3.17 Fly River floodplain sediments D10, D50, and D90 as a function of distance from the nearest channel.

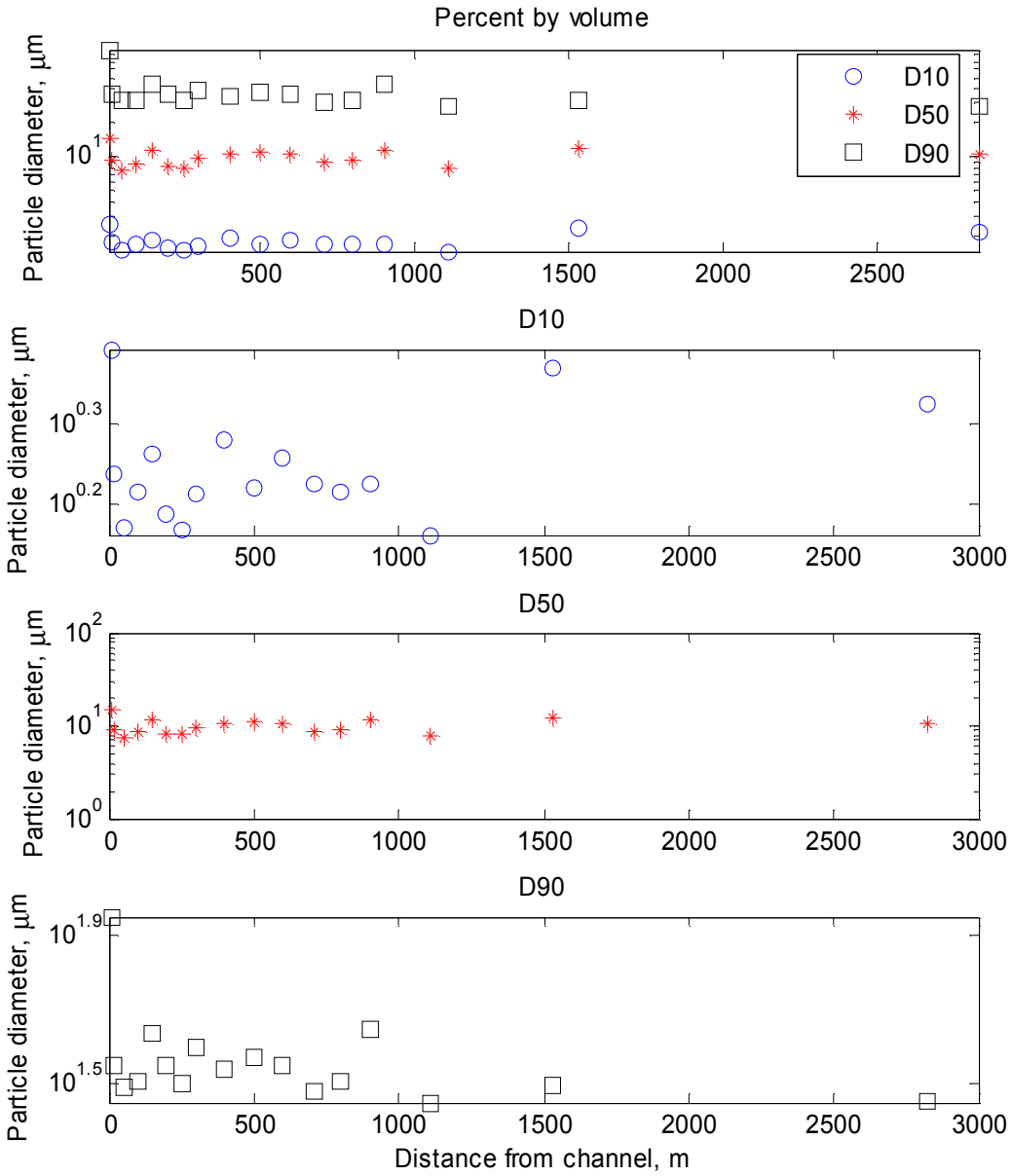


Figure 3.18 Binned-average Fly River floodplain sediments D10, D50, and D90 as a function of distance from the nearest channel.

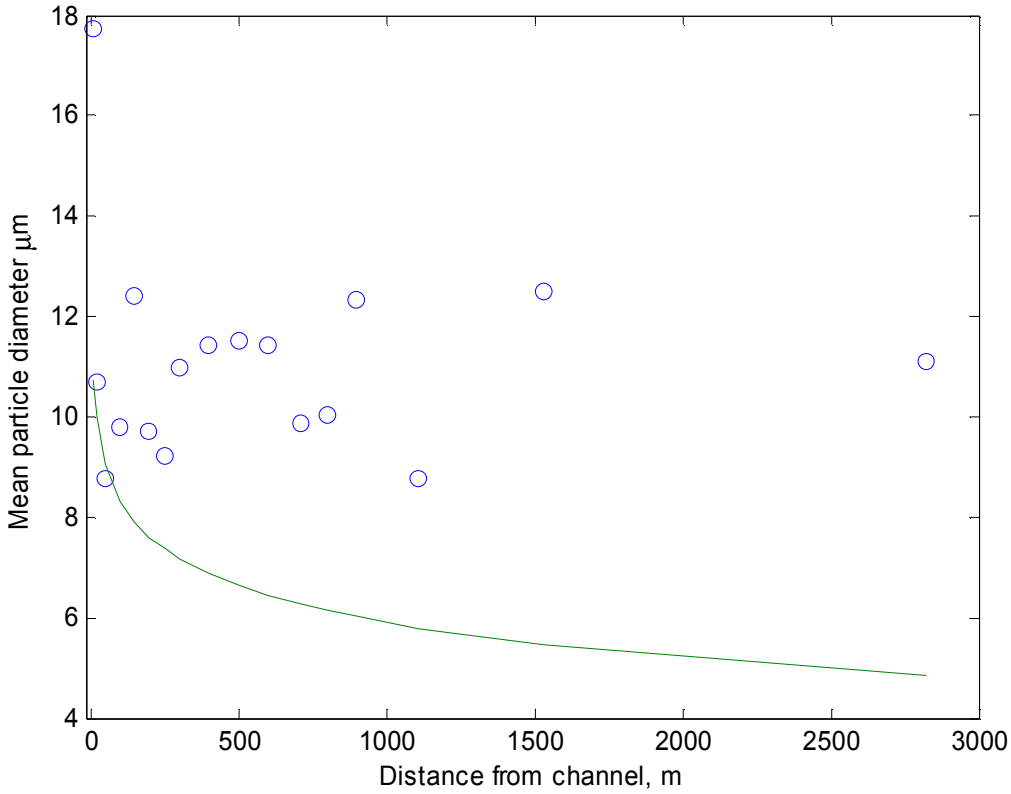


Figure 3.19 Mean particle size for binned Fly River PSD data. The green line represents the best fit function $y = -0.452\ln(x) + 13.633$ and $R^2=0.1078$.

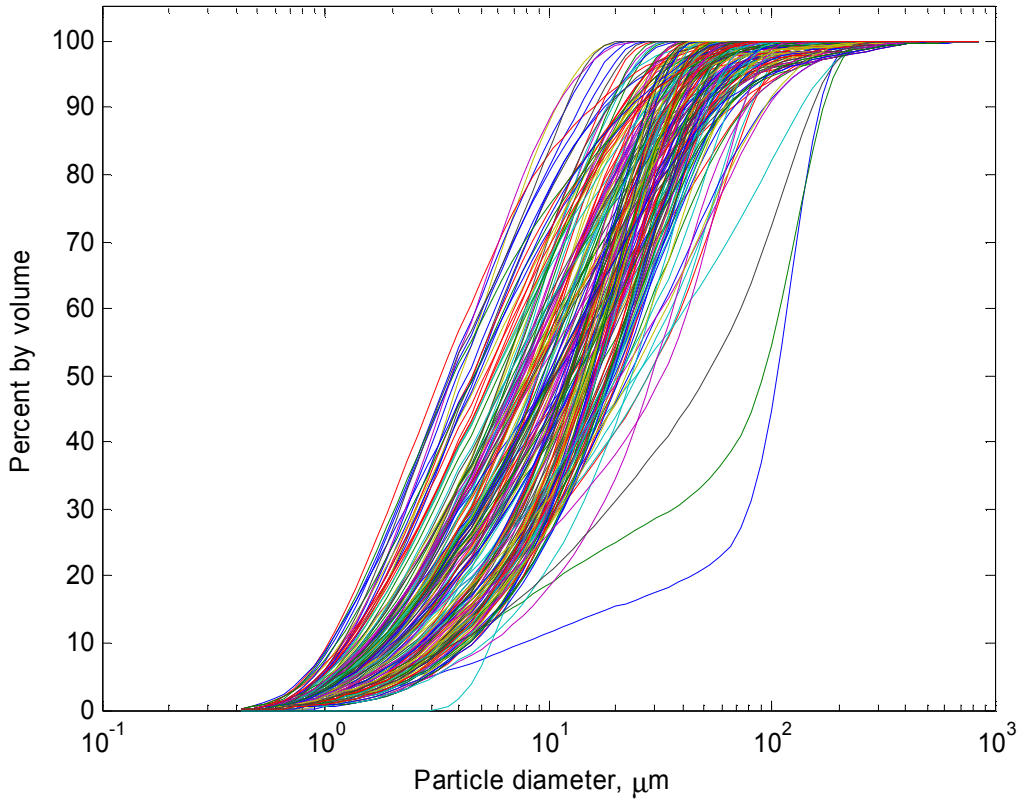


Figure 3.20 Cumulative percent finer than by volume for all Fly River samples.

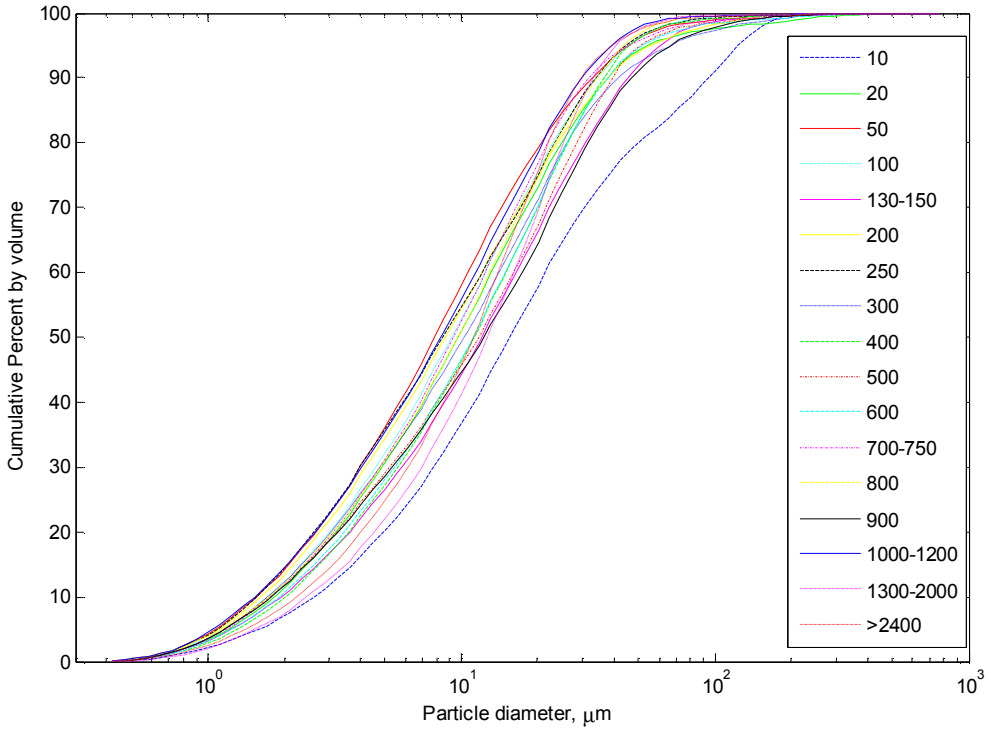


Figure 3.21 Cumulative percent finer than by volume for Fly River floodplain sediment for each distance bin (m). The coarsest sediments are found 10m from the channel, but no discernable trend in grainsize is obvious at increasing distances beyond the channel bank.

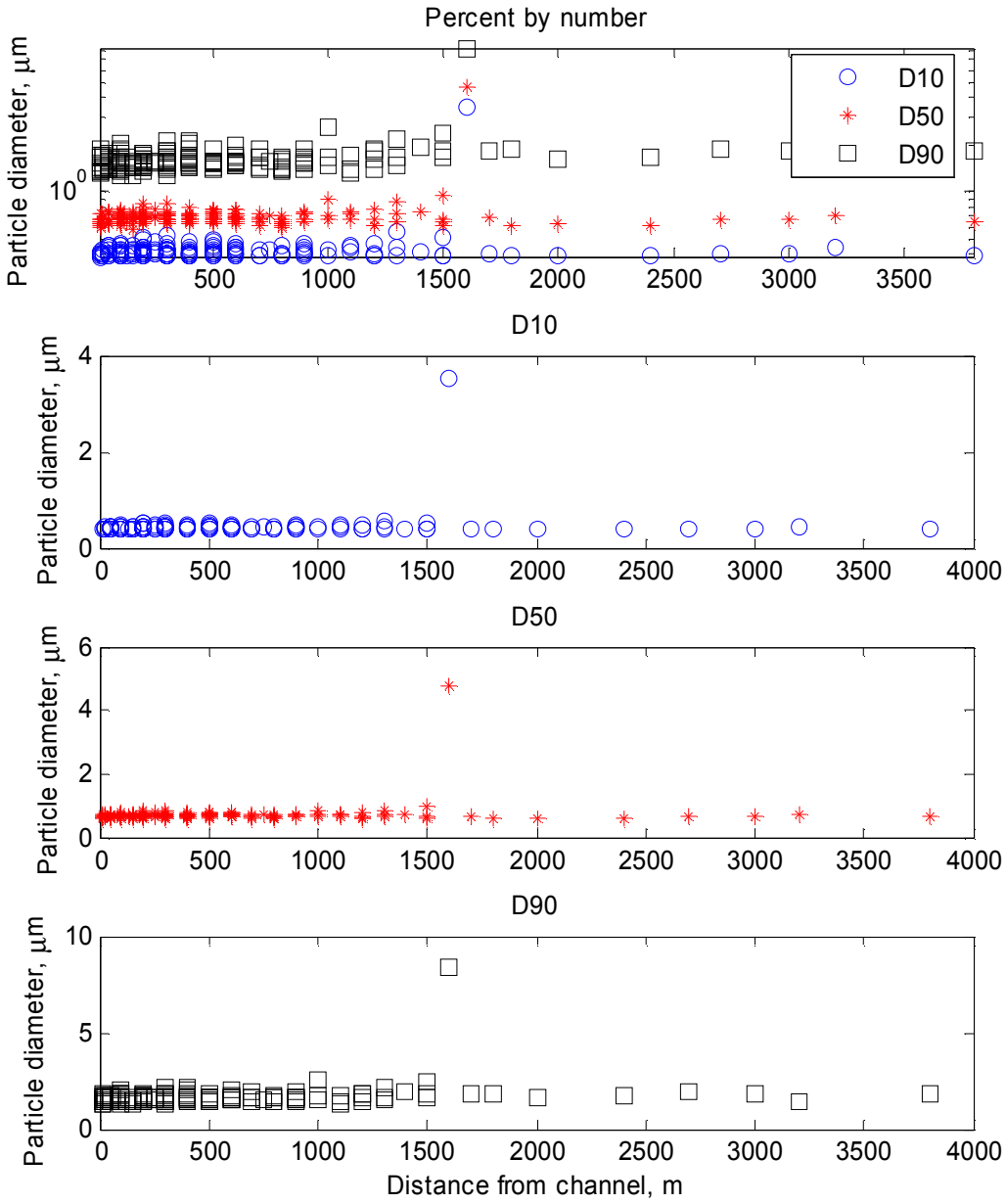


Figure 3.22 Fly River floodplain particle D10, D50, and D90 from percent by number plotted versus distance from the nearest channel.

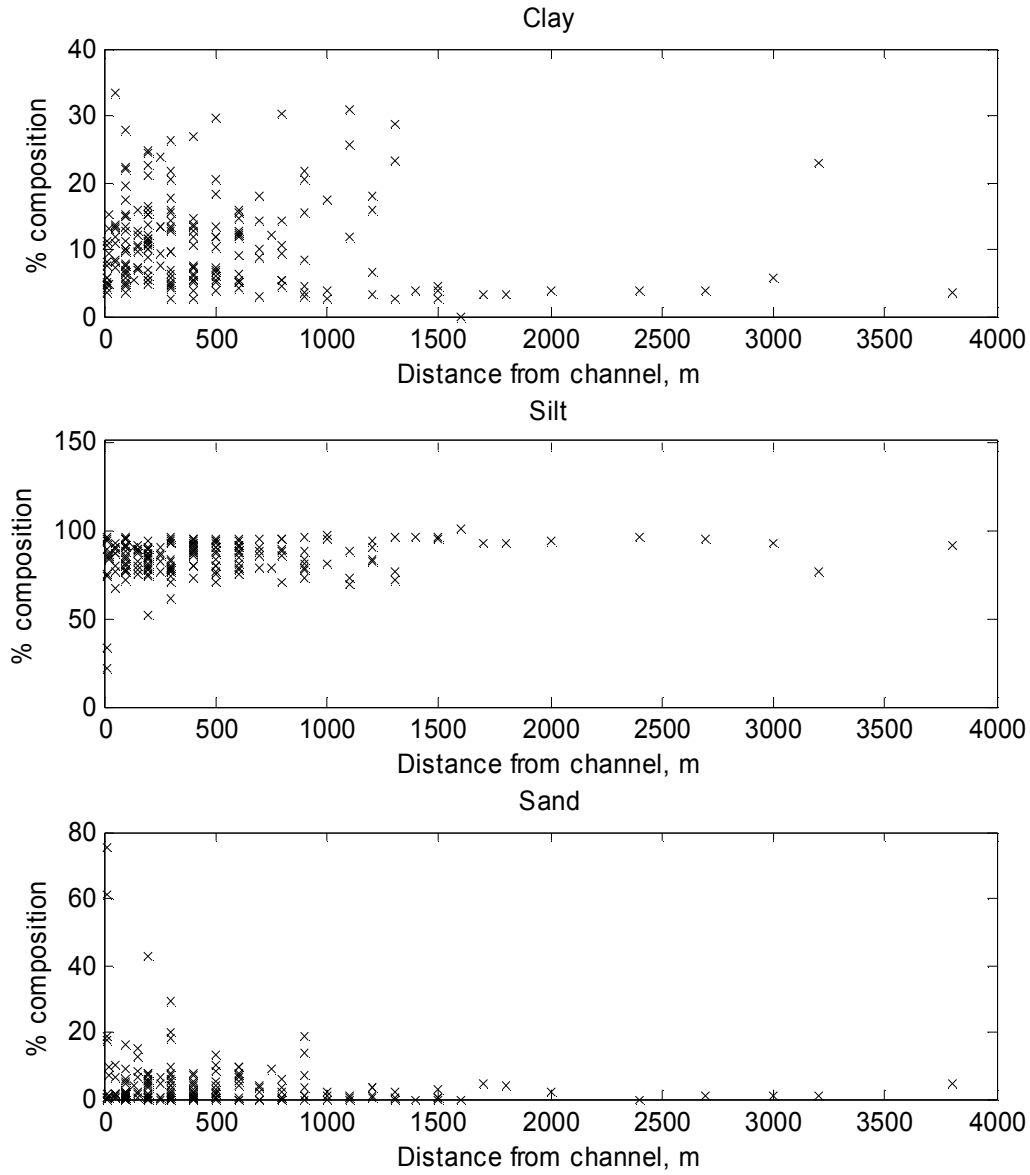


Figure 3.23 Fraction of clay, silt and sand in Fly River floodplain sediments as a function of distance from the nearest channel.

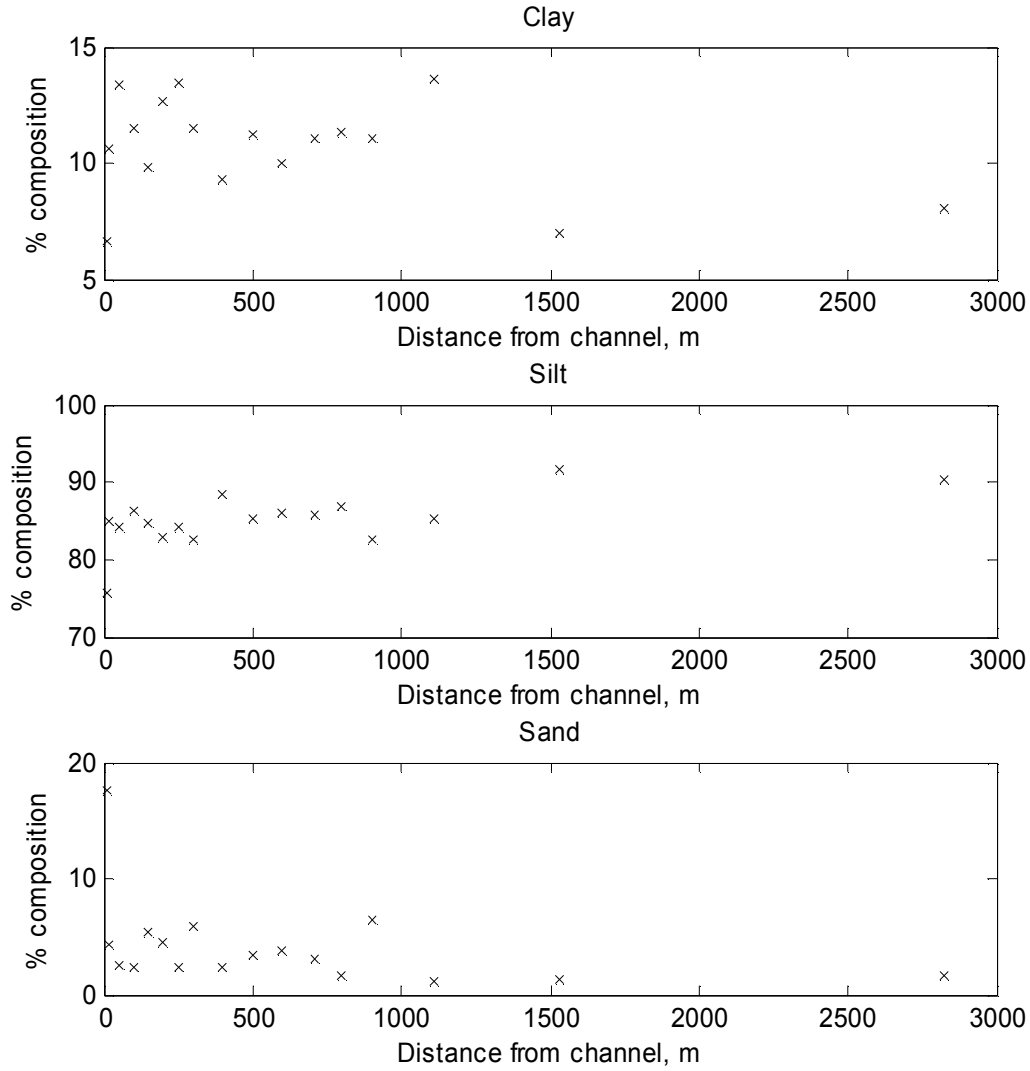


Figure 3.24 Binned-average percent clay, silt and sand in Fly River floodplain sediment versus distance from the nearest channel.

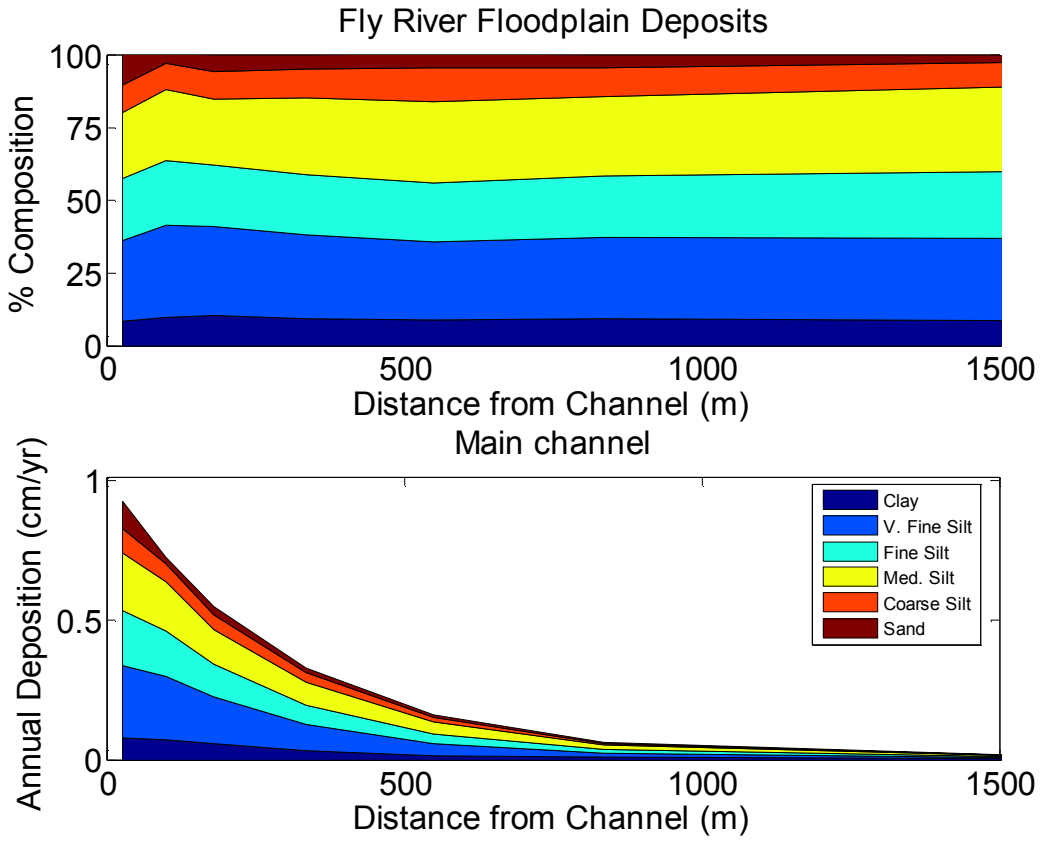


Figure 3.25 Binned-average percent composition by volume of Fly River floodplain deposits for each size class of clay (<2 μm), very fine silt (2-8 μm), fine silt (2-16 μm), medium silt (16-32 μm), coarse silt (32-62 μm) and sand (>62 μm). The lower panel shows both the relative contribution and magnitude of deposition of each size class. The deposition function is defined by $h=1.01e^{(-.003357y)}$ (from Geoff Day, 1993 data).

Chapter 4

A 1-D model to explore the lateral variation of floodplain deposition

Abstract

The Fly and Strickland Rivers in Papua New Guinea share geologic history, climate and a legacy of mine tailings from active mines in their headwaters, but have vastly different floodplain sediment trapping efficiencies and depositional mechanisms as evidenced by the measured decadal deposition rates and sediment size distributions on their respective floodplains. A 1-D model of turbulent kinetic energy and sediment transport across a lateral section of floodplain was developed to explore the differences in the depositional patterns of these two large floodplains. The model analysis indicated that lateral advection was the primary transport mechanism of sediment across both floodplains and that the key difference in the depositional pattern may be explained by flocculation of all sediment particle sizes transported on the Fly River floodplain and flocculation of primarily fine sediment transported across the Strickland River floodplain. Lateral variability in accretion from overbank deposition can be explained by a mechanistically-derived exponential function that was solved by balancing a simple advection-deposition transport formula, however the parameters needed to apply this function are difficult to measure directly. A simple scaling of the modeled depositional length-scale was explored to calculate the possible duration of active deposition, effective settling velocity of flocculated particles, and floodplain flow velocity. These parameters are used to investigate the mechanisms which explain the differences between the exponential deposition observed on the Fly River floodplain and non-exponential deposition pattern observed on the Strickland River floodplain. The results of the model indicate that the non-exponential deposition pattern observed on the Strickland River floodplain was the result of differential deposition of a distribution of particles sizes and effective settling velocities. The observed non-exponential accretion on the floodplain was the sum of the exponential functions for each particle size. The flocculated particles on the Fly River floodplain likely have a single effective settling velocity resulting in the observed exponential pattern of accretion resulting from overbank deposition.

4.1 Introduction

The observed differences in the spatial pattern of deposition rate and sediment texture on the Fly and Strickland Rivers described in Chapter 3 indicated a difference in the processes controlling the rate and pattern of deposition on the floodplain (Figures 4.1 and 4.2). Sediment deposition on the Strickland River floodplain decreases in a non-exponential manner and fines rapidly with distance from the channel. Sand delivered to the Strickland River floodplain deposits near the channel and fine silt and clay deposit much farther from the channel. On the swampy Fly River floodplain deposition decreases exponentially, but there was very little observed change in sediment size with increasing distance from the nearest channel. There was negligible decrease in sand deposition with increasing distance beyond the natural levee with several percent of the deposited material beyond 1 km from the channel consisting of fine sand. Here I propose and develop a 1-D model of the lateral overbank deposition pattern to explore the primary processes controlling the rate and pattern of overbank floodplain deposition as a function of distance from the channel and use this model to explain the differences in process that lead to the observed distance-dependent patterns of deposition on the Fly and Strickland River floodplains. Motivated by these observed differences in depositional pattern, the three questions that this model will attempt to answer are:

1. What process is the primary control on the spatial variation in the rate of deposition?
2. What process is the primary control on the spatial variation in particle size distribution (PSD)?
3. Is there a difference in the primary process controlling transport or deposition that makes Fly and Strickland River floodplains so different?

The Middle Fly River is much less steep and more swampy than the lower Strickland River floodplain. Day et al. (2008) observed on the Fly distinct levees that responded to increased sediment load by elevating and the exponential decline in sedimentation rate as a function of distance from the nearest channel, but also noted that lack of lateral fining across the floodplain could not be explained by any observed depositional process. The model developed here was used to examine the relative importance of diffusion and advection on overbank sediment transport on the Fly and Strickland River floodplains. Model results were compared to the observed patterns of deposition on the two floodplains.

Quantitative assessments of the variability of lowland river floodplain sediment sizes are not abundant and the two datasets presented in the previous chapter appear to be the most extensive to date. Overbank deposition has been described empirically as a power law function (Kesel et al., 1974) or exponential function (Pizzuto, 1987) of lateral distance from the channel edge. Following Bridge and Mackey (1993) these two general forms of

overbank deposition described by Kesel et al. (1974) and Pizzuto (1987) are shown in equations 4.1 and 4.2

$$\frac{r}{a} = (1 + \frac{z}{z_m})^{-b} \quad (4.1)$$

$$\frac{r}{a} = e^{-b\frac{z}{z_m}}. \quad (4.2)$$

These non-dimensional relationships describe $\frac{r}{a}$, the rate deposition rate at position z from the channel edge, r, relative to the mean deposition rate. a, within a fixed floodplain width, z_m, and a dimensionless exponent, b, that controls the spatial variability of deposition. The measurements by Kesel et al. (1974) of overbank flood deposits on the Mississippi River after a single flood event showed a power law decline in both the thickness of flood deposit and median grain diameter, D50, of the deposited sediments with increasing distance from the channel. The exponential pattern described by Pizzuto (1987) is a generalized from of both modeled and measured sediment deposition and is discussed in detail below. These generalized formulations do not describe the mechanics of overbank deposition, but describe the lateral decline of overbank deposition with increasing distance from the channel. Walling and He (1997) fit an exponential deposition pattern to measurements of overbank deposition rates on several small catchments in the UK, though it should be noted that the r^2 values of the exponential fit to the data do not exceed 0.22 for any of the 5 catchments in their study. An exponential deposition pattern was measured up to nearly 1 km from the channel belt for coarse sediment on the Brahmaputra-Jamuna and a constant deposition of fine sediment was noted for distances beyond 1-km (Allison et al., 1998). Non-exponential patterns of deposition have been measured on the Beni and lower Strickland Rivers (Aalto et al., 2003; Aalto et al., 2008; Swanson et al., 2008). Advective flow through crevasse splays was identified as the primary sediment transport mechanism on the Beni River floodplain (Aalto et al., 2003), but have not been reported along the lower Strickland River floodplain.

It is widely noted that there is an abrupt decrease in flow velocity and transport capacity from the channel to the floodplain resulting in the deposition of the coarsest suspended sediment near the channel bank (Allen, 1965; Pizzuto, 1987; Asselman and Middelkoop, 1995; Walling et al., 1996; Asselman and Middelkoop, 1998). As the water spreads across the floodplain frictional losses and increasing flow depth can often result in additional decreases in flow velocity and transport capacity leading to a fining of deposited sediment with increasing distance from the channel (Walling et al., 1992; Asselman and Middelkoop, 1995; Asselman et al., 2003). It was theorized that the grain size would decrease gradually across a broad plain in floodplains where advective

transport dominates while floodplains that are dominated by diffusive transport will fine more rapidly and have steeper transitions adjacent to the channel (Pizzuto, 1987; Adams et al., 2004). No current theory of floodplain sediment transport can explain a deposition pattern like that observed on the Fly River floodplain with decreasing deposition and constant particle size with increasing distance from the channel. Particle interactions may provide a mechanism that would alter the sediment transport dynamics. Nicholas and Walling (1996) note the importance of incorporating the effective (flocculate) settling velocity, not the ultimate settling velocities of the dispersed individual particles into any model of floodplain sedimentation to accurately predict both the rate and pattern of deposition. They measured the relative strength of flocculation of particles depositing on the floodplain of the River Exe basin and developed an effective distribution of settling velocities and the corresponding actual particle size distributions. In their experiments sand was not incorporated into the flocs and was considered separately from flocs and fine sediment transport.

Numerical models can be used to investigate the mechanisms that control the observed overbank deposition patterns. The most important early models used to explore the lateral pattern of overbank floodplain deposition were James (1985) and Pizzuto (1987). Figure 4.3 illustrates the flow regime of an idealized compound channel-floodplain where the main channel flows through a wide, confined, shallow floodplain. In a straight compound channel-floodplain mean advective flow is in the downstream direction and the difference in flow velocity between the channel and floodplain generates turbulent mixing. Turbulence mixes sediment laterally from the high sediment concentration zone in the channel to the low-sediment concentration zone of the floodplain in a process that can be mathematically described as a diffusion process (Rowland et al., 2010). James (1985) formulated the transfer of sediment by longitudinal advection and turbulence generated diffusion resulting in sediment transport normal to the channel. The model described by James (1985), an elliptic partial differential equation, numerically solves for sediment concentration across the floodplain perpendicular to the channel and was parameterized by empirical relationships. This model was applied to the floodplain of the River Severn, UK, by Marriot (1992) and the model was able to predict the relative distribution of particle size across the floodplain. The measured floodplain grain sizes decreased with increasing distance from the channel and fine sand contributed to deposited sediments at all distances from the channel up to 575 m from the channel (Marriot, 1992). The modeled floodplain sediment concentrations are shown in Figure 4.4. The model predicted that the coarsest fraction was only found in suspension up to ~100 m from the channel and the silt fraction was mixed nearly uniformly across the entire width of the floodplain. This result was comparable to the deposition pattern observed on the Middle Fly floodplain, though the along-channel floodplain flows incorporated in the model developed for the compound channel modeled and the modeled fining of sediment with distance from the channel predicted using the James (1985) model are not consistent with observations of transport and deposition on the Middle Fly River.

Pizzuto (1987) also modeled overbank floodplain transport as a diffusion process in a compound channel. The model includes diffusion, erosion and deposition and was solved explicitly for a steady-state solution of lateral sediment concentration when the erosional and depositional terms are equal. Depositional thickness, H [L], is then solved as the integral of the instantaneous difference between erosion and diffusion for the duration of the flood. Depositional thickness is given by

$$H = \frac{w_s^2}{e_z} Z_0 t \cdot \left(\frac{\sinh(Gy)e^{-G}}{\cosh(Gy)} + e^{-Gy} \right) \tag{4.3}$$

where w_s is the sediment settling velocity [L/T], e_z is the vertical sediment diffusivity [L^2/T], Z_0 is model parameter of depth integrated excess sediment concentration [L], t is time, y is distance from the channel [L]. G is a dimensionless function of floodplain width, W [L], settling velocity, and the lateral and vertical sediment diffusivity e_y and e_z respectively,

$$G = Ww_s / (e_y e_z)^{1/2} \tag{4.4}$$

(Pizzuto, 1987). The Pizzuto (1987) model does predict declining deposition with increasing distance from the channel and fining of deposited sediments with increasing distance from the channel. This general pattern was observed in the flood deposit of a field site where the model was used to predict flood deposition. However, the model generally under predicts deposition on the floodplain during the flood (Pizzuto, 1987). The observed deposition of coarse material far from the channel was significantly under predicted. Pizzuto concludes that advection across the floodplain must be included in order to accurately predict the transport and deposition of sediment across a floodplain.

Howard (1992) defined the long term distance-dependent sedimentation rate, r [L/T], as a function of the accommodation space of the floodplain. Accommodation space was defined as the difference of the maximum and local floodplain elevations, $E_{\max}$ and E_{act} [L] in the floodplain basin. The rate, *r*,

$$r = (E_{\max} - E_{act})(v + m * e^{-y/l}), \tag{4.5}$$

allows for a constant rate of deposition of fine material expressed as a weighting coefficient, v [T^{-1}], and a spatially variable deposition rate for coarse material, weighting coefficient m [T^{-1}], that decreases exponentially with distance from the channel relative to a characteristic diffusion/advection length-scale, y/l. The rates of deposition, v and m, are not determined by the model itself, but must be specified as model inputs. This proposed exponential deposition relationship was used as a motivation to explore large

floodplain systems in order to better describe the processes controlling floodplain development and overbank deposition.

Landscape models incorporate the 2- and 3-dimensional complexities of flow and deposition over complex floodplain geometries and variable topography. Landscape models often focus on restoration efforts, contaminant dispersal or environmental response to anthropogenically induced changes in flow and sediment flux (Kondolf et al., 2005). Nicholas and Walling (1997) modeled deposition rates and grain size distributions as a result of advection, diffusion and particle settling on a reach of the River Culm, UK. Their depth-averaged 2-D model solves for floodplain hydraulic conditions at each grid node (Figure 4.5) for a limited number of flows and uses these instantaneous, steady solutions as a proxy for floodplain flow over varying discharges. Sediment transport and deposition are determined using8 a 2-D model that incorporates advection, diffusion, and settling in a mass balance. The model predicted the magnitude of deposition within an order of magnitude up to 200 m from the channel, but consistently under predicted deposition on the distal floodplain (Figure 4.6).

Middelkoop and Van der Perk (1998) used a 2-D raster-based model embedded in GIS to model flow and sedimentation over small floodplain sections on the Rhine River and the River Waal in the Netherlands. Their depth-averaged, unsteady flow model combined an existing hydrologic model with the SEDIFLUX, a sediment flux model, and was calibrated for a single flood event in 1993. Their mass balance sedimentation model consisted of a simple sediment flux calculation. The predicted total amount of overbank sediment deposition during a single flood event was consistent with measurements, but the pattern of deposition in single raster cells of the model did not agree well with observations (Middelkoop and Van der Perk, 1998). They observed that general patterns of floodplain deposition are attributed to differences in frequency and duration of inundation. Thonon et al. (2007) built upon the approach of raster map sedimentation model used by Asselman and Middlekoop (1995) by applying a particle tracking model to predict sediment deposition on the lower River Rhine floodplain during a flood event. Thonon et al. (2007) were able to roughly recreate the spatial pattern of deposition in the downstream direction, but were unable to match the magnitude of deposition.

Hardy et al. (2000) were able to replicate the amount of sediment deposited on the floodplain, but were unable to replicate the spatial variability of deposition. Their 2-D depth-averaged, non-steady-state model captures routing of the flood flow as well as the wetting and drying effect of a flood wave passing through the model domain of the otherwise dry floodplain. Their model solves the Navier-Stokes equations for flow and calculated the sediment concentration from transport by hydrodynamics, settling and erosion, or resuspension, and solves for sediment flux within a finite element framework. This model was applied to an 11km reach of the River Culm, UK and was able to predict conveyance loss between the upstream and downstream ends of the modeled reach. However, the spatial variability of modeled deposition, both laterally and downstream on the floodplain, was more difficult to replicate with the model (Hardy et al., 2000). Hardy

et al. (2000) note that a vast amount of data was required to properly calibrate and validate the model and that a 3-dimensional model would be more appropriate to predict deposition at smaller scales. However, their 2-D depth-averaged model was adequate to predict reach-scale deposition patterns.

Asselman and Wijngaarden (2002) conceptualized the flooded, embanked, narrow floodplain of the Rhine River as a series of aligned downstream "flow tubes" (Figure 4.7). Sediment conveyance decreases downstream along any individual flow tube due to deposition and, by virtue of the geometry of these floodplain flow corridors, flow at increasing distances perpendicular to the main channel travels longer distances from the upstream channel. Sedimentation thus decreased in both the downstream direction and with increasing distance from the channel. The assumption that flow was along the path of flow tubes without the inclusion of sediment transport by advection perpendicular to the channel or diffusion (as included in the James (1985) and Pizzuto (1987) models) resulted in even smaller predicted magnitude of deposition at greater distances from the channel across the floodplain (Asselman and Wijngaarden, 2002).

An additional class of numerical floodplain models have been used to hindcast the adjustment of the channel belt elevation, slope and avulsion frequency, and can be used to forecast future channel belt response to sea-level, hydrological and sediment supply changes. A 1-D (along channel), unsteady model of floodplain elevation, developed by Moody and Troutman (2000), describes the relationship between decreasing floodplain accretion and constant frequency and magnitude of river discharge with time, assuming that there was not a corresponding increase in vertical elevation of the channel bed. Karssenberg and Bridge (2008) developed a channel network model to explore bifurcation, avulsion and alluvial architecture. Their model does not explicitly include floodplain sedimentation, but instead computes the total deposition within a grid cell at each time step and assumes that a channel of fixed geometry avulses to an adjacent cell when a threshold of superelevation is reached. Evolution of the channel and floodplain long profile of the Clark Fork River (Lauer and Parker, 2008) and the Fly and Strickland Rivers (Lauer et al., 2008; Parker et al., 2008) was described by the solution of the Exner equation for sand transport and deposition within the active floodplain width. Floodplain deposition of mud was assumed to be a constant proportional to the calculated sand deposition and lateral variability of deposition rate and PSD are not considered (Lauer and Parker, 2008; Lauer et al., 2008; Parker et al., 2008). Many other models are used to explore the relationships between flood flow and the complex topography of floodplains, but these do not directly address the question of the process that drives mean lateral variability of floodplain deposition.

Though all of these models of floodplain sedimentation processes provide valuable insight into the development and morphodynamics of floodplains, none can be easily applied to explore the 1-D lateral variability of overbank deposition of the Fly and Strickland Rivers at a process level. The models of James (1985) and Pizzuto (1987) provide the best insights into the mechanisms that may dominate the lateral variability in

the mean depositional pattern. Later models are either site specific, require much more detailed flow modeling than was possible given the limited data available for the Fly and Strickland Rivers, or are not applicable to answer the questions of lateral variability motivating this study.

In this chapter a simple lateral overbank deposition model that requires minimal parameterization was developed to explore the lateral variability in the deposition rate and PSD on the Middle Fly and lower Strickland River floodplains. The model was used to explore the mechanism that result in starkly different overbank deposition patterns on the two lowland river floodplains. Since advection was not measureable on the Middle Fly River floodplain (ether because only diffusion was responsible for sediment transport on the Fly River floodplain or advection events did not coincide with the timing and location of field work) it has been hypothesized that shear flow between the mainstem and still water in the floodplain could be responsible for focused deposition that builds the levees on the Fly River bank (Day et al., 2008). Observations of flooding on the Strickland River are not available, but the steeper, better drained and less swampy floodplain is likely dominated by advective transport of sediment from the channel by floodplain flows and that the difference in transport mechanisms may lead to the different deposition patterns. A scaling of typical deposition length for the advection and diffusion models was compared to the observed patterns of deposition to evaluate the applicability of each of the models. This comparison of modeled and observed deposition patterns enhanced our understanding of the dominant overbank transport mechanisms on each of the floodplains where observation of individual floods are not available but where the pattern of deposition has been documented.

4.2 Theory

Since the focus of the proposed model was to evaluate the lateral variability in floodplain deposition, a straight, longitudinally uniform, steady flow, channel-floodplain system was considered (Figure 4.8). The idealized floodplain was modeled as depth-averaged flow over a flat (constant depth), vegetated floodplain with a uniform lateral velocity and negligible longitudinal floodplain velocity. Instead of modeling a compound channel floodplain (James, 1985; Pizzuto, 1987), this model allows for the transport of water and sediment across a wide plain of fixed width and allows the water and sediment to exit the system at the distal boundary. Though this formulation does not conserve mass in the sense that all sediment mass transported into the system at the channel edge is not necessarily stored in the floodplain. However, it is a reasonable assumption that the mean flow perpendicular to the channel transports sediment away from the channel and across the floodplain, a flow dynamic that cannot exist in a bounded, compound, straight channel. Additionally, both the Fly and Strickland River systems occupy scroll-bar belts of plains elevated relative to their adjacent floodbasins and can be drained by parallel drainage systems, the Agu and Mamboi Rivers respectively (Day et al., 2008; Swanson et al., 2008). The Fly floodplain is characterized by a distributary network of channels that can collect floodplain flow and convey it downstream or return it to the main channel

once the stage retreats (Day et al., 2008; Rowland et al., 2005). In the meander belt of a river there may be flow across meanders in the down-valley direction rather than perpendicular to the valley axis. However, differences in deposition between curved and straight reaches were small on the Strickland River floodplain (Swanson et al., 2008) and are not observed on the Fly River floodplain. Additionally, observations indicate that most deposition occurs within 1-2 channel widths from the channel on both of these large floodplains such that down-valley flow would still deposit much if not all of its suspended load within 1/2 a meander wavelength before returning to the channel (~11 times the channel width; Leopold and Wolman, 1960).

The model developed here was used to calculate deposition patterns for both the middle Fly and lower Strickland River floodplains for diffusion, advection and diffusion, and advection only transport processes. The diffusion only scenario was used to describe the conditions of direct precipitation inundation of the floodplain prior to the river stage exceeding bankfull flow that has been observed on the Middle Fly River floodplain. When this occurs, the sediment-laden, brown water of the channel remains confined within the natural levees and can be observed mixing only slightly with the organic-rich, black water on the floodplain (Figure 4.9).

4.2.1 Floodplain deposition model

A model of floodplain deposition was developed and applied to both the middle Fly and lower Strickland River floodplains. Three scenarios of transfer of sediment from the channel and deposition on the plain were considered for each floodplain (for a total of six scenarios): diffusion only, advection and diffusion, and advection only. The reasonability of each of the scenarios was evaluated based on a deposition length-scale and the full model results were computed either numerically or analytically.

For a longitudinally-uniform depth-averaged floodplain, the diffusion and advection of sediment onto the plain are balanced by the difference between sediment settling and entrainment. For the purposes of this model, it was assumed that all overbank sediment was transported all suspended load. Sediment deposition was modeled based on a 1-D mass balance of sediment transport and settling much like the 2-D sediment deposition model used by Nichols and Walling (1997). From conservation of mass, the change in depth-averaged sediment concentration, c_n, (a surrogate for mass in the water column for the floodplain of uniform depth) for particle size *n*, with respect to time is equal and opposite to the rate of change of sediment flux for that same grainsize, q_{sn}, or

$$\frac{\partial c_n}{\partial t} + \nabla \cdot q_{sn} = 0 \qquad (4.6)$$

The depth-averaged sediment flux, $\nabla \cdot q_{sn}$, can be expressed as the transport of sediment by advection and turbulent diffusion, erosion and deposition

$$\frac{\partial c_n}{\partial t} + \frac{\partial}{\partial y}\overline{c_n'v'} + \bar{v}\frac{\partial c_n}{\partial y} + \frac{c_n E}{H} - \frac{c_n w_{sn}}{H} = 0 \qquad (4.7)$$

where the overbar indicates a temporal average, *y* is the lateral distance from the channel edge, $\overline{c_n'v'}$ is the Reynolds flux of sediment [M/L^{3}t], $\bar{v}$ is the lateral flow velocity [L/t], E is an entrainment rate [L/t], w_{sn} is the settling velocity for particle size *n* and *H* is the depth of flow on the floodplain. The Reynolds flux of sediment can be expressed as

$$\overline{c_n'v'} = -K_s \frac{\partial c_n}{\partial y} \qquad (4.8)$$

where K_s is the sediment diffusivity. Sediment diffusivity is calculated as the product of the turbulent velocity, q, the turbulent mixing length, l_t, and a coefficient, C_s, (Pizzuto 1987):

$$K_s = C_s q l_t \qquad (4.9)$$

and C_s is set equal to the diffusivity of water, 0.13, after Fischer et al. (1979). The turbulent velocity, *q*, is used in the formulation of diffusivity in place of the friction velocity, u_*, here because u_* defined a depth-slope definition as a fraction of the mean velocity would be zero in all or some scenarios. The limiting length-scale for turbulent mixing, l_t, is set as the depth of flow for a shallow floodplain system. Entrainment is set equal to zero for the low-energy floodplain and the sediment balance can be obtained by substitution of equations 4.8 and 4.9, into equation 4.7:

$$\frac{\partial c_n}{\partial t} + \frac{\partial}{\partial y}(-C_s q l_t \frac{\partial c_n}{\partial y}) + \bar{v}\frac{\partial c_n}{\partial y} - \frac{c_n w_{sn}}{H} = 0 \quad . \qquad (4.10)$$

The second term of the equation can be expanded using the product rule yielding

$$\frac{\partial c_n}{\partial t} - C_s l_t \frac{\partial q}{\partial y}\frac{\partial c_n}{\partial y} - C_s l_t q \frac{\partial^2 c_n}{\partial y^2} + \bar{v}\frac{\partial c_n}{\partial y} - \frac{c_n w_{sn}}{H} = 0 \qquad (4.11)$$

.

For the scenarios of diffusion only ($\bar{v} = 0$), and the scenarios where advection and diffusion are both considered, the turbulent velocity, *q*, is solved for as a function of *y* in

order to solve for the steady-state concentration function ($\frac{\partial c_n}{\partial t}$=0). The sediment concentration as a function of distance from the channel for each size class can then be solved numerically. If advection only is considered (*q=0*), equation 4.7 simplifies to

$$\frac{\partial c_n}{c_n} = \frac{w_{sn}}{\bar{\nu} H} \partial y , \tag{4.12}$$

a linear differential equation that can be solved explicitly by integration. Integration from the channel boundary, y=0, to some distance, y, yields

$$c_n(y) = c_n(0) e^{\frac{w_{sn}}{\bar{\nu} H} y} . \tag{4.13}$$

Once the sediment concentration has been determined as a function of lateral distance for each scenario, the annual sedimentation rate for size class *n*, r_n, with units of L/t, is calculated as

$$r_n(y) = \frac{c_n(y) w_{sn} I}{r_b} \tag{4.14}$$

or

$$r_n(y) = \frac{c_n(0) e^{\frac{w_{sn}}{\bar{\nu} H} y} w_{sn} I}{r_b} \tag{4.15}$$

where *I* is the fractional time that the floodplain is active and r_b is the bulk density of the deposited material. The total annual deposition rate is then equal to the sum of r_n for all particle sizes considered.

4.2.2 Turbulence model

The lateral variability of turbulence needs to be determined in order to solve the lateral sediment concentration relationship for the diffusion and advection-diffusion scenarios from equation 4.11. Turbulent kinetic energy (TKE) per unit mass, $\frac{1}{2} q^2$, is defined as half the root of the sum of the temporally averaged (indicated by overbars) squares of the deviatoric velocities in the three coordinate directions in the fluid flow, *u'*, *v'* and *w'*:

$$\frac{1}{2}q^2 = \frac{1}{2}\sqrt{\overline{u'^2} + \overline{v'^2} + \overline{w'^2}} \quad . \tag{4.16}$$

For the idealized floodplain in Figure 4.8, turbulence is transported across the floodplain by lateral flow, dispersed by turbulent mixing, produced by the drag of the flow through the floodplain vegetation and dissipated by the viscosity of the fluid. Since pressure and buoyancy can be ignored in this idealized floodplain, the TKE balance can be written as

unsteadiness transport diffusion shear production - dissipation

$$\frac{\partial}{\partial t}\left(\frac{1}{2}q^2\right) + \overline{U}\cdot\nabla\frac{1}{2}q^2 = \nabla\cdot\left(K_q\nabla\left(\frac{1}{2}q^2\right)\right) + P \qquad \varepsilon \tag{4.17}$$

where $\overline{U}$ is the temporally averaged velocity that is the sum of the mean velocities in the three coordinate directions in the fluid flow, $\overline{u}$, $\overline{v}$, and $\overline{w}$

$$\overline{U} = \overline{u} + \overline{v} + \overline{w} \tag{4.18}$$

and K_q is the eddy diffusivity (Kundu and Kohen, 2004). Eddy diffusivity is defined as

$$K_q = C_q q l_t \tag{4.19}$$

where C_q is equal to 0.13 (Fischer et al., 1979). Substitution of equation 4.19 into 4.17 and simplification for longitudinally-uniform, depth-averaged, steady flow with advection only in the lateral direction yields

$$\frac{\partial}{\partial t}(\frac{1}{2}q^2) + \overline{v}\frac{\partial}{\partial y}(\frac{1}{2}q^2) = \frac{\partial}{\partial y}(K_q\frac{\partial}{\partial y}(\frac{1}{2}q^2)) + P - e \; . \tag{4.20}$$

Turbulence production for flow through a vegetated floodplain is assumed to be a function of mean velocity, bulk drag, $\overline{C_d}$, and vegetation density, *a*, after Nepf (1999) so that

$$P = \frac{1}{2}a\overline{C_d}\overline{v}^3 \quad . \tag{4.21}$$

The drag coefficient, $\overline{C_d}$, decreases with increasing vegetation cover and $a\overline{C_d} = l^{-1}$ where l is the length-scale of shear mixing (Nepf, 1999).

Viscous dissipation of turbulent energy is assumed to be equal to

$$\varepsilon = \frac{q^3}{BH} \tag{4.22}$$

where B is an empirically defined constant defined to be 16.6 by Blumberg et al. (1992). Equations 4.21 and 4.22 are substituted into equation 4.20 resulting in a relationship for TKE that can be discretized and solved numerically for the steady-state turbulence relationship

$$\frac{\partial}{\partial t}(\frac{1}{2}q^2) + \bar{v}\frac{\partial}{\partial y}(\frac{1}{2}q^2) = \frac{\partial}{\partial y}(K_q \frac{\partial}{\partial y}(\frac{1}{2}q^2)) + \frac{1}{2}\frac{\bar{v}^3}{l} - \frac{q^3}{BH} \tag{4.23}$$

with the appropriate boundary conditions described in the model parameterization. The advection and production terms are equal to zero in the diffusion only case resulting in a steady-state balance between diffusion and dissipation. When advection is considered, the distal floodplain is characterized by a balance between turbulent production and dissipation. This relationship does not need to be solved for the advection only scenarios, since turbulence is not considered in those scenarios.

4.2.3 Model scaling

Scaling provides a simple test to determine the reasonableness of applying the described models for each of the scenarios. The scaled deposition length for the diffusion-only and advection-only scenarios can be calculated in order to determine the applicability of the model to the observed floodplain system. For the diffusion only scenarios, the depositional length-scale, L_d, is computed as

$$L_d = \sqrt{K_s T} \tag{4.24}$$

where K_s is the sediment diffusivity described in equation 4.9 and T is the time required for settling to clear the water column

$$T = \frac{H}{w_s}. \tag{4.25}$$

The deposition length-scale was computed for each size class individually.

The depositional length-scale for advective transport, L_a, was calculated as the product of mean lateral velocity, $\bar{v}$, and T:

$$L_a = \bar{v}T . \quad (4.26)$$

The calculated depositional length-scales were compared to the observed mean distance from the channel bank that particles of similar size are transported, which was calculated as the center of mass of the lateral floodplain deposit for a given size.

The Peclet number was used to assess if one transport mechanism dominates in either of the advection-diffusion scenarios rendering it redundant with the end member case. The Peclet number, Pe, a dimensionless number describing the relative strength of diffusion and advection in a flow, is defined as

$$Pe = \frac{K_q}{vH} . \quad (4.27)$$

If $Pe >> 1$, diffusion is the dominant transport process and if $Pe << 1$ advection is the dominant transport process.

4.3 Model parameterization

Estimates and measurements of channel and floodplain characteristics are needed in order to solve the above sediment and turbulence relationships. The input parameters needed to run the model are the concentration of sediment and sediment PSD at the channel-floodplain boundary, the depth of flow on the floodplain, the fractional annual time of active overbank deposition, lateral velocity across the floodplain, turbulence at the channel boundary, and the length-scales of turbulence and shear mixing on the floodplain. Settling velocity is defined as a function of particle diameter. Many of these input parameters are not routinely observed and must be estimated based on the limited data available.

The time of flow above bankfull flow was used to approximate the fractional time of active overbank deposition. Lauer et al. (2008) estimated this fractional time of flows in excess of bankufll was equal to 0.25 or 91.25 days a year for the Strickland and Middle Fly Rivers. While this may be reasonable for the Middle Fly River, the estimate seems too large for the Strickland River floodplain which, unlike the Middle Fly floodplain, does not remain inundated for months at a time. This was indicated by the by the low frequency of occurrence of bank-overtopping flows at SG4 (Figure 4.10). Channel geometry is very consistent on the lowland Strickland River with bankfull areas of 3440-3480 m^2 and bankfull depths of 11 to 14 m on transects 2, 3 and 4. A Manning's n value of 0.03 yields a calculated channel flow velocity of ~1.8 m/s for this lowland reach and bankfull discharge of ~6300 m^3/s. This flow was exceeded at SG4, near the gravel sand transition, 5 to 6 days a year. A fractional annual flood duration, I, of 91 days/year was used for the Middle Fly River as proposed by Lauer et al. (2008). For the Strickland

River a flood duration of 5 days/year was used in order to explore these two end member scenarios.

Lateral velocity, $\bar{v}$, across the floodplain can be estimated such that the measured mass of sediment deposited, per unit width, within 1-km of the channel boundary on each of the floodplains in one year, M_{sed}, is equal to the flux across the sediment-channel boundary for the flood durations described above. This approach assumes that all sediment transported from the channel was deposited on the floodplain. Thus, lateral velocity is

$$\bar{v} = \frac{M_{sed}}{HbcI} \tag{4.28}$$

where c is sediment concentration in the channel and b is a unit width. On the Strickland River, suspended sediment concentration (SSC), c, of about 500 mg/L was typical for during bankfull flows. This estimate is similar to the 455 mg/L that can be calculated from bankfull the discharge estimates in Lauer et al. (2008). The bankfull discharge values for the Fly River provided by Lauer et al. (2008) yield a suspended sediment concentration of 130 mg/L at bankfull discharge. Particle size distributions of the measured floodplain sediments are described in Chapter 3 for the Fly and Strickland River floodplains. The volumetrically integrated floodplain deposit PSDs are assumed to represent the sediment that was transported overbank during flood flows. These size distributions are summarized in Tables 4.1 and 4.2. A floodplain flow depth, H, of 3 m was used for all scenarios (Geoff Day, unpublished data).

The calculated lateral floodplain velocities were 0.064 m/s and 0.00014 m/s on the Strickland and Fly River floodplains respectively. These velocities should be considered to be low estimates because the flux of sediment to the floodplain does not have to equal the mass deposited. Field observations over several years on the Fly failed to detect significant floodplain velocities. It seems likely that rare events likely create the advective velocities to deliver the sediment and that these back calculations represent some gross time average. As such these estimates may be reasonable first-order approximations of the lateral velocity to explore the relative importance of advection and diffusion in generating the observed deposition patterns.

Boundary conditions at the distal floodplain boundary were constant TKE and SSC with respect to y. The turbulent velocity at the channel boundary, $q(0)$, was assumed to equal the friction velocity, calculated as a fraction, $1/10$, of the mean bankfull channel velocity for each of the channels. Lauer et al. (2008) defined the bankfull velocities as 1.63 and 0.93 m/s for the Strickland and Middle Fly Rivers, respectively. The characteristic length-scale of turbulent eddies in the floodplain flow was assumed to be the depth of the flow, H. The length-scale of shear eddies on the floodplain were assumed to be equal to $1/2$ the width of the natural levees observed on the floodplain and was set equal to 70 m

for all scenarios. The input parameters for each of the 6 scenarios are summarized in Table 4.3.

The sediment concentrations and deposition rates were calculated explicitly for equation 4.15 for the advection only scenarios (scenarios 5 and 6). The model input parameters in Table 4.3 inputs were used to solve equations 4.11 and 4.23 numerically for scenarios 1-4 in which diffusion was considered. The partial differential equations were discretized using a central difference formulation and solved for a steady-state solution. The turbulence at the channel edge results from the mean downstream velocity in the channel. Turbulent production at the channel boundary provided one boundary condition for equation 4.23. The balance of production and dissipation at the distal edge of the floodplain model domain provided the other boundary condition required to solve equation 2.23. Similarly, the sediment concentration was defined at the channel boundary, and the distal boundary condition was defined as zero variability in sediment concentration or

$$\frac{\Delta c}{\Delta y} = 0 \ . \tag{4.29}$$

This boundary condition allows for the sediment concentration at the distal boundary to be positive, so within this model framework sediment can be transported across the floodplain without depositing. A 5000-m wide floodplain was modeled so that the zone where deposition was measured, 1000-2000 m on the Fly and Strickland River floodplains, is not strongly influenced by the distal boundary. The lateral node spacing, Δy, was 1m and a timestep of 0.01s was used to calculate the convergence of the discretized equations for a steady-state solution using MATLAB.

4.4 Results

Deposition length

The calculated and observed depositional length-scales for the Fly and Strickland River floodplains are shown in Table 4.4. These results indicate that diffusion only is not sufficient to transport sediment significant distances across the floodplain. Sediment with a diameter of 8 μm or more would typically be transported less than 60 m from the channel boundary by diffusion alone. Because clay has a very long settling time, T, the typical deposition length for diffusion alone would be greater than the observed center of mass of clay deposits adjacent to the Fly River, but about ½ the magnitude of the center of mass of deposits on the Strickland floodplain.

The weak advection calculated for the long flood duration on the Fly River floodplain is even less effective at transferring sediment coarser than clay significant distances from the channel based on the calculated deposition length for advection (≤7.3m; Table 4.4).

However, the very small settling velocity for clay size particles leads to a length-scale of deposition much greater than the center of mass of observed deposits.

The scaling of deposition length for the advection model of sediment transport and floodplain deposition on the Strickland River floodplain yields slightly more promising results by predicting significant transport of silt to the median and distal floodplain, but the characteristic deposition depths for fine silt and clay are larger than the observed range of deposition (Table 4.4). However, the calculated depositional length-scales are generally larger than the observed centers of mass and increase for decreasing particle sizes much more rapidly than is observed in the floodplain deposits.

Either advection or diffusion would lead to fining based on the decrease in calculated deposition length with increasing grainsize, which is not observed on the Fly River floodplain where the center of mass for deposits of all grainsizes is ~250m.

Advection and diffusion

For the scenarios that considered both advection and diffusion, scenarios 3 and 4 for the Fly and Strickland, respectively, the Peclet numbers were respectively 86.35 and 0.37 at the channel boundary and 0.72 and 0.10 500 m from the channel edge. This indicates a dominance of diffusion in scenario 3 near the channel and a dominance of advective transport everywhere in scenario 4, particularly far from the channel. There was a reversal in the dominant mechanism of transport in scenario 3 between the channel boundary and 500m distal, but so little sediment was transported away from the channel boundary that the reversal in mechanisms was not apparent in the pattern of deposited sediment (See Appendix B). The strong advection in scenario 4 yielded nearly identical results to the advection-only case for the Strickland River, scenario 6. A Pe less than one but not very small near the channel indicates that diffusion played a small role in transport in the near-channel section of the floodplain but the distal floodplain was completely dominated by advective transport. Advection was necessary for sediment to be transported significant distances from the channel and diffusion played a small role in only the near-channel transport of sediment.

Model results

The full suite of solutions for the six scenarios is presented in Appendix B. In all of the modeled scenarios, deposition decreases and sediment particle size decreased with increasing distance from the channel. All of the scenarios over-predicted deposition directly adjacent to the channel and under-predict deposition in the distal floodplain, especially for clay sized sediment on the Strickland floodplain (Figure 4.11). As indicated by the model scaling, the advection-diffusion scenarios were redundant with the single-process scenarios and only the single-process models required further consideration. Of the single-process scenarios, only scenario 6, advection on the Strickland River floodplain, was competent at transporting and depositing sediment significant distances from the channel (Figure 4.12). Despite the depositional length-scale analysis indicating a disparity between the modeled and measured depositional

lengths, the model approximately reproduced the observed rate of deposition with increasing distance from the channel (Figure 4.11). However, examination of the observed pattern of deposition for each grainsize shows that the model over-predicted sand and coarse silt deposition near the channel and under-predicted fine silt and clay deposition throughout (Figures 4.12 and 4.13). While the calculated deposition rate for each grainsize in scenario 6 is an exponential function (Equation 4.15 and Figure 4.13), the resulting sum of exponentials is a non-exponentially decreasing deposition function (Figure 4.12).

4.5 Discussion

The model scaling and scenario solutions and indicated that deposition decreases and sediment particle size decreased with increasing distance from the channel. All of the scenarios over-predicted deposition directly adjacent to the channel and under-predicted deposition in the distal floodplain, especially for clay-sized sediment on the Strickland floodplain. The diffusion-only scenarios and weak-advection scenarios (Fly) did not transport significant sediment across the plain while the strong advection scenarios (Strickland) were nearly identical regardless of the inclusion of diffusion, as would be expected based on the Pe analysis. None of the scenarios resulted in a uniform exponential deposition pattern that does not fine with distance from the channel as was observed on the Fly floodplain. Qualitatively the model results do recreate some key observed patterns of magnitude and lateral variability of PSD in overbank deposits on the lowland floodplains modeled. This allows for the exploration of the key processes of diffusion and advection across a floodplain that may result in the observed patterns of deposition.

The prediction of deposition near the channel boundary was controlled by the concentration at the channel boundary, the settling velocities of the specified particle sizes and the duration of flooding. On real floodplains, one would expect significant downstream flow along the levee that may be competent to keep fine sediment in suspension and inhibit deposition immediately adjacent to the channel. This process was both observed and modeled on the Rhine-Meuse floodplain by Asselman and Middlekoop (1995), but was not considered in this study resulting in the overestimation of deposition directly adjacent to the channel boundary.

The diffusion-only scenarios for the Strickland and Fly Rivers and weak advection in the advection-diffusion scenario of the Fly River did not provide a reasonable transport mechanism for overbank sediment deposition beyond the area immediately adjacent to the channel. The model was simplified to exclude downstream velocities and did not explicitly incorporate coherent eddies that would exchange sediment and momentum between the floodplain and channel which could increase the lateral extent of sedimentation. Absent these or other mechanisms that could increase turbulent production and transport across the entire width of the floodplain, diffusion alone is clearly insufficient to transport sediment across the floodplain in a manner that would

match the observed floodplain deposition patterns on the Fly and Strickland River floodplains. The models of Pizzuto (1987) and James (1985) that exclude sustained advection in the cross-stream direction explicitly incorporated a downstream velocity and were applied to much narrower floodplain sections which may account for the apparently significant deposition that was predicted by these earlier models and that was not predicted here. However, diffusive transport of sediment from the channel to the plain when advection of water and sediment is inhibited by floodwaters on the plain (as in Figure 4.9) is likely an important process in natural levee formation and should be considered an important process for near-channel deposition (Adams et al., 2004).

The depositional length-scale analysis and all scenario solutions predict fining of sediment with increasing distance from the channel (Table 4.4, Appendix B), but all of the scenarios over-estimated sand deposition near channel and under-predicted the total clay deposition on the floodplain. In the case of a real flood, the sediment-laden water in the water column when the flood recedes would likely pond on the floodplain and the sediment settle onto the plain. This could account for some of the "missing" clay in the modeled floodplain deposits. However, when calculated from the predicted sediment concentration curves the mass of sediment in the water column was very small and the resulting deposition does not account for the difference between modeled and measured clay deposition. On the contrary, the model was not a closed model and both water and sediment could exit the model domain at the distal boundary. Conceptually this is similar to water flowing from the floodplain to tributary channels or adjacent flow basins like the Agu or Mamboi Rivers. It is more likely that fine particles form flocculates and the effective settling velocity of these particles is much larger than the settling velocity of a single clay or fine silt particle. A larger settling velocity would result in increased deposition similar to the deposition curve modeled for the larger particle sizes.

It is clear from the model results that only the scenarios with relatively strong advection provide a realistic magnitude of deposition across the floodplain. Though the Fly River remains above flood stage for months every year, it is likely that the floodplain is only connected to these flood flows by advective transport from the channel across the plain for much shorter durations (e.g. during the rising limb of a flood when the floodplain is not already inundated by direct precipitation). More realistic parameterization of the Fly River floodplain model would likely include a lateral velocity of the same order of magnitude as that calculated for the Strickland River floodplain. This would result in a deposition pattern similar to the results of scenarios 4 and 6 on the Strickland River floodplain. Though these scenarios captured decreasing magnitude of deposition across the plain they did not predict the observed exponentially declining depositing rate and nearly constant PSD on Fly River floodplain.

It is possible that the assumption of constant depth across the plain, constant sediment concentration at the boundary and constant velocity used in the model were too simple. The simplest scenario to explore is the lateral variation of floodplain depth – a floodplain that slopes away from the channel ridge. If we consider advection only where flux of

water and sediment are held steady at the channel boundary and the water surface remains horizontal, the calculation of sediment concentration across the floodplain would not yield an exponential function. Taking a Lagrangian approach, a parcel of water flowing across the floodplain would slow as it moved across the floodplain to deeper sections of the floodplain. The residence time of water over a given section of floodplain would increase linearly with depth allowing the time for additional sediment to settle, however, since the model assumes a well mixed water column, this would yield a lower sediment concentration at a given distance than the comparable case with a constant floodplain depth. This would result in an identical mass of sediment in suspension over a unit area at any location on the floodplain in both scenarios. Though the concentration would decrease with depth relative to the flat floodplain scenario, the residence time of a parcel of water would increase correspondingly with depth yielding an equal mass flux for both the flat and sloping floodplain profiles. The resulting deposition pattern for either scenario would be equal to the calculated deposition curve (equation 4.15) for the flat floodplain scenario despite the differing sediment concentration curves.

If one considers a temporally variable scenario where velocity, depth or concentration are allowed to change in time a simplifying assumption that these changes are immediately translated across the floodplain can be made. It is then trivial to solve any set of parameters for their steady-state solutions from equation 4.15 and apply these solutions over discrete time intervals as was done by Nicholas and Walling (1997). The sum over all time intervals could then be compared to the deposition pattern observed on the floodplain. No matter what reasonable parameterization was chosen, the resultant pattern would have decreasing magnitude of deposition and fining of sediment sizes away from the channel and would not result in the observed pattern on the Middle Fly River floodplain.

The only feasible formulation which allows for the advection-only model to result in an exponential deposition pattern is for the application of a single particle size. This may be realistic on some rivers like the Brahma-Putrah where coarse sediment deposition decreases exponentially and fine sediment deposition is nearly constant and small in magnitude (Allison et al., 1998). Despite the exponential decrease in deposition rate the deposited sediments fine as the relative proportion of coarse sediment decreases with increasing distance from the channel. However, on the Fly River floodplain the PSD is not bi-modal and the deposition pattern of all size classes is nearly identical. Basd on the solution to equation 4.1, this seems to indicate that the particles all have the same effective settling velocity or are being advectively transported together as a single floc size.

In field measurements of the effective settling velocity of suspended material and laboratory analysis of dispersed ultimate particle sizes from the River Culm, UK, floodplain aggregation was found to be important for the cohesive material and increased the proportion of fine material found on the floodplain. Understanding this relationship was fundamental to modeling the floodplain accurately (Nicholas and Walling, 1996).

McNally and Mehta (2001) found that aggregation dominated the deposition of high-cohesion material and was important for medium-cohesion material in laboratory experiments of estuarine sediments. In experiments in San Francisco Bay both Kranck and Milligan (1992) and Maning and Schoellhamer (in review) noted the presence of fine sands in some flocs during in situ studies of particle dynamics within the water column despite the fact that these coarse particles are thought to be non-cohesive and therefore non-participatory in flocculation. These studies indicate that not only is flocculation an important control in sediment transport, but also that it is possible for all particle sizes, even sand, to flocculate as they are transported across the Fly River floodplain.

The swamps adjacent to the Fly River may provide the floodplain flows with organic matter that can increase the cohesion of fine sediments in the low-energy environment and allow for the trapping of coarse particles in the flocculates. The flocculation of all particle sizes in a Fly River scenario combined with reasonable advection could result in the observed deposition pattern. If one assumes that the flood interval of 91 days/year and suspended sediment concentration at the channel boundary of 130 mg/L are correct, the effective settling velocity can be calculated from the coefficient on the exponential fit to the measured deposition pattern and equation 4.15. This yields an effective settling velocity of $1.2*10^{-3}$ cm/s. The lateral floodplain flow velocity can then be calculated from the exponent term in equation 4.15 from this assumed effective settling velocity for all particle sizes and a depth of 3 m to be 0.12 cm/s. It is more likely that the total time that the floodplain is receiving sediment from the channel is less than the time that the channel is above flood stage. There may be very short periods of time when the river stage rises rapidly prior to inundation of the floodplain that deliver the majority of the overbank sediment to the adjacent floodplain. The relationship between inundation time, I, and settling velocity can be further explored by equating the depositional length-scale, L_a, to the observed center of mass of deposition, ~250m, and by substitution of equations 4.25 and 4.28 into 4.26 yielding

$$I = \frac{M_{sed}}{L_a b c w_s} \quad . \tag{4.30}$$

Using this approach, inundation period and settling velocity vary inversely with one another and the depth of floodplain flow is no longer required for the calculation. The calculated inundation period for an effective particle diameter, the diameter of a single particle with an equivalent settling velocity of the flocculated sediment, of 12 μm is 25 days and an effective diameter of 48 μm requires only 1.6 days of active transport from the channel to the floodplain (Figure 4.14). This analysis indicates that if advective transfer of sediment from the channel to the floodplain did occur for 91 days, the effective particle diameter would be ~6 μm. Figure 4.15 shows the relationship between inundation period, floodplain flow velocity, and depth described in equation 4.28. Flow velocities of the order 1 cm/s occur for flood durations of ~10-30 days for depths

generally greater than 2 m. This indicates that an effective particle diameter of 12 μm and duration of active flow from the channel to the floodplain of 25 days are not unreasonable.

On the steeper, better drained Strickland River floodplain, flow is likely more turbulent and less organic-rich than the Fly River floodplain water resulting in less flocculation, though the cohesive clays and very fine silts are probably transported as flocs and the settling velocities of these particles should be carefully parameterized in future model applications to accurately predict their deposition. The under-prediction of clay and fine silt deposition by the model results from using the Stokes settling velocity rather than the effective floc settling velocity for these cohesive size classes.

The effective settling velocities of the observed floodplain deposits on the Strickland River can be approximated using the relationship in equation 4.30 for each particle size class, *n*,

$$w_{sn} = \frac{M_{sedn}}{L_{an} b c_n I}. \tag{4.31}$$

This calculation indicates that the effective settling velocities of clay, very fine silt and fine silt are higher than the settling velocities of individual particles by factors of 31, 3 and 3.5 respectively (Figure 4.16). This indicates that coarse silt and fine sand may be settling at an effectively lower velocity due to flocculation (as is hypothesized for the Fly River floodplain), but it is more likely that the narrow band adjacent to the channel where these coarser sediments are deposited experiences higher flow velocities in the along-channel or down-valley direction inhibiting deposition.

4.6 Conclusions

The results of the modeling and model scaling lend themselves to the conclusion that advection is the dominant transport mechanism for overbank deposition and that flocculation plays a critical role in determining the pattern of overbank deposition. The Fly River floodplain may be unique in that no fining is observed with increasing distance from the channel. Studies on the Brahma-Putrah and small basins in the UK have both measured exponentially decreasing sediment deposition rates, but in both cases coarse sediment deposition decreased exponentially and fine sediment deposition was nearly constant and small in magnitude (Allison et al., 1998; Walling and He, 1998). Walling and He (1998) identified two distinct processes leading to this unique deposition pattern: the advection of coarse sediment from the channel to the floodplain and the settling of clay from waters impounded on the floodplain after the initial flood pulse. Aalto et al. (2003) measured an exponentially decreasing deposition pattern on the Beni River as the result of crevasse splays, but noted that these high-energy sediment-laden flows were

very different than the overbank deposition of clay and fine sediments carried as wash load in the channel.

Because of the difficulty of sampling and the spatial and temporal scales involved, very little documentation of the grain size distribution of deposited sediments is available for the world's larger rivers such as the Amazon (Dunne et al., 1998; Mertes, 1994). The Strickland River floodplain deposition pattern is perhaps more typical for large lowland rivers with decreasing deposition rate and grainsize with increasing distance from the channel. Previous studies of overbank deposition have noted an exponential decrease in median grainsize with distance from the channel on the Saskatchewan River floodplain (Adams et al. 2004). Grainsize and deposition also decreased for an unconstrained reach of the Rhine system, but size and deposition rate were nearly uniform on a confined channel reach where flow velocities are more likely to be large and in the downstream direction.

The rate and pattern of sediment deposition measured on both the Fly and Strickland River floodplains were explained using a simple advection model resulting in an exponential deposition pattern for an individual effective particle size or a non-exponential deposition pattern for a distribution of effective particle sizes. However, the data available were inadequate to properly parameterize particle settling, the duration of active floodplain deposition and floodplain flow velocity. It seems reasonable to infer that exponential deposition patterns are the result of lateral advection across the floodplain and a single effective settling velocity for the majority of the sediment in suspension (e.g. Walling and He, 1997; Allison et al., 1998, Day et al., 2008). A bimodal distribution of particles in suspension may result in an exponential deposition pattern of the coarser material and an apparently uniform layer of fine sediment as observed on the Brahma-Putrah (Allison et al., 1998). Non-exponential deposition patterns are likely to result from lateral advection of sediment with a distribution of effective settling velocities (e.g. Aalto et al, 2003; Swanson et al., 2008).

The floodplain deposition model developed here indicated that the floodplain sediment transport mechanisms which control the spatial variation of the rate and pattern of deposition were the velocity of lateral floodplain flow and the effective settling velocity of the sediment in suspension. A simple scaling of the model resulted in reasonable estimates of some of some critical model parameters (that are typically difficult on unfeasible to measure) based on the observed deposition patterns. In terms of the three questions motivating this work, this analysis suggests the following answers:

1. The primary controls on the lateral variation in the rate of deposition are the lateral floodplain velocity and the ratio of that velocity to the effective settling velocity of the sediment in suspension.
2. The primary control on the spatial variation in particle size distribution is the variation of the effective settling velocity

3. The controlling deposition mechanism that makes the Fly and Strickland River floodplain systems so different is the relative strength of flocculation of the sediments in suspension.

The differences between the Fly and Strickland may arise from the difference is sediment supply such that in response to sea level rise the rate of infilling of accommodation space was more rapid on the Strickland, and distinctly far from complete on the Fly. Consequently, the Fly experiences extensive periods of floodplain inundation and the swampiness of the floodplain influences sedimentation patterns by driving flocculation whereas the Strickland floodplain drains more rapidly.

Further refinements to the model could include improved parameterization of floodplain velocity, floodplain-channel connectivity, and suspended sediment settling characteristics. Future studies of floodplain sediment transport processes should include long-term monitoring of flow velocity on the floodplain and *in situ* measurements of floc properties. Because these properties have not been measured on the floodplain I can only hypothesize that flocculation and advection are the mechanisms that are primary controls on the pattern of deposition observed on the two floodplains. The comparison of model results to field observations indicated that diffusion alone cannot transport sediment sufficient distances from the channel to replicate observed deposition patterns on these large floodplains.

Tables

Total distance considered (m)	Grain size class μm					
	1	8	12	24	48	100
1000	0.31%	24.21%	12.11%	40.00%	16.40%	6.96%
2000	0.49%	33.14%	14.38%	33.63%	12.89%	5.47%

Table 4.1 Model input PSD for all Fly River floodplain model scenarios.

Total distance	Grain size class µm						
	0-2	2-8	8-16	16-32	32-62	62-128	>128
1000	22.5%	36.9%	17.3%	13.5%	7.6%	2.1%	0.1%
2000	28.1%	40.2%	14.4%	10.3%	5.4%	1.4%	0.1%

Table 4.2 Model input PSD for all Strickland River floodplain scenarios.

Scenario		Parameter			
		T days	***c(0)*** mg/L	**U_{bf}** m/s	***V*** Cm/s
1	Fly, diffusion	91	130	0.93	0
2	Strickland, diffusion	5	500	1.63	0
3	Fly, advection and diffusion	91	130	0.93	0.014
4	Strickland, advection and diffusion	5	500	1.63	6.4
5	Fly, advection	91	130	-	0.014
6	Strickland, advection	5	500	-	6.4

Table 4.3. Model input parameters for all model scenarios.

Particle size (μm)	Depositional length-scale (m)						Size class range (μm)
	Diffusion only		Advection only		Observed center of mass		
	Fly	Strickland	Fly	Strickland	Fly	Strickland	
1	348	461	468	213730	242	845	<2
8	44	58	7.3	3340	239	561	2-8
12	29	38	3.2	1484	242	25	8-16
24	15	19	0.8	371	259	36	16-32
48	7.3	9.6	0.2	93	254	10	32-64
100	3.5	4.6	0.05	21	213	22	64-900

Table 4.4 Calculated depositional length-scales for the diffusion-only and advection-only model scenarios (scenarios 1, 2, 5 and 6) as well as the observed center of mass of floodplain deposits. Calculated length-scales reflect the settling time for a particle with the diameter shown in the left column while center of mass calculations were completed for the size-range indicated in the right column.

References

Aalto, Rolf, et al. "Episodic sediment accumulation on Amazonian flood plains influenced by El Nino/Southern Oscillation." *Nature* 425.6957 (2003): 493-497.

Aalto, Rolf, J. Lauer, and William E. Dietrich. "Spatial and temporal dynamics of sediment accumulation and exchange along Strickland River floodplains (Papua New Guinea) over decadal.to.centennial timescales." *Journal of Geophysical Research: Earth Surface (2003–2012)* 113.F1 (2008).

Adams, Peter N., Rudy L. Slingerland, and Norman D. Smith. "Variations in natural levee morphology in anastomosed channel flood plain complexes."*Geomorphology* 61.1 (2004): 127-142.

Allen, John RL. "A review of the origin and characteristics of recent alluvial sediments." *Sedimentology* 5.2 (1965): 89-191.

Allison, M. A., et al. "Importance of flood-plain sedimentation for river sediment budgets and terrigenous input to the oceans: Insights from the Brahmaputra-Jamuna River." *Geology* 26.2 (1998): 175-178.

Asselman, Nathalie EM, and Hans Middelkoop. "Floodplain sedimentation: quantities, patterns and processes." *Earth Surface Processes and Landforms*20.6 (1995): 481-499.

Asselman, Nathalie EM, and Hans Middelkoop. "Temporal variability of contemporary floodplain sedimentation in the Rhine–Meuse delta, The Netherlands." *Earth Surface Processes and Landforms* 23.7 (1998): 595-609.

Asselman, Nathalie EM, Hans Middelkoop, and Paul M. Van Dijk. "The impact of changes in climate and land use on soil erosion, transport and deposition of suspended sediment in the River Rhine." *Hydrological Processes* 17.16 (2003): 3225-3244.

Asselman, Nathalie EM, and Marjolein van Wijngaarden. "Development and application of a 1D floodplain sedimentation model for the River Rhine in The Netherlands." *Journal of Hydrology* 268.1 (2002): 127-142.

Blumberg, Alan F., Boris Galperin, and Donald J. O'Connor. "Modeling vertical structure of open-channel flows." *Journal of Hydraulic Engineering* 118.8 (1992): 1119-1134.

Bridge, J. S., and S. D. Mackey. "A revised alluvial stratigraphy model."*Alluvial sedimentation* (1993): 317-336.

Bridge, John S. *Rivers and floodplains: forms, processes, and sedimentary record*. Wiley. com, 2009.

Day, Geoff, et al. "The depositional web on the floodplain of the Fly River, Papua New Guinea." *Journal of Geophysical Research: Earth Surface (2003–2012)* 113.F1 (2008).

Dunne, Thomas, et al. "Exchanges of sediment between the flood plain and channel of the Amazon River in Brazil." *Geological Society of America Bulletin*110.4 (1998): 450-467.

Fischer, Hugo B., ed. *Mixing in inland and coastal waters*. Access Online via Elsevier, 1979.

Hardy, R. J., P. D. Bates, and M. G. Anderson. "Modelling suspended sediment deposition on a fluvial floodplain using a two-dimensional dynamic finite element model." *Journal of Hydrology* 229.3 (2000): 202-218.

Howard, Alan D. "Modeling channel migration and floodplain sedimentation in meandering streams." *Lowland floodplain rivers: Geomorphological perspectives* (1992): 1-41.

James, C. S. "Sediment transfer to overbank sections." *Journal of Hydraulic Research* 23.5 (1985): 435-452.

Karssenberg, Derek, and John S. Bridge. "A three.dimensional numerical model of sediment transport, erosion and deposition within a network of channel belts, floodplain and hill slope: extrinsic and intrinsic controls on floodplain dynamics and alluvial architecture." *Sedimentology* 55.6 (2008): 1717-1745.

Kesel, Richard H., et al. "Lateral erosion and overbank deposition on the Mississippi River in Louisiana caused by 1973 flooding." *Geology* 2.9 (1974): 461-464.

Kondolf, G. Mathias, et al. "Geomorphic classification of rivers and streams."*Tools in fluvial geomorphology* (2003): 171-204.

Kundu, P. K., and I. M. Cohen. "Fluid Mechanics, 759 pp." (2004).

Kranck, Kate, and T. G. Milligan. "Characteristics of suspended particles at an 11.hour anchor station in San Francisco Bay, California." *Journal of Geophysical Research: Oceans (1978–2012)* 97.C7 (1992): 11373-11382.

Lauer, J. Wesley, and Gary Parker. "Modeling framework for sediment deposition, storage, and evacuation in the floodplain of a meandering river: Theory." *Water Resources Research* 44.4 (2008): W04425.

Lauer, J., Gary Parker, and William E. Dietrich. "Response of the Strickland and Fly River confluence to postglacial sea level rise." *Journal of Geophysical Research: Earth Surface (2003–2012)* 113.F1 (2008).

Leopold, Luna B., and M. Gordon Wolman. "River meanders." *Geological Society of America Bulletin* 71.6 (1960): 769-793.

Manning, A.J., and D.H. Schoellhamer, "Sediment floc characteristics in San Francisco Bay, USA" *Marine Geology* (*In review)*.

Marriott, Susan. "Textural analysis and modelling of a flood deposit: River Severn, UK." *Earth Surface Processes and Landforms* 17.7 (1992): 687-697.

McAnally, W. H., and A. J. Mehta. "Collisional aggregation of fine estuarial sediment." *Proceedings in Marine Science* 3 (2000): 19-39.

Mertes, Leal AK. "Rates of flood-plain sedimentation on the central Amazon River." *Geology* 22.2 (1994): 171-174.

Middelkoop, Hans, and Marcel Van Der Perk. "Modelling spatial patterns of overbank sedimentation on embanked floodplains." *Geografiska Annaler: Series A, Physical Geography* 80.2 (1998): 95-109.

Moody, John A., and Brent M. Troutman. "Quantitative model of the growth of floodplains by vertical accretion." *Earth Surface Processes and Landforms*25.2 (2000): 115-133.

Nepf, H. M. "Drag, turbulence, and diffusion in flow through emergent vegetation." *Water resources research* 35.2 (1999): 479-489.

Nicholas, A. P., and D. E. Walling. "The significance of particle aggregation in the overbank deposition of suspended sediment on river floodplains." *Journal of Hydrology* 186.1 (1996): 275-293.

Nicholas, A. P., and D. E. Walling. "Modelling flood hydraulics and overbank deposition on river floodplains." *Earth Surface Processes and Landforms* 22.1 (1997): 59-77.

Parker, Gary, et al. "Unravelling the conundrum of river response to rising sea.level from laboratory to field. Part II. The Fly–Strickland River system, Papua New Guinea." *Sedimentology* 55.6 (2008): 1657-1686.

Pizzuto, James E. "Sediment diffusion during overbank flows." *Sedimentology*34.2 (1987): 301-317.

Rowland, Joel C., et al. "Tie channel sedimentation rates, oxbow formation age and channel migration rate from optically stimulated luminescence (OSL) analysis of floodplain deposits." *Earth Surface Processes and Landforms* 30.9 (2005): 1161-1179.

Rowland, Joel C., William E. Dietrich, and Mark T. Stacey. "Morphodynamics of subaqueous levee formation: Insights into river mouth morphologies arising from experiments." *Journal of Geophysical Research: Earth Surface (2003–2012)* 115.F4 (2010).

Swanson, Kathleen M., et al. "Sediment load and floodplain deposition rates: Comparison of the Fly and Strickland rivers, Papua New Guinea." *Journal of Geophysical Research: Earth Surface (2003–2012)* 113.F1 (2008).

Thonon, Ivo, et al. "Modelling floodplain sedimentation using particle tracking."*Hydrological processes* 21.11 (2007): 1402-1412.

Walling, D. E., T. A. Quine, and Q. He. "Investigating contemporary rates of floodplain sedimentation." *Lowland floodplain rivers: Geomorphological perspectives* (1992): 165-184.

Walling, D. E., Qand He, and A. P. Nicholas. "Floodplains as suspended sediment sinks." *Floodplain processes* (1996): 399-440.

Walling, D. E., and Q. He. "Investigating spatial patterns of overbank sedimentation on river floodplains." *The Interactions Between Sediments and Water*. Springer Netherlands, 1997. 9-20.

Figures

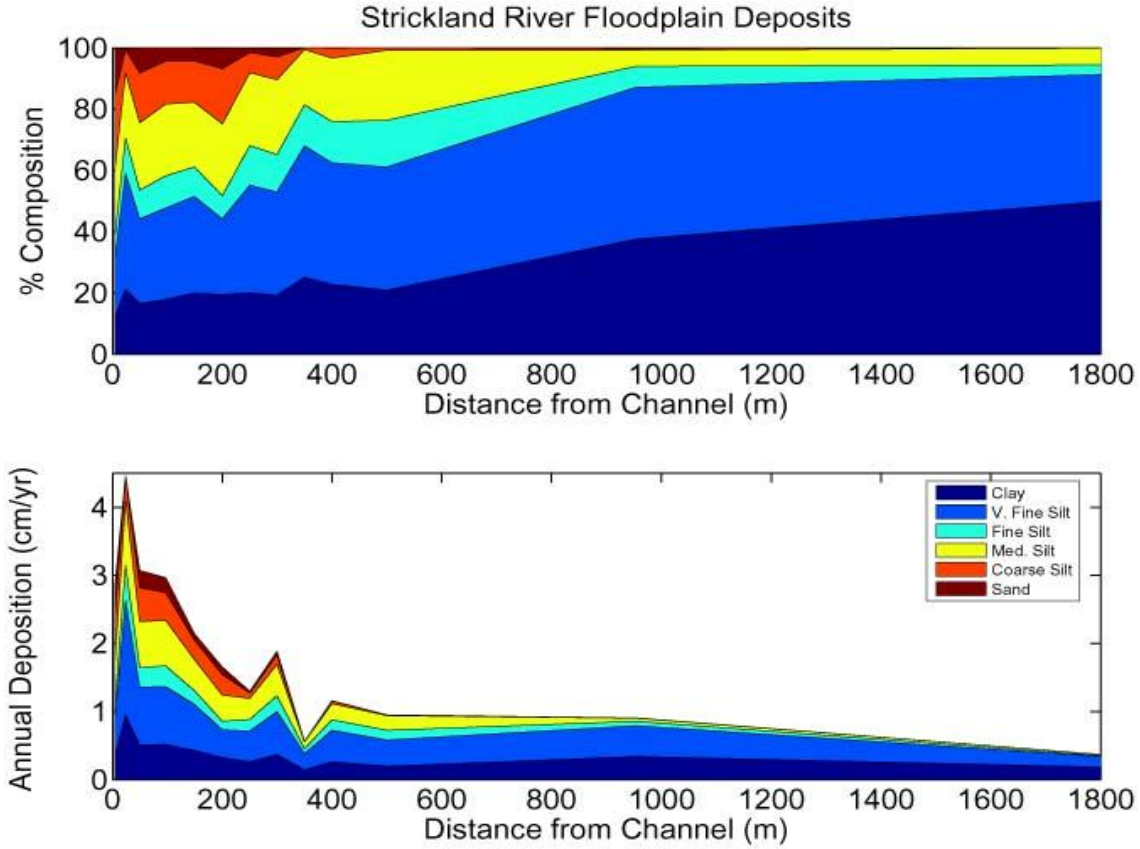


Figure 4.1 Binned average percent composition by volume of Strickland River floodplain deposits for each size class of clay (<2 μm), very fine silt (2-8 μm), fine silt (2-16 μm), medium silt (16-32 μm), coarse silt (32-62 μm) and sand (>62 μm). The lower panel shows both the relative contribution and magnitude of deposition of each size class.

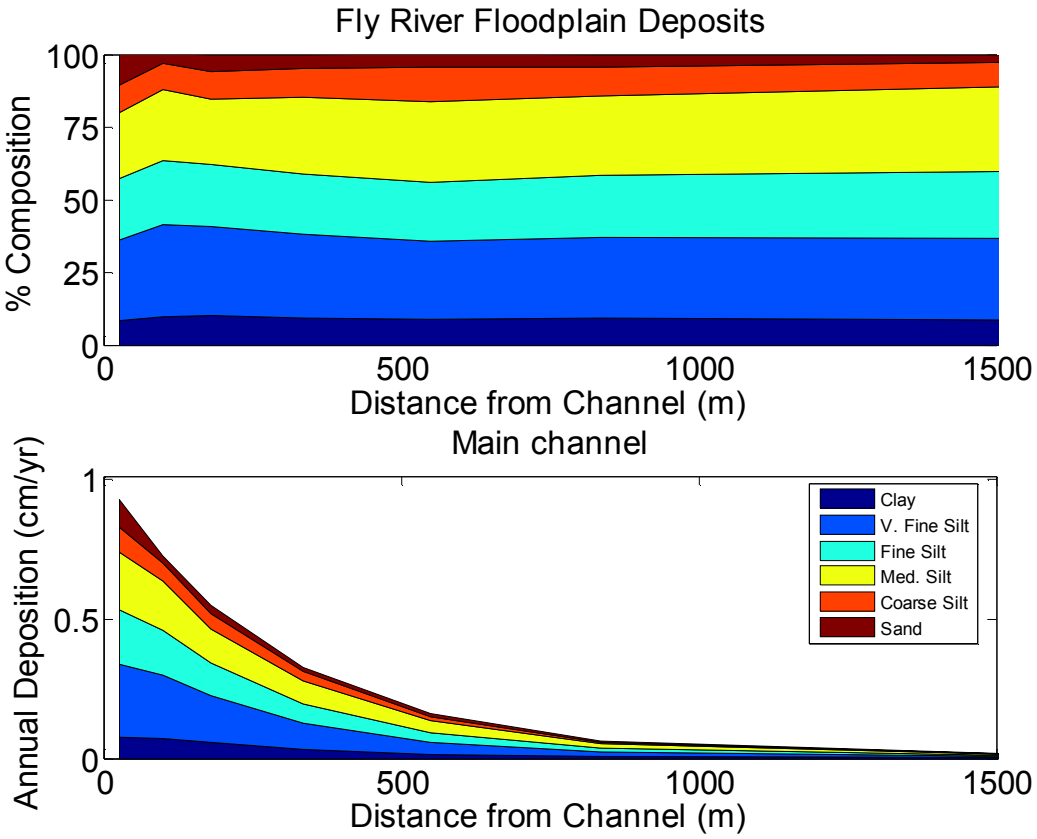


Figure 4.2 Binned average percent composition by volume of Fly River floodplain deposits for each size class of clay (<2 μm), very fine silt (2-8 μm), fine silt (2-16 μm), medium silt (16-32 μm), coarse silt (32-62 μm) and sand (>62 μm). The lower panel shows both the relative contribution and magnitude of deposition of each size class. The deposition function is defined by $h=1.01e^{(-.003357y)}$ (from Geoff Day, 1993 data, Day et al., 2009).

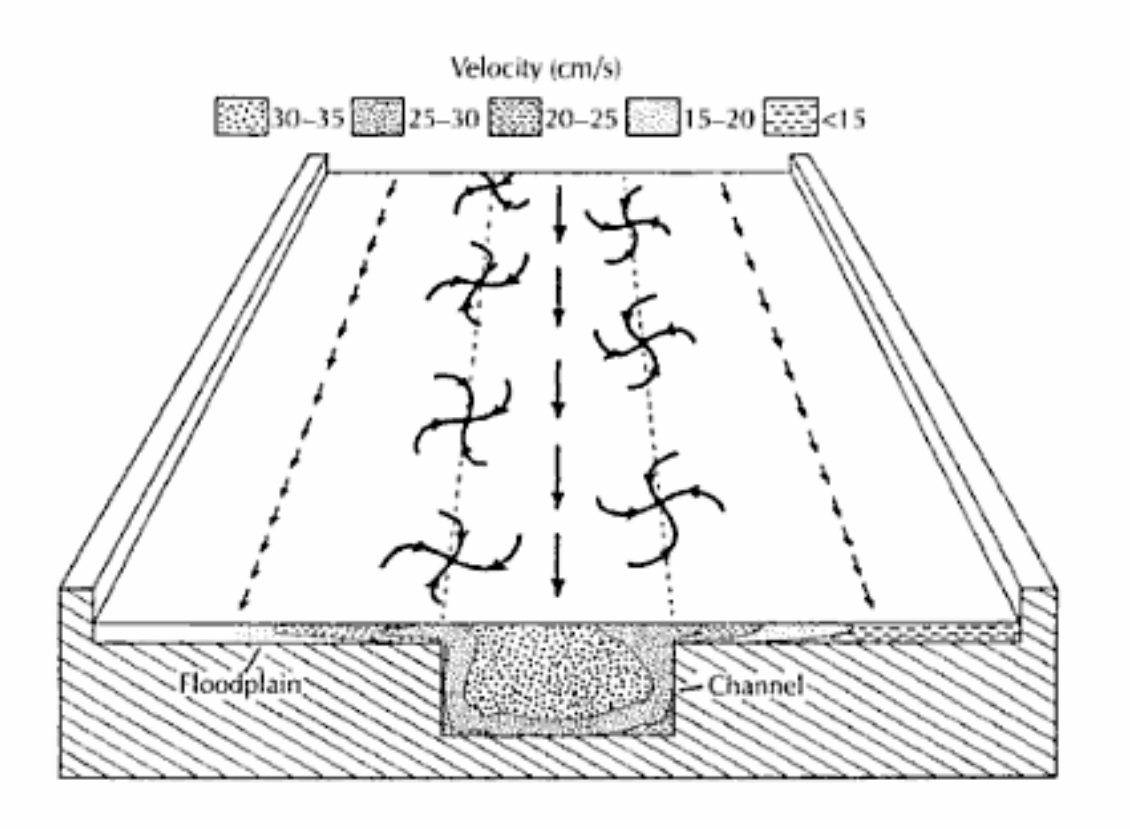


Figure 4.3 Model of floodplain flow idealized as a compound channel from Bridge (2003), based on Sellin (1964) and Allen (1970).

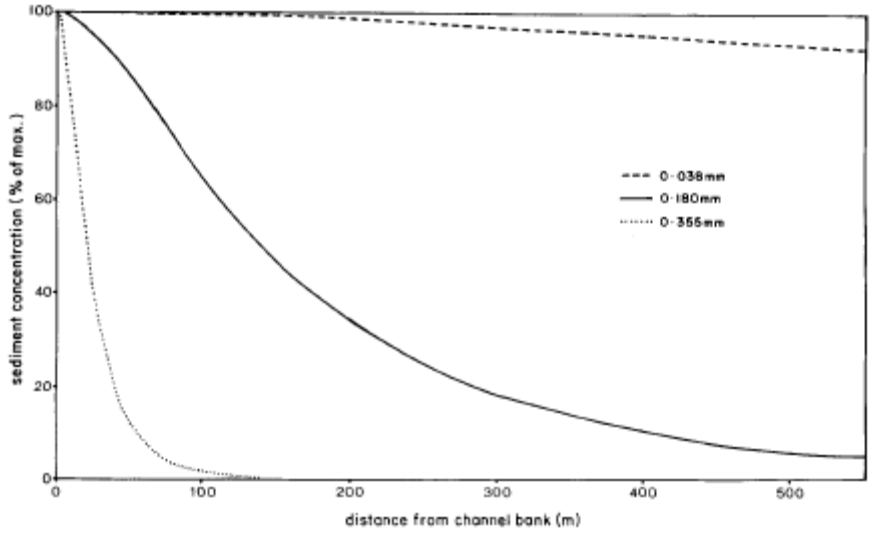


Figure 4.4 Modeled sediment concentration on the River Severn floodplain during a flood event calculated using the James (1985). Reproduced from Marriott (1992).

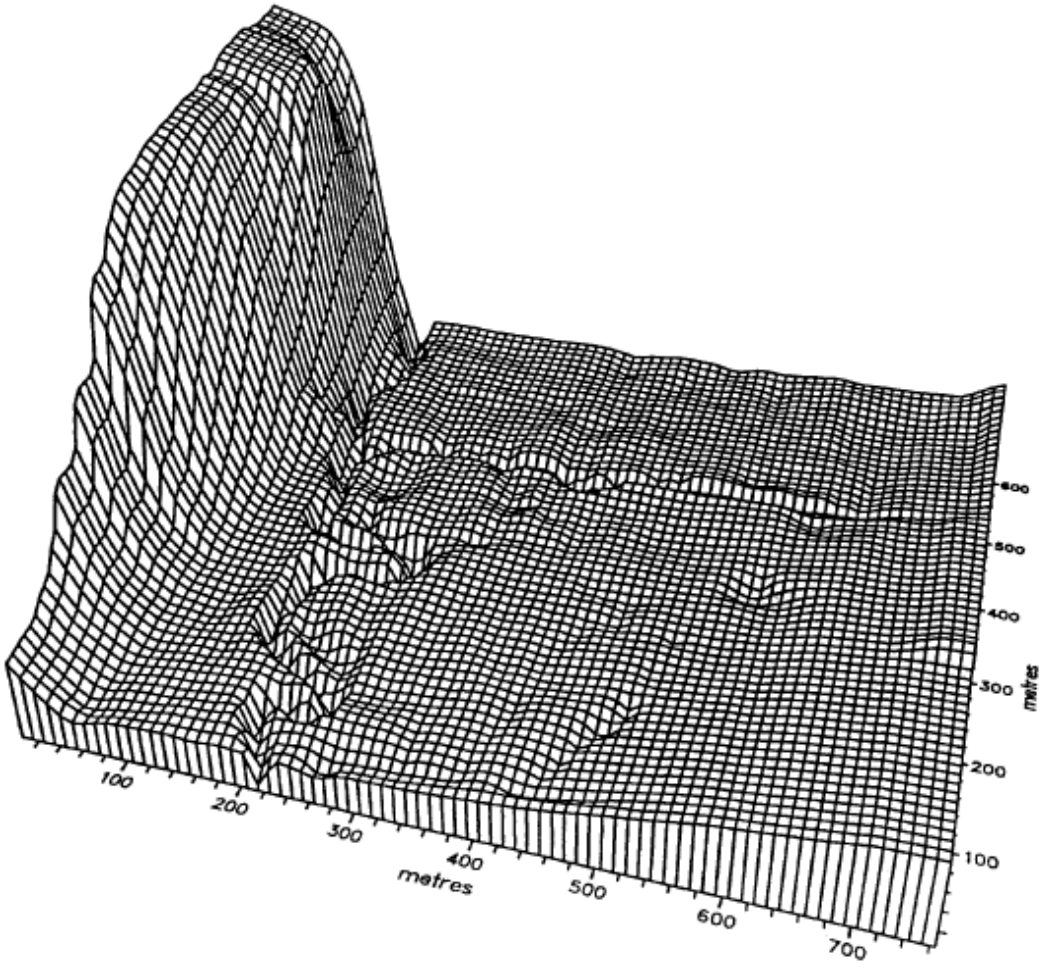


Figure 4.5 The finite element grid used by Nicholas and Walling (1997). Grid spacing is 10 x 10 m and the vertical exaggeration is 1:25.

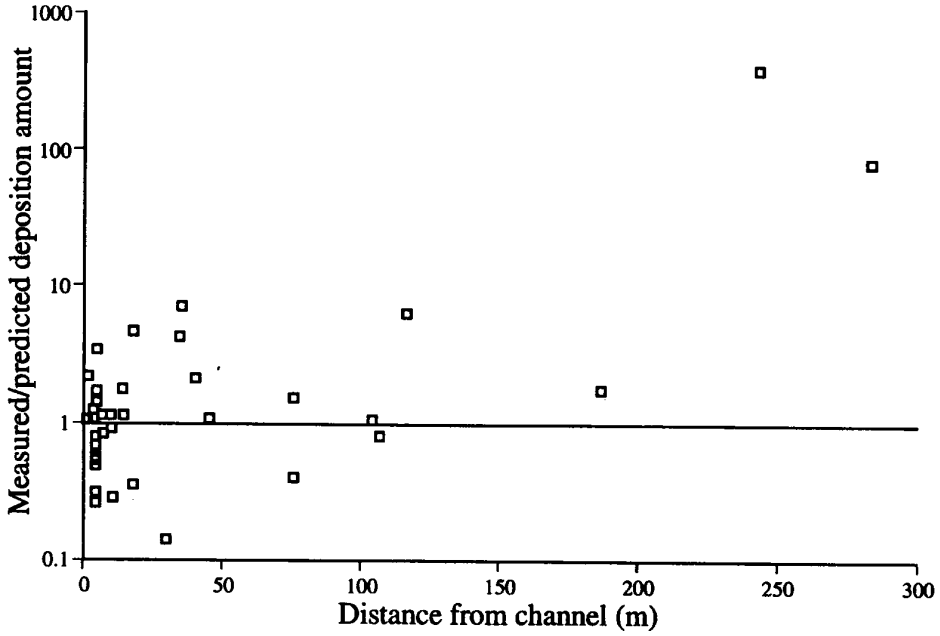


Figure 4.6 Performance of the model of floodplain deposition developed by Nicholas and Walling (1997) for the River Culm, UK.

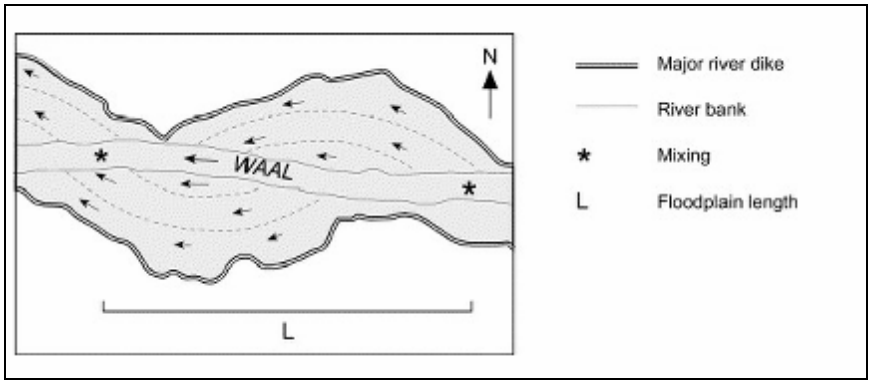


Figure 4.7 Conceptual drawing of floodplain flow along “flow tubes” in the River Waal, Netherlands (Asselman and Wijngaarden, 2002).

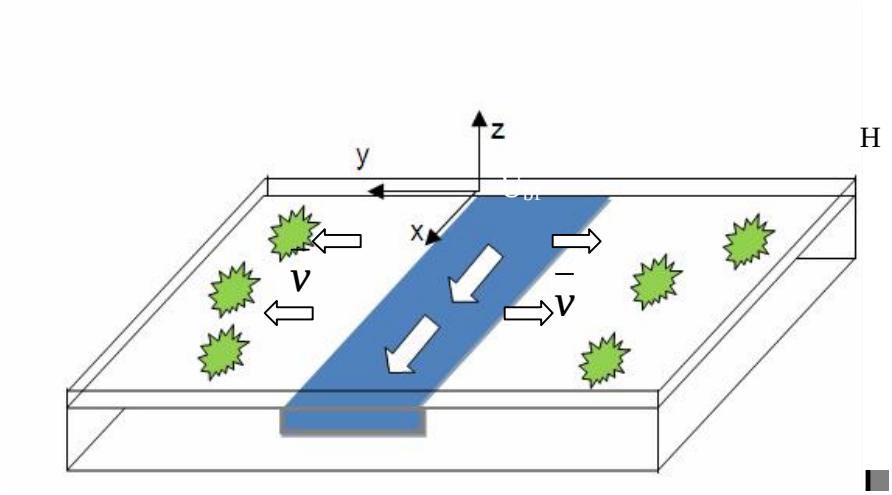


Figure 4.8 Conceptual drawing of the idealized floodplain. Channel flow, U_{bf}, in blue, is downstream out of the page. Floodplain flow, $\bar{v}$, is perpendicular to channel flow. The depth of flow, H, is the difference between the water surface and the sediment surface of the vegetated floodplain.



Figure 4.9 Photograph of sediment-laden flood flow following the path of the Fly River (top left to bottom left) through the already inundated floodplain. Photo credit: W.E. Dietrich.

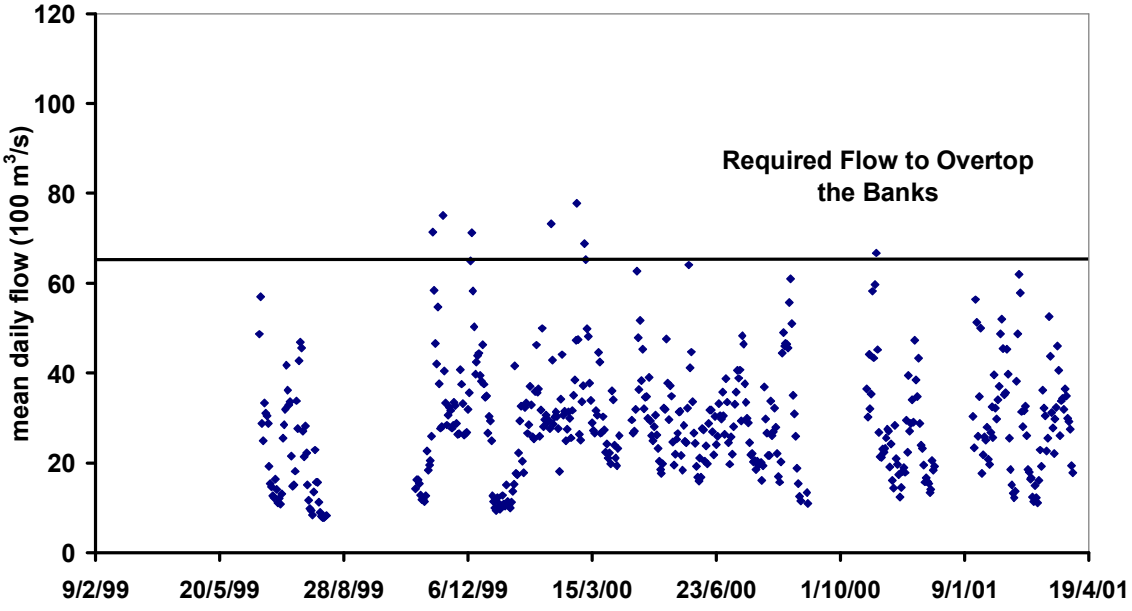


Figure 4.10 Mean daily flow measured at Strickland River Gauging station 4 (GS4).

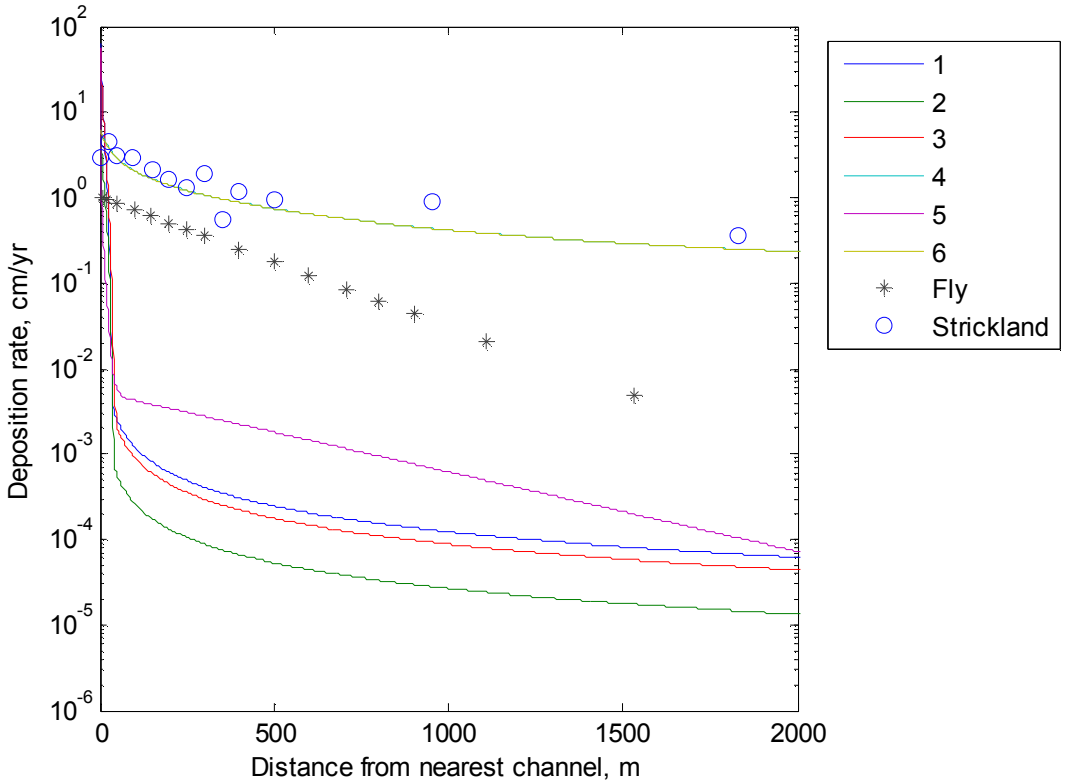


Figure 4.11 Total deposition rate for all model scenarios (lines) and measured annual rates (points).

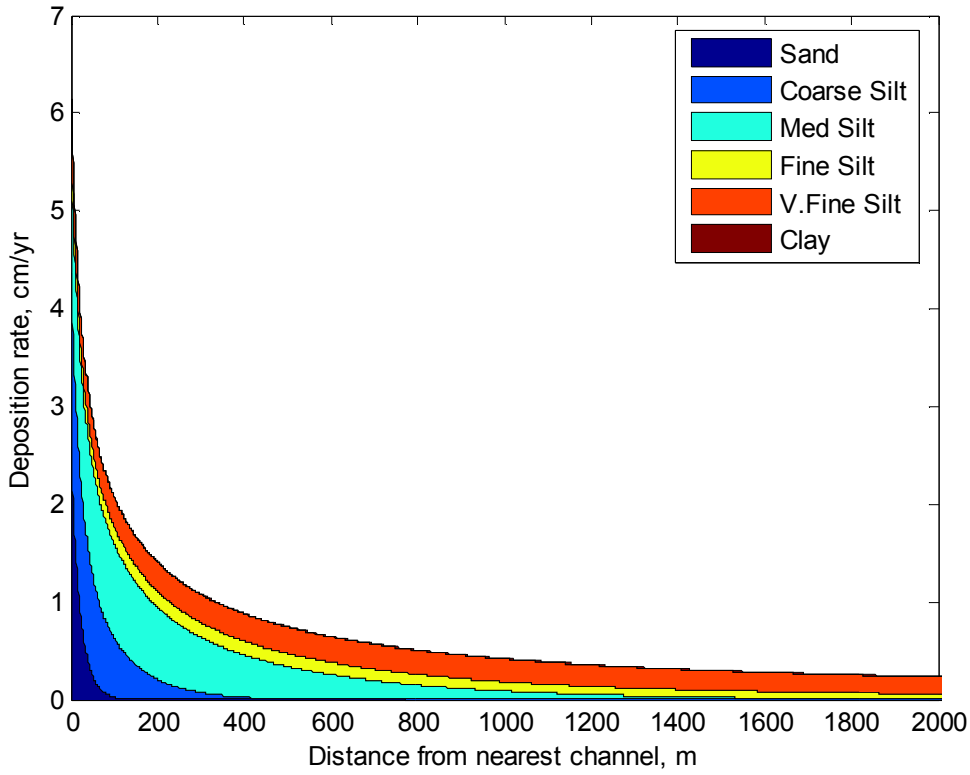


Figure 4.12 Modeled deposition pattern resulting from scenario 6: Strickland River floodplain, advection only.

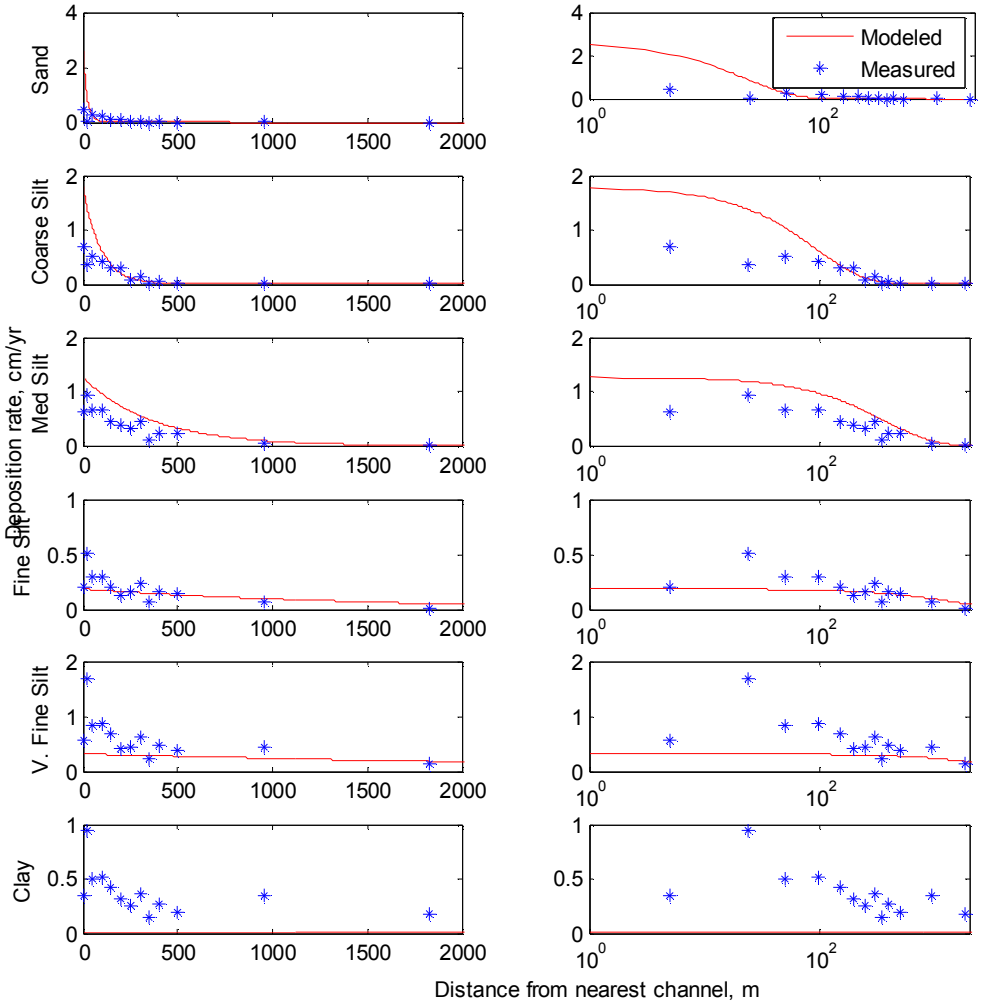


Figure 4.13 Modeled and measured deposition rate by particle size for scenario 6: Strickland River floodplain, advection only. Left column shows data on a linear x-axis and the right column shows the data for a log-scale distance from the channel to better illustrate the near-channel data.

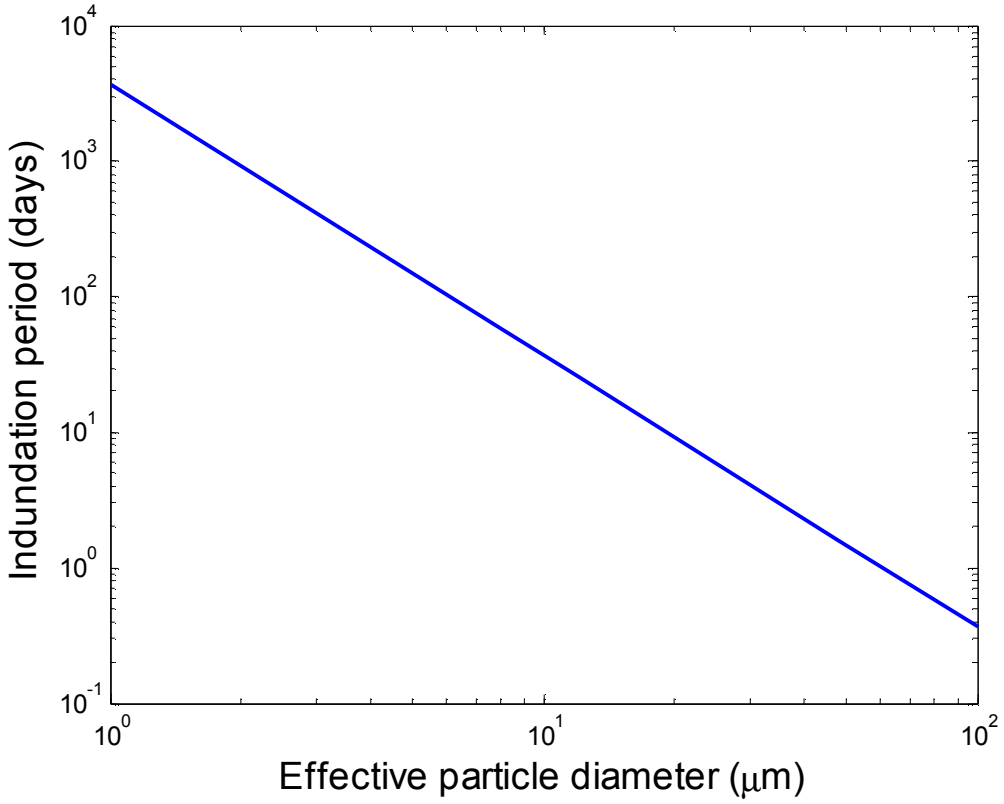


Figure 4.14 Calculated inundation period for effective particle diameters of flocculated material for the Fly River floodplain deposition length of 250 m.

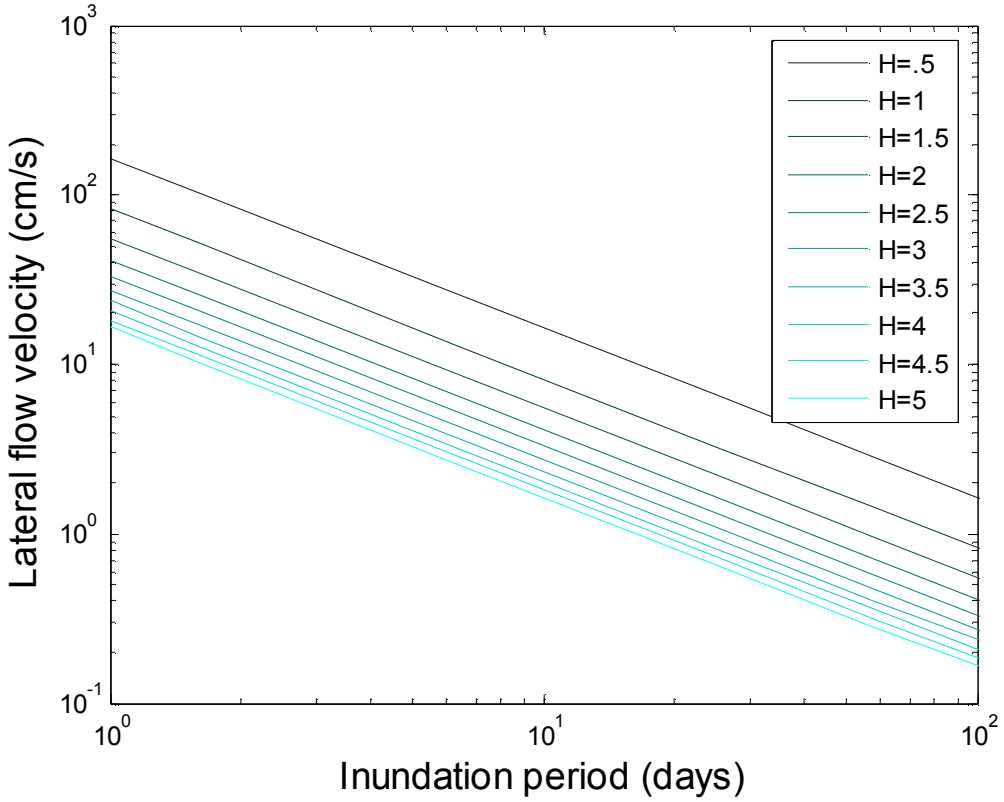


Figure 4.15 Variation in flow velocity with time of active floodplain deposition (inundation period), and flow depth, *H* (m), for the Fly River floodplain.

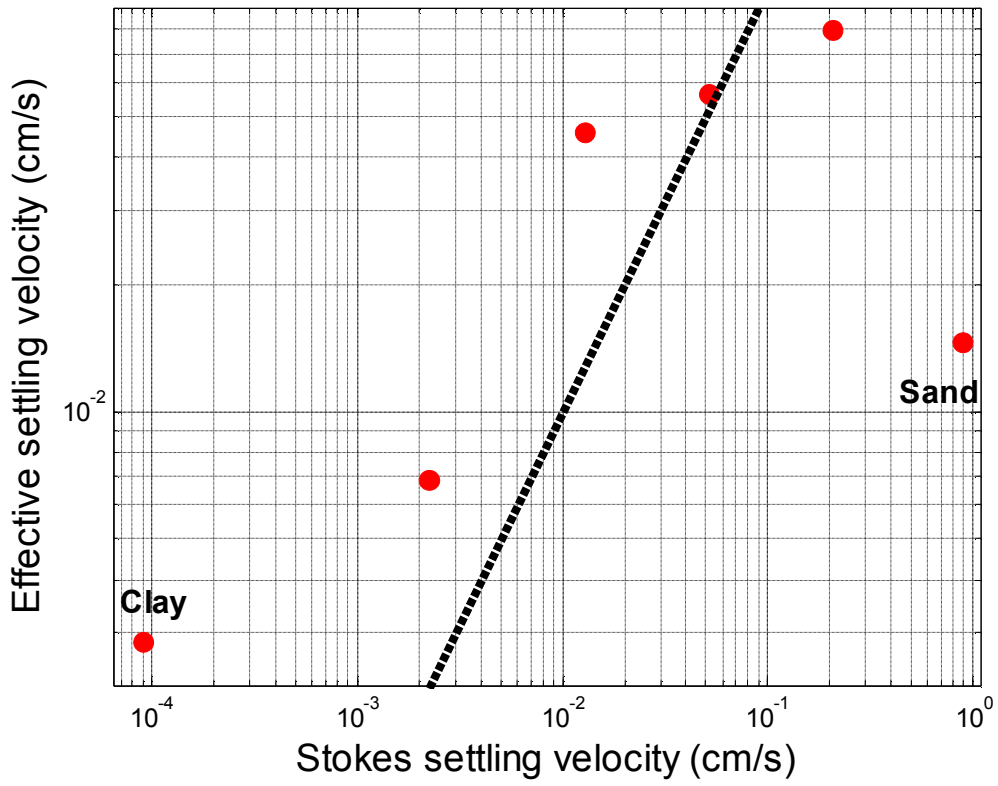


Figure 4.16 Stokes settling velocity versus calculated effective settling velocity with a dashed 1:1 line. The calculation indicates that flocculation may have a strong effect on clay and fine silt deposition.

Appendix A

Calculated deposition rates for each sediment core for different background AG and Pb concentrations described in Chapter 2. Bank designations are L for Left, R for right and U or D for upstream and downstream respectively where applicable.

			Calculated deposition rate (cm/yr)			
			Background metal concnetration			
Transect	Bank	Distance (m)	0.16 mg/g Ag	25 mg/g Pb	0.1 mg/g Ag	22 mg/g Pb
1	L	2000	0.62	1.07	1.19	1.68
1	L	1000	1.42	1.48	2.79	1.66
1	L	500	2.35	2.35	2.35	2.35
1	L	250	3.17	3.17	3.17	3.17
1	L	50	3.90	3.90	3.90	3.90
1	L	5	3.90	3.90	3.90	3.90
1	R	5	3.05	3.05	3.05	3.05
1	R	22	1.70	1.62	2.01	1.75
1	R	50	1.55	1.69	1.78	1.98
1	R	500	0.96	0.47	2.55	0.82
1	R	1000	2.46	1.89	2.96	2.06
2	L	1000	2.08	1.76	3.12	2.42
2	L	500	0.86	0.92	1.12	1.01
2	L	300	2.45	2.92	2.50	2.95
2	L	240	2.49	2.35	3.05	2.58
2	L	200	0.96	0.96	1.12	0.98
2	L	150	2.15	2.05	2.75	2.34
2	L	100	3.39	3.28	3.51	3.35
2	L	50	2.29	2.35	2.64	2.50
2	L	25	9.80	9.80	9.80	9.80
2	R	5	3.08	2.90	4.81	3.02
2	R	25	4.02	3.97	4.13	4.03
2	R	50	2.51	1.91	3.03	2.08
2	R	75	0.15	0.19	0.22	0.20
2	R	100	0.62	0.85	3.29	0.91
2	R	150	1.12	0.92	2.61	1.53
2	R	200	0.52	0.80	0.90	0.90
2	R	250	1.16	1.85	2.35	2.18
2	R	350	0.17	0.30	0.40	0.36
2	R	435	0.29	0.35	3.29	0.56
2	R	1000	0.59	1.10	0.99	1.44

			Calculated deposition rate (cm/yr)			
			Background metal concnetration			
Transect	Bank	Distance (m)	0.16 mg/g Ag	25 mg/g Pb	0.1 mg/g Ag	22 mg/g Pb
3	**L**	**652**	0.00	0.00	1.94	0.15
3	**L**	**350**	0.05	0.00	0.72	0.05
3	**L**	**250**	0.00	0.00	0.00	0.00
3	**L**	**150**	0.00	0.00	2.57	0.00
3	**L**	**100**	1.49	0.59	1.94	0.67
3	**L**	**50**	0.80	0.71	0.92	0.73
3	**L**	**5**	8.51	8.54	9.05	8.76
3	**R**	**5**	1.38	1.47	3.29	1.48
3	**R**	**50**	0.66	0.70	0.82	0.77
3	**R**	**100**	0.95	0.89	1.44	0.90
3	**R**	**150**	0.64	0.63	0.98	0.65
3	**R**	**250**	0.87	0.84	2.88	0.88
3	**R**	**350**	2.63	2.48	3.03	2.67
3	**R**	**600**	2.79	2.79	3.29	3.29
4	**L**	**2000**	0.00	0.00	0.06	0.00
4	**L**	**150**	2.01	1.21	2.01	2.01
4	**L**	**100**	0.00	0.00	0.00	0.00
4	**L**	**50**	0.27	0.31	0.73	0.33
4	**L**	**5**	0.00	0.54	3.23	0.57
4	**R**	**5**	1.00	1.10	1.85	1.16
4	**R**	**50**	0.00	0.00	1.12	0.00
4	**R**	**100**	0.05	0.15	1.24	1.02
4	**R**	**150**	0.00	0.00	1.12	0.15
4	**R**	**250**	0.00	0.07	1.62	0.72
4	**R**	**350**	0.00	0.00	0.00	0.00
4	**R**	**475**	0.00	0.11	1.41	0.15

			Calculated deposition rate (cm/yr)			
Transect	Bank	Distance (m)	Background metal concnetration			
			0.16 mg/g Ag	25 mg/g Pb	0.1 mg/g Ag	22 mg/g Pb
5	**L**	**500**	2.43	2.30	3.16	2.56
5	**L**	**250**	1.50	1.48	2.19	1.76
5	**L**	**150**	1.68	1.58	1.86	1.88
5	**L**	**100**	2.50	1.57	4.18	2.05
5	**L**	**50**	9.05	9.05	9.05	9.05
5	**L**	**5**	6.22	6.22	6.22	6.22
5	**R**	**5**	4.75	6.15	7.21	6.90
5	**R**	**50**	6.22	6.22	6.22	6.22
5	**R**	**100**	7.18	7.18	7.18	7.18
5	**R**	**150**	4.44	4.43	6.19	4.44
5	**R**	**800**	0.98	1.28	3.29	1.90
10d	**L**	**5**	0.51	0.51	0.51	0.51
10d	**L**	**25**	1.86	6.90	2.03	6.90
10d	**L**	**50**	1.60	1.91	1.94	5.95
10d	**L**	**100**	6.14	6.37	7.82	7.26
10d	**L**	**135**	0.72	0.98	0.93	0.98
10d	**L**	**150**	1.98	2.19	2.05	2.57
10d	**L**	**300**	1.41	0.92	2.07	8.68
10U	**Ld**	**5**	1.03	1.03	1.03	1.03
10U	**L**	**5**	3.95	4.07	5.62	4.21
10U	**L**	**50**	2.21	6.82	5.88	7.25
10U	**L**	**100**	7.32	7.32	7.32	7.32
10U	**L**	**150**	8.76	8.76	8.76	8.76
10U	**L**	**200**	3.63	4.43	4.65	4.65
10U	**L**	**300**	1.47	2.64	2.40	5.03
10U	**L**	**400**	1.27	3.66	4.53	5.03
10U	**L**	**600**	0.51	0.51	0.51	0.51
10	**R**	**5**	2.58	3.77	3.77	3.77
10	**R**	**50**	7.32	7.32	7.32	7.32
10	**R**	**75**	7.04	7.04	7.04	7.04
10	**R**	**100**	5.95	5.95	5.95	5.95

			Calculated deposition rate (cm/yr)			
Transect	Bank	Distance	Background metal concnetration			
			0.16 mg/g Ag	25 mg/g Pb	0.1 mg/g Ag	22 mg/g Pb
12	A	850	0.08	0.14	0.14	3.41
12	C	1875	0.00	0.56	0.57	3.11
12	E	1446	0.00	0.12	0.12	3.41
12	F	1025	0.09	0.28	0.28	3.41
12	G	425	0.17	0.31	0.31	3.41
13	L	250	2.55	2.73	2.84	3.10
13	L	100	5.95	5.95	5.95	5.95
13	L	50	2.98	2.85	3.15	2.97
13	L	5	3.42	3.40	3.63	3.51
13	R	5	2.58	2.58	2.58	2.58
13	R	25	5.55	5.55	5.55	5.55
13	R	50	5.95	5.95	5.95	5.95
13	R	150	4.02	4.07	4.16	4.13
15	L	100	0.96	1.24	1.45	1.58
15	L	50	8.46	8.46	8.46	8.46
15	L	5	2.93	2.93	2.93	2.93
15	R	5	4.52	4.52	4.52	4.52
15	R	5	6.35	6.35	6.35	6.35
15	R	50	6.35	5.02	6.35	5.96
15	R	100	8.76	8.76	8.76	8.76
15	R	150	6.86	7.96	7.93	8.68
15	R	250	1.97	2.05	2.04	2.07
15	R	285	2.93	2.93	2.93	2.93

Appendix B

Results from the modeling effort described in Chapter 4 are presented here. Scenario definitions are included in Table B.1. Scenarios 1 and 2 are for transfer to and deposition of sediment on the floodplain by diffusion only for the Fly and Strickland Rivers respectively. Scenarios 3 and 4 are the advection-diffusion scenarios and scenarios 5 and 6 are advection only. As expected based on the model scaling, the modeled scenarios did not reproduce the observed pattern of deposition. The two scenarios that included advective transport on the Strickland River floodplain did a reasonable job recreating the observed magnitude of deposition and pattern of fining, but underestimated clay and fine silt deposition. All of the scenarios of deposition on the Middle Fly River floodplain underestimated floodplain deposition and predict fining when none is observed.

The turbulent kinetic energy (TKE) field resulting from the solution of equation 4.24 is solved for scenarios 1-4 is plotted in Figures B.1 and B.2 as a fraction of the TKE at the channel boundary, $\frac{1}{2}q(0)^2$, for each scenario. Scenarios 5 and 6 consider only advection of sediments across the floodplain. The relative strengths of TKE for scenarios 1, 2 and 3 are nearly indistinguishable from one another despite the inclusion of an advection term in scenario 3. The magnitude of that advection is very small and has little impact on the shape of the resulting lateral variability in TKE across the floodplain in scenario 3. In each of the first 3 scenarios the turbulent energy from the channel is only transported ~20m laterally and is negligible beyond that distance. The larger lateral velocity in scenario 4 transports TKE ~80m from the channel, beyond which the local production of turbulence is balanced by dissipation.

The modeled sediment deposition on the Fly River floodplain for scenario 1 is plotted in Figures B.3-B4. Percent error in Figure B.5 is calculated as

$$\%Error = \frac{|r_{meas} - r_{\mathrm{mod}}|}{r_{meas}} * 100 . \qquad \text{(B.1)}$$

Deposition decreases from 62 cm/y at the channel boundary to less than 1 mm/yr, 32 m from the channel. Since diffusion, which penetrates only tens of meters across the floodplain, is the only mechanism transporting sediment across the plain in this scenario (1), sediment deposition is limited to a very narrow floodplain width near the channel. Additionally, the long time period assumed for this scenario, 91 days, and the fixed concentration at the channel boundary result in a very large deposition rate at the channel boundary. An exponential function does not fit the modeled deposition pattern well for the cumulative deposition rate (R^2=0.42) or the deposition pattern of any individual grain size.

Similarly, the diffusion only scenario for the Strickland River floodplain, scenario 2, predicts a deposition rate that decreases non–exponentially from 6.1 cm/yr at the channel boundary to less than 1 mm/yr 30m from the channel (Figures B.6-B.8).

The weak advection combined with diffusion in scenario 3 on the Fly River floodplain is also insufficient to transport sediment significant distances from the channel (Figures B.9-B.11). Modeled deposition decreases non-exponentially from nearly 60 cm/year at the channel bank to less than 1 mm/year 35m from the channel.

Stronger advection on the Strickland river floodplain in the advection and diffusion scenario, 4, is capable of transporting sediment farther from the channel that the previous scenarios (Figures B.12-B.14). Modeled deposition is 6.1 cm/yr at the channel margin and decreases non-exponentially to 0.23 cm/yr 2000 m from the channel. Only a very small amount of clay is deposited while deposition of all other particle sizes is much more substantial. While the total deposition pattern is non-exponential, within each particle size class, the deposition pattern is exponential and described accurately by equation 4.15 (r^2=1 for the exponential function fit to the modeled deposition for each particle size).

Scenario 5, advection only on the Fly River floodplain, results in a similar deposition pattern to scenario 3 (Figures B.15-B.17). The weak advection is not capable of transporting sediment beyond the first few m from the channel edge and deposition sums less than 1mm/yr just 19m from the channel boundary. Advection only on the Strickland river floodplain in scenario 6 (Figures B.18-B.20) resembles the advection-diffusion scenario 4 as modeled by equation 4.15 for each particle size with r^2 =1 for each particle size.

Scenarios 4 and 6 (advection and diffusion on the Strickland River floodplain and advection only on the Strickland River floodplain) are the only scenarios to provide a qualitatively similar deposition pattern across the floodplain. Though the pattern of deposition is similar in each case, the magnitude of total deposition in each of these scenarios can differ from the measured deposition rate by 100%. The error in modeled vs. measured total deposition rate is plotted for scenarios 4 and 6 in Figure B.21.

Particle size decreases with increasing distance from the channel in all of the scenarios (Figures B.23-B.26). Fining occurs across the plain in all cases because successively smaller particle sizes are depleted from the suspended load as the water is transported across the plain. The 10^{th} percentile particle size, D10, is less than 3 μm at all points on the Fly and Strickland floodplains. Modeled D10 decreases to very fine silt size within a few decimeters of the channel bank in scenarios 4 and 6. Modeled D10 is clay size at this distance in the other scenarios in all other scenarios (Figure B.23). It should be noted that the decrease in modeled D10 and comparable particle size measures are step functions because the input sediment size distribution was of a limited number of discrete particle sizes.

Median particle size, D50, on the Fly and Strickland floodplains decreases from ~20 μm to 10 μm decimeters from the channel edge. Measured D50 remains nearly constant with additional increases in distance from the channel on the Fly floodplain but continues to decrease to just a clay particle sizes at the distal edge of the Strickland River floodplain. Modeled D50 decreases from the diameter of coarse silt to that of very fine silt in a stepwise manner over the first few decimeters from the channel in scenarios 1, 2, and 3 and the first 800 m in scenarios 4 and 6 (Figure B.24). Median size modeled in scenario 5 decreases to that of clay within a few decimeters of the channel.

The 90th percentile particle diameter, D90, decreases from coarse sand to coarse silt over the first few decimeters on the Fly River floodplain and varies little with additional changes in distance from the channel. The D90 of Strickland River floodplain sediments decrease more gradually from fine sand to fine silt over the entire width of the floodplain where sediment cores were collected. Modeled D90 decreases to fine silt just decimeters from the channel in scenarios 1, 2, and 3 and more gradually declines to that of fine silt in scenarios 4 and 6 1400 m from the channel (Figure B.25). D90 for scenario 5 rapidly declines to clay size decimeters from the channel indicating that only clay is deposited any significant distance from the channel boundary.

Mean particle diameter measured on the Fly River floodplain decreases from ~18 μm to ~10 μm within the first few decimeter from the channel boundary and remains nearly constant across the remainder of the width of the floodplain where cores were collected. The measured mean particle diameter of Strickland River floodplain sediments decreases across the whole width of the active floodplain from ~12 μm at the channel bank to ~3 μm more than 1800 m from the channel. Modeled mean particle diameter in scenario 5 quickly converges to 1 μm decimeters from the channel boundary (Figure B.26). Mean particle diameter in scenarios 1, 2, and 3 rapidly approach ~10 μm decimeters from the channel boundary. Modeled mean particle diameter in scenarios 4 and 6 decrease exponentially from just over 60 μm at the channel boundary to 10 μm ~1500 m from the channel boundary.

Tables

Scenario		Parameter			
		T days	***c(0)*** mg/L	**U_{bf}** m/s	***V*** cm/s
1	Fly, diffusion	91	130	0.93	0
2	Strickland, diffusion	5	500	1.63	0
3	Fly, advection and diffusion	91	130	0.93	0.014
4	Strickland, advection and diffusion	5	500	1.63	6.4
5	Fly, advection	91	130	-	0.014
6	Strickland, advection	5	500	-	6.4

Table B.1. Model inputs for all model scenarios.

Figures

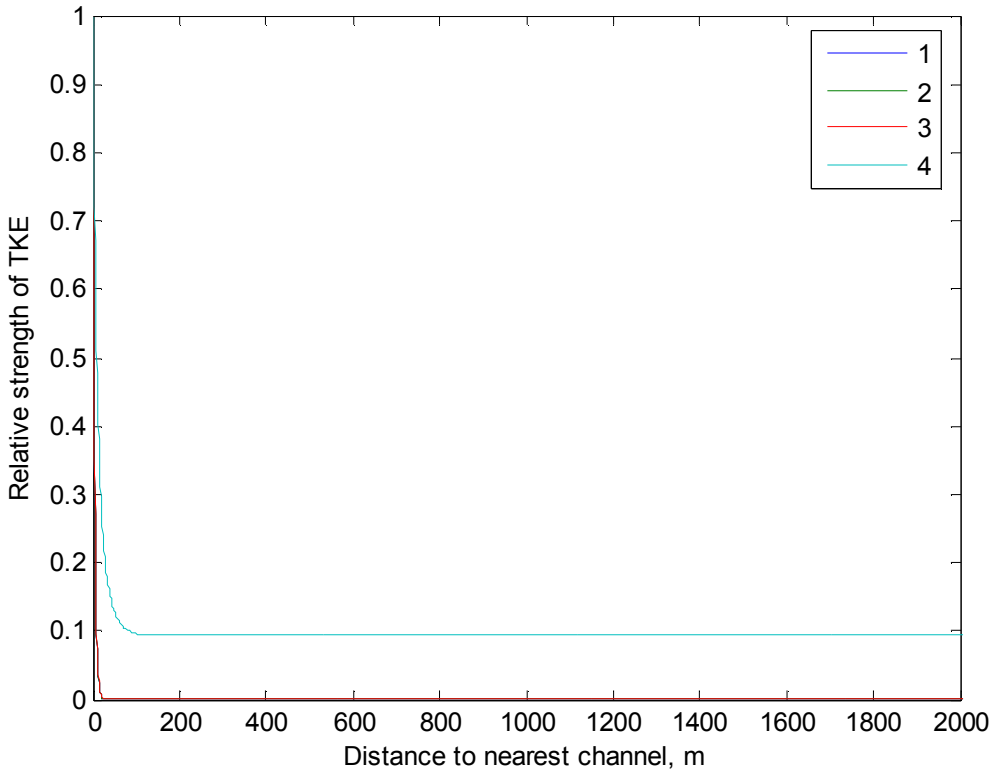


Figure B.1 Relative strength of TKE, $\frac{\frac{1}{2}q(y)^2}{\frac{1}{2}q(0)^2}$, for 1) Fly River, diffusion only 2) Strickland River, diffusion only 3) Fly River, advection and diffusion, and 4) Strickland River, advection and diffusion scenarios as a function of distance from the nearest channel.

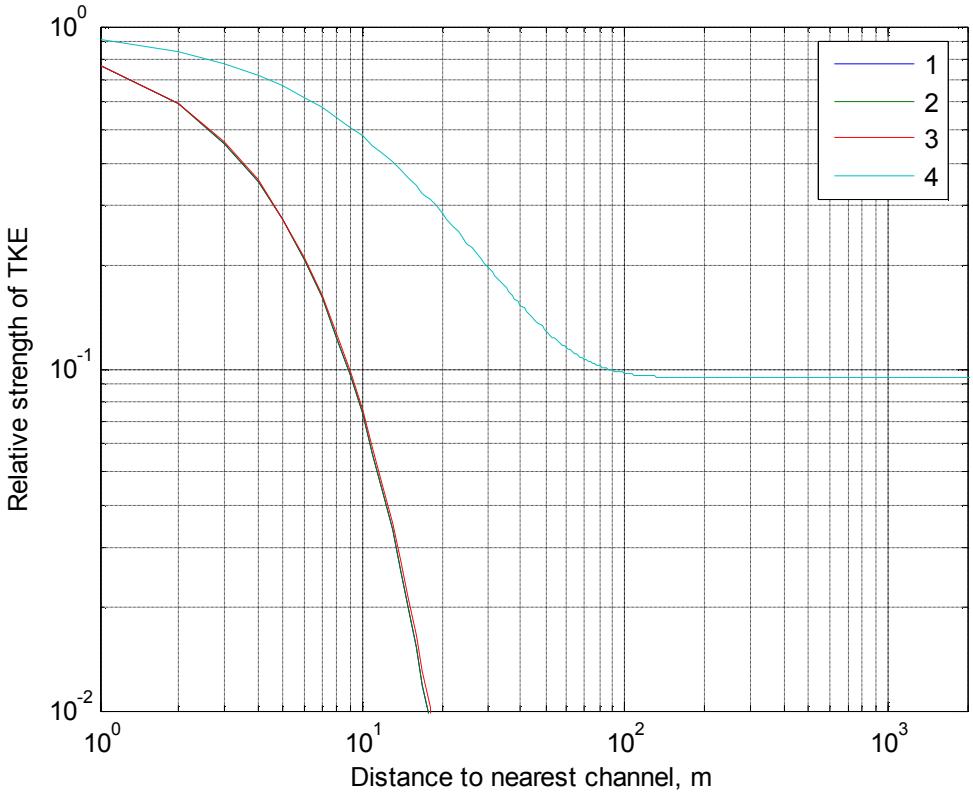


Figure B.2 Relative strength of TKE, $\frac{\frac{1}{2}q(y)^2}{\frac{1}{2}q(0)^2}$, for 1) Fly River, diffusion only 2) Strickland River, diffusion only 3) Fly River, advection and diffusion, and 4) Strickland River, advection and diffusion scenarios as a function of distance from the nearest channel plotted on logarithmic axes.

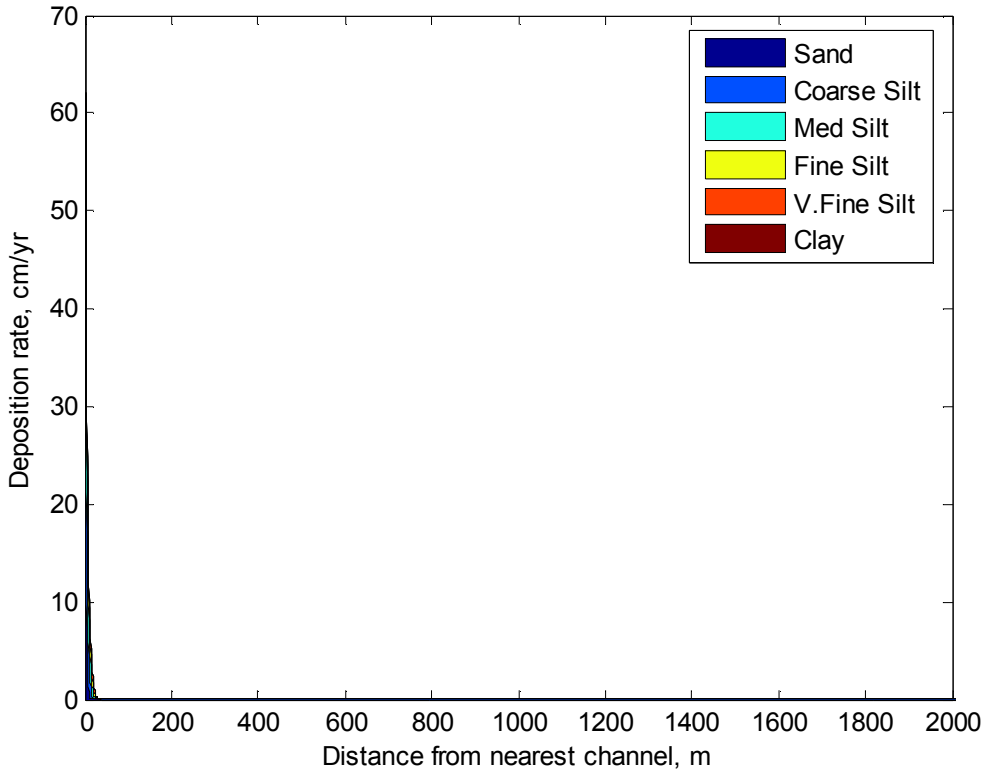


Figure B.3 Modeled deposition pattern resulting from scenario 1: Fly River floodplain, diffusion only.

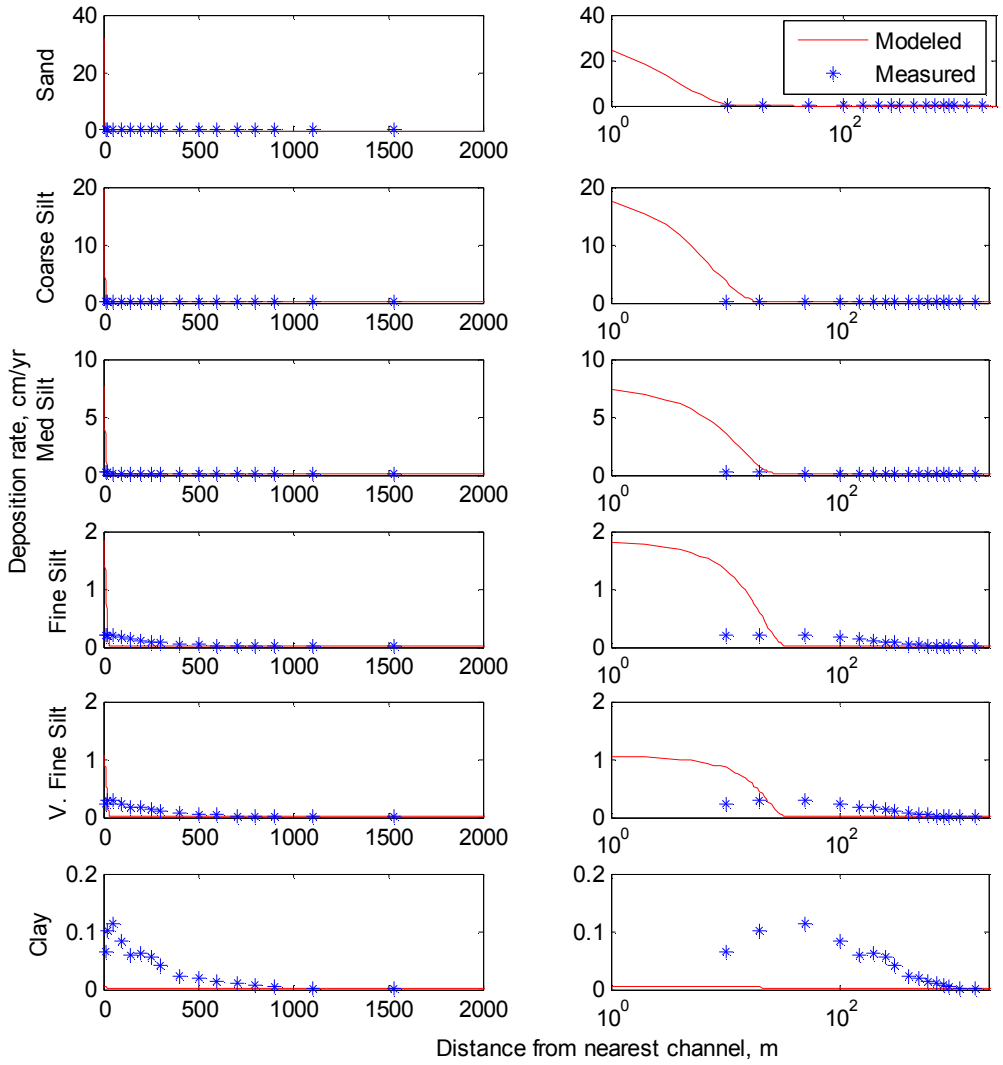


Figure B.4 Modeled and measured deposition rate by particle size for scenario 1: Fly River floodplain, diffusion only.

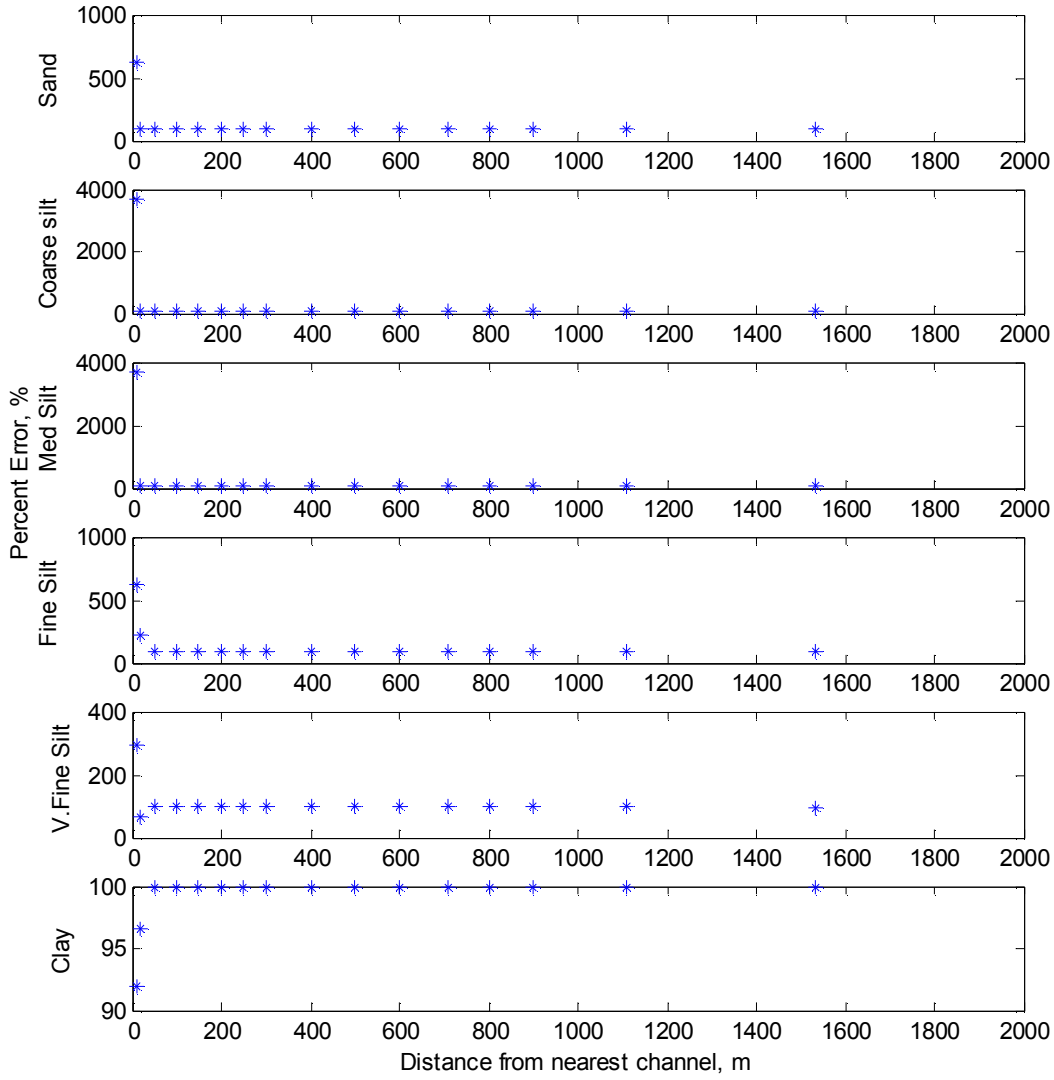


Figure B.5 Percent error modeled vs. measured deposition by particle size for scenario 1: Fly River floodplain, diffusion only.

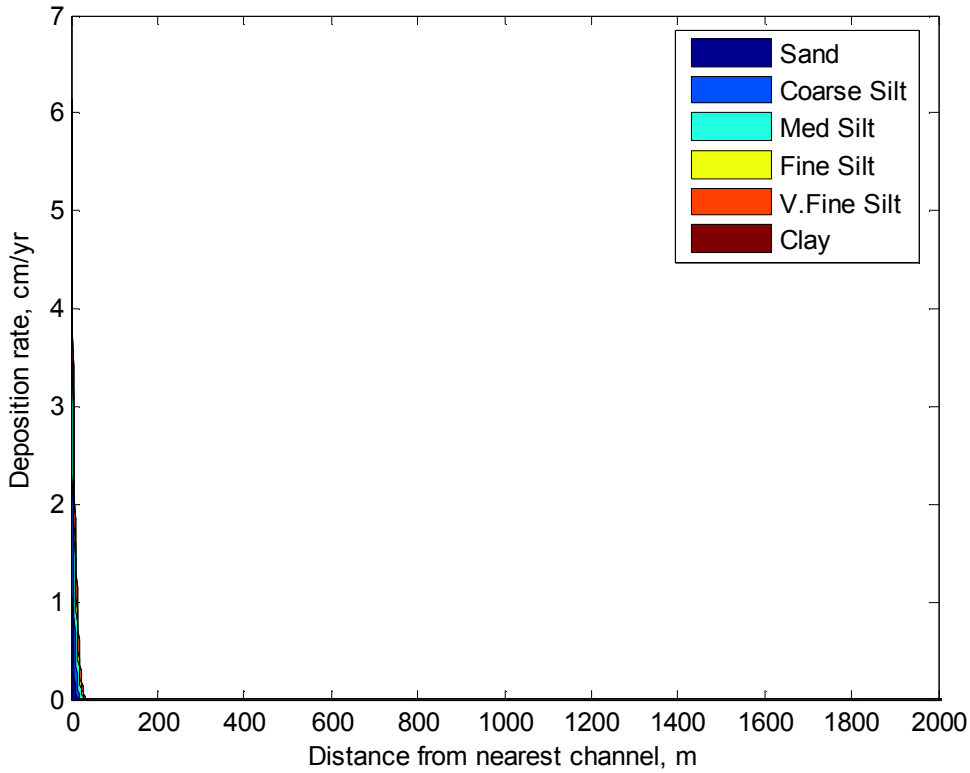


Figure B.6 Modeled deposition pattern resulting from scenario 2: Strickland River floodplain, diffusion only.

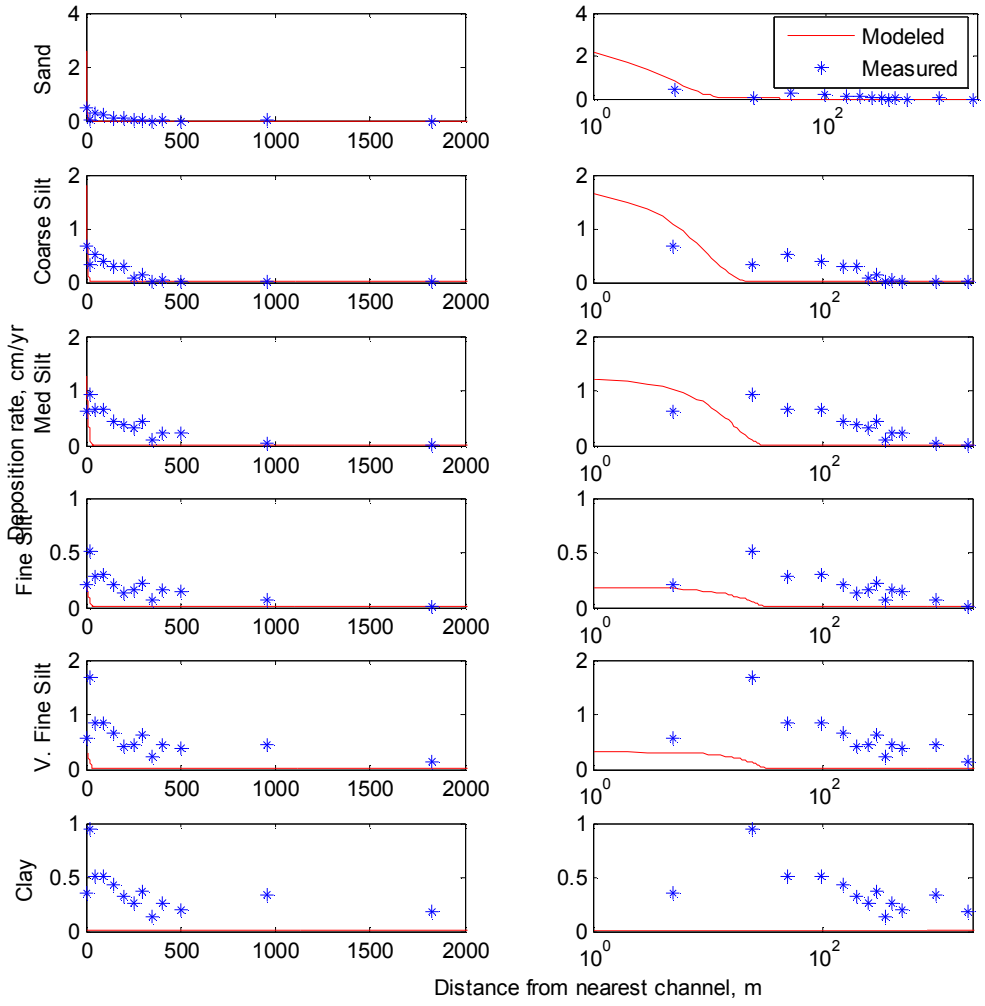


Figure B.7 Modeled and measured deposition rate by particle size for scenario 2: Strickland River floodplain, diffusion only.

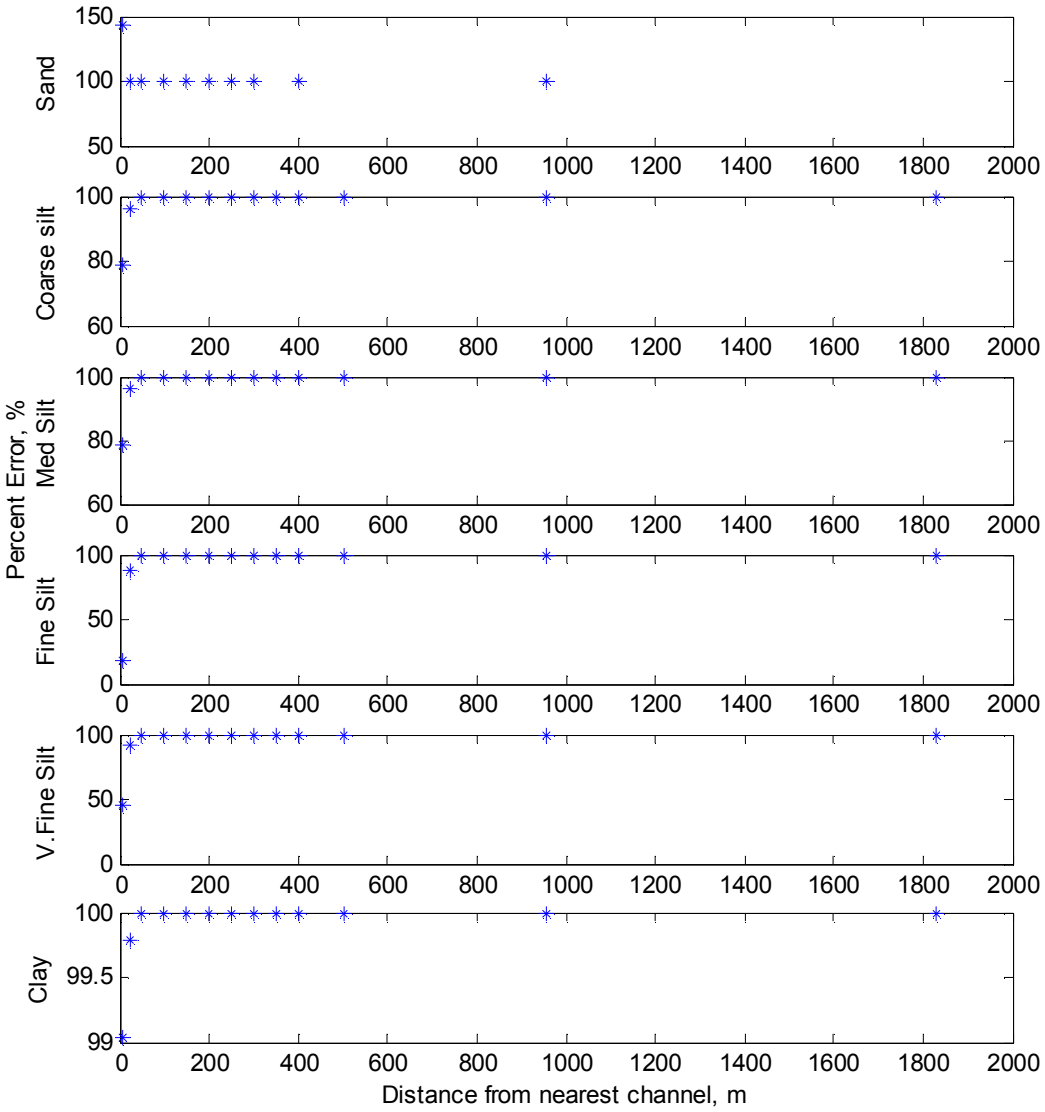


Figure B.8 Percent error modeled vs. measured deposition by particle size for scenario 2: Strickland River floodplain, diffusion only.

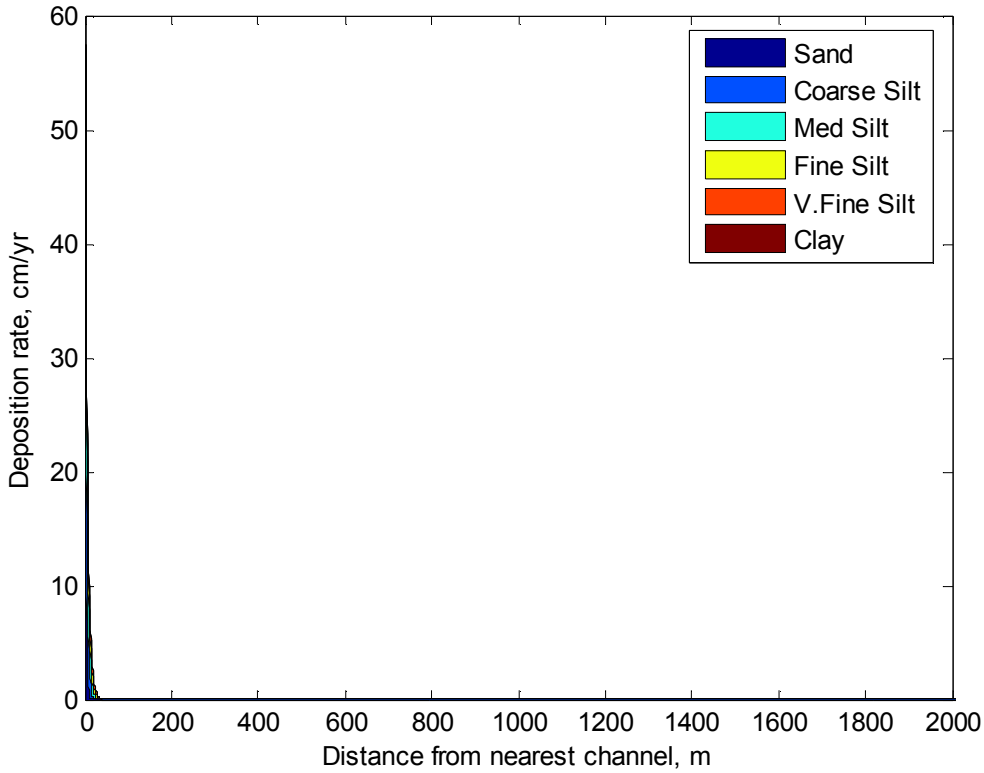


Figure B.9 Modeled deposition pattern resulting from scenario 3: Fly River floodplain, advection and diffusion.

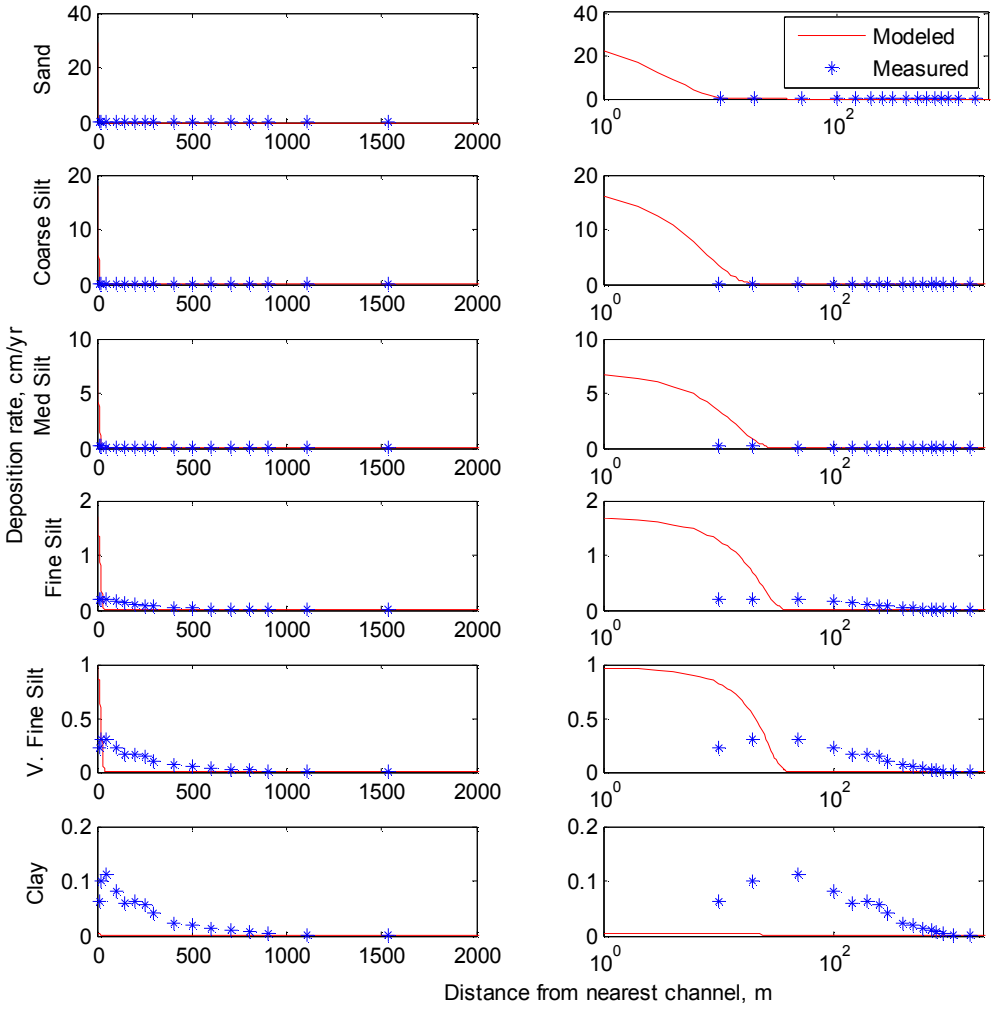


Figure B.10 Modeled and measured deposition rate by particle size for scenario 3: Fly River floodplain, advection and diffusion.

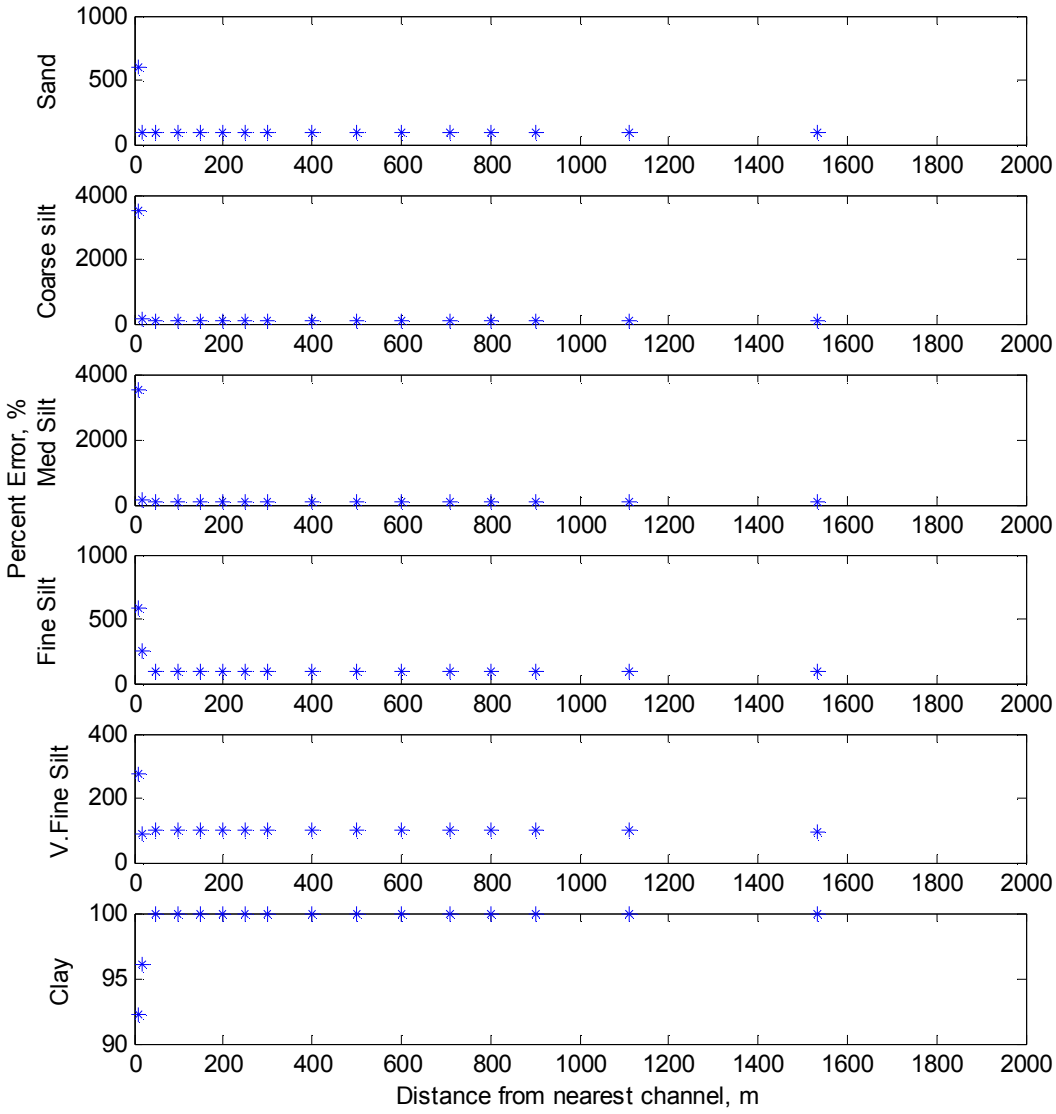


Figure B.11 Percent error modeled vs. measured deposition by particle size for scenario 3: Fly River floodplain, advection and diffusion.

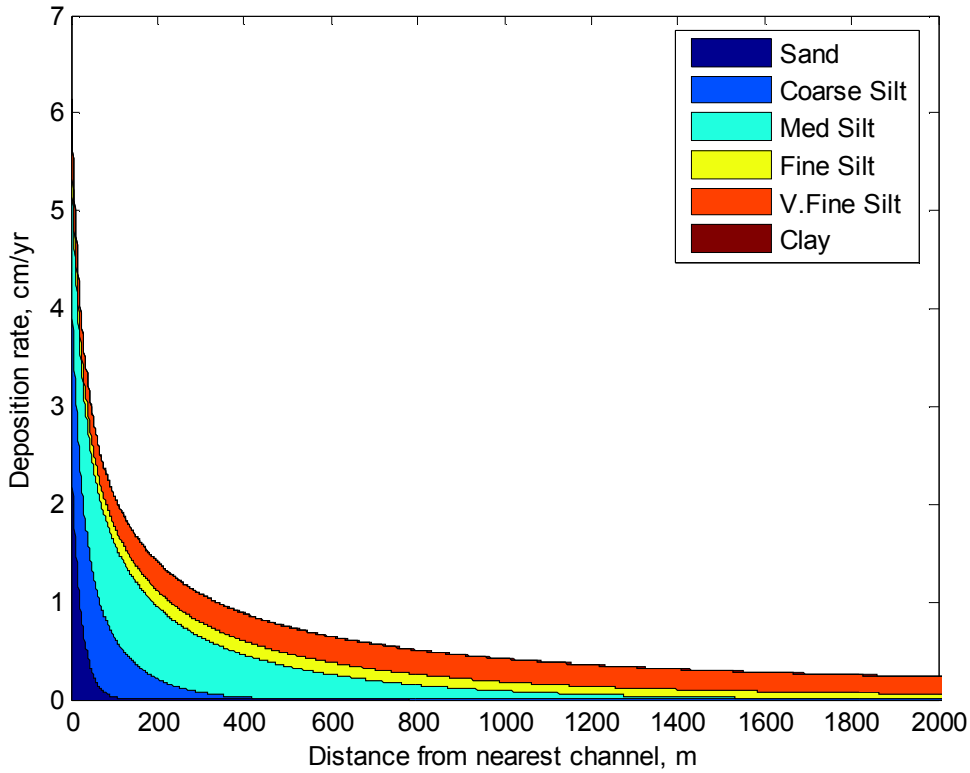


Figure B.12 Modeled deposition pattern resulting from scenario 4: Strickland River floodplain, advection and diffusion.

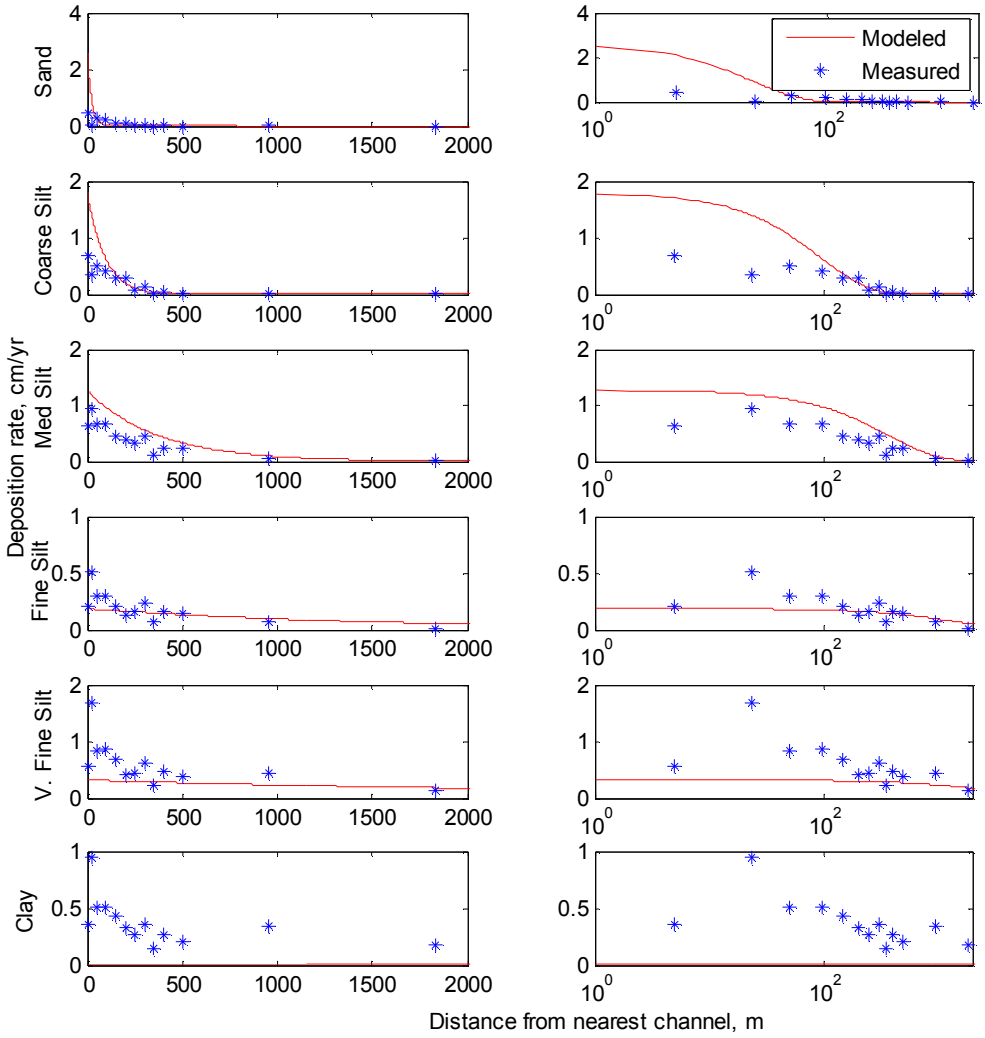


Figure B.13 Modeled and measured deposition rate by particle size for scenario 4: Strickland River floodplain, advection and diffusion.

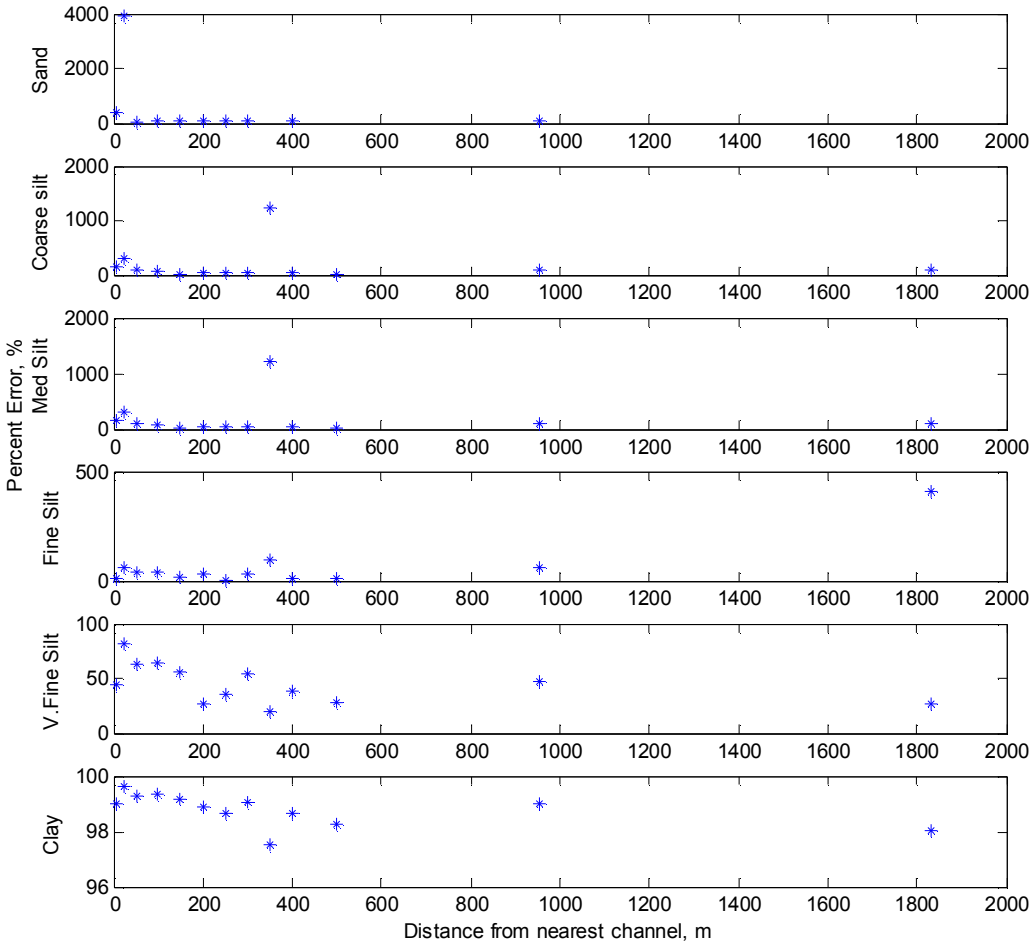


Figure B.14 Percent error modeled vs. measured deposition by particle size for scenario 4: Strickland River floodplain, advection and diffusion.

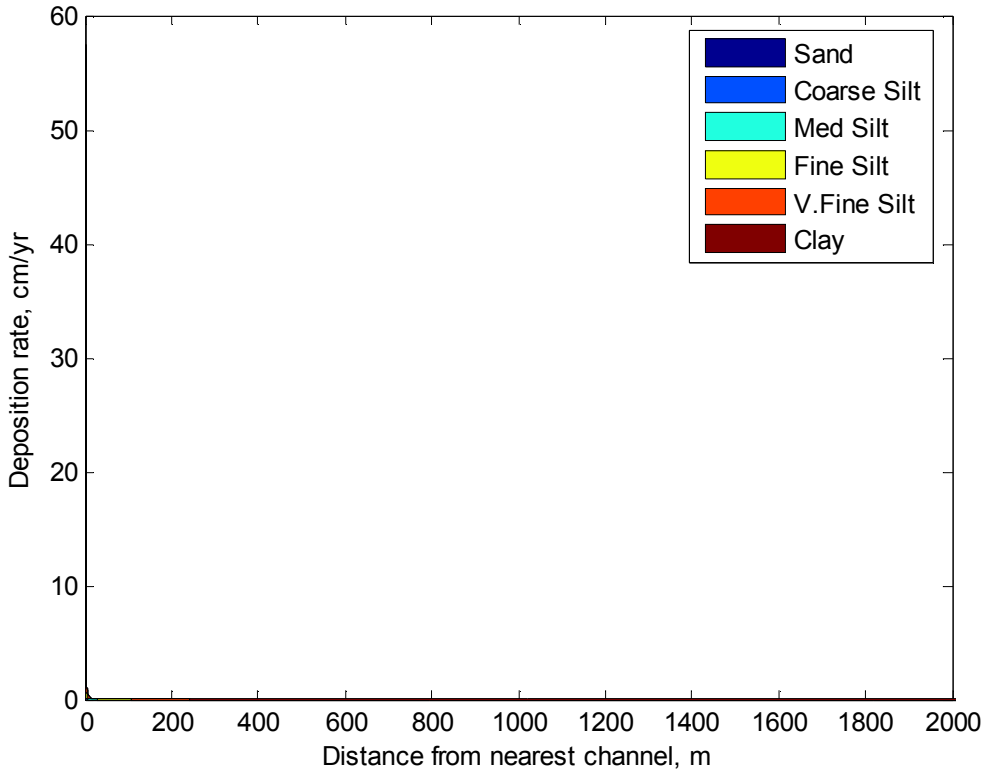


Figure B.15 Modeled deposition pattern resulting from scenario 5: Fly River floodplain, advection only.

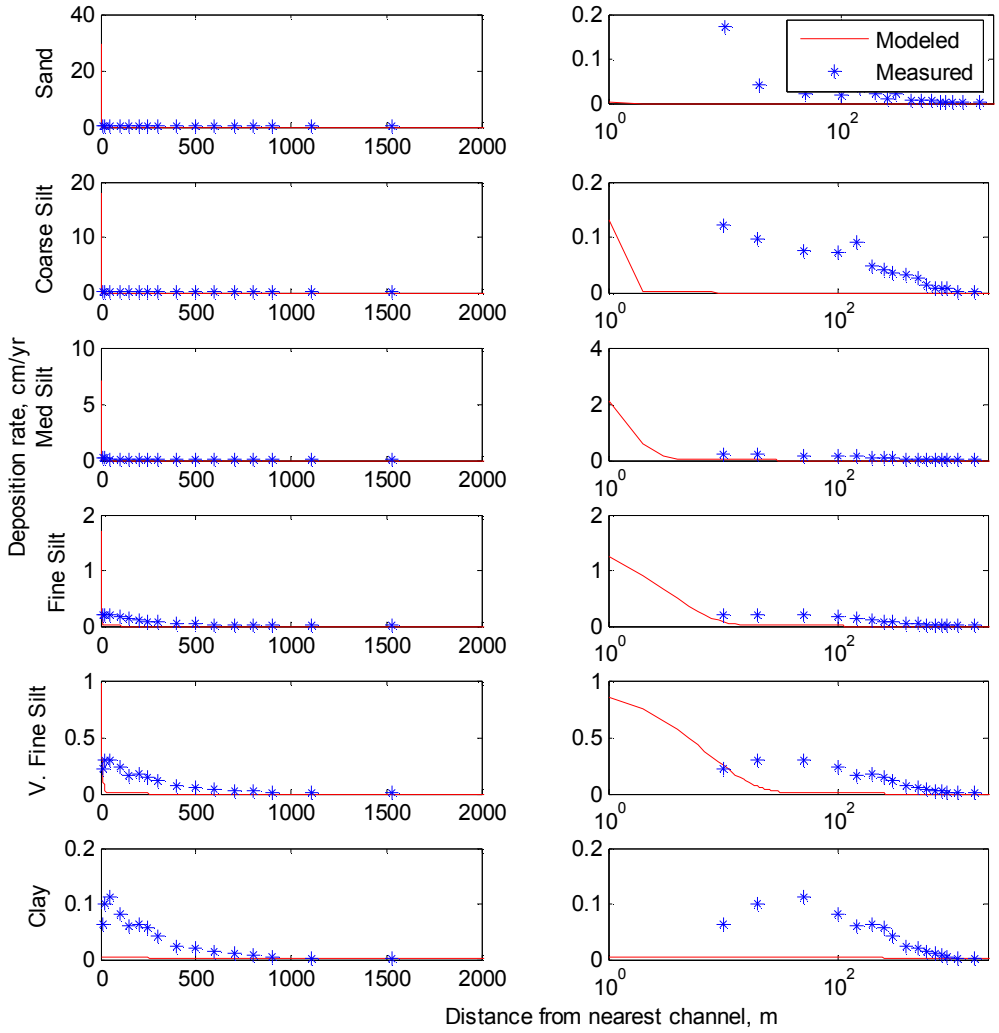


Figure B.16 Modeled and measured deposition rate by particle size for scenario5: Fly River floodplain, advection only.

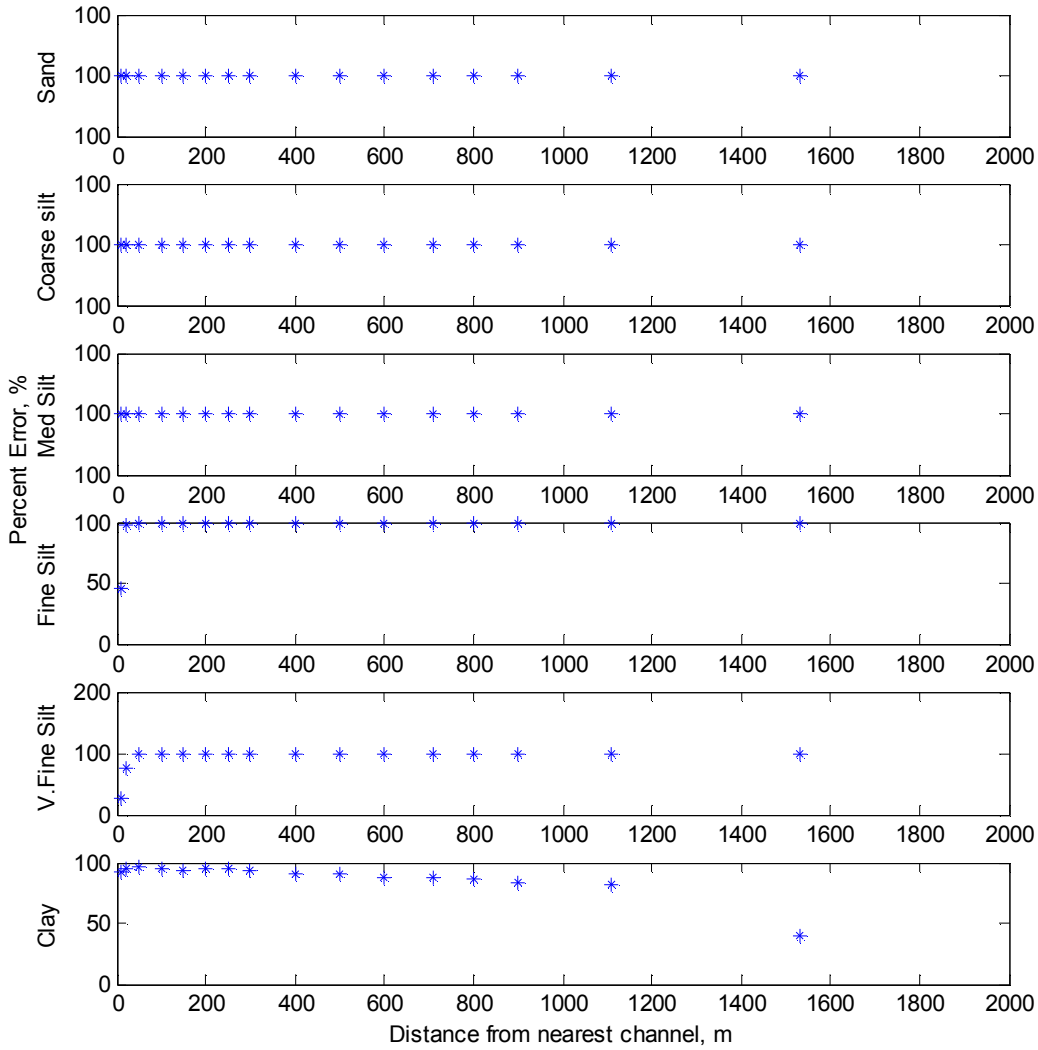


Figure B.17 Modeled deposition pattern resulting from scenario 5: Fly River floodplain, advection only.

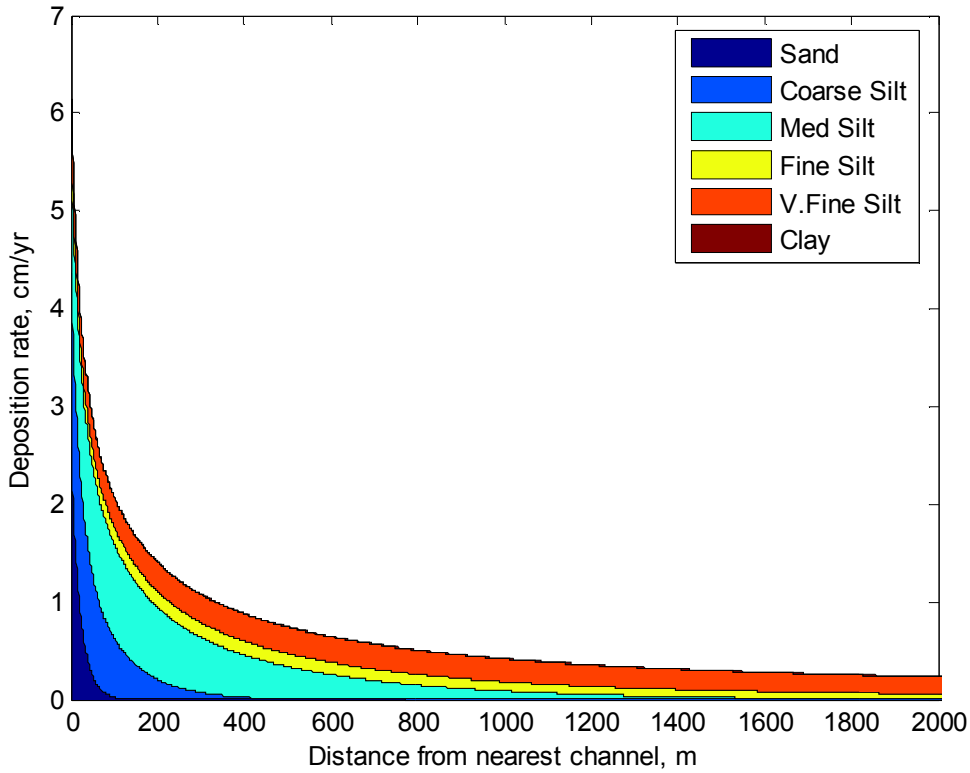


Figure B.18 Modeled deposition pattern resulting from scenario 6: Strickland River floodplain, advection only.

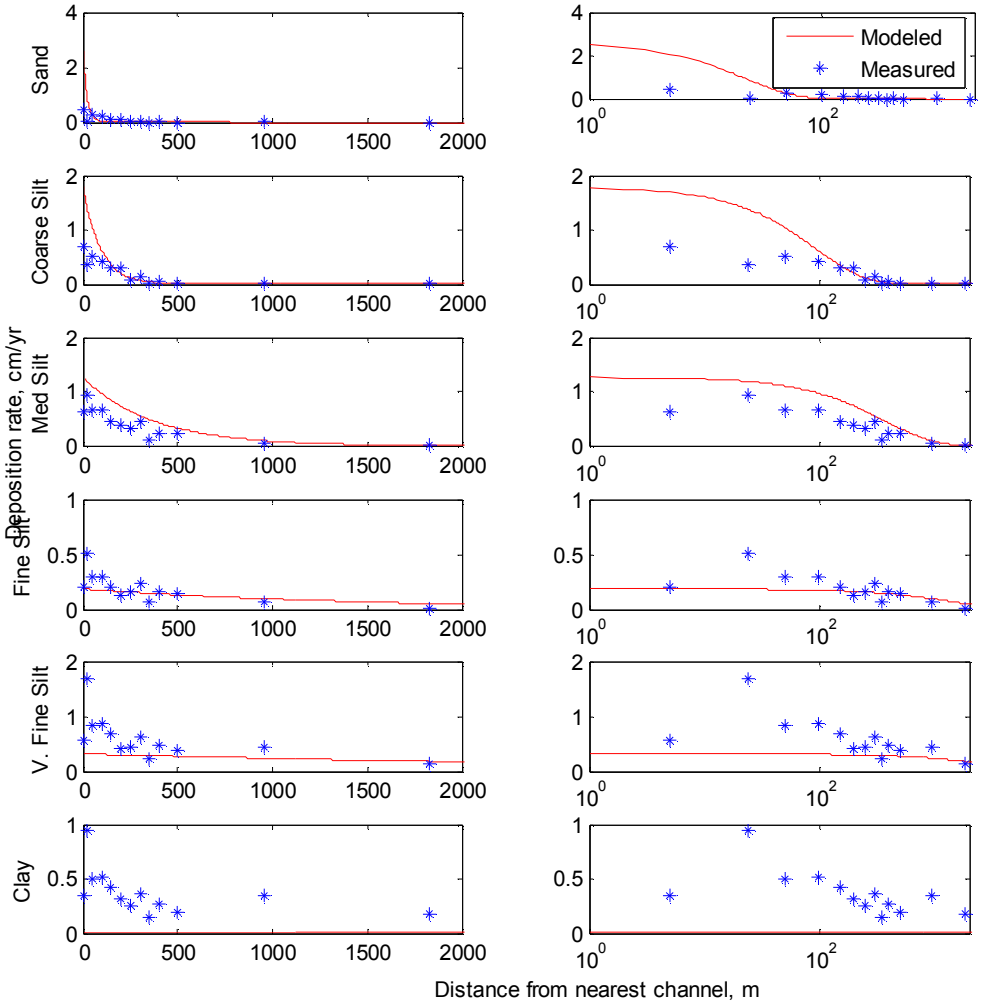


Figure B.19 Modeled and measured deposition rate by particle size for scenario 6: Strickland River floodplain, advection only.

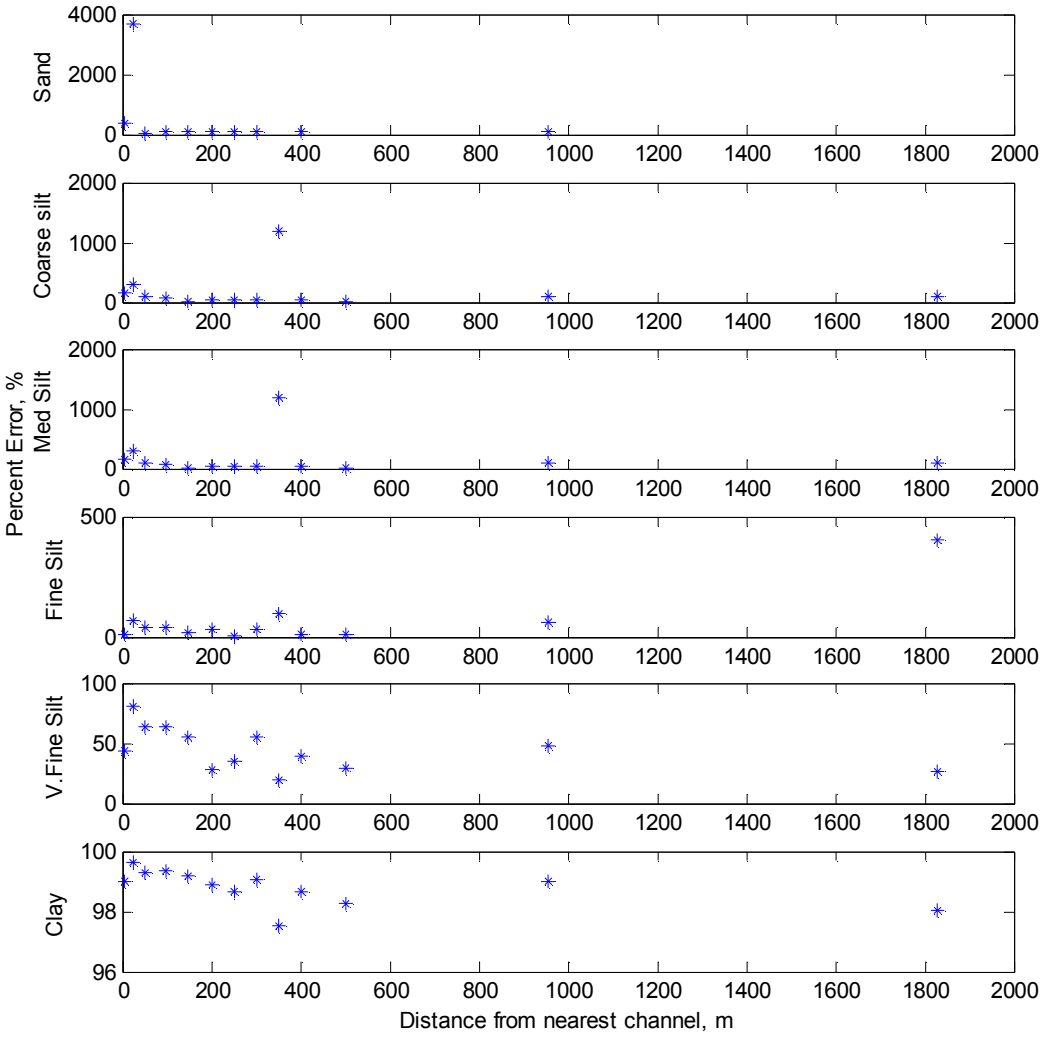


Figure B.20 Percent error modeled vs. measured deposition by particle size for scenario 6: Strickland River floodplain, advection only.

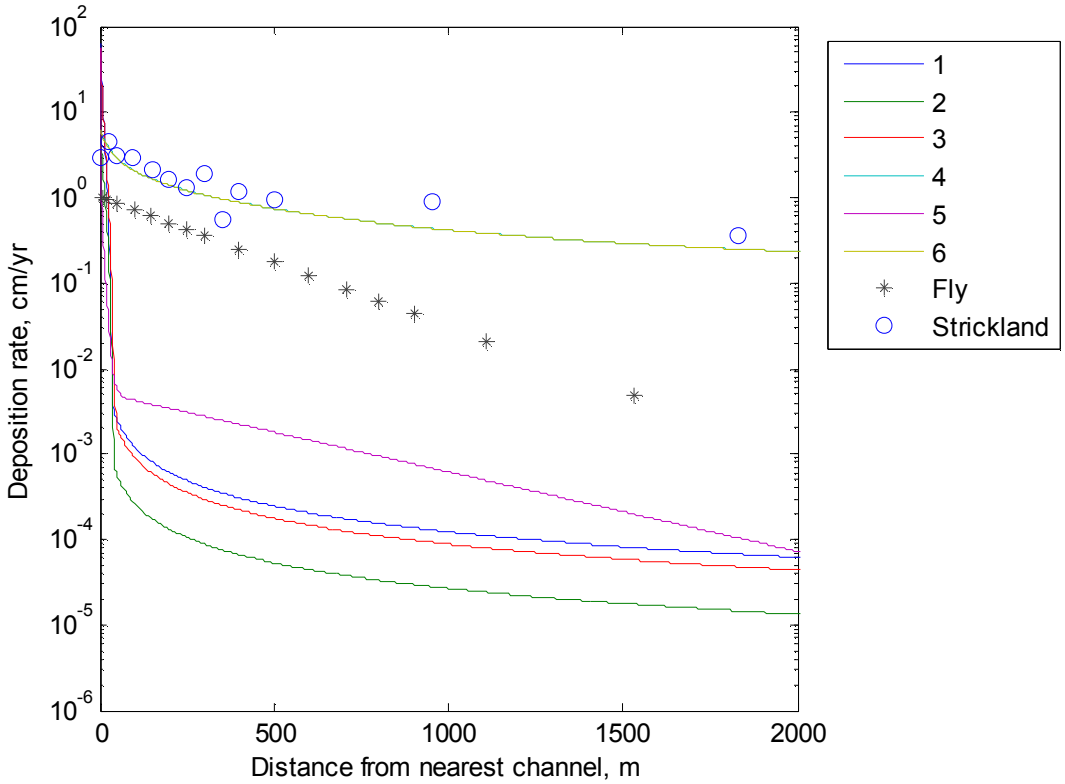


Figure B.21 Total deposition rate for all model scenarios (lines) and measured annual rates (points).

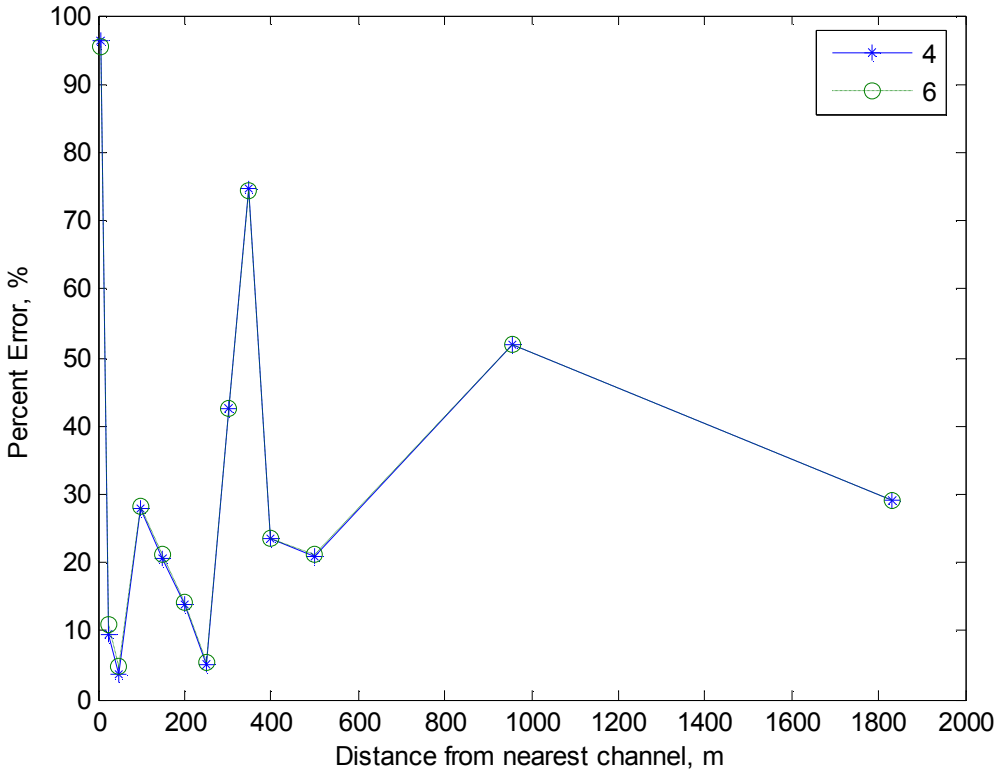


Figure B.22 Percent error between scenarios 4 and 6 modeled total deposition rates and Strickland River measured deposition rates. Total deposition is modeled reasonably well 50-250 m from the channel but errors increase where the model underestimates clay deposition on the distal floodplain and the magnitude of deposition is small.

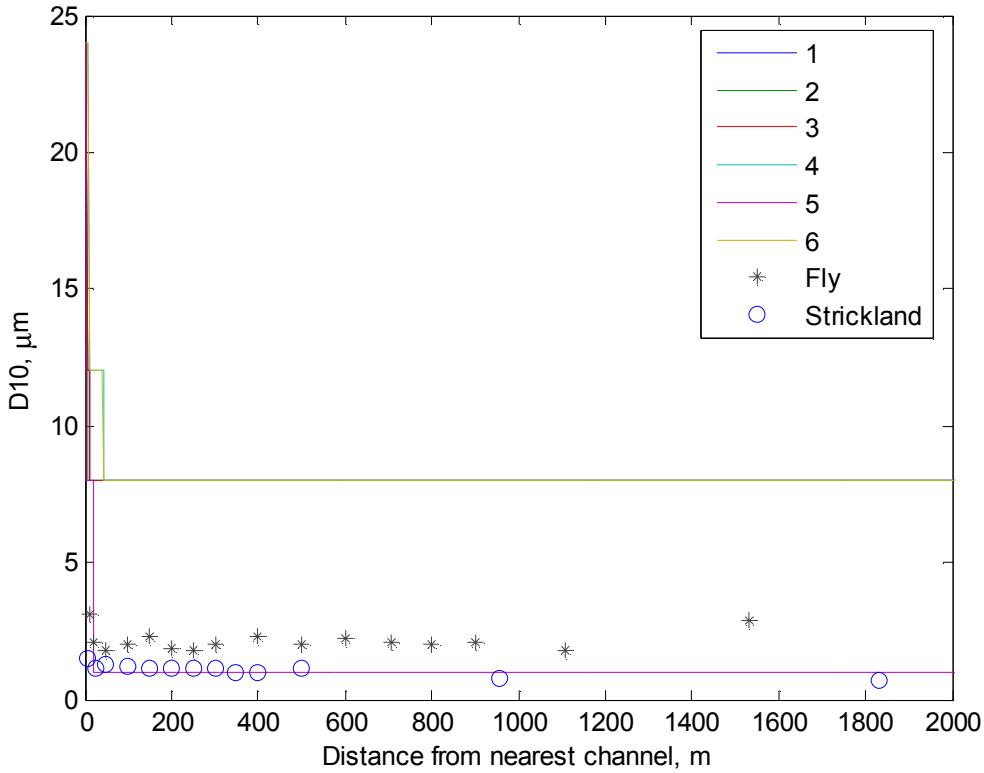


Figure B.23 Modeled and measured D10 for scenarios 1-6 and the Fly and Strickland River floodplains. The models generally overestimate D10 because the settling velocity for clay is very small and little is deposited within the model domain.

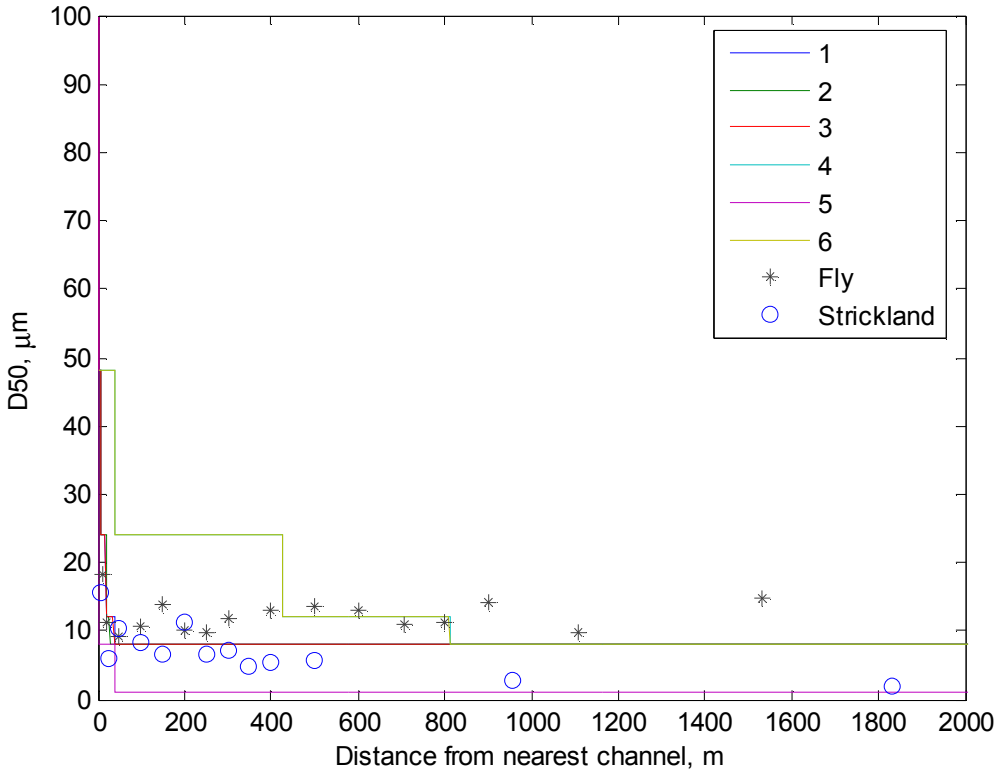


Figure B.24 Modeled and measured D50 for scenarios 1-6 and the Fly and Strickland River floodplains. The models generally cannot reproduce the observed median grainsize which are coarser than predicted on the Fly river where no fining occurs and finer on the Strickland where very little deposition of clay is predicted.

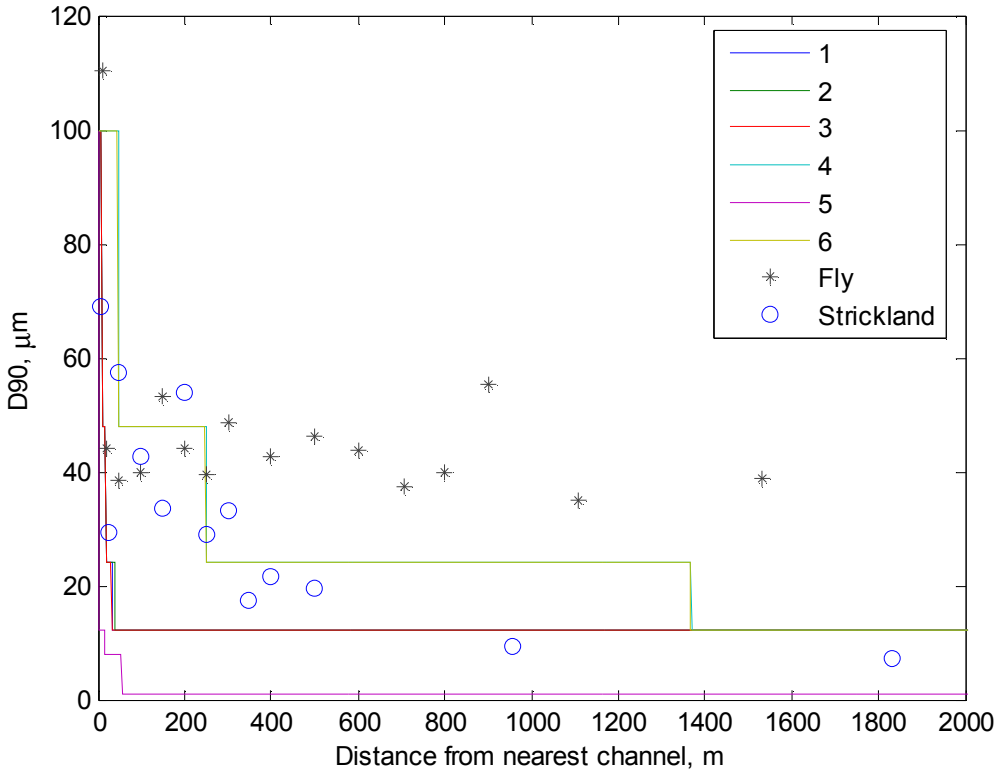


Figure B.25 Modeled and measured D90 for scenarios 1-6 and the Fly and Strickland River floodplains. Fly River floodplain D90 is consistently under-predicted by the modeled scenarios which all predict fining. The modeled scenarios of Strickland River floodplain deposition that include advection transport a fair amount of sand coarse and medium silt away form the channel and reasonably reproduce the decrease in D90 with increasing distance from the channel to ~500m.

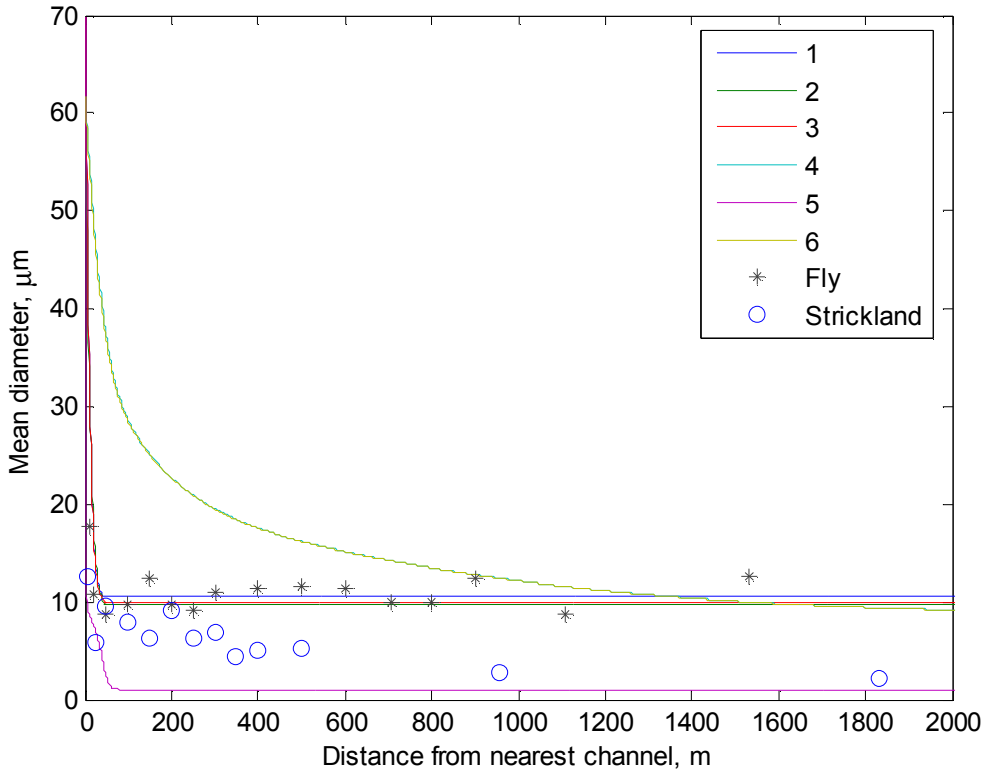


Figure B.26 Modeled and measured mean particle diameter for scenarios 1-6 and the Fly and Strickland River floodplains.